



**HAL**  
open science

**Thermodynamic and structural study of the mechanism  
of competitive retention of azo dyes and inorganic  
anions at the solid-liquid interface with the use of such  
model sorbents as mineral oxides, anionic clays, and  
organic exchangers**

Ganna Darmograi

► **To cite this version:**

Ganna Darmograi. Thermodynamic and structural study of the mechanism of competitive retention of azo dyes and inorganic anions at the solid-liquid interface with the use of such model sorbents as mineral oxides, anionic clays, and organic exchangers. Material chemistry. Université Montpellier, 2015. English. NNT : 2015MONT015 . tel-01331366

**HAL Id: tel-01331366**

**<https://theses.hal.science/tel-01331366v1>**

Submitted on 13 Jun 2016

**HAL** is a multi-disciplinary open access archive for the deposit and dissemination of scientific research documents, whether they are published or not. The documents may come from teaching and research institutions in France or abroad, or from public or private research centers.

L'archive ouverte pluridisciplinaire **HAL**, est destinée au dépôt et à la diffusion de documents scientifiques de niveau recherche, publiés ou non, émanant des établissements d'enseignement et de recherche français ou étrangers, des laboratoires publics ou privés.

# THÈSE

Pour obtenir le grade de  
**Docteur**

Délivré par l'**Université Montpellier**

Préparée au sein de l'école doctorale  
**Sciences Chimiques Balard**  
Et de l'unité de recherche **UMR5253**

Spécialité : **CHIMIE ANALYTIQUE, PHYSIQUE ET THEORIQUE**

Présentée par **Ganna DARMOGRAI**

**Etude thermodynamique et structurale  
des mécanismes de rétention  
compétitive des colorants azoïques et  
d'anions inorganiques à l'interface  
solide-liquide sur des matériaux  
modèles de type oxydes, lamellaires  
et échangeurs organiques**

Soutenue le 26 novembre 2015 devant le jury composé de

M. L. STIEVANO, Professeur, UM	Président du jury
M. C. FORANO, Professeur, Université Blaise Pascal	Rapporteur
M. A. MASON, DR CNRS, CEREGE	Rapporteur
M. D. BERGE-LEFRANC, MC, Aix-Marseille Université	Examineur
Mme D. LAURENCIN, CR, UM	Invité
Mme G. MARTIN-GASSIN, MC, UM	Invité
M. J. ZAJAC, Professeur, UM	<i>Directeur de thèse</i>
Mme B. PRELOT, CR CNRS, UM	<i>Co-directrice de thèse</i>



# THÈSE

Pour obtenir le grade de  
**Docteur**

Delivered by **University of Montpellier**

Prepared within the doctoral school  
**Sciences Chimiques Balard**  
and the research unit **UMR5253**

Speciality: **ANALYTICAL, PHYSICAL AND THEORETICAL  
CHEMISTRY**

Presented by **Ganna DARMOGRAI**

**Thermodynamic and structural study  
of the mechanism of competitive  
retention of azo dyes and inorganic  
anions at the solid-liquid interface  
with the use of such model sorbents as  
mineral oxides, anionic clays, and  
organic exchangers**

Defended 26 november 2015

M. L. STIEVANO, Professeur, UM	President of the jury
M. C. FORANO, Professeur, Université Blaise Pascal	Reviewer
M. A. MASON, DR CNRS, CEREGE	Reviewer
M. D. BERGE-LEFRANC, MC, Aix-Marseille Université	Examiner
Mme D. LAURENCIN, CR, UM	Invited
Mme G. MARTIN-GASSIN, MC, UM	Invited
M. J. ZAJAC, Professeur, UM	Supervisor
Mme B. PRELOT, CR CNRS, UM	Co-supervisor



## *Remerciements*

---

Tout d'abord je remercie vivement Prof. Jurek ZAJAC en tant que Responsable de l'équipe AIME pour l'accueil dans son équipe et également en tant que directeur de ma thèse, qui malgré son emploi du temps chargé, était disponible pour partager ces connaissances sur la Sorption et de m'avoir fait réaliser l'importance de mon travail. *Bardzo dziękujemy!*

De plus, je remercie vivement Mme Bénédicte PRELOT, ma tutrice, pour le temps qu'elle m'a consacré tout au long de cette période, pour avoir répondu à toutes mes interrogations avec patience et d'avoir partagé sa riche expérience dans la science. Je n'oublie pas son soutien au cours de ma thèse.

J'adresse mes remerciements à M. Armand Masion et M. Claude FORANO d'avoir accepté de juger ce travail et d'être les rapporteurs de ce manuscrit. Je veux remercier également M. Lorenzo STIEVANO, M. David BERGE-LEFRANC, Mme Danielle LAURENCIN et Mme Gaëlle GASSIN pour leur participation au jury.

J'adresse ma gratitude à Mr Didier TICHIT, « Dieu des HDL en France », pour sa collaboration, ses grandes idées et sa grande disponibilité pour m'accueillir à la Galera. Je n'oublie pas son soutien au cours de la préparation de ma soutenance. Je suis ravie de vous connaître et d'avoir travaillé avec vous ! Merci !

Je remercie également tous les personnes qui ont fait les synthèses des matériaux, avec qui j'ai eu de la chance de travailler et sans qui c'aurait été difficile d'effectuer ce travail : Géraldine LAYRAC, Sara CAVALIERE, Monika KUS et Vera MEYNEN. Merci les filles je suis très contente de travailler avec vous.

Je veux aussi donner mes remerciements à Mr Amine GENESTE, « Козак » de notre équipe, tout d'abord pour sa gentillesse, ses qualités humaines. Ce fut un énorme plaisir de travailler avec lui. Amine, je te remercie pour ta contribution dans mon travail, même si tu dis que tu as fait rien, sans ton aide avec TAM, je n'aurais jamais obtenus autant de résultats. Merci !

Je tiens à remercier Vanessa, Delhia et Brian qui m'ont aidé à corriger l'anglais de ce manuscrit et qui m'ont permis d'améliorer mes connaissances dans la langue de Shakespeare.

## *Remerciements*

---

Je tiens à remercier mes collègues de bureau : Nejib, Brian, Delhia, Fabrice et Muhammad. Qui ont fait ces trois ans plus vifs et plus agréables. Je vous souhaite plein de bonnes choses dans la vie.

Je souhaite également remercier mes amis proches de travail : Tahra, Julia, Rakhi, Cristina, Anna, Vanessa, Marie-Pierre qui m'ont beaucoup soutenue. Merci pour vos paroles, vos encouragements qui ont été parfois indispensables. Merci d'avoir été à mes côtés aux moments de la joie et de tristesse. Je suis ravie que vous soyez dans ma vie !

Je souhaite également témoigner toute ma reconnaissance à tous les membres de l'équipe AIME avec qui j'ai travaillé en étroite collaboration, l'expérience fut très enrichissante et pleine d'intérêt tout au long de ces trois ans.

Enfin je tiens à remercier toute ma famille : mon père et ma mère, Max, Papie et Mamie pour son soutien à distance et pendant la soutenance. Ils ne savent pas trop ce que j'ai fait mais qui ont été toujours très fiers de moi, ma famille d'accueil, Jannick et Gérard, qui a toujours pensé à moi, ma famille française : Béa, Chloé, Gil, Papi et Mamie. Sans oublier mes amis que je considère comme ma famille : Оля, Миша, Ангелина, Юлик и Pierre. Merci pour tout !

Enfin je veux remercier une personne qui m'a soutenu énormément et sans qui j'aurais pas réussi, mon compagnon Alexis. Merci d'avoir été avec moi, de me soutenir aux moments où j'ai voulu tout lâcher, merci d'avoir tenu ma main quand j'en avais besoin. Je suis ravie que tu sois dans ma vie.

# **Etude thermodynamique et structurale des mécanismes de rétention compétitive des colorants azoïques et d'anions inorganiques à l'interface solide-liquide sur des matériaux modèles de type oxydes, lamellaires et échangeurs organiques**

La présence combinée de différents types de polluants dans les effluents industriels est une problématique assez complexe à résoudre pour les chercheurs dans le domaine de la protection de l'environnement. Dans ce contexte, le principal objectif de ce travail de thèse a été d'améliorer la compréhension des mécanismes de sorption à l'interface solide liquide, processus impliqués dans la rétention compétitive pour une sélection de colorants organiques et d'espèces inorganiques sur des matériaux adsorbants modèles.

Ce manuscrit comprend une étude détaillée de l'adsorption combinant différentes approches et techniques expérimentales complémentaires, principalement à partir de mesures de cinétiques et d'isothermes d'adsorption, une étude structurale par diffraction des rayons X, et une approche thermodynamique par calorimétrie isotherme de titrage. Trois colorants azoïques: Méthyl Orange (MO), Orange II (OII) et Orange G (OG) ont été retenus pour ce travail. Ils ont la particularité de présenter différentes tailles de molécules, différentes charges et caractères hydrophile/ hydrophobe, ... D'autre part, deux types de matériaux chargés positivement et considérés comme échangeurs anioniques ont été choisis comme solides adsorbants modèles : Mg-Al Hydroxyde Double Lamellaire (HDL) contenant dans son espace interfoliaire soit des contre-ions nitrate (Mg-Al-HDL-NO<sub>3</sub>) soit des chlorures (Mg-Al-HDL-Cl) et une résine échangeuses d'ions Amberlite® IRN-78. Enfin, l'impact des oxoanions comme les carbonates (IV), les sulfates (VI), les chromates (VI) et phosphates (V) sur les propriétés de rétention des colorants sur ces adsorbants a été évalué.

Dans un premier temps, l'adsorption des colorants a été réalisée sur ces trois matériaux dans des systèmes mono-composant afin d'étudier en détail les mécanismes de rétention. L'étude

des Mg-Al-HDL échangés par diffraction des rayons X a permis de montrer que l'échange d'anions est accompagné de l'intercalation dans l'espace interfoliaire de la nouvelle espèce sorbée, générant des modifications structurales. En systèmes mono- et multi-composant, la rétention des MO semble supérieure à la capacité d'échange anionique (CEA) théorique des HDL. Ce comportement a été attribué à l'adsorption du colorant sur les surfaces externes, ainsi qu'à la co-adsorption des cations sodium, contre-ions du colorant. Il a aussi été montré que la capacité d'adsorption dépend fortement du caractère hydrophile-hydrophobe des colorants et de leur capacité à établir des interactions latérales (de  $\pi$ -stacking) avec les autres espèces voisines directement au sein de l'espace interfoliaire. La calorimétrie de titrage isotherme a mis en évidence des comportements inhabituels dans les thermogrammes décrivant l'évolution de l'enthalpie cumulative de déplacement, en lien avec la formation d'agrégats fibrillaires provenant de l'interaction entre l'OII et les espèces Mg(II), issues de la dissolution partielle des HDL au contact du colorant.

Dans un second temps, l'étude de la compétition entre les colorants organiques et des anions inorganiques sur ces matériaux a démontré que l'élimination de colorant est fortement influencée par la présence d'anions phosphate ainsi que d'anions carbonate. L'analyse détaillée des différentes espèces compétitives a permis de proposer une classification sur la base de trois types de schémas de compétitions, en lien avec la forme des isothermes individuelles et les données calorimétriques, comme l'enthalpie cumulative en système mono-composant.

L'ensemble de cette description des mécanismes de rétention dans des systèmes mono- ou multi-composants a été complété par des études plus applicatives comme les phénomènes de cinétiques de sorption, de réversibilité.

Mots-clés: Hydroxydes double lamellaires, résines échangeuses d'ions, Méthyl Orange, Orange II, Orange G, Cr(VI), anions inorganiques, adsorption en système mono- ou multi-composant, étude structurale par DRX, calorimétrie isotherme de titrage.

## **Thermodynamic and structural study of the mechanism of competitive retention of azo dyes and inorganic anions at the solid-liquid interface with the use of such model sorbents as mineral oxides, anionic clays, and organic exchangers**

The co-occurrence of various pollutants in industrial effluents is one of the most difficult problems the researchers have to face in the field of Environmental Remediation. In this context, the main objective of the present Ph.D. thesis has been to improve the comprehension of the sorption mechanisms involved in the competitive retention of selected organic dyes and inorganic species at the Solid-Liquid interface by using some model sorbents.

The manuscript reports the results of advanced sorption studies made by combining several experimental techniques, mainly including kinetic and equilibrium adsorption measurements, XRD diffraction, as well as isothermal titration calorimetry. Three Orange-type dyes differing in the molecular size, electric charge, and hydrophobic/hydrophilic character, i.e., Methyl Orange (MO), Orange II (OII), and Orange G (OG), were selected for the purpose of this work. Two types of solid materials possessing positively charged surface sites were considered as model sorbents: layered double hydroxide structures based on Mg and Al (molar Mg:Al ratio of 2) with either nitrate (Mg-Al-LDH-NO<sub>3</sub>) or chloride counter-ions (Mg-Al-LDH-Cl) localized in the interlayer space, on the one hand, and strongly basic anion-exchange resin, Amberlite<sup>®</sup> IRN-78, on the other hand. The impact of carbonate(IV), sulfate(VI), chromate(VI), and hydrogen phosphate(V) oxyanions on the retention capacity of model sorbents towards the three dyes was also investigated thoroughly.

In the first step, the single-component adsorption onto three sorbents was analyzed in regards with the detailed mechanism of retention. In all cases, an ion-exchange pathway between the pristine compensating anions (NO<sub>3</sub><sup>-</sup>, Cl<sup>-</sup>, OH<sup>-</sup>) or anions coming from the ambient atmosphere (e.g., carbonates) and the oncoming anionic species was identified as the principal retention mechanism. In the case of LDH sorbents, this anion exchange was accompanied by the

## Summary

---

intercalation of the adsorbing species within the interlayer space with the concomitant changes in the layered structure, as inferred from the XRD study of the LDH samples loaded with the appropriate solute species. The retention of monovalent MO anions, both from the single-solute and bi-solute solutions, was found to exceed the anionic exchange capacity (AEC) of the LDH samples, which was ascribed to the dye adsorption on the external surface paralleled by the co-adsorption of sodium cations. The adsorption capacity was demonstrated to depend strongly on the hydrophilic-hydrophilic character of the dye units and their capacity of generating lateral interactions (e.g.,  $\pi$ -stacking) with other adsorbed species within the LDH structure. The use of isothermal calorimetry allowed the unusual shape of the curve representing the cumulative enthalpy of displacement to be attributed to the formation of OII aggregates/fibers induced by the presence of Mg and Al cations originating from the partial dissolution of the LDH sample. Competitive adsorption of dye and selected inorganic anions on the three model sorbents was studied in the second step in view of increasing the efficiency of dyes removal by optimizing experimental conditions. One of the main achievements was to categorize the dye uptake schemes in the presence of inorganic anions in regards with the shape of the experimental adsorption isotherms and to correlate them with the individual adsorbate affinities for the LDH sample, as inferred from the calorimetry measurements of the cumulative enthalpy of displacement in single-solute systems.

The discussion on the mechanisms of dye retention in the single- and multi-component systems was supplemented by experimental studies of such applicative aspects of sorption phenomena as kinetics, reversibility, and selectivity.

### Keywords:

Layered double hydroxides, anion-exchange resin, Methyl Orange, Orange II, Orange G, Cr(VI), inorganic anions, single-solute and multi-solute adsorption, XRD study, isotherm titration calorimetry



# Contents

<b><u>Introduction</u></b>	1
1. Environmental impact of textile industry	4
2. Aims and objectives	6
3. Structure of the thesis	8
4. References	10
<b><u>Chapter I: Background</u></b>	11
INTRODUCTION	13
1. Theory of adsorption	14
1.1. Adsorption	14
1.2. Solid-liquid interface	16
1.3. Ion exchange	18
2. Study of adsorption	20
2.1. Isotherm	20
2.2. Classification of liquid-solid adsorption isotherms	20
3. Dyes	21
3.1. Definition and structure	21
3.2. Classification of the dyes	23
3.3. Azo dyes	25
4. Adsorbent used for multi-component adsorption	27
4.1. Layered Double Hydroxides (LDHs)	27
4.1.1. Structure of the layer	27
4.1.2. Interlamellar anions	28

4.1.3.	Anion intercalation into the layers	29
4.2.	Synthetic organic ion exchanger	31
5.	Literature review on competitive adsorption	33
5.1.	Competitive adsorption between organic species.	36
5.2.	Competitive adsorption between inorganic species.	37
5.3.	Competitive adsorption between organic and inorganic species.	38
	References	41

## **Chapter II: Mechanism of dye uptake onto Mg-Al-NO<sub>3</sub> Layered Double Hydroxide** 49

	INTRODUCTION	51
	<b>I. Study of Adsorption and Intercalation of Orange-Type Dyes into Mg-Al Layered Double Hydroxide</b>	52
	ABSTRACT	53
	1. Introduction	54
	2. Experimental	57
	2.1. Materials and synthesis	57
	2.2. Characterization	59
	2.3. Adsorption experiments	59
	2.4. Kinetic study	60
	2.5. Calorimetry measurements	61
	2.6. XRD study of the dye-loaded LDH samples	61
	3. Results and discussion	62
	4. Conclusions	73
	Acknowledgment	74
	References	74
	<b>SUPPORTING INFORMATION I</b>	78
	S1. Characteristics of Mg-Al-LDH-NO <sub>3</sub> solid and dye molecules	78
	S2. Repeatability and experimental uncertainties	79
	S3. Kinetic Models	80

<b>II. On the origin of anomalous enthalpy effects accompanying the adsorption of Orange II onto Mg-Al Layered Double Hydroxide from aqueous solutions</b>	86
1. Introduction	87
2. Materials and methods	89
3. Results and Discussion	90
4. Conclusion	95
Acknowledgements	96
References	96
<b>SUPPORTING INFORMATION II</b>	98
Experimental	98
1. Materials	98
2. Adsorption studies	98
3. Ionic chromatography of the supernatant	99
4. XRD and TEM analysis	99
CONCLUSIONS	101

**Chapter III: Competitive adsorption of Dyes and Inorganic divalent anions onto Mg–Al –NO<sub>3</sub> Layered Double Hydroxide** 103

INTRODUCTION	105
1. Introduction	107
2. Experimental	110
2.1. Materials	110
2.2. Measurements of the cumulative enthalpy of displacement in single-solute systems by isothermal titration calorimetry (ITC)	110
2.3. Measurements of the adsorption isotherms in single-solute and bi-solute systems	111
2.4. X-ray diffraction (XRD) study of the LDH samples loaded with the adsorbate	113

3. Results and discussion	113
3.1. Competitive adsorption of dye and inorganic anions from equimolar bi-solute solutions	117
3.2. Effects of the molar ratio between the dye and inorganic anion on their competitive adsorption from bi-solute solutions	124
3.3. Effects of the controlled carbonate addition to the aqueous phase on the dye adsorption from bi-solute carbonate-dye solutions	128
4. Conclusion	132
Acknowledgments	132
References	133
<b>SUPPORTING INFORMATION</b>	136
<b>CONCLUSIONS</b>	156

**Chapter IV: Single-component and competitive adsorption of Dyes and inorganic anions onto Mg-Al-LDH-Cl** 157

1. INTRODUCTION	159
2. Characterization of uncalcined Mg-Al-LDH-Cl adsorbent	160
3. Adsorption of azo dyes from single-component aqueous solutions	162
4. Competitive adsorption of dye and inorganic anions from equimolar bi-solute and tri-solute solutions	170
5. CONCLUSIONS	175
6. References	177

**Chapter V: Single-component and competitive adsorption of Dyes and Cr (VI) oxoanion onto strongly basic Anion -Exchange Resin** 179

INTRODUCTION	181
1. Introduction	183
2. Experimental	184
2.1. Materials	184

2.2. Measurements of the adsorption isotherms in single-solute and bi-solute systems _____	185
2.3. Reversibility and selectivity tests of solute retention by the resin _____	186
2.3. Calorimetry measurements of the enthalpy changes accompanying single-component and competitive adsorption of dye and chromate anions _____	187
2.4. <sup>13</sup> C CP/MAS NMR study of the resin samples loaded with dye anions _____	188
3. Results and discussion _____	188
3.1. Single-component adsorption of dye and chromate anions from single-solute solutions _____	189
3.2. Competitive adsorption of dye and chromate anions from bi-solute equimolar solutions _____	199
4. Conclusions _____	205
References _____	206
<b>SUPPORTING INFORMATION</b> _____	209
<b>CONCLUSIONS</b> _____	215
<b><u>Conclusions and Perspectives</u></b> _____	217
<b><u>List of the Figures and Tables</u></b> _____	225
<b><u>Appendices</u></b> _____	241
APPENDIX I _____	242
APPENDIX II _____	261

# Introduction



## ***1. Environmental impact of textile industry***

Nowadays, environmental issues, especially those concerning chemical water pollution, have become a major concern for the whole population. Textile industries are the main contributors of water contamination worldwide. They consume large volumes of water through different processes. For example a traditional textile finishing industry consumes around 100 liters of water to process 1 kg of material [1]. Therefore, numerous suggestions have been made to reduce the water use by improving the production methods [2]. The following processes could be found in the next textile producing steps: scouring, bleaching, dyeing, printing, washing-off, etc., and each of these wet processes gives its own contribution to effluent's pollution.

The wastewater varies extensively in terms of composition due to the impurity in fibers and the chemical compounds used in different processes. Nevertheless, the main problem in water pollution from textile industry concerns mainly *dye*, which is used to impart color to the matter of which it becomes an integral part. The estimated annual production of dye is more than  $7 \cdot 10^3$  metric tons [3], in which 2% are directly discharged in aqueous effluents and about 10% are lost during the coloration process [4]. The release of the dyes into water is undesirable for different reasons: it colors the water, changes the pH or the salinity of the wastewater media as well as leaves residual pigment intermediates. Consequently, it has a harmful impact on the photosynthesis of aquatic plants and brings changes to aquatic systems. Moreover, many of the used dyes and their breakdown products present a potentially toxic hazard. Indeed, more than 90% of over 4000 dyes tested in survey have median lethal dose ( $LD_{50}$ ) values greater than  $0.002 \text{ mg kg}^{-1}$ .

To evaluate the degree of pollution of wastewaters streams, many parameters should be compared. Among the most important ones are [2]: Chemical and Biological Oxygen Demands (COD and BOD), Dissolved Organic Carbon (DOC) and Total Organic Carbon (TOC). It should be noted that DOC and TOC values contain all the organic pollutants rejected from textile industry, including dye contents. All the above-mentioned parameters are independent, i.e. the knowledge of one of them cannot be used to identify the others. Besides, other parameters may

also be taken into account such as color, temperature, pH of discharged water or contents of inorganic additives.

The accurate determination of the chemical composition of wastewater is important since this allows better understanding of the reactions and interactions between organic and inorganic compounds. Wastewater can be described as a complex mixture of many polluting substances ranging from organic chlorine-based pesticides to heavy metals associated with dyes [5]. To have an idea about the multiplicity of the component from the textile effluents, Table 1 gathers a classification of the main pollutants.

Table 1. Classification of pollutants in textile effluents [2]

<b>Inorganic contaminants</b>	Neutral salts ( <i>chlorides, sulfates, phosphates, etc.</i> ), alkalis, mineral acids, oxidizing agents
<b>BOD easily biodegradable</b>	Vegetable oils, biodegradable surfactants, organic acids ( <i>formic, acetic, oxalic</i> )
<b>Dyes and polymers difficult to biodegrade</b>	Dyes, polymeric impurities, most fibers, silicones
<b>BOD difficult to biodegrade</b>	Mineral oils, surfactants resistant to biodegradation, anionic or non-ionic softeners
<b>BOD unsuitable for conventional biological treatment</b>	Heavy-metal salts ( <i>Cr(VI), Cu(II), Hg(II), Cd(II), Sb(III), As(III, V), Zn(II)</i> ), formaldehyde reactant, chlorinated solvents, cationic retarders and softeners

Therefore identifying pollutants in wastewaters is not trivial as the latter can contain highly variable distinct components. Indeed, heavy metals such as chromium, copper, zinc and mercury can be found in many textile processing waters, especially those from wool and synthetic finishing processes [3]. The presence of salts like sodium chloride and sodium sulfate salts are used to assist in exhaustion of anionic dyes [6, 7]. They are not toxic for the plants and animals in normal concentrations but it becomes dangerous at very high doses [8].

Researchers from different continent have evaluated the samples from several textile industries [9, 10] as well as from different processes occurring in a textile mill [11] in order to measure the composition and amount of discharged contaminants, as well as different physico-

chemical parameters such as the pH, the total dissolved of solids (TDS), the conductivity and so on. This information are important in order to improve the purification procedure of the water.

Due to the complexity of mills effluents, the purification process have to be divided in two main steps : the first step is to separate all the solid particles or suspended matter which can be present in water followed by the second treatment, which is to mineralize or decompose completely all organic pollutants. The separation process is mainly physical (screening, sedimentation, flotation and flocculation) or chemical (neutralization, extraction, oxidation, precipitation or coagulation) [12]. Thus, solid - free wastewater can either be divided into biodegradable or non-biodegradable parts and these following treatments such as biological, chemical or physical methods can be used to eliminate the rest of the polluting residues.

In this line, *adsorption* is rapidly gaining prominence as an effective means for lowering pollutants in effluent at a relatively low cost [13]. The key point of adsorption process is in the choice of adsorbent material. The latter has to follow next requirements:

- Low cost (the cheapest adsorbents are often produced from locally, abundantly and easily available materials).
- Regenerative (reuse of the adsorbent after easy regeneration method)
- Competitive performance (adsorption properties of adsorbent in multi-component wastewater conditions).

One of the most popular adsorbent nowadays is activated carbon. This material is used as the main adsorbent in pre-treatment stage for adsorption treatment methodology [12, 14]. Activated carbon is highly efficient for large, negatively charged or polar molecules of the dyes and even more, for anionic mordant and acid dyes [9] (see classification of dyes in Chapter I). But the main disadvantage of this adsorbent is its' high cost. Therefore, a large variety of low-cost adsorbents, named non-conventional, is presented in the literature (ex.: anion-exchange resins, zeolites, silica, chitosane, clays, etc.).

Despite the numerous peer-reviewed papers found in the literature on the adsorption of contaminants using activated carbon, anion exchange resins, zeolites and activated alumina, not a lot of them give a comprehensive and deep understanding of the mechanisms occurring during the adsorption process. Few information on the selectivity of the adsorbent for the dye removal from a real industrial effluent is given in the literature.

## ***2. Aims and objectives***

There is a real necessity to estimate the selectivity of the sorbent under competing conditions among the variety of organic and inorganic solutes, which are currently present in wastewaters during the sorption processes [9, 10]. In order to have an insight on selectivity, it is vital to understand the nature of the interactions (competitive or synergic) between the organic dyes and the inorganic species during the adsorption at the solid/liquid interface as well as the possible interactions of the adsorbates with the adsorbent.

Therefore, the first objective of this thesis was to choose an adsorbent material, which potentially exhibit a good adsorbing properties for organic dyes. The chosen adsorbent was then characterized using different characterization techniques, followed by the study of the sorption of the organic dye.

Titanium dioxide ( $\text{TiO}_2$ ) famously known for its photocatalytic properties was studied during the first year. The adsorption properties of this synthetic mineral with the Rhodamine 6G dye were investigated as a photocatalyst for the degradation of organic dye impurities in wastewater. Initially, further objective was to evidence the effect of adsorption (dye, intermediate and other organic or inorganic species in solution) on photocatalytic performance. Nevertheless, the study demonstrates that Rhodamine 6G adsorbs to a very small extent on  $\text{TiO}_2$ . The adsorption of this dye onto  $\text{TiO}_2$  was so insignificant that the investigation of the multi-component adsorption was not possible. However, it was possible to show the competition between the Rhodamine 6G and inorganic ions (provided from phosphate buffer which was added for pH stabilization) that was quite unexpected. This work is presented in more details in Appendix I.

This thesis deals mainly with the investigation of mono- and multi-component adsorption on the two solids, chosen as adsorbents-references for this work. The first is an anionic clay known as Layered Double Hydroxide (LDH). It has excellent exchange properties for polluting dyes, therefore is a good candidate for this study. The second adsorbent is a synthetic anion exchanger – commercially available resin Amberlite<sup>®</sup> IRN-78. For both solids, the same dye

systems were used in order to compare their sorption properties. The following approaches were used:

- adsorption of the organic dyes from a single-solute system on the adsorbents;
- isothermal study of the competitive adsorption between organic and inorganic anions from the multi-component solutions;
- XRD, ITC and NMR measurements were performed to investigate the single- and multi- component sorption.

The primary target of this work was to elucidate the sorption process of three dyes: Methyl Orange, Orange II and Orange G onto Layered Double Hydroxide. Different parameters such as the amount adsorbed, energy of the interactions, kinetic, possible sorption mechanisms were evaluated. It was possible to use the LDH system to study the competition without adding any supplementary anionic species in the bulk. The aim was to investigate whether the intrinsic anion present in the LDH system, that could be exchanged by the dye molecules as well as carbonate ions that are naturally present in the bulk solution as we were working in an open air system.

The second objective was to investigate the competitive adsorption between the dyes and inorganic anions (discharged with dyes in wastewaters) onto the LDH. Different dye:inorganic anion molar ratios were tested, with analysis of two competing species *i.e.* the dye and inorganic ion removal. XRD studies were performed for different competitive systems with the aim to determine from the d-spacing of the LDH's interlayer the different steps of the exchange. In order to investigate the energetic aspects of adsorption in the competitive systems, as well as influence of pH on adsorption, bi-solute adsorption was also performed onto strongly basic anion-exchange resins between the dyes and Cr (VI).

### ***3. Structure of the thesis***

This thesis reports the study of dyes adsorption mechanisms from the aqueous solution towards simple- and multi-component systems onto different sorbent particles. Chapter I summarized the theory of adsorption and ion-exchange mechanisms, with a literature review concerning dyes, used in textile industries and adsorbent used as effective exchangers for pollutant removal. Moreover, the literature review concerning competitive adsorption studies was summarized to better understand the system investigated in this work. The results obtained during this thesis are presented in four chapters in the form of articles.

Chapter II focus primarily on the comprehension of the mechanisms of orange-type dyes adsorption onto the Mg-Al-LDH containing nitrate as interlayer anions. This chapter is divided into two articles where the mechanisms of adsorption of dyes onto the LDH are described based on experimental studies. In the first article, named "Study of Adsorption and Intercalation of Orange-type Dyes into Mg-Al Layered Double Hydroxide" the sorption of Orange-type dyes onto Mg-Al-NO<sub>3</sub> is explained. Different analysis such as: kinetic of sorption, global energetic effect of sorption, expansion of the LDH's layers after the dye sorption and finally competitive adsorption between the dyes and carbonates provided from air as well as the co-adsorption of the sodium - counter-ion were performed and reported in this article. The second article "On the origin of anomalous enthalpy effects accompanying the adsorption of Orange II onto Mg-Al Layered Double Hydroxide from aqueous solutions" described the sorption of Orange II dye adsorption only using ITC analysis in order to shed some more light on the different phenomena involved during this dye uptake.

Chapter III is dedicated to the competitive adsorption of the Orange-type dyes and inorganic anions onto Mg-Al-LDH-NO<sub>3</sub>. This chapter contains one article and deals with the competitive adsorption from the bi-solute systems. Three different molar ratios of the dye and the inorganic ions (sulfates, phosphates, carbonates or chromates) were investigated in order to comprehend the competitive adsorption of these compounds onto the LDH. This study allows the classification of the three schemas of species adsorption from the bi-component systems, based on the shape of the individual adsorption isotherms of the dye and inorganic anion.

Chapter IV is also devoted to the Mg<sub>2</sub>Al Layered Double Hydroxide, however in this chapter the interlayer anions are the chloride ions. The same type of studies were performed. In

analogy with Mg-Al-LDH-NO<sub>3</sub>, mechanism of the Orange-type dyes adsorption was established. The competitive adsorption was investigated for dye from bi-solute and tri-solute component systems. Phosphates and carbonates were presented as the main competing species in this chapter. Analysis of the difference in adsorption properties between the two LDH solids (Mg-Al-NO<sub>3</sub> and Mg-Al-Cl) is also reported.

Last Chapter V is dedicated to dye adsorption from mono- and bi-solute solutions onto anion exchange resins Amberlite® IRN-78. The analysis of all the main parameters (e.g. pH) influencing the adsorption of dyes on this sorbent was performed and confirmed by <sup>13</sup>C CP/MAS NMR. This adsorbent permits us to perform some complementary studies of the competitive adsorption, as reversibility and selectivity tests of solute retention by the resin.

#### 4. References

1. Shah, M.P., et al., *Microbial degradation of Textile Dye (Remazol Black B) by Bacillus spp.* ETL-2012. J Bioremed Biodeg, 2013. **4**(180): p. 2.
2. Park, J. and J. Shore, *Water for the Dyehouse: Supply, Consumption, Recovery and Disposal.* Journal of the Society of Dyers and Colourists, 1984. **100**(12): p. 383-399.
3. Robinson, T., et al., *Remediation of dyes in textile effluent: a critical review on current treatment technologies with a proposed alternative.* Bioresource Technology, 2001. **77**(3): p. 247-255.
4. Pearce, C.I., J.R. Lloyd, and J.T. Guthrie, *The removal of colour from textile wastewater using whole bacterial cells: a review.* Dyes and Pigments, 2003. **58**(3): p. 179-196.
5. Mansour, H.B., et al., *Alteration of in vitro and acute in vivo toxicity of textile dyeing wastewater after chemical and biological remediation.* Environmental Science and Pollution Research. **19**(7): p. 2634-2643.
6. Shore, J., *Advances in direct dyes.* Indian Journal of Fibre and Textile Research, 1996. **21**: p. 1-29.
7. Khandegar, V. and A.K. Saroha, *Electrocoagulation for the treatment of textile industry effluent. A review.* Journal of Environmental Management. **128**(0): p. 949-963.
8. Tufekci, N., N.k. Sivri, and I. Toroz, *Pollutants of textile industry wastewater and assessment of its discharge limits by water quality standards.* Turkish Journal of Fisheries and Aquatic Sciences, 2007. **7**(2): p. 97-103.
9. Anjaneyulu, Y., N.S. Chary, and D.S.S. Raj, *Decolourization of industrial effluents–available methods and emerging technologies–a review.* Reviews in Environmental Science and Bio/Technology, 2005. **4**(4): p. 245-273.
10. Singh, D., V. Singh, and A. AK, *Study of textile effluent in and around Ludhiana district in Punjab, India.* International Journal of Environmental Sciences, 2013. **3**(4): p. 1271-1278.
11. Imtiazuddin, S., M. Mumtaz, and K.A. Mallick, *Pollutants of wastewater characteristics in textile industries.* Journal of Basic & Applied Sciences, 2012. **8**: p. 554-556.
12. Crini, G. and P.-M. Badot, *Traitement et épuration des eaux industrielles polluées: Procédés membranaires, bioadsorption et oxydation chimique.* 2008: Presses Univ. Franche-Comté.
13. Mehali J. Mehta, K.K.C., *Adsorptive Removal Of Dye From Industrial Dye Effluents Using Low-Cost Adsorbents: A Review.* Journal of Engineering Research and Applications, 2014. **4**(12): p. 40-44.
14. Carmen, Z. and S. Daniela. *Textile organic dyes–characteristics, polluting effects and separation/elimination procedures from industrial effluents–a critical overview.* in *Organic Pollutants Ten Years After the Stockholm Convention-Environmental and Analytical Update.* 2012. InTech: Croatia.

# Chapter 1: Background



## **INTRODUCTION**

Many industrial wastewaters contain pollutants that are difficult to remove via conventional treatment, some contaminants are present in very small concentration, and therefore the removal of these impurities is quite difficult using the conventional methods. Hence, sorption processes are very efficient techniques for the decontamination of wastewaters. Adsorption processes are not only limited to the removal of pollutants but also widely used in the pharmaceutical industries, chemical and biological processes to name a few.

This thesis focuses on the competitive interactions between solid and pollutants of wastewaters system at the solid-solution interface. Organic and inorganic compound will be used to mimic the wastewater systems. The sorption processes on different systems were studied by means of adsorption isotherm. The aims of this chapter is first to give a brief description on the basic aspects of the theory of adsorption. The emphasis will be mainly on the solid-liquid interface, where both adsorption and ion-exchange processes occur. Adsorption isotherms are classified according to the nature of the sorbate-sorbent interactions. The classification can be used to correlate macroscopic observations with microscopic phenomena occurring at the solid-liquid interface.

The systems used in this study are then described. Dyes, frequently used in textile industry, are persistent pollutants and to our knowledge, only few low-cost adsorbents have been proposed so far to treat such species. In order to illustrate why dyes are persistent pollutants, a detailed description of different types of dyes commonly used in industry is given. More attention has been paid to *azo* dyes, one of the most used types of dyes in numerous different industrial processes. In order to address the specific challenge of low-cost and effective sorbents, we have chosen to focus on Layered Double Hydroxide and ion-exchange resins whose structural features and reactivity are described.

The originality of our approach is to consider the competition of different species for adsorbent's surface, these competing species being important for real wastewater application. The use of multi-component adsorption processes is not straightforward since species can interact in different ways (cooperate, compete and do not have any interaction). Therefore, a comprehensive

literature review in this specific field is proposed, taking into account organic-organic, inorganic-inorganic and organic-inorganic types of interaction.

## ***1. Theory of adsorption***

### ***1.1. Adsorption***

The term "sorption" is used to describe the attachment of a substance to a surface with the creation of an interaction. Depending on the type of interactions occurring between the sorbate and the sorbent, sorption can be divided into physical, chemical or electrostatic terms [1].

**Physical sorption** or physisorption involves the formation of weak physical interactions, where no exchange of electrons is observed. Moreover, only relatively weak long-range van der Waals forces can be formed between the surface and the adsorbate, as well as among adsorbates. Because the adsorbate - surface interactions are weak, this type of adsorption can be easily reversed by heating. Physisorption usually has a low heat of adsorption ranging from 20 to 40 kJ mol<sup>-1</sup>, hence this type of adsorption is stable only to temperatures below 150°C. Because of the weak Van der Waals forces between the adsorbate and adsorbent, lateral interactions are very important for sorbed molecules [2].

**Chemical sorption** or chemisorption involves the formation of new chemical bonds between the adsorbate and the surface site. In chemical sorption an exchange of electrons takes place between the adsorbed molecule and the surface site. This sorption mechanism is characterized by higher energies of interactions, equivalent to strong chemical bonds ( $\geq 100$  kJ mol<sup>-1</sup>) and therefore can be more stable at high temperatures.

**Electrostatic sorption** involves the formation of Coulomb attractions between adsorbed ions and charged functional groups. The term "electrostatic sorption" is used specifically to ion exchange.

The term "adsorption" is used to describe the uptake of the components (gaseous, liquid or solids) on external or internal surfaces of the solids. According to the second law of thermodynamics, adsorption of substances on solids takes place to reduce the surface tension, so free surface energy of the solids.

The energy of formation of a chemical bond on the surface on a solid can be depicted by means of Lennard-Jones potential energy curve [3]. Therefore, Lennard Jones potential can be used to explain the energetic phenomenon occurring during an adsorption or desorption process. Figure 1 represents the energy of the molecule as a function of the distance ( $z$ ) from the mass center of the molecule to the surface. The well is the result of the balance of two forces: van der Waals attraction and repulsion present between the clouds of electrons in the atoms, from the surface and those of the sorbed molecule. When a molecule reaches the well, it is trapped or another term “adsorbed” by this potential energy until the molecule has sufficient energy to be desorbed. Thus, the lower the energy of the molecule, the easier it is for the molecule to fall in the well and stick in the chemisorption well. As shown, there are two types of wells presented on the curve, chemisorption and physisorption wells. The physisorption well is located further than the chemisorption one (i.e when the distance is large), because the bonds formed are short-ranged and stronger in the case of chemisorption.

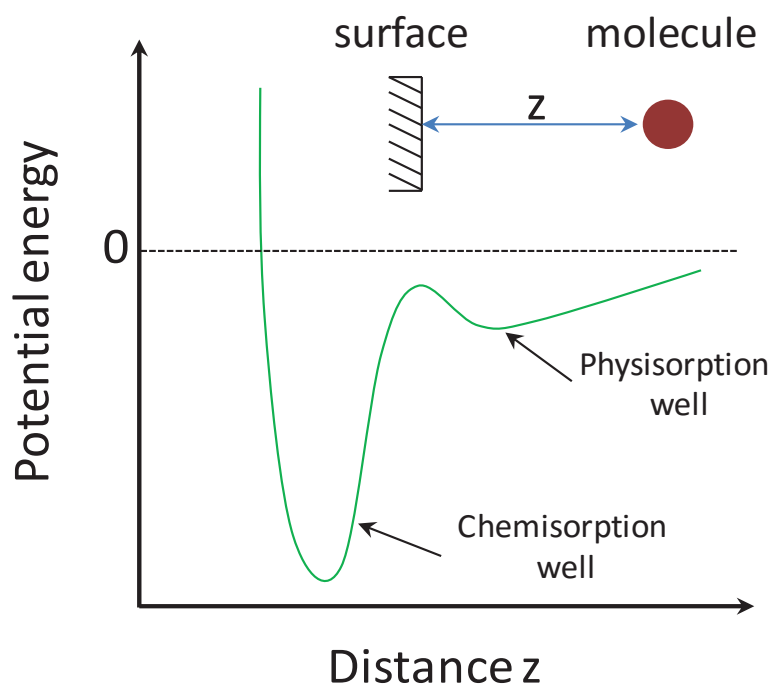


Figure 1. Lennard - Jones type diagrams (non-activated adsorption): potential energy versus distance.

From the thermodynamic point of view, any systems will try to reduce its energy to reach the lowest values of Gibbs energy  $G$ . Adsorption is the process that occurs in the isolated system

with a constant temperature. Therefore, for such system Gibbs free energy describes by the following relation:

$$\Delta G = \Delta H - T\Delta S$$

where,  $\Delta H$  and  $\Delta S$  are respectively, the changes in enthalpy and entropy during the process.

A spontaneous process is always accompanied by a decrease in the Gibbs energy, leading to  $\Delta G < 0$ , this implies the increase in the disorder of the system or entropy changes during the process  $\Delta S > 0$ .

### 1.2. Solid-liquid interface

The solid-liquid interface is the common boundary surface formed by two different phases of matter (e.g., solid and liquid), where many important chemical, physical and biological processes occur. The solid – liquid interface formed during the sorption process will be discussed in this section. Adsorption at the solid-liquid interface is of a very complex nature compared to solid-gaseous interface. As adsorption takes place at an interface covered by the solvent molecules, which can potentially be strongly adsorbed must be displaced from the surface to make way for the adsorbent.

The distributions or accumulation of ions in the vicinity of the solid surface can be described using different model based on the double layer structure. One of the oldest model of such electrolyte-solid system was developed by Helmholtz in 1874 [4]. This model states that two layers of opposite charge form at the surface/electrolyte interface and are separated by an atomic distance. The Helmholtz model was modified by Gouy and Chapman, where the latter introduced the creation of a diffuse layer. Later Stern combined the two previous models. Thus, in Stern's model it is possible to recognize two regions of ion distribution - the inner region (compact or *Stern layer*) and the diffuse layer. *Stern layer* consists of *inner (IHP)* and *outer (OHP) Helmholtz planes*. The graphical representation of hydration shell in double layer is represented in Figure 2.

All ions in solution bear around them a shell from the solvent molecules and interact strongly with the solvent as well as with the solid. The ionic compound can be sorbed on the surface of the solid in well-defined adsorbate geometry and this type of chemisorption is called *specific adsorption*. The ion exists with a hydration shell in the solution but if it is specifically

adsorbed, it must discard this shell, at least partially, when it attaches to the surface. This will happen only if the formation of the bond between the ion and the surface can overcome that part of energy of solvation between the solvent and the ion that is lost owing to specific adsorption. Specifically sorbed ions do not lose all their interactions with the solvent but there are no solvent molecules between ions and the solid surface. If the solvent-ion interactions are stronger than ion-surface interactions, ions preserve their hydration shell. In this case, adsorption is *non-specific*. Specifically adsorbed ions are principally bound by chemical interactions (covalent or coordinate bond), but non-specifically sorbed ions are principally bound by electrostatic attraction.

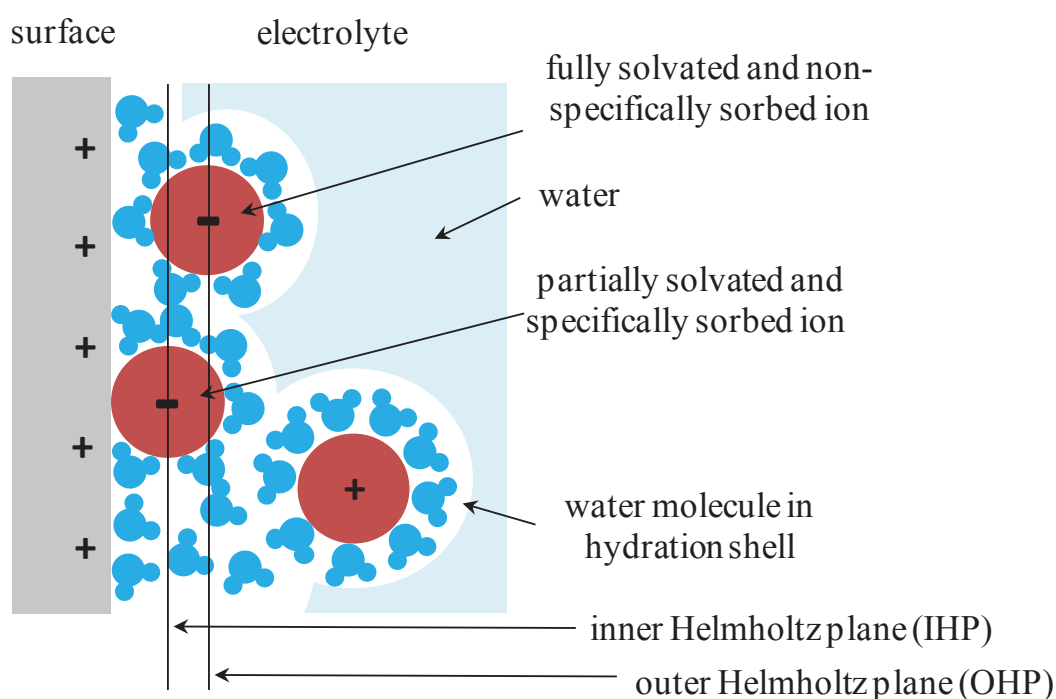


Figure 2. Model of double layer structure of the solid-liquid interface with examples of specific and non-specific ion adsorption [5], together with their hydration shell.

Specifically adsorbed ions form Inner Helmholtz plane, while the outer Helmholtz plane is formed by non-specifically sorbed ions.

Different sorption mechanisms can be found at the solid-liquid interface: co-precipitation or dissolution (when solid is partially dissolute in suspension with an ion liberation, that can precipitate on the surface with species presented in solution); surface complexation (sorption of reactive solute occurs on the specific sites of adsorbent); surface precipitation (at variance with

latter, this sorption mechanism is independent from the number of sorption sites) and ion exchange that will be described in the following part.

### 1.3. Ion exchange

The notion of *ion exchangers* comes from the property of insoluble solid materials to contain exchangeable ions (named, counter-ions). These charged ions can be replaced or exchanged in stoichiometric amount with other anions in contact with the surrounding solution. For example,  $\text{Na}^+$  neutralizes negative charges of clay platelets (of cationic clays). If the clays particles are placed in  $\text{CaCl}_2$  electrolyte solution, the  $\text{Ca}^{2+}$  ions present in the solution displace  $\text{Na}^+$  from clay interlayer to take up its place [6] based on an exchange mechanism as demonstrated in Figure 3. The ability to exchange ions is due to the properties of the structure of the materials.

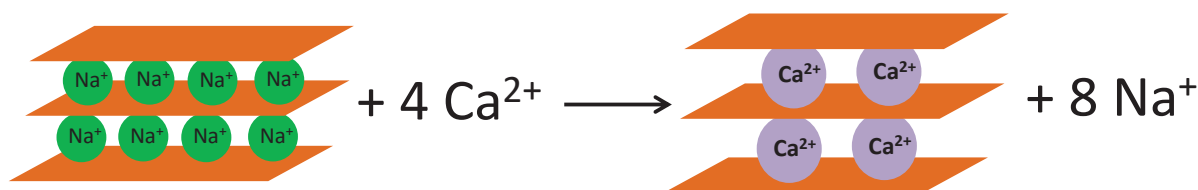


Figure 3. Schematic representation of  $\text{Na}^+$  -  $\text{Ca}^{2+}$  exchange [6].

If a solid contains exchangeable anions, it is called *anion exchanger*. In contrast, if the sorbent contains cations, this is a *cation exchanger*. The name *amphoteric* ion exchanger is used when exchanger contains both anions and cations.

Ion exchange is similar to the adsorption process, as both process described the uptake of substances by a solid in solution. However, there is a specific difference between these two processes. Ion exchange is only a stoichiometric process in contrast to adsorption, which can be also nonstoichiometric. It means that in the ion exchange process for every charged specie removed from solution another charge compensator of the equal charge is released from the solid. However, the aim is to neutralize the structure's charge of exchanger that is why if one di-charged ion is released from the structure it will be replaced by another di-charged or two mono-charged ions. Both ions, exchanged and removed must have the same, positive or negative charge [7]. Secondly, in ion exchange only ions are sorbed, whereas in adsorption processes, electrically neutral species

can also be removed [8]. However, it is difficult to differentiate them practically, because sometimes common sorbent material can be adsorbent and exchanger at the same time (ex: activated alumina, with its exchangeable hydroxide ions [7]).

A water-swollen ion exchange material surrounded by an aqueous solution can be used as an example to demonstrate what is a complex ion exchange system [9]. The exchanger is composed of a dimensional framework with either positive or negative electric charges, compensated by the counter-ions, as mentioned above. Counter-ions are free to move within the framework and can diffuse in the pores. In contact with the electrolyte solution, the exchanger takes up the solvent with additional mobile ions. This term includes the counter-ions, different from those in the structure and co-ions with charge of the same sign as the framework charge. Hence, counter-ion can leave the framework, simultaneously with the incorporation of another counter-ion in the framework to compensate the charge of the system. The ion exchange process has been established as diffusion controlled, with the rate determining mechanism being the inter-diffusion of the two counter-ions [10]. The counter-ion content of the ion exchanger is a specific property of the material, named – *ion-exchange capacity*. It depends on the framework charge and it is independent from the nature and the charge of the counter-ions. For cationic exchangers, the constant is named *cation-exchange capacity (CEC)* and for anionic *anion-exchange capacity (AEC)*.

Ionic exchanger is sometimes able to preferentially select some ions. This preference can be caused by different factors:

- the nature of the interactions between the solid and the counter-ions
- the size and the valence of the counter-ions
- other interactions than electrostatic (London forces between the counter-ion and the matrix, as well as interactions of the solvent molecules with one another)
- the steric exclusion of large ions from the framework.

This ability to choose between the counter-ions is called the *selectivity* of exchanger.

Many different natural and synthetic solids possessed exchange properties. But the main ones are: natural and synthetic inorganic ion exchangers (MOFs), ion exchange resins and ion exchange coals [7].

## 2. Study of adsorption

### 2.1. Isotherm

The amount of solute species ( $q$ ) adsorbed per gram of adsorbent can be expressed in terms of the mole fraction of the solute on the surface  $N$  and the number of moles of adsorption sites per gram  $m$  according to:

$$q = Nm = f(T, C_{eq})$$

$q$  is a function of equilibrium concentration  $C_{eq}$  and the temperature  $T$ . At constant temperature  $q = f_T(C_{eq})$ , and this is called the *adsorption isotherm function* [11].

To evaluate the adsorption from solution, the amount of adsorbed species can be obtained by measuring the decrease in its concentration after its uptake by the solid. The *adsorption isotherm* is then plotted with amount adsorbed  $q$  against the equilibrium concentration  $C_{eq}$ . The adsorption isotherm represents the main property of the adsorbent, i.e., its ability to remove the species from the solution. Moreover, each part of the adsorption curve can give us information about the potential sorption mechanisms. The real value of amount adsorbed can be evaluated only when equilibrium is reached, that is why it is necessary to measure the kinetic of adsorption, to know the necessary time to reach equilibrium.

### 2.2. Classification of liquid-solid adsorption isotherms

For the sorption onto liquid-solid interface, according to the nature of the initial portion of the curve and its slope, Giles et al. proposed a classification of adsorption isotherms [12]. This classification divides the various types of isotherms onto four main groups:  $S$ ,  $L$  (Langmuir type),  $H$  (high affinity) and  $C$  (constant partition), see Figure 4. The isotherm of  $L$  type is the most classical and widespread form among the sorption curves. For  $L$  type, species adsorption is favored in the beginning of the process, when all adsorption sites are vacant. It is usually indicative of molecules adsorbed flat on the surface.  $S$  curve arises due to the vertical orientation of the adsorbed molecules at the surface during the adsorption process. The  $S$  curve isotherm occurs as a result of the interactions among the adsorbed molecules.  $H$  type curve is characterized by a sharply vertical

part of the initial slope, indicating highly strong interactions between the adsorbate and the adsorbent. All the molecules in the solute are adsorbed onto the solid. H curves arise in special cases where the adsorbate has a high affinity with the substrate.

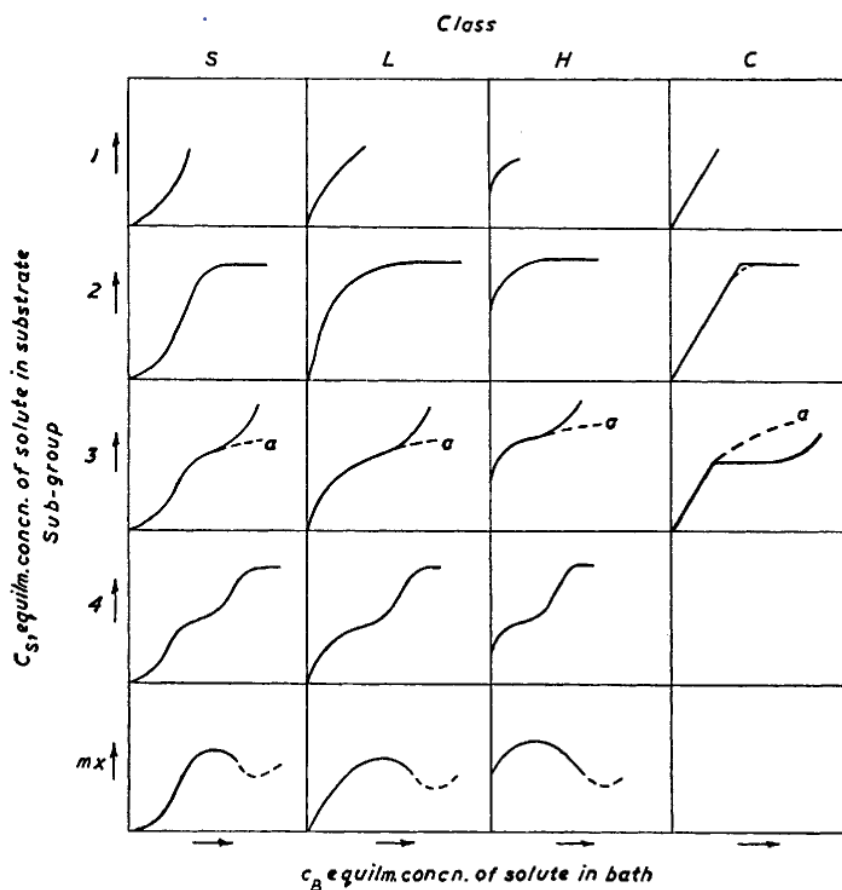


Figure 4. Classification of solution adsorption isotherms according to Giles et al. [12].

The last group of the isotherm curves is the C type and this can only be found in special cases. In the latter, the solutes penetrate into the solid more readily than the solvent.

### 3. Dyes

#### 3.1. Definition and structure

Organic colored compounds could be named *dyes* in the case if they can share their color with other materials. Thus, the color of the dye becomes an integral part of these materials. Not all

organic compound could be dyes, because of the existence of different characteristics. They should:

- ✓ have at least one *chromophore* group, which is the color-bearing group (acceptor of electrons);
- ✓ absorb light in the visible spectrum (400-750 nm);
- ✓ have conjugated system with alternating single and double bonds ( $\pi$  bonds);
- ✓ have *auxochrome* groups (donor of electrons). These groups can be ionizable, and they confer to dyes the binding capacity onto the textile material (color helpers).

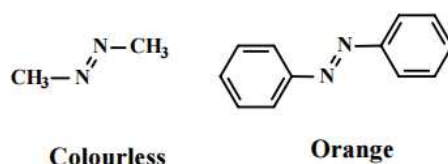


Figure 5. Example of chromophores related with non-conjugated (left) and conjugated (right) systems [13].

It is very important to have chromophore as part of a conjugated system. On the contrary, the production of colorless substances occurs by the placement of chromophoric, azo-group between methyl groups, as it is illustrated in Figure 5. However, if the azo-group is placed between conjugated systems – benzene aromatic rings, the organic substances give the color. Some examples of chromophoric and auxochrome groups are presented in Table 1.

Table 1. Examples of chromophoric groups presented in organic dyes.

Chromophoric groups [14]	Auxochrome groups [15]
Azo (-N=N-)	Amino (-NH <sub>2</sub> )
Sulfur (=C=S)	Chlorine (-Cl)
Nitroso (-N=O, -N-OH)	Hydroxyl (-OH)
Carbonyl (=C=O)	Methyl (-CH <sub>3</sub> )
Vinyl or methane (-C=CH <sub>2</sub> , =C=)	Sulphonic acid and sodium salts (-SO <sub>3</sub> H)

### 3.2. Classification of the dyes

Dyes can be classified in several ways: according to their chemical structure [14, 16], their method of applications onto substrate [17] or fibers type, i.e. for nylon, cotton, polyester,... Here,

two different classifications will be presented: the classification of the dyes by their chemical structure, which is the most appropriate system as it is based on chromogenic moieties. The second classification based on auxochromes groups, can help to understand the nature of the dye and substrate interactions (ionic, hydrogen, Van der Waals or covalent bonding).

### 3.2.1. Chemical classification based on chromogen [14]

♣ *Azo dyes*. The compounds of this class are characterized by the presence of one or more azo groups (-N=N-). The most used dyes in textile industry.

♣ *Anthraquinone dyes*. The general formula of these dyes is based on anthraquinone molecules, which contain chromophoric carbonyles. It is the most important class of dyes after azo dyes (Figure 6 (a)).

♣ *Indigoid dyes*. The name of this class comes from the main representative member – indigo dye. These dyes give large range of colors, from orange to turquoise (Figure 6 (b)).

♣ *Xanthene dyes*. The compounds of this class provide intensive fluorescence, and can be used as markers for underground rivers. The most representative member is fluorescein (Figure 6 (d)).

♣ *Phthalocyanine dyes*. It is a class of synthetic dyes based on complex structures with a central atom of metal (ex: Cu, Co, Pb, Fe, Mg) (Figure 6 (c)). These dyes are often used for painting of trains, and for organic photoconductors of electrophotography.

♣ *Nitro and nitroso dyes*. These dyes have the sample structure composed of a nitro group (-NO<sub>2</sub>) bonded with group, donor of electrons (amine or hydroxyl group) (Figure 6 (e)).

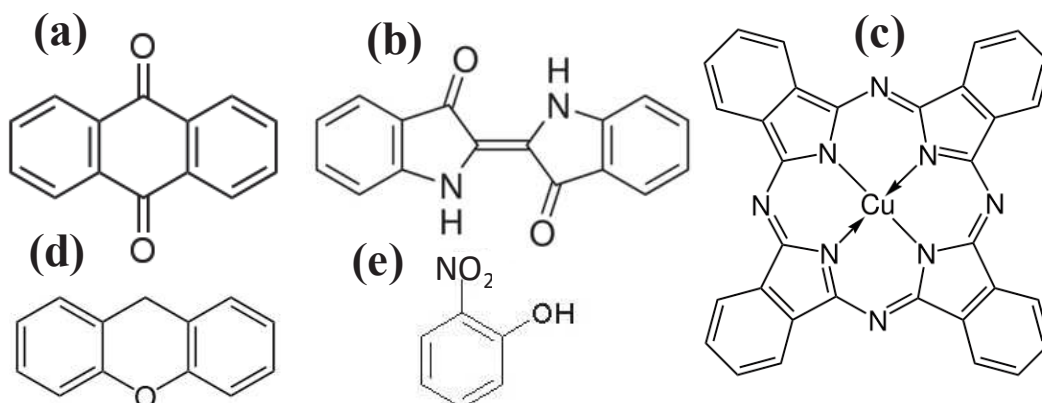


Figure 6. Examples of molecules that represent different chemical classes: anthraquinone (a), indigoid (b), phthalocyanine (c), xanthene (d) and nitroso (e) dyes.

### 3.2.2. Chemical classification based on auxochrome [15]

♣ *Acid dyes.* Acid or anionic dyes contain sulfonic or carboxylic acid groups in their structure, they are therefore soluble in water. Moreover, such functional groups help to create ionic bonds with amino groups for textile fibers [14]. These dyes are used for coloring animal fibers, nylon, silk, modified acrylic, wool, paper, food and even cosmetic.

♣ *Basic dyes.* Basic or cationic dyes mainly consist of big soluble molecules. These dyes have a high affinity for wool, silk, acrylic, paper and polyesters. Some of these dyes are used in medicine, because of their biological activity.

♣ *Direct dyes.* These dyes are mainly used for dyeing cotton, cellulose, or even cotton-wool or cotton-silk. They are water-soluble anionic dyes and have high affinity for fibers. Most of the dyes in this particular class are constituted of azo compounds, along with some triazoles, phthalocyanines and oxazines.

♣ *Reactive dyes.* These dyes are chemically constituted from azo compounds, anthraquinones and phthalocyanines, with high fixing properties. The presence of reactive chemical functions like triazinic or vinylsulfone, reactive dyes allow to create covalent bonds with the fibers (cotton, wool or nylon).

♣ *Sulfurous dyes.* It is a small group of dyes, insoluble in water but applied in form of soluble derivative. A next re-oxidation to their insoluble form occurs directly on the fibers.

Sulphurous dyes are low cost and process good fixing properties. But they are sensitive to chlorine and light. However, they are often applied to cotton.

♣ *Vat dyes*. The dyes of this class are insoluble in water (anthraquinones and indigo) that is why they are impregnated into fibers under reducing conditions and then they are reoxidized to an insoluble form directly on fiber.

♣ *Dispersive dyes*. They are almost insoluble in water and applied in the form of dispersive powder in suspension, preferentially onto hydrophobic fibers. The dyeing process occurs in the presence of dispersing agents of long chains which stabilize the dyes suspension and facilitate the contact with the hydrophobic fibers. They are applied to cellulose acetate, nylon, polyester and polyamide.

♣ *Mordant dyes* generally contain a functional ligand able to strongly react with aluminum, chromium, cobalt, nickel and copper salts to form different colored metal complexes with textile materials. They are formed directly on the fibers by in situ precipitation.

These classifications show us the huge diversity of the dyes existing and used in textile industries. Adsorption of azo dyes will be investigated in this work that is why they are described in the following part.

### 3.3. Azo dyes

Almost two-third of all organic dyes are azo dyes ( $R_1-N=N-R_2$ ) used in numerous different industrial processes such as textile dyeing and printing, color photography, finishing process of leather, pharmaceutical, cosmetics, etc.

The reactivity of azo dyes depends on different parameters. The first factor is the nature of the substituent in the molecular structure. Thus, the azo dyes can be found in different forms: acid (if the functional groups are in protonated form), basic (deprotonated with free electron pair on nitrogen) or non-ionic depending on the pH values. The basicity of dyes is influenced by additional factors. For example, the presence of acceptors substituents in aromatic rings such as  $-Cl$  or  $-NO_2$  groups decreases the basicity of the amino groups. The basicity is also decreased by the donor substituents in the ortho position, which sterically impedes the protonation [18]. However, the basicity is increased by the presence of donor groups ( $-CH_3$  or  $-OR$ ) in meta and para positions. The azo dyes also have amphoteric properties if they contain additional acidic groups (hydroxyl,

carboxyl or sulfoxyl groups). The chromophore distribution in reactive dyes indicates that a great majority of unmetallised (do not contain a chelated metal on negative ion group) azo dyes have a range of colors from yellow to red.

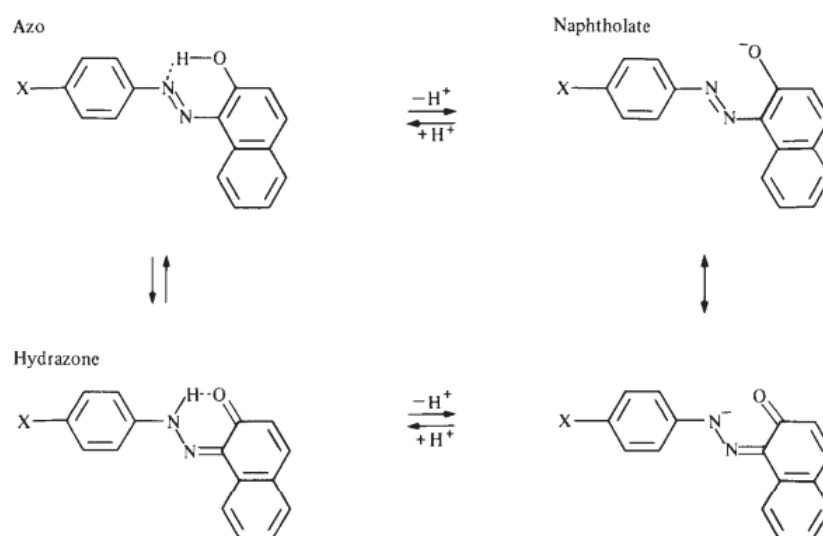


Figure 7. Tautomeric forms of Orange II molecules depending from pH [19].

Other structural particularities of the azo dyes like the position of the substituent compared to azo groups or electronic repetition can have an influence on the reactivity. For example, many azo molecules have two isomeric forms – cis and trans, where the cis form is unstable and can be obtained by photoisomerization method of the trans form (Figure 7). Thus, the transition between these two forms can change the absorption wavelength ( $\lambda$ ) of the molecule and consequently the color of the dye [16]. Some dyes have different tautomeric forms, (for example Orange II molecule (see the Figure 7)). As a result, the different tautomers usually have different molecular fingerprints, hydrophobicity and pKa's values as well as different structural and electrostatic properties [20].

Azo dyes are widely used for coloring mostly because of their affordable cost and their good fixation properties [21]. However, the high values of acute toxicity are found among these dyes as well as their intermediates therefore a very high potential risk to human health (toxicity, carcinogenicity and allergic sensation) and aquatic life [22]. That is why, it is very important to remove completely or to reduce the level of these species in aqueous effluents.

## 4. Adsorbent used for multi-component adsorption

In this work, two different materials are chosen as the adsorbent for the study of simple and multi-component adsorption: the layered double hydroxides and the anion exchange resins. Thus, this section describes the main structural features of these two materials.

### 4.1. Layered Double Hydroxides (LDHs)

One of the potential adsorbent for anionic pollutant removal is the Layered Double Hydroxides (LDHs), which belongs to the anionic (anion exchanger) clays class. Hydrotalcite-like compounds (HTlc) are another name currently used in the literature for this kind of materials, since the first natural mineral found was the hydrotalcite [23] and therefore becomes the most representative mineral of the group. LDHs are not as prevalent in the nature as cationic clays, however, they have both natural and synthetic origins. The synthesis of such material is easy and non-expensive.

#### 4.1.1. Structure of the layer

The structure of LDHs is related to the mineral brucite ( $\text{Mg}(\text{OH})_2$ ), where, the  $\text{Mg}^{2+}$  cations is surrounded by six hydroxide ions to make up octahedral units. These units share their edges to organize an infinite two-dimensional layer (see Figure 8 (A)). Then, the layers are stacked to form a three-dimensional structure with electrostatic interactions and hydrogen bonds between the layers [24, 25]. The brucite-like layer can be stacked on top of one another by forming rhombohedral (3R) or hexagonal (2H) sequences.

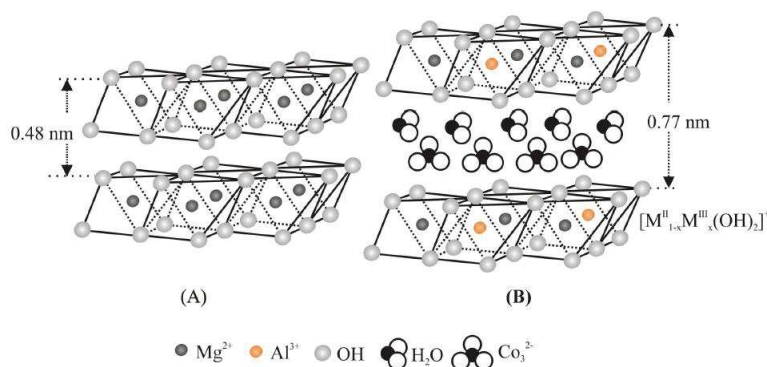


Figure 8. Schematic representation of brucite layer (A) and that of LDHs (B) [26].

Layered double hydroxides are formed by substitution of a fraction of divalent  $Mg^{2+}$  cations from the brucite layers by trivalent ones (i.e.  $Al^{3+}$ ). As a result, the layers acquire a positive charge, which is compensated by negative interlayer anions (Figure 8 (B)). The composition of LDHs is generally written as  $[M^{2+}_{1-x}M^{3+}_x(OH)_2]^{x+}[(X^n)_{x/n} \cdot mH_2O]^{x-}$ , where  $M^{2+}$  and  $M^{3+}$  are divalent and trivalent cations and  $(X^n)_{x/n}$  is the interlayer anion, with different nature (organic or inorganic) (see Figure 8 (B)). Cations that can be incorporated into the brucite-like layers are:  $M^{2+} = Ca^{2+}, Mg^{2+}, Zn^{2+}, Ni^{2+}, Mn^{2+}, Co^{2+}$  or  $Fe^{2+}$  and  $M^{3+} = Al^{3+}, Cr^{3+}, Mn^{3+}, Fe^{3+}, Ga^{3+}, Co^{3+}, Ni^{3+}$ , etc [27]. Tetravalent anions based LDH was also reported ( $Zr^{4+}, Ti^{4+}, Sn^{4+}$ ) [28-30]. The molar ratio of trivalent cations ( $x = M^{3+}/(M^{2+} + M^{3+})$ ) determines the charge density, and thus the number of potential sites occupied by the compensating anions. Although, some authors claim that the x value could be situated in the range of 0.1 - 0.5, the limit of composition generally admitted is 0.2 – 0.33 [31].

#### 4.1.2. Interlamellar anions

The compensating interlayer anions are part of complex network of hydrogen bonding between the hydroxyl groups of the layer and the water molecules. They also dictate the interlamellar spacing. The water molecules, situated in the interlayer are not fixed in one position but rotate freely and move around the hydroxide oxygen sites [32].

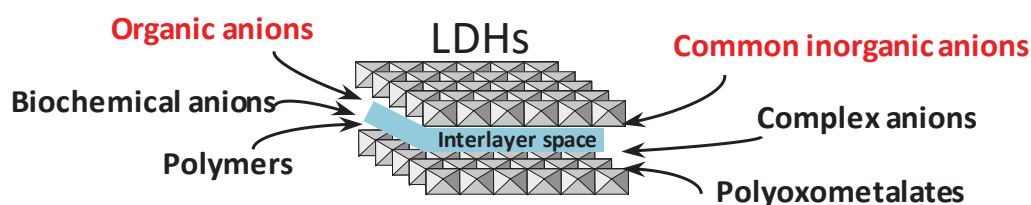


Figure 9. Different kinds of anions, which could be intercalated in the LDHs.

The most important feature of the LDHs material is the nature of the interlamellar anions. There are no limitations, as long as the anions have sufficient charge density (around  $3.0 \text{ e/nm}^2$ ) [31] and are stable in the operating conditions. Figure 9 presents the possible species that can be accommodated in the interlayer of the LDHs structure. The intercalation of organic anions

(carboxylates, alkylsulfates, alkanesulfonates, dyes, etc.), common inorganic anions (halides, oxoanions), biochemical anions (amino acids, DNA, etc), polymeric anions (poly(vinylsulfonate), polyanilin, etc.), complex anions ( $\text{CoCl}_4^{2-}$ ,  $\text{Fe}(\text{CN})_6^{4-}$ ,  $\text{Mo}(\text{CN})_8^{4-}$ , etc.), iso- and heteropolyoxometalates ( $\text{Mo}_4\text{O}_{24}^{6-}$ ,  $\text{W}_7\text{O}_{24}^{6-}$ , etc.) are often reported in the literature [31]. The intercalation of these different anions can potentially modify the interlayer distance i.e. causing an expansion or a reduction of the separation between the two layers, depending on the nature of the species involved. This variety of cations in the layers and of anions in the interlayer offers to LDHs numerous different potential structure, reactivity, etc.

#### 4.1.3. Anion intercalation into the layers

Compositional diversity in the layers and in the interlayer anions of LDH leads to the formation of divers compounds that allowed such material to be used for a variety of material science applications. The main examples are presented in Figure 10 [33].

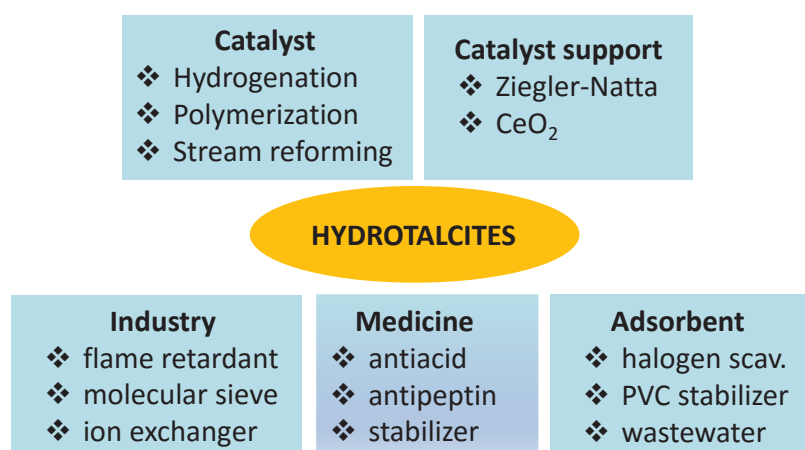


Figure 10. Schema of the possible applications of LDHs [33].

One of the most interesting applications of LDHs is their use as adsorbent or ion exchanger, as these two mechanisms can take place. Moreover, the main advantage of the LDHs compounds over traditional cationic clays is their higher AEC values. For example, the CEC values for cationic clays, like montmorillonites and bentonite are 0.7 and 1.2 meq/g, respectively [34]. While for LDHs the AEC value can reach 4.2 meq/g [35]. Different methods exist to incorporate the anion into the layer:

- ✓ by *co-precipitation method* of LDH structure;
- ✓ by *ion exchange*, usually performed onto pristine LDHs without any previous treatments;
- ✓ by “*reconstruction*” method, which requires the heat treatment of LDHs.

***Co-precipitation method*** is one of the most common ways for the preparation of LDHs solid. It suggests the simultaneous precipitation of cations at a fixed ratio, determined by the initial salt solutions. This method consists of continuous addition of a solution of anions and a basic solution under vigorous stirring, with the relative rates of addition regulated so that the overall pH is maintain constant [31]. The use of different salts can vary the metal cations in the layers, as well as the compensating anions. However, if the preparation is performed at very high pH values, the interlamellar anion can be hydroxyl anion, coming from the alkaline solution, as well as carbonate species, coming from atmospheric CO<sub>2</sub>. That is why LDHs prepared by co-precipitation method could often contain the carbonates contamination if no care was taken.

Many other various methods have been developed for LDHs compounds: hydrothermal synthesis, salt-oxide method, sol-gel process, etc [36-38]. However, they are rarely used and only in the special cases.

***Ion exchange method*** is based on exchange properties of LDHs. In order to use LDH materials as anion-exchanger, the affinity of the intercalated anions of the pristine phases must be lower than the affinity of the anion in the solution to be treated. Miyata [39] gave a comparative list of the ion selectivity for monovalent anions: OH<sup>-</sup> > F<sup>-</sup> > Cl<sup>-</sup> > Br<sup>-</sup> > NO<sub>3</sub><sup>-</sup> > I<sup>-</sup>. The affinity for divalent anions is also presented: CO<sub>3</sub><sup>2-</sup> > CrO<sub>4</sub><sup>2-</sup> > SO<sub>4</sub><sup>2-</sup>. They demonstrated that the monovalent anions have lower affinity for the LDHs than divalent ones. Hence, LDHs containing nitrates and chloride anions in the interlayer are preferred as starting materials for exchange processes.

***Reconstruction method*** is based on the unique property of the LDHs structure, named “memory effect” [40, 41]. After calcination of the solid (around 500°C), the reconstruction of the parent structure can spontaneously occur within the solution, incorporating any anions that are present in the solution where the reconstruction is performed. The anion intercalation using this method should be held in an inert N<sub>2</sub> atmosphere, to prevent the intercalation of the carbonate species.

It should be mentioned that the anion intercalation can be influenced by different factors: the charge, nature, size and orientation of the anion (important in the case of large molecule intercalation), as well as the interactions between the negatively charged guest and the positively charged layer (affinity of the anions onto LDHs).

#### 4.2. Synthetic organic ion exchanger

The synthetic organic resin is one of the most common ion exchangers. They exist in powder (5-150  $\mu\text{m}$ ) or bed (0.5-2 mm diameter) form [42]. The introduction of synthetic organic ion exchange resins in 1935 [43] resulted from the synthesis of phenolic condensation products, containing either sulfonic or amine groups, which could be used for the reversible exchange of cations or anions. Later, a variety of different functional groups has been added as well as polymer serving as a base of the resin structure. Conventional ion exchange resin consists of a cross-linked polymer matrix with a relatively uniform distribution of fixed ions (ion-active sites) throughout the structure. To preserve the neutrality of the resins, each ion contains a counter-ion, which is mobile and can be exchanged by other positively or negatively charged species (depending on the ionic nature of the resins). Figure 11 shows a schematic representation of two structures, i.e. a cationic and anionic resin.

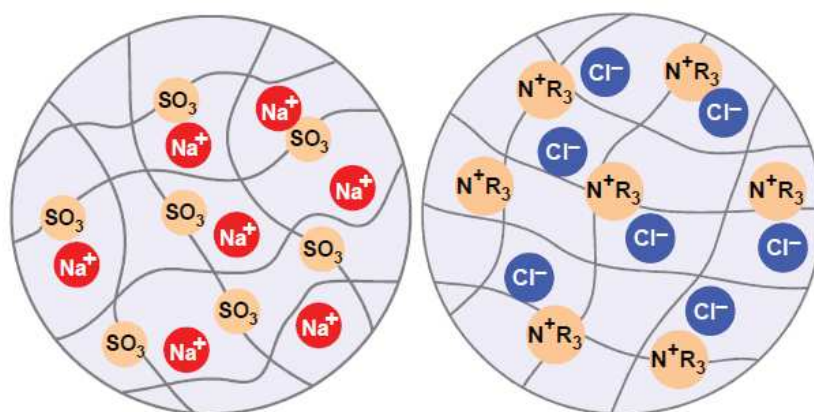


Figure 11. Cation (left) and anion (right) exchange resins, with schematic representation of negatively charged matrix and positively charged functional groups [44].

The widely used form of ion exchange resins is based on the copolymer of styrene and divinylbenzene. The degree of cross-linking is adjusted by varying the divinylbenzene content and

is expressed as the percentage of divinylbenzene in the matrix (for example, 5% cross-linking means 5 mol % divinylbenzene in the matrix) [42]. If the divinylbenzene content in the resins is low, they are soft, gelatinous and swell strongly in solvents. Fixed ionic groups are introduced into resin matrices to enable the ion exchange process. In the case of cation exchange resins, it can be sulphonate ( $-\text{SO}_3^-$ ) groups, with the mobile counter ions  $-\text{H}^+$  or  $\text{Na}^+$ . The anion exchangers can be produced by creating  $-\text{NH}_3^+$  or  $-\text{N}_2^+$  functional groups on the matrix with  $\text{OH}^-$ ,  $\text{Cl}^-$  or other anions as the counter-ions. Figure 12 shows two types of anionic resins, containing the styrene divinylbenzene copolymer matrix with trimethylammonium functional groups attached.

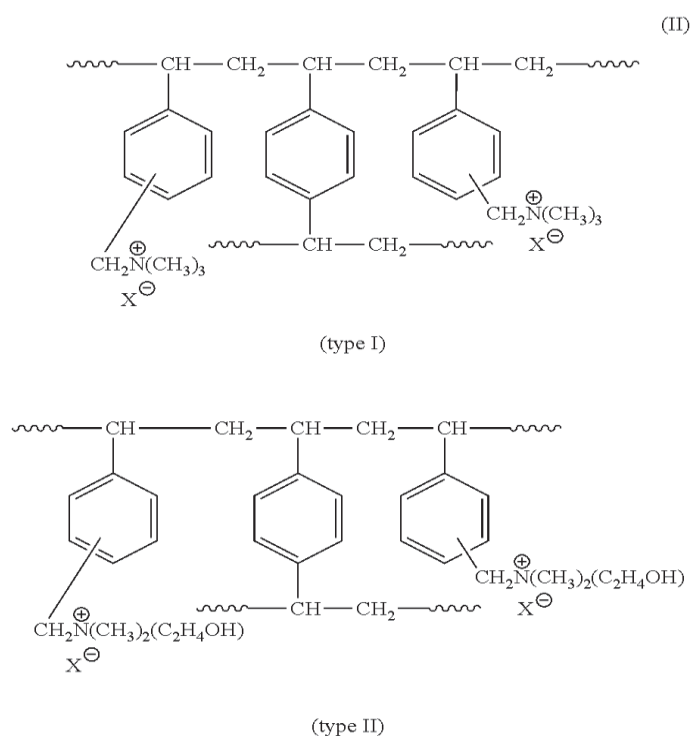
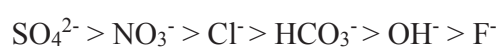


Figure 12. Structure of the anionic resin, which contains styrene divinylbenzene copolymer matrix with trimethylammonium functional groups.

Thanks to the difference of affinity for the different ions, the ion exchange resins can be used to remove selectively ions from water. Thus, the company Rohm & Haas [44] reports, that sulphates and nitrates have more affinity for anionic resins:



The trend of affinity onto cationic resins was also established:



Kim et al. reviewed that synthetic resins could be also used to remove the different kind of organic substances from water [45]. The adsorption of such organic contaminants like: phenols [46, 47], alkylbenzene sulphonate [48] as well as carboxylic acids were investigated. Dye adsorption onto resin was also studied and reported in the literature [49-53]. From this, it can be concluded that the same resins are able to remove different anions available in solution. They can be considered as good potential adsorbent for multi-component adsorption.

Moreover, the main advantages of the synthetic organic ion exchange resins are their high capacity, wide versatility and low cost relative compared to some synthetic inorganic media. There are many types of anionic resins, which are commercially available nowadays. Amberlite® IRN-78 is an example of such type of resins. It is usually supplied in the hydroxide form, and will be the solid-reference used in this work.

### ***5. Literature review on competitive adsorption***

The wastewater systems are a complex multi-compositional system [54]. Table 2 shows an example of the main physico-chemical characterization of textile mills effluence as well as the analysis of mills on heavy metal concentrations [55]. Some authors in addition report the salts composition of industrials wastewaters [56]. However, the main conclusion is the same: a real aqueous system usually contain numerous different species, which can interact and compete between each other on adsorption sites of the solid. Therefore, talking about competitive adsorption, solid-adsorbate interactions can be highly influenced by the presence of other species in the complex solute or by the adsorbate-adsorbate interactions. Therefore, it is very important to understand the nature of these interactions, which can change the result of the pollutants uptake from multi-component systems.

Table 2. Physico-chemical characterization and heavy metals concentrations in textile mills effluents [57].

Parameters	NEQS	Mill-1	Mill-2	Mill-3	Mill-4	Mill-5	Mill-6	Mill-7
pH Value	6 - 9	7.5	8.6	9.5	10.4	11.5	10.6	11.3
Temperature	Upto 40° C	36	36.6	39.7	38.3	49.2	45.0	42.5
TSS	Upto 200 mg/l	934	1875	1619	1236	954	1159	1050
TDS	Upto 3500 mg/l	2469	5408	6481	4868	7295	4025	3687
EC	400 mS/cm	295.3	282.4	175.7	196.3	345.0	320.1	256.5
BOD	Upto 80 mg/l	125.55	185.35	653.75	156.50	312.61	262.54	220.30
COD	Upto 150 mg/l	115.66	612.16	431.61	251.25	705.25	342.21	342.24
Metals	NEQS	Mill-1	Mill-2	Mill-3	Mill-4	Mill-5	Mill-6	Mill-7
Cd	0.1 mg/l	0.001	0.001	N.D	0.05	0.18	0.08	0.15
Cr	1.0 mg/l	1.53	1.86	1.66	1.20	1.05	1.12	1.32
Cu	1.0 mg/l	0.07	1.37	5.14	2.66	4.51	3.33	1.96
Fe	2.0 mg/l	1.08	1.16	1.86	2.00	2.61	1.88	3.11
Ni	1.0 mg/l	0.75	0.96	1.00	0.66	1.21	0.82	1.53
Mn	1.5 mg/l	1.31	1.10	0.95	0.88	1.85	1.16	1.65
Zn	5.0 mg/l	2.36	3.21	4.65	4.55	6.03	4.95	5.85

NEQS- National Environmental Quality Standards; TSS- Total Suspended Solids; TDS- Total Dissolved Solid; Mill № - samples collected from different textile factories.

Generally, different factors can influence sorption of the adsorbates onto solid surface. At first, it depends on the solid properties: specific surface area, porosity (macro-, micro- or mesoporosity), nature of the solid (functional groups) as well as the charge of the surface (PZC, IEP), etc. The second parameter that influences the sorption is the adsorbate properties, such as polarity, chemical structure, molecular size and charge of the adsorbate species, etc. However, the main factor governing the species uptake is the nature of the interaction between the solid and the adsorbate. Such parameter as pH of the working solution is another important factor influencing adsorption properties. Firstly, because the charge of the adsorbent's surface can be dependent of pH (ex: natural or synthetic oxides). Thus, adsorption of the positively charged species can be higher at high pH, where charge of the adsorbent surface is more negative (depending on the PZC). Secondly, information about pKa of adsorbed species, diagrams of speciation and pH measured in the beginning of adsorption process as well as at equilibrium can give us valuable data about the charge of potential adsorbates. Therefore, this parameter should be always taken into account during the study of adsorption processes.

Studies on multi-component adsorption from gaseous and liquid media hold a great importance since the separating properties of adsorbents affect the pollutant removal in different industrial processes [58]. Many studies, reviews [6, 11, 50, 54, 55, 59-111] and dissertations [112-114] have been devoted to this topic. In multi-component adsorption process two competing species can react with each other in three different ways, they can cooperate, compete or do not interact between them. In the first case, the sum of the two adsorbed species will be higher than in the individual system, in the second one, the competition will decrease the sum of the adsorbed species. Finally, the third possibility describes the independent adsorption between the species, where the mixture has no effect on the adsorption of each sorbate from the mixture.

From the sorption points of view, during adsorption from multi-component systems, the interactions can be formed between different species. They can be divided in three main groups: Organic – Organic; Inorganic – Inorganic and Organic - Inorganic interactions (Figure 13).

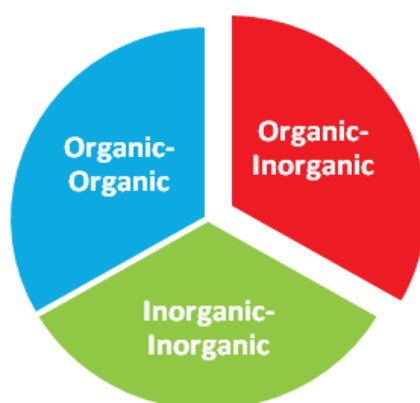


Figure 13. Schema of different competing species presented in solutes.

### **5.1. *Competitive adsorption between organic species.***

In order to investigate multi-component adsorption between organic species, authors often use a variety of dyes to mimic the effluents that are released in rivers and oceans by mainly the textiles industries [54]. The first investigation of competitive adsorption between organic compounds were performed onto activated carbon [65-70, 113]. At first, the authors mainly

focused their studies on the use of empirical models to simulate aqueous multi-solute adsorption equilibria [65-67]. Noroozi et al. summarized all the theories applied for the adsorption of multi-component systems for dyes (among them widespread Langmuir, Redlich–Peterson, and Freundlich models, as well as Ideal adsorbed solution theory (IAST) [62]). However, today more and more authors investigate the experimental study of adsorption from multi-dye solution.

Multi-component adsorption of a range of dyes has been investigated on various adsorbents such as: peat [71], bentonite [63, 72, 73], chitosan [115], melon husk [74], fly ash [75] and LDHs [76]. On the other hand, the use of different binary and ternary dye systems like: Remazol reactive Yellow, Black and Red [70]; Astrazon Blue BG, Yellow 7 GL and Maxilon Red BL-N [71]; Basic Yellow 28 and Red 46 [63]; Acid Scarlet GR, Acid Turquoise Blue 2G and Indigo Carmine [72]; Methylene blue, Congo Red and Methyl Orange [74]; as well as Basic Blue BG, Red, Violet and Yellow [73] allowed to analyze dyes behavior in competitive conditions. Moreover, research groups work with dyes of different classes [75, 115]. For example, they investigate the competition between an acid (metanil yellow) and reactive (reactive blue 15) dyes on cross-linked chitosan. They showed that for an equimolar dye concentrations adsorption is favored for the reactive dye [115]. Nevertheless, when the acid dye concentration is increased, the opposite trend is observed. They explained this phenomenon by measuring the kinetic behavior of each dye in single and multi-component systems and they concluded that the initial adsorption rate of the acid dye onto chitosan is faster. Hence, the time to reach the adsorption equilibrium for the acid dye is shorter than for the reactive dye. Another study investigated the competitive adsorption of dispersive and anionic dyes (see classification of the dyes in section 3.2.) on fly ash (FA). They showed that the anionic dye adsorbed preferentially on FA can compared to than dispersive dye [75]. In addition, they demonstrate that the adsorption rate of dispersive dye was affected apparently by the existence of the anionic compounds during the competitive adsorption, while the rate of anionic dyes was almost unaffected at all.

Based on the above studies and considering the empirical models (mentioned earlier) the following conclusions can be drawn from these studies:

- The adsorption rate of one dye is reduced in the presence of other competing dyes in solution. Thus, the presence of competing dyes has an influence on the desired dye uptake [71].

- The competitive adsorption between dyes in solution depends on the dye properties (structure and functional group) and the interactions between each other [75].
- The dye properties like molecular weight and size also have an influence on the competitive adsorption.
- The nature of the adsorbent - dye interactions are predominant on the molecular weight of the dye. Thus, large chemisorbed molecules will be adsorbed faster than small physisorbed dyes [62].

## 5.2. *Competitive adsorption between inorganic species.*

To study the inorganic-inorganic interactions in adsorption process, several authors preferred to deal with heavy metal ions (Cd(II), Hg(II), Pb(II), Zn(II), Ni(II), Cu(II)) [77-86] or toxic oxyanions ( $\text{AsO}_4^{3+}$ ,  $\text{CrO}_4^{2-}$ ,  $\text{VO}_4^{3-}$ ,  $\text{MoO}_4^{2-}$ ,  $\text{BrO}_3^-$ ) [87-90], because of the abundant presence of these species in wastewaters. However, the competitive adsorption of radioisotopes: Sr(II), Cs(I) and Co(II) was also investigated [91]. Some common anions like nitrates, phosphates or fluorides are present in nature with higher concentration than the standards allowed. Hence, it is important to remove this species in water according to the treatment policy of wastewater [92-94, 116, 117]. The investigation of adsorption of these common anions was also studied using the competitive adsorption process. But there is no limit for the competition between inorganic substances and scientists begin to study the influence of common anions on heavy metal together with oxyanions [89, 95-98].

Oxy- and common anions can compete with each other for the same adsorptive sites onto ferrihydrite or LDHs solids [87, 89] with the preference for oxyanion adsorption onto ferrihydrite [87]. The authors explained this behavior with the presence of some surface sites that exhibited much higher affinity for oxyanions than for common ones. Another study on competition between phosphate, arsenate and molybdate shows that the presence of phosphate reduces As(V) uptake onto oxide minerals. However, molybdate partly decreases the As(V) removal below pH 6 [88]. Therefore, Mohan concluded in his review on As(V) removal that the interpretation of multi-component systems is complex and depends on different factors such as oxyanions ionic radii, electronegativity, pH and availability of the active sites [99]. Other example of the decrease in

species uptake from competitive system was described by Mien et al. [100]. In multi-component sorption between Pb(II), Cd(II) cations and Cr(VI) anions onto clinoptilolite, which is natural zeolite, the presence of Cr(VI) diminishes the cations removal efficiencies because of the ionic complex formation between Cr(VI) anions and the two other cations.

According to Ghorbel-Abid, the removal of Cr(III) was strongly influenced by the presence of Cd(II) into smectic clays. The Cr uptake was increased to 70 % while the Cd uptake decreased to 67 % in comparison with simple systems of Cr and Cd [77]. This is a good example of cooperative adsorption of Cr(III) species onto clays. The work on competitive adsorption between halide ions ( $\text{BF}_4^-$ ,  $\text{ClO}_4^-$ ,  $\text{BrO}_3^-$ ,  $\text{IO}_3^-$ ) and common anions shows low affinity of LDHs for oxyanions of halogen in comparison with common anions. It is concluded that anionic clays prefer anions with multiple charges instead of monocharged species [98]. However, opposite results could be found on activated carbon, where sulfates discharged species cannot compete with monocharged nitrates and perchlorates [101]. Because of the stronger affinity of nitrate and perchlorate toward the activated carbon surface, than those of sulfate.

### **5.3. Competitive adsorption between organic and inorganic species.**

Complex organic - organic and inorganic - inorganic interactions can change the results of removal of desired pollutant. However, organic-inorganic interactions could induce new competitive mechanisms and they may change our vision about adsorption from multi-component system. Several works present different complex organic-inorganic systems combined with solid adsorbents.

The bi-solute systems: phenol or humic acid with Cd(II) or Cr(VI) onto activated carbon was reported by Jiang et al [102]. The uptake of organic species is hardly affected by the presence of metals, while organic molecules negatively influence the sorption of heavy metals. However, it was concluded that organic species were physisorbed onto carbon while inorganic species are chemisorbed. Another work on activated carbon cloth describes the relation between organic and inorganic substances as dependent of the pH of the media. Hence, the deprotonated form of benzoic acid can form ligands with Cu(II) and Pb(II) cations and increase the total amount adsorbed of these inorganic species [103]. Abdel-Ghani et al. worked with multiwalled carbon nanotubes and performed multi-component adsorption between phenol and Ni(II) ions. They reported that the

competitive adsorption results with a decrease of species uptake of up to 70% and 60%, respectively for organic and inorganic substances [55]. It was also mentioned that two species compete for the same adsorptive sites. Mier et al. [100] also worked on similar organic-inorganic system: phenol with Pb(II) and Cd(II) ions but on clinoptilolite. The authors concluded that the formed organic-inorganic complexes were too bulky to enter in the sorbent pores. Thus, the heavy metals uptake was hindered by the presence of organic matter.

Another study was performed on the same zeolite by Wang and co-workers [104]. Wang and Ariyano worked on multi-component sorption between malachite green and Pb(II) onto clinoptilolite. They concluded that the inorganic ions have higher affinity for zeolite than organic ions in the binary systems. In spite of the presence of competing species, the total amount adsorbed (sum of two species) is higher than that of malachite green and Pb(II) amount adsorbed in individual system. The same conclusion concerning the competition of another organic dyes and inorganic ions onto zeolitic structures was reached by Hernandez-Montoya et al. [105]. However, it was demonstrated that using two zeolites with different textural properties, the opposite outcome is found. Therefore a zeolite having an acidic nature and a high specific surface area prefers the adsorption of organic species from binary solutions, whereas a zeolite with low specific surface prefers inorganic compounds [105].

Other interesting works based on competition were also investigated onto montmorillonite-based adsorbents [106, 107]. Margulies et al. reported competitive adsorption of Thioflavin (TFT) and Cs. They concluded that Cs did not change the uptake of TFT and could not compete with organic species during sorption on clays [106]. In the case of competitive adsorption between Pb(II), Cd(II) with Methyl Orange (MO) onto composites of lignocellulose - montmorillonite, sorption was found to be synergic. MO uptake was greater in the presence of metals. A different range of dye:metal concentrations were tested and it was found that the amount of MO adsorbed increased with the metal ion concentration in solution. Indeed, adsorbed heavy metals can act like adsorption sites for MO adsorption, through electrostatic interactions [107]. Other example of synergic co-adsorption was found for the adsorption between Methylene Blue (MB) and Cu(II) onto fly ash [108]. Here, the mechanism of sorption of the organic-inorganic complex plays a major role. It could be divided into two steps. MB has the highest affinity to sorbent, therefore dye is firstly adsorbed on the substrate and then copper is adsorbed on this new layer with good efficiency.

Co-adsorption of dyes and common anions was also investigated onto anion exchange resins, MgAl - mixed metal oxides with magnetic iron oxide, and LDHs [50, 109, 111]. These results showed that competing anions strongly affect the dye adsorption process. Moreover, carbonates and phosphates have the highest influence on dye uptake, because of the high affinity of these anions onto LDHs layers.

All these works invite us to draw the following conclusions about synergy, competition and no-interactions for adsorption in multi-component system:

- The synergic organic-inorganic interaction can be judiciously used for treating wastewaters. Indeed, in most cases, the addition of inorganic or organic species can greatly improve the adsorbed quantities of the target species. However, the synergic behavior between organic and inorganic substances can be negative as there is also a possibility for undesired species to be adsorbed during the sorption process. This illustrates well the importance of knowing the synergic mechanisms.

- The competitive adsorption can also be positively useful and efficient. If one wants to adsorb one species (A) and not another (B), both present in solution, a third species (C) can be added to compete with the undesirable one (B). A good example to explain such system was described by Ali et al [110]. They studied competitive sorption of organic acids (phthalic and chelidamic) with sulfate onto goethite. As a result, sulfate can effectively compete with organic acids for surface sites of goethite. Therefore, sulfate ion can significantly influence the sorption of organic acids in natural aquatic system. It was also claimed that the humic substances influence the sorption of trace of metal ions. Therefore, sulfate could influence the metal ion uptake by reducing the adsorption of humic compounds. The negative point of such interactions is that in some cases the presence of organic/inorganic ions can completely inhibit or suppress the sorption of the desirable species.

- No-interaction or independent adsorption also occurs between organic-inorganic species [106]. In reality, only few systems present this type of interactions.

Most literature review based on multi-component sorption deal mainly with the investigation of quantity adsorbed of only one species in this type of system. However, it is very important to measure the equilibrium concentration of all possible compound that is susceptible to be adsorbed in such complex system. Complementary information about quantitative co-

adsorption of competing ions can give valuable information about the real adsorption capacity and selectivity of the adsorbent (sum of two or more species absorbed).

Thermodynamic contributions of the mono-component and multi-component adsorption should be compared to obtain a better understanding of the nature of interactions during adsorption process. Thus, isothermal titration calorimetry could be a powerful tool for the measurement of heat changes involved in the mono and multi-component system during the adsorption process.

### References

1. Inglezakis, V. and S. Pouloupoulos, *Adsorption, ion exchange and catalysis: design of operations and environmental applications*. Vol. 3. 2006: Elsevier. pp. 602.
2. Kolasinski, K.K. and K.W. Kolasinski, *Surface science: foundations of catalysis and nanoscience*. 2012: John Wiley & Sons. pp. 574.
3. Lennard-Jones, J., *Processes of adsorption and diffusion on solid surfaces*. Transactions of the Faraday Society, 1932. **28**: p. 333-359.
4. Von Helmholtz, H., *Studien über electrische Grenzschichten*. Annalen der Physik, 1879. **7**: p. 337-382.
5. Kolb, D.M., *An atomistic view of electrochemistry*. Surface Science, 2002. **500**(1-3): p. 722-740.
6. Chin, P., C. O'Melia, and J. Morgan, *Aquatic Chemistry-Interfacial and Interspecies Processes*. Colloids and Surfaces A: Physicochemical and Engineering Aspects, 1996. **3**(110): p. 293-294.
7. Helfferich, F.G., *Ion exchange*. 1962, New York: McGraw-Hill. pp. 624.
8. Noble, R.D. and P.A. Terry, *Principles of chemical separations with environmental applications*. 2004: Cambridge University Press. pp. 336.
9. Kumar, S. and S. Jain, *History, Introduction, and Kinetics of Ion Exchange Materials*. Journal of Chemistry, 2013. **2013**: p. 1-13.
10. Helfferich, F. and M.S. Plesset, *Ion exchange kinetics. A nonlinear diffusion problem*. The Journal of Chemical Physics, 1958. **28**(3): p. 418-424.
11. Adamson, A.W. and A.P. Gast, *Physical chemistry of surfaces*. 1967, New York: Wiley-Interscience. pp. 808.
12. Giles, C.H., et al., *786. Studies in adsorption. Part XI. A system of classification of solution adsorption isotherms, and its use in diagnosis of adsorption mechanisms and in measurement of specific surface areas of solids*. Journal of the Chemical Society, 1960: p. 3973-3993.

13. IARC *General Introduction to the Chemistry of Dyes*. IARC monographs on the evaluation of carcinogenic risks to humans 2010. **99**, 55-67.
14. Mansour, H.B., *Colorants textiles: Biodégradation & Toxicité* 2012: Editions universitaires européennes.
15. de Campos Ventura-Camargo, B. and M.A. Marin-Morales, *Azo dyes: characterization and toxicity—a review*. Textiles and Light Industrial Science and Technology, 2013. **2**(2): p. 85-103.
16. Hedayatullah, M., *Les colorants synthétiques*. Vol. 15. 1976: Presses universitaires de France.
17. Waring, D.R. and G. Hallas, *The chemistry and application of dyes*. 2013: Springer Science & Business Media.
18. Carmen, Z. and S. Daniela. *Textile organic dyes—characteristics, polluting effects and separation/elimination procedures from industrial effluents—a critical overview*. in *Organic Pollutants Ten Years After the Stockholm Convention-Environmental and Analytical Update*. 2012. InTech: Croatia.
19. Barnes, A.J., et al., *The resonance Raman spectra of Orange II and Para Red: molecular structure and vibrational assignment*. Spectrochimica Acta Part A: Molecular Spectroscopy, 1985. **41**(4): p. 629-635.
20. Martin, Y.C., *Let's not forget tautomers*. Journal of Computer-Aided Molecular Design, 2009. **23**(10): p. 693-704.
21. Burkinshaw, S.M. and A. Gotsopoulos, *The pre-treatment of cotton to enhance its dyeability — Sulphur dyes*. Dyes and Pigments, 1996. **32**(4): p. 209-228.
22. Shore, J., *Advances in direct dyes*. Indian Journal of Fibre and Textile Research, 1996. **21**: p. 1-29.
23. Feitknecht, W. and G. Fischer, *Zur Chemie und Morphologie der basischen Salze zweiwertiger Metalle. II. Über basische Kobaltsulfate. (IX. Mitteilung über basische Salze)*. Helvetica Chimica Acta, 1935. **18**(1): p. 40-60.
24. Blasco, T., et al., *Influence of the acid-base character of supported vanadium catalysts on their catalytic properties for the oxidative dehydrogenation of n-butane*. Journal of Catalysis, 1995. **157**(2): p. 271-282.
25. Duan, X. and D.G. Evans, *Layered double hydroxides*. Vol. 119. 2006, Berlin - Heidelberg: Springer Science & Business Media. pp. 234.
26. Costa, F.R., *Mg-Al Layered Double Hydroxide: A Potential Nanofiller and Flame-Retardant for Polyethylene*. 2007, Technischen Universität Dresden: Dresden.
27. Khan, A.I. and D. O'Hare, *Intercalation chemistry of layered double hydroxides: recent developments and applications*. Journal of Materials Chemistry, 2002. **12**(11): p. 3191-3198.
28. Chitrakar, R., et al., *Synthesis and phosphate uptake behavior of Zr<sup>4+</sup> incorporated MgAl-layered double hydroxides*. Journal of Colloid and Interface Science, 2007. **313**(1): p. 53-63.

29. Das, N., et al., *Adsorption of Cr (VI) and Se (IV) from their aqueous solutions onto Zr<sup>4+</sup>-substituted ZnAl/MgAl-layered double hydroxides: effect of Zr<sup>4+</sup> substitution in the layer*. Journal of Colloid and Interface Science, 2004. **270**(1): p. 1-8.
30. Shen, Y., et al., *Simultaneous incorporation of palladium and zirconium ions in Mg–Al layered double hydroxides by co-precipitation*. Applied Clay Science, 2011. **54**(2): p. 179-183.
31. Auerbach, S.M., K.A. Carrado, and P.K. Dutta, *Handbook of layered materials*. 2004, New York: Marcel Dekker. pp. 650.
32. Kagunya, W., P.K. Dutta, and Z. Lei, *Dynamics of water in hydrotalcite*. Physica B: Condensed Matter, 1997. **234–236**(0): p. 910-913.
33. Cavani, F., F. Trifirò, and A. Vaccari, *Hydrotalcite-type anionic clays: preparation, properties and applications*. Catalysis Today, 1991. **11**(2): p. 173-301.
34. Kahr, G. and F.T. Madsen, *Determination of the cation exchange capacity and the surface area of bentonite, illite and kaolinite by methylene blue adsorption*. Applied Clay Science, 1995. **9**(5): p. 327-336.
35. Rives, V., *Layered double hydroxides: present and future*. 2001, New York: Nova Publishers. 439.
36. Xu, Z.P. and G.Q. Lu, *Hydrothermal synthesis of layered double hydroxides (LDHs) from mixed MgO and Al<sub>2</sub>O<sub>3</sub>: LDH formation mechanism*. Chemistry of Materials, 2005. **17**(5): p. 1055-1062.
37. Prinetto, F., et al., *Synthesis and characterization of sol–gel Mg/Al and Ni/Al layered double hydroxides and comparison with co-precipitated samples*. Microporous and Mesoporous Materials, 2000. **39**(1): p. 229-247.
38. Boehm, H.P., J. Steinle, and C. Vieweger, *[Zn<sub>2</sub>Cr (OH)<sub>6</sub>]<sub>x</sub> · 2H<sub>2</sub>O, New layer compounds capable of anion exchange and intracrystalline swelling*. Angewandte Chemie International Edition in English, 1977. **16**(4): p. 265-266.
39. Miyata, S., *Anion-exchange properties of hydrotalcite-like compounds*. Clays Clay Miner, 1983. **31**(4): p. 305-311.
40. Miyata, S., *Physico-chemical properties of synthetic hydrotalcites in relation to composition*. Clays Clay Miner, 1980. **28**(1): p. 50-56.
41. Sato, T., et al., *Preparation and chemical properties of magnesium aluminium oxide solid solutions*. Reactivity of Solids, 1986. **2**(3): p. 253-260.
42. IAEA, *Application of ion exchange processes for the treatment of radioactive waste and management of spent ion exchangers*. 2002, International Atomic Energy Agency. p. 115.
43. Adams, B.A. and E.L. Holmes, *Absorptive properties of synthetic resins*. Journal of Indian Chemical Society 1935. **54** (2): p. 1-6.
44. Rohm and Haas, *Ion exchange for dummies*. 2008: Lenntech.
45. Kim, B.R., V.L. Snoeyink, and F.M. Saunders, *Adsorption of organic compounds by synthetic resins*. Journal (Water Pollution Control Federation), 1976: p. 120-133.

46. Anderson, R. and R. Hansen, *Phenol sorption on ion exchange resins*. Industrial & Engineering Chemistry, 1955. **47**(1): p. 71-75.
47. Chasanov, M., R. Kunin, and F. McGarvey, *Sorption of phenols by anion exchange resins*. Industrial & Engineering Chemistry, 1956. **48**(2): p. 305-309.
48. Abrams, I.M. and S.M. Lewon, *Removal of ABS from water by chloride cycle anion exchange*. Journal - American Water Works Association 1962: p. 537-543.
49. Liu, C.-H., et al., *Removal of anionic reactive dyes from water using anion exchange membranes as adsorbers*. Water Research, 2007. **41**(7): p. 1491-1500.
50. Karcher, S., A. Kornmüller, and M. Jekel, *Anion exchange resins for removal of reactive dyes from textile wastewaters*. Water Research, 2002. **36**(19): p. 4717-4724.
51. Suteu, D., D. Bilba, and S. Coseri, *Macroporous polymeric ion exchangers as adsorbents for the removal of cationic dye basic blue 9 from aqueous solutions*. Journal of Applied Polymer Science, 2014. **131**(1): p. 39620.
52. Kaušpėdienė, D., et al., *Removal of the phthalocyanine dye from acidic solutions using resins with the polystyrene divinylbenzene matrix*. Chemija, 2013. **24**(3): p. 171-181.
53. Dulman, V., et al., *Adsorption of anionic textile dye Acid Green 9 from aqueous solution onto weak or strong base anion exchangers*. Journal of Applied Polymer Science, 2009. **113**(1): p. 615-627.
54. Park, J. and J. Shore, *Water for the dyehouse: supply, consumption, recovery and disposal*. Journal of the Society of Dyers and Colourists, 1984. **100**(12): p. 383-399.
55. Abdel-Ghani, N.T., G.A. El-Chaghaby, and F.S. Helal, *Individual and competitive adsorption of phenol and nickel onto multiwalled carbon nanotubes*. Journal of Advanced Research, 2015. **6**(3): p. 405-415.
56. Nergis, Y., et al., *Quality characterization and magnitude of pollution implication in textile mills effluents*. Journal of Quality and Technology Management, 2009. **5**(11): p. 27-40.
57. Imtiazuddin, S., M. Mumtaz, and K.A. Mallick, *Pollutants of wastewater characteristics in textile industries*. Journal of Basic & Applied Sciences, 2012. **8**: p. 554-556.
58. Gun'ko, V.M., *Competitive adsorption*. Theoretical and Experimental Chemistry, 2007. **43**(3): p. 139-183.
59. Toth, J., *Adsorption Theory, Modeling and Analysis*. 2002, New York: Marcel Dekker, Inc. . pp. 878.
60. Do, D.D., *Adsorption analysis: equilibria and kinetics*. Vol. 2. 1998, London: Imperial College Press. pp. 916.
61. Murali, V. and L. Aylmore, *Competitive adsorption during solute transport in soils: 3. A review of experimental evidence of competitive adsorption and an evaluation of simple competition models*. Soil Science, 1983. **136**(5): p. 279-290.
62. Noroozi, B. and G.A. Sorial, *Applicable models for multi-component adsorption of dyes: A review*. Journal of Environmental Sciences, 2013. **25**(3): p. 419-429.

63. Turabik, M., *Adsorption of basic dyes from single and binary component systems onto bentonite: Simultaneous analysis of Basic Red 46 and Basic Yellow 28 by first order derivative spectrophotometric analysis method*. Journal of Hazardous Materials, 2008. **158**(1): p. 52-64.
64. Lipatov, Y.S., et al., *Adsorption of polymers from concentrated solutions*. Advances in Colloid and Interface Science, 1976. **6**(1): p. 1-91.
65. Jain, J.S. and V.L. Snoeyink, *Adsorption from bisolute systems on active carbon*. Journal (Water Pollution Control Federation), 1973: p. 2463-2479.
66. McKay, G. and B. Al Duri, *Prediction of multicomponent adsorption equilibrium data using empirical correlations*. The Chemical Engineering Journal, 1989. **41**(1): p. 9-23.
67. Fritz, W. and E.U. Schlünder, *Competitive adsorption of two dissolved organics onto activated carbon — I: Adsorption equilibria*. Chemical Engineering Science, 1981. **36**(4): p. 731-741.
68. Jossens, L., et al., *Thermodynamics of multi-solute adsorption from dilute aqueous solutions*. Chemical Engineering Science, 1978. **33**(8): p. 1097-1106.
69. Noroozi, B., et al., *Adsorption of binary mixtures of cationic dyes*. Dyes and Pigments, 2008. **76**(3): p. 784-791.
70. Al-Degs, Y., et al., *Competitive adsorption of reactive dyes from solution: equilibrium isotherm studies in single and multisolute systems*. Chemical Engineering Journal, 2007. **128**(2): p. 163-167.
71. Allen, S.J., G. McKay, and K.Y.H. Khader, *Multi-component sorption isotherms of basic dyes onto peat*. Environmental Pollution, 1988. **52**(1): p. 39-53.
72. Shen, D., et al., *Adsorption kinetics and isotherm of anionic dyes onto organo-bentonite from single and multisolute systems*. Journal of Hazardous Materials, 2009. **172**(1): p. 99-107.
73. Turabik, M. and B. Gozmen, *Removal of Basic Textile Dyes in Single and Multi-Dye Solutions by Adsorption: Statistical Optimization and Equilibrium Isotherm Studies*. CLEAN–Soil, Air, Water, 2013. **41**(11): p. 1080-1092.
74. Olajire, A., A. Giwa, and I. Bello, *Competitive adsorption of dye species from aqueous solution onto melon husk in single and ternary dye systems*. International Journal of Environmental Science and Technology, 2015. **12**(3): p. 939-950.
75. Sun, D., et al., *Kinetic mechanism of competitive adsorption of disperse dye and anionic dye on fly ash*. International Journal of Environmental Science and Technology, 2013. **10**(4): p. 799-808.
76. Sumari, S.M., Z. Hamzah, and Y. Yasin. *Competitive adsorption of reactive dyes from binary mixture by MgAlNO<sub>3</sub>-layered double hydroxide*. in *Business, Engineering and Industrial Applications (ISBEIA), 2011 IEEE Symposium 2011*. IEEE.
77. Ghorbel-Abid, I. and M. Trabelsi-Ayadi, *Competitive adsorption of heavy metals on local landfill clay*. Arabian Journal of Chemistry, 2015. **8**(1): p. 25-31.

78. Srivastava, P., B. Singh, and M. Angove, *Competitive adsorption behavior of heavy metals on kaolinite*. Journal of Colloid and Interface Science, 2005. **290**(1): p. 28-38.
79. Igwe, J.C. and A.A. Abia, *Competitive adsorption of Zn (II), Cd (II) and Pb (II) ions from aqueous and non-aqueous solution by maize cob and husk*. African Journal of Biotechnology, 2005. **4**(10): p. 1113-1116.
80. Benjamin, M.M. and J.O. Leckie, *Competitive adsorption of Cd, Cu, Zn, and Pb on amorphous iron oxyhydroxide*. Journal of Colloid and Interface Science, 1981. **83**(2): p. 410-419.
81. Elliott, H., M. Liberati, and C. Huang, *Competitive adsorption of heavy metals by soils*. Journal of Environmental Quality, 1986. **15**(3): p. 214-219.
82. Mahamadi, C. and T. Nharingo, *Competitive adsorption of Pb<sup>2+</sup>, Cd<sup>2+</sup> and Zn<sup>2+</sup> ions onto Eichhornia crassipes in binary and ternary systems*. Bioresource Technology, 2010. **101**(3): p. 859-864.
83. Gomes, P.C., et al., *Selectivity sequence and competitive adsorption of heavy metals by Brazilian soils*. Soil Science Society of America Journal, 2001. **65**(4): p. 1115-1121.
84. Usman, A.R.A., *The relative adsorption selectivities of Pb, Cu, Zn, Cd and Ni by soils developed on shale in New Valley, Egypt*. Geoderma, 2008. **144**(1): p. 334-343.
85. Fontes, M.P.F. and P.C. Gomes, *Simultaneous competitive adsorption of heavy metals by the mineral matrix of tropical soils*. Applied Geochemistry, 2003. **18**(6): p. 795-804.
86. Seco, A., et al., *Adsorption of heavy metals from aqueous solutions onto activated carbon in single Cu and Ni systems and in binary Cu-Ni, Cu-Cd and Cu-Zn systems*. Journal of Chemical Technology and Biotechnology, 1997. **68**(1): p. 23-30.
87. Jain, A. and R.H. Loeppert, *Effect of competing anions on the adsorption of arsenate and arsenite by ferrihydrite*. Journal of Environmental Quality, 2000. **29**(5): p. 1422-1430.
88. Manning, B.A. and S. Goldberg, *Modeling competitive adsorption of arsenate with phosphate and molybdate on oxide minerals*. Soil Science Society of America Journal, 1996. **60**(1): p. 121-131.
89. Goh, K.-H. and T.-T. Lim, *Influences of co-existing species on the sorption of toxic oxyanions from aqueous solution by nanocrystalline Mg/Al layered double hydroxide*. Journal of Hazardous Materials, 2010. **180**(1-3): p. 401-408.
90. Goh, K.-H., T.-T. Lim, and Z. Dong, *Application of layered double hydroxides for removal of oxyanions: A review*. Water Research, 2008. **42**(6-7): p. 1343-1368.
91. Gutierrez, M. and H.R. Fuentes, *Modeling adsorption in multicomponent systems using a Freundlich-type isotherm*. Journal of Contaminant Hydrology, 1993. **14**(3-4): p. 247-260.
92. Violante, A. and L. Gianfreda, *Competition in adsorption between phosphate and oxalate on an aluminum hydroxide montmorillonite complex*. Soil Science Society of America Journal, 1993. **57**(5): p. 1235-1241.
93. Lv, L., et al., *Factors influencing the removal of fluoride from aqueous solution by calcined Mg-Al-CO<sub>3</sub> layered double hydroxides*. Journal of Hazardous Materials, 2006. **133**(1): p. 119-128.

94. Das, J., et al., *Adsorption of phosphate by layered double hydroxides in aqueous solutions*. Applied Clay Science, 2006. **32**(3–4): p. 252-260.
95. Hongshao, Z. and R. Stanforth, *Competitive adsorption of phosphate and arsenate on goethite*. Environmental Science & Technology, 2001. **35**(24): p. 4753-4757.
96. Violante, A., et al., *Sorption/desorption of arsenate on/from Mg–Al layered double hydroxides: Influence of phosphate*. Journal of Colloid and Interface Science, 2009. **333**(1): p. 63-70.
97. Dadwhal, M., M. Sahimi, and T.T. Tsotsis, *Adsorption isotherms of arsenic on conditioned layered double hydroxides in the presence of various competing ions*. Industrial & Engineering Chemistry Research, 2011. **50**(4): p. 2220-2226.
98. Theiss, F.L., et al., *A review of the removal of anions and oxyanions of the halogen elements from aqueous solution by layered double hydroxides*. Journal of Colloid and Interface Science, 2014. **417**(0): p. 356-368.
99. Mohan, D. and C.U. Pittman Jr, *Arsenic removal from water/wastewater using adsorbents—A critical review*. Journal of Hazardous Materials, 2007. **142**(1–2): p. 1-53.
100. Mier, M.V., et al., *Heavy metal removal with mexican clinoptilolite: multi-component ionic exchange*. Water Research, 2001. **35**(2): p. 373-378.
101. Mahmudov, R. and C.P. Huang, *Selective adsorption of oxyanions on activated carbon exemplified by Filtrasorb 400 (F400)*. Separation and Purification Technology, 2011. **77**(3): p. 294-300.
102. Jiang, Z., et al., *Competitive Adsorption of Several Organics and Heavy Metals on Activated Carbon in Water*. Influence and Removal of Organics in Drinking Water, 1992: p. 79.
103. Faur-Brasquet, C., K. Kadirvelu, and P. Le Cloirec, *Removal of metal ions from aqueous solution by adsorption onto activated carbon cloths: adsorption competition with organic matter*. Carbon, 2002. **40**(13): p. 2387-2392.
104. Wang, S. and E. Ariyanto, *Competitive adsorption of malachite green and Pb ions on natural zeolite*. Journal of Colloid and Interface Science, 2007. **314**(1): p. 25-31.
105. Hernández-Montoya, V., et al., *Competitive adsorption of dyes and heavy metals on zeolitic structures*. Journal of Environmental Management, 2013. **116**: p. 213-221.
106. Margulies, L., H. Rozen, and S. Nir, *Model for competitive adsorption of organic cations on clays*. Clays Clay Miner, 1988. **36**(3): p. 270-276.
107. Bunhu, T. and L. Tichagwa, *Adsorption of Methyl Orange, Pb<sup>2+</sup> and Cd<sup>2+</sup> from Aqueous Solution by Composites of Lignocellulose-Montmorillonite Modified with Methacryloxypropyl Trimethoxysilane*. Macromolecular Symposia, 2012. **313-314**(1): p. 146-156.
108. Visa, M., C. Bogatu, and A. Duta, *Simultaneous adsorption of dyes and heavy metals from multicomponent solutions using fly ash*. Applied Surface Science, 2010. **256**(17): p. 5486-5491.

109. Jiao, F., et al., *Excellent adsorption of Acid Flavine 2G by MgAl-mixed metal oxides with magnetic iron oxide*. Applied Clay Science, 2014. **101**(0): p. 30-37.
110. Ali, M.A. and D.A. Dzombak, *Competitive sorption of simple organic acids and sulfate on goethite*. Environmental Science & Technology, 1996. **30**(4): p. 1061-1071.
111. Alexandrica, M.C., et al., *Layered double hydroxides as adsorbents for anionic dye removal from aqueous solutions* Environmental Engineering and Management Journal, 2015. **14**(2): p. 381-388.
112. Ding, L., *Mechanisms of competitive adsorption between trace organic contaminants and natural organic matter on activated carbon*. 2010, University of Illinois at Urbana-Champaign.
113. Dash, B., *Competitive Adsorption of dyes (congo red, methylene blue, malachite green) on Activated Carbon*. 2010, National institute of Technology, Rourkela.
114. Lee, C.K.M. and M.K. Stenstrom, *Competitive adsorption of cyclotrimethylenetrinitramine (RDX) and cyclotetramethylenetetranitramine (HMX)*. 1996, University of California: Los Angeles.
115. Chiou, M.-S. and G.-S. Chuang, *Competitive adsorption of dye metanil yellow and RB15 in acid solutions on chemically cross-linked chitosan beads*. Chemosphere, 2006. **62**(5): p. 731-740.
116. Shin, H.-S., et al., *Phosphorus removal by hydrotalcite-like compounds (HTLcs)*. Water Science and Technology, 1996. **34**(1-2): p. 161-168.
117. Cai, P., et al., *Competitive adsorption characteristics of fluoride and phosphate on calcined Mg-Al-CO<sub>3</sub> layered double hydroxides*. Journal of Hazardous Materials, 2012. **213-214**(0): p. 100-108.

**Chapter II:**  
**Mechanism of Dye uptake onto**  
**Mg-Al-NO<sub>3</sub>**  
**Layered Double Hydroxide**



## INTRODUCTION

This chapter summarizes the investigation of the adsorption mechanisms of three pollutants, which are the Azo dyes (Methyl Orange, Orange II and Orange G) from a single-solute component solution onto Mg-Al Layered Double Hydroxide (LDH). The structure of the LDH was previously described in Chapter I section 4.1. The results presented here concern the LDH, containing the nitrate anions as the interlayer charge compensator. Nitrates are known as anions having the lowest affinity with the interlayer, therefore the latter can be exchanged easily. This adsorbent was characterized using standard methods such as elemental analysis (for chemical composition), SEM imaging and XRD before using it for any adsorption experiments. All the main parameters of adsorption (kinetic of adsorption, adsorption isotherms, thermal effect of process, and expansion of the layers) were studied and then reported in the first article “Study of Adsorption and Intercalation of Orange-Type Dyes into Mg-Al Layered Double Hydroxide”.

The competition between the interlayer anion and the adsorbing species, which is in this case the dyes, were investigated in an open system i.e. the systems were exposed to ambient atmosphere. Hence, the second competitive species is the carbonate anions that are formed during exposure to air. The latter has a very good affinity with the LDH. X-ray diffraction measurements were performed to inform on the nature of the interlayer anions after exchange.

Information about energetic aspects of adsorption processes will be evaluated using *Isothermal Titration Calorimetry*. This method will help in the understanding of the mechanism of dye adsorption on the LDH. Moreover, the complexity of the sorption mechanism of Orange II dye will be explained in detail in the second article, named “On the origin of anomalous enthalpy effects accompanying the adsorption of Orange II onto Mg-Al Layered Double Hydroxide from aqueous solutions”.

# I. Study of Adsorption and Intercalation of Orange-Type Dyes into Mg-Al Layered Double Hydroxide

*Ganna Darmograi, Benedicte Prelot, Géraldine Layrac, Didier Tichit, Gaelle Martin-Gassin,*

*Fabrice Salles, Jerzy Zajac*

Institut Charles Gerhardt de Montpellier, UMR-5253 CNRS-UM-ENSCM,  
C.C. 1502 Place Eugène Bataillon, F-34095 Montpellier cedex 5, France

Accepted in *Journal of Physical Chemistry C*

DOI: 10.1021/acs.jpcc.5b05510

***ABSTRACT:***

In the context of depollution and textile wastewater treatment, the sorption-based processes are good candidates to achieve the efficient removal of such toxic substances as dyes. In the present study, the exchange – adsorption from aqueous solutions of three azoic dyes, methyl orange (MO), orange II (OII), and orange G (OG), onto Mg-Al-LDH-NO<sub>3</sub> layered double hydroxides (LDH, molar Mg:Al ratio of 2) was investigated through monitoring all retained and removed species in combination with direct calorimetry and X-ray diffraction measurements. Kinetic curves, determined for several initial concentrations of the three dyes, indicated that the process was fast (between 60 and 100 min) and followed the pseudo-second order model in line with the passage of the removed dye through a chemisorption stage, thus constituting the rate-limiting step. Dye adsorption isotherms (H2-type) showed some differences in the maximum adsorption quantity (5.5 mmol g<sup>-1</sup>, MO; 2.7 mmol g<sup>-1</sup>, OII; 1.7 mmol g<sup>-1</sup>, OG), consistent with anionic exchange capacity and adsorption on the external surface, depending on the cross-sectional area of the dye species and with their hydrophobic-hydrophilic character. The uptake of sodium cations as a function of the dye type and the surface coverage ratio pointed that the counter-ions can either stay in solution or be adsorbed to neutralize the free –SO<sub>3</sub><sup>-</sup> moieties or other anionic species in the interlayer space. The cumulative enthalpy of displacement was negative in conformity with the exothermic character of the overall process. The intercalation of dye anions into the interlayer space of LDH materials led to its expansion with various distances being dependent both on the dye type and on the overall exchange balance. The latter included also the desorption of nitrates as well as the presence of carbonate species within the interlayer space, due to exchange in open systems exposed to the ambient atmosphere.

Keywords :

Layered double hydroxides, Methyl Orange, Orange II, Orange G, adsorption, intercalation, expansion of the layers, XRD study, calorimetry, co-adsorption, counter-ion.

### ***1. Introduction***

The release of textile wastewater to the aquatic environment is known to cause many detrimental effects [1]. Among a wide variety of toxic substances present in the effluents generated by textile industry, dyes have the mostly diversified harmful impact on aquatic and terrestrial ecosystems, as well as on human health. Tackling and achieving the goal of ‘zero discharge’ is a complex challenge, especially in economically weaker regions where textile is one of the most important sectors of the local economy. Chemical coagulation and flocculation is by far the mostly used technology for dyes removal, though its implementation requires significant quantities of inorganic polymers or chemical coagulants that generally involve higher cost and it results in a high sludge production, thereby posing further handling and disposal problems. Sorption-based processes with the use of solid sorbents are good candidates for the economically and technically viable method to achieve adequate level of dyes removal at low operating cost [2]. However, the necessity of ensuring good binding affinity between the adsorbent and the adsorbing species is the principal limitation to the effectiveness of treatment technologies. The development of a new adsorbent material for efficient and economic removal of dyes from textile wastewater should be always followed by a detailed study on its working mechanism under given conditions.

The removal of anionic azo dyes from aqueous streams by layered double hydroxides (LDHs) or modified layered materials such as pillared clays is a good example of sorption-based processes proposed in the literature based on a partial comprehension of the removal mechanism and the physical factors governing it [3-22]. It is worth mentioning here that two types of adsorption systems may be considered for the study of dye retention mechanism by LDHs and it is really crucial to be sure to which system a given study is related. In a more classical case, the uptake of dye species is studied from dye-containing aqueous solutions directly by a pristine LDH sample, which includes a specific anion (e.g., NO<sub>3</sub><sup>-</sup>, CO<sub>3</sub><sup>2-</sup>, OH<sup>-</sup>, Cl<sup>-</sup>) compensating the positive charge of the LDH layers. In the other case referred to as ‘reconstruction procedure’ [23], the starting LDH structure is calcined to obtain a mixed oxide intermediate and the latter, in turn, is immersed in an aqueous solution containing a dye solute at a given concentration. It is usually claimed that, in the presence of water and dye anionic species, the mixed oxide intermediate is

reversibly transformed back into the LDH structure, in line with the so-called ‘memory effect’. Therefore, further description of the state-of-the-art is made by referring either to ‘uncalcined’ (i.e., pristine) or ‘calcined’ (i.e., reconstructed) LDH samples.

Among various reports dealing with uncalcined samples, Costantino *et al.* considered the intercalation of methyl orange (MO<sup>-</sup>) anions into the hydrotalcite-like compound Zn<sub>0.67</sub>Al<sub>0.33</sub>(OH)<sub>2</sub>Cl<sub>0.33</sub>·0.6H<sub>2</sub>O via ion exchange with the pristine chloride ions up to the saturation state corresponding to 94% of the overall anionic exchange capacity (AEC) of the host [3]. X-ray diffraction (XRD) patterns recorded on uncalcined LDH samples with increasing dye uptake evidenced a step-wise increment of the interlayer spacing from 0.774 nm (the pure Cl<sup>-</sup> phase) to 2.42 nm (the pure MO<sup>-</sup> phase). For MO<sup>-</sup> uptake quantities smaller than 4% of AEC, the ion exchange pathway was restricted only to the external surface of the microcrystals. The two containing phases Cl<sup>-</sup> and MO<sup>-</sup> were postulated to coexist in the intermediate samples up to 70% of AEC, where the Cl<sup>-</sup> phase was completely transformed into the pure MO<sup>-</sup> one. Further retention was regarded as solubilization of MO<sup>-</sup> ion in the already formed phase. The computer-aided molecular modeling of the Zn-Al hydrotalcite-like layered structure with some intercalated MO anions, undertaken on the basis of the chemical composition and interlayer distance of the composite, indicated the monolayer packing of dye anions in perpendicular orientation with respect to the layer plane (their charged SO<sub>3</sub><sup>-</sup> moieties in a ‘flip-flop’ arrangement interacting with the positively charged sites). In another paper [10], the distance of interlayer spacing in Ca-Al-LDH was shown to increase to 2.45 nm upon MO intercalation by exchange, which was regarded as reflecting a tilted orientation of the intercalated MO<sup>-</sup> species with an angle of 49°. The intercalation of MO<sup>-</sup> species via anionic exchange with NO<sub>3</sub><sup>-</sup> counter-ions among the layers of the host Mg-, Ni-, and Zn-containing LDHs was monitored by UV-Vis absorption spectroscopy and XRD [6]. The interlayer spacing was proven to be expanded following a two-phase transition mechanism. The maximum exchange ratio equal to 100% of the AEC was obtained only for Mg-Al-LDH, whereas it was limited to about 90% in the case of Ni- and Zn-Al-LDH. This discrepancy was rationalized by referring to a limited diffusion of MO due to a larger crystalline size of the last two LDH particles. Besides the chemisorbed MO<sup>-</sup> ions, the compensating interlayer anions were represented mostly by OH<sup>-</sup> and by CO<sub>3</sub><sup>2-</sup> coming from air. Several authors applied Langmuir, Freundlich, Temkin, or Redlich-Peterson equations to fit the experimental adsorption isotherms of MO retained by various LDHs containing either nitrate or carbonate counter-ions [12-14]. The

kinetics of MO<sup>-</sup> retention by LDH materials was intensely studied and often analyzed by using pseudo-first-order, pseudo-second-order, Elovich, intraparticle diffusion, and Boyd models [5, 12-14]. The pseudo-second-order model provided the best fit of kinetic data in most cases and the adsorption equilibrium, at different initial concentrations of MO, was obtained after 2 h at the most.

In the second group of papers focusing on the reconstruction and ‘memory effect’ procedures, Zhang *et al.* demonstrated, on the basis of XRD and FT-IR studies, the successful intercalation of MO<sup>-</sup> anions into calcined calcium-aluminium layered double hydroxides (Ca-Al-LDHs) in the form of interpenetrating bilayer, paralleled by the expansion of the basal spacing of Ca-Al-LDH to 2.48 nm [8]. The results of powder XRD, FTIR, UV-Vis, as well as <sup>27</sup>Al and <sup>13</sup>C CP/MAS NMR studies were also exploited by Laguna *et al.* to show that MO species adsorbed onto calcined Mg-Al-LDH (with a Mg:Al atomic ratio of 3) to achieve a MO content of *c.a.* 6 wt.% could not be incorporated in the interlayer space, but rather on the external surface of the LDH crystals [19]. The interlayer space was postulated to be occupied by hydroxyl and carbonate anions not eliminated in the calcinations stage. The possibility of intercalation of MO<sup>-</sup> ions in flat configuration within the interlayer space of Zn-Al-LDH (with a Zn:Al molar ratio of 3) was inferred from XRD, Inductively Coupled Plasma (ICP) emission spectroscopy, and TG-DTA measurements [4]. Taking advantage of such fitting procedures, the MO adsorption was regarded as a spontaneous (negative Gibbs free energy) and endothermic (positive enthalpy of adsorption) phenomenon.

Contrary to numerous papers dealing with the removal of methyl orange from aqueous solutions by LDH materials, only a few reports were published on the mechanism of adsorption of orange II (OII) and orange G (OG) [16-18]. Bouhent *et al.* carried out an extended study on the adsorption of OII onto Mg-Al-LDH with the aid of powder XRD, FT-IR, UV-Vis, TGA-DTA techniques [16]. They showed that OII<sup>-</sup> anions were first adsorbed on the external surface and then intercalated within the interlayer space via ion exchange with the pristine NO<sub>3</sub><sup>-</sup> counter-ions. The endothermic character of the adsorption phenomenon was deduced when fitting the experimental adsorption isotherms with the Langmuir model. The adsorption of OG onto Mg-Fe-LDH and Mg-Al-LDH was also investigated with the use of similar characterization methods [17, 18]. The kinetic data fitted well the pseudo-second-order model and the thermodynamic consideration based on the Langmuir isotherm equation indicated that the sorption process was endothermic in nature

[17]. The intercalation of OG anions into the Mg-Al-LDH interlayer space, initially containing CO<sub>3</sub><sup>2-</sup> ions, was demonstrated to induce an increase in the basal spacing from 0.77 nm to 1.77 nm [18]. There are also previous studies reporting exothermic effects of sorption of dyes onto lamellar materials [24]. However they do not describe the exchange of ionized species in pure intercalated layered anionic clays, but rather sorption on clay materials, sometimes as mixtures with other inorganic compounds.

The objective of this study was to shed more light on the mechanism of individual adsorption of three azo dyes, i.e., methyl orange, orange II, and orange G, from aqueous solutions onto the same pristine Mg-Al-LDH-NO<sub>3</sub> (molar Mg:Al ratio of 2). The equilibrium and kinetic aspects of the phenomenon in open systems exposed to the ambient atmosphere were examined in view of its potential uses in Environmental Remediation. Unlike previous papers reported on the subject, special attention was paid to the balance of various species involved in the ion exchange. The intercalation of dye anions was followed by XRD in a large 2θ range from 2° to 30°, which allowed a correct assignment of diffraction peaks. Direct calorimetry measurements of the enthalpy change accompanying the dye retention by LDH were carried out to demonstrate the exothermic character of the overall mechanism, at variance with the current state-of-the-art.

## ***2. Experimental***

### ***2.1. Materials and synthesis***

The Mg-Al LDH was prepared by co-precipitation method at constant pH (≈ 10). 300 mL of aqueous solution containing 30.76 g of Mg(NO<sub>3</sub>)<sub>2</sub>•6H<sub>2</sub>O (Sigma Aldrich), and 22.5 g of Al(NO<sub>3</sub>)<sub>3</sub>•9H<sub>2</sub>O (Sigma Aldrich) was delivered by peristaltic pump into a beaker and the pH was maintained constant at pH = 10 by addition of NaOH (2 mol L<sup>-1</sup>) with pH-STAT Titrino (Metrohm). After complete precipitation, the suspension was refluxed at 80 °C for 17 h, and then the gel was separated by centrifugation, thoroughly washed three times with deionized water (Na < 100 ppm). Finally, the product was dried overnight at 80 °C.

According to Table 1, the molar Mg:Al ratio was equal to 2 and the material achieved contained nitrate anions as the main interlayer compensator of the positive layer charge. Therefore, this sample was further referred to as Mg-Al-LDH-NO<sub>3</sub>.

**Table 1.** Chemical composition and proposed formula of Mg-Al-LDH-NO<sub>3</sub> as inferred from the elemental analysis (the element contents are given in wt %).

Mg	Al	N	C	Chemical formula	AEC (meq g <sup>-1</sup> )
15.85	8.78	3.81	0.32	[Mg <sub>0.67</sub> Al <sub>0.33</sub> (OH) <sub>2</sub> ](CO <sub>3</sub> ) <sub>0.027</sub> •(NO <sub>3</sub> ) <sub>0.276</sub> •1.32H <sub>2</sub> O	3.25

The SEM micrographs (see Supporting Information) evidenced well-defined layered platelets. The appearance below 35° 2θ of three symmetric and intense peaks in the XRD pattern (see Figure S1 in Supporting Information) corresponding to the (003), (006) and (009) harmonic reflections and above 35° 2θ of broad and asymmetric (012), (015), (110) peaks were in agreement with a well crystallized LDH exhibiting an hexagonal lattice with *R-3m* rhombohedral symmetry. The values of the lattice parameter *c* = 2.67 nm and the basal spacing *d*<sub>003</sub> = 0.89 nm agreed well with those previously reported in literature for Mg-Al-LDH-NO<sub>3</sub> [16, 25, 26]. The interlayer spacing of 0.41 nm was found to be consistent with the diameter of nitrate anion (i.e., 0.40 nm [27]).

Methyl Orange, Orange II (Acid Orange 7) and Orange G (Acid Orange 10), purchased from Sigma-Aldrich, were designated MO, OII and OG, respectively. All dyes had high purity > 99% and they were used without any further purification. The maximum absorption (*λ*<sub>max</sub>) in the UV-Vis spectra was obtained at a wavelength of 466 nm, MO; 483 nm, OII; and 480 nm, OG. The structural formulas of the three dye anions together with their 2D molecular sizes are given in **Figure 1**. The estimated molecular sizes in two dimensions of the dyes were calculated with ChemDraw 3D 5.0 software package.

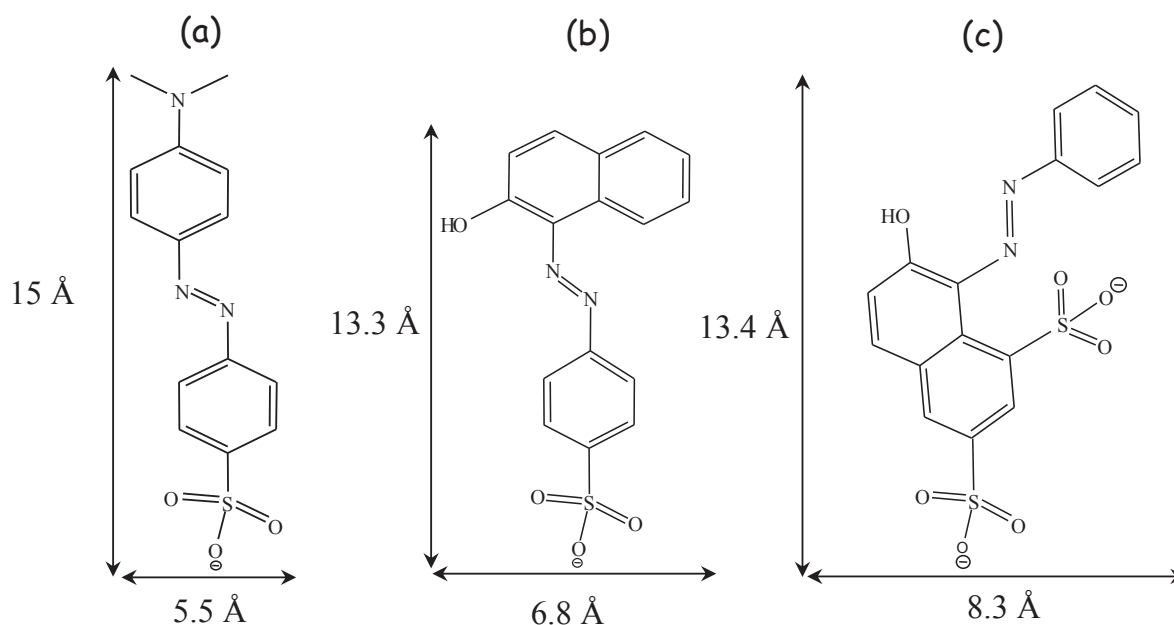


**Figure 1.** Structural formulas of MO (a), OII (b), OG (c), and their 2D molecular sizes, as estimated with the aid of ChemDraw 3D 5.0 software package.

## 2.2. Characterization

The LDH morphology was observed by using a scanning electron microscope (SEM) Hitachi S-4800. The percentages of Mg and Al in the as-synthesized LDH sample were determined using Energy-Dispersive X-ray analysis with Quanta 200 FEG Electron Microscopy spectrometer. The C, N and O contents were obtained by means of CHNS-O elemental analysis (Flash EA 1112). X-ray diffraction patterns of the pristine sample were recorded with a X'Pert diffractometer over the  $2\theta$  range from  $3^\circ$  to  $70^\circ$  under the Cu  $K\alpha$  radiation ( $\lambda = 1.5418 \text{ \AA}$ ) and nickel filter. In the case of LDH samples containing different amounts of retained dye species, the XRD patterns were collected at a scan rate of  $0.003 \text{ deg mn}^{-1}$  in the  $2\theta$  range from  $2^\circ$  to  $30^\circ$  at 30 mA, 45 kV, using incident beam mask 10 mm, and zero background sample holder.

## 2.3. Adsorption experiments

Classical batch adsorption studies were carried out to evaluate the retention properties of Mg-Al-LDH-NO<sub>3</sub>. For this purpose, a LDH sample (2.5 mg) was poured into a 30 ml Nalgene™

tube containing 10 mL of dye solution at a given concentration. The initial concentration of dyes varied from 0.02 to 5 mmol L<sup>-1</sup> for MO and OII; from 0.02 to 3 mmol L<sup>-1</sup> for OG molecule. The pH of each suspension was carefully checked before and after the attainment of adsorption equilibrium. The tubes were stirred overnight at 298 K. The separation of solid phase from the supernatant liquid was achieved by centrifugating at 10 000 rpm for 12 min. The supernatant was then analyzed by using V-670 UV-Vis Spectrophotometer (wavelength range 350 – 550 nm) to determine the equilibrium concentration of dye, C<sub>eq</sub>. The amount adsorbed, Q<sub>ads</sub>, is calculated as follows,

$$Q_{ads} = \frac{V_0 (C_i - C_{eq})}{m_s}$$

C<sub>i</sub> is the initial dye concentration in the tube, V<sub>0</sub> is the initial solution volume, and m<sub>s</sub> denotes the mass of the adsorbent. The supernatant was also analyzed with the aid of ionic chromatography analyzer (Shimadzu HPLC) equipped with a CDD-6A conductivity detector operating at 313 K (Shim-pack IC-A1 column, 2 mmol L<sup>-1</sup> potassium hydrogen phthalate at pH 4.2 as the mobile phase) so as to study the amount of nitrate anions released from the LDH sample during dye adsorption. The presence of sodium counter-ions in the supernatant was also evaluated by the same technique (Shim-pack IC-C1 column, 5 mmol L<sup>-1</sup> nitric acid as the mobile phase). The HPLC operating conditions were kept the same in both cases: flow rate of 1.5 mL min<sup>-1</sup>, injection volume of 45 μL, column temperature of 40 °C. The repeatability and experimental uncertainties of the adsorption measurements were carefully evaluated, and results were detailed in SI-S2.

#### 2.4. Kinetic study

Sorption kinetics was studied by using experimental procedures similar to those described in the previous paragraph. The quantities of dye adsorption were determined at different time intervals. Three common kinetics models were subsequently applied to fit the experimental data: Lagergren-pseudo-first order [28], pseudo-second order [29], and Weber's intraparticle diffusion [30] one. The related analytical expressions are reported in Supporting Information.

### 2.5. Calorimetry measurements

A differential TAM III microcalorimeter was used to measure the enthalpy changes accompanying the removal of dye species from aqueous solutions by Mg-Al-LDH-NO<sub>3</sub>. To achieve a higher sensitivity on longer time scale, the calorimeter was run in a heat flow mode. The operating procedures and data processing are detailed elsewhere [31]. Taking advantage of the oil bath system, the temperature was kept constant within  $\pm 0.0001$  °C and the isothermal heat flow was measured at 25 °C. Prior to each calorimetric run, a sample of about 1-2 mg of LDH powder was introduced into the calorimetric cell initially containing 0.8 mL of deionized water. Only the same volume of deionized water was put in the reference cell. Then, both cells were placed inside the microcalorimeter and the thermal equilibrium was reached after 2 h. The injection system was equipped with a syringe filled with the appropriate stock solution of a given dye: 8.5 mmol L<sup>-1</sup>, MO; 14 mmol L<sup>-1</sup>, OII; 12 mmol L<sup>-1</sup>, OG. Successive injections of the 10  $\mu$ L aliquots of a given stock solution during 10 sec resulted in an electric signal directly fed into a computer; the digitized signal representing the related thermal peaks was recorded with an equilibration time of 90 min applied between 2 injections. Integration of the areas under the thermal peaks was performed and the resulting enthalpy values were related to the mass of LDH in the cell. Similar procedures were applied to evaluate the effects of dilution and to correct the enthalpy values accordingly [31]. The repeatability of the enthalpy measurement, including the data processing step to determine the cumulative enthalpy of displacement, was within 6%, MO; 17%, OII; 4%, OG, respectively, nevertheless, the same trends in the enthalpy of displacement with the amount of dye uptaken were recorded in two separate runs.

### 2.6. XRD study of the dye-loaded LDH samples

Several LDH samples loaded with increasing amounts of dye were analyzed by XRD. For this purpose, 5 mg of LDH were dispersed in 20 mL of dye solution at known initial concentration. The supernatant solution was analyzed after having attained the sorption equilibrium and the corresponding dye equilibrium concentration and amount adsorbed were determined. The dye-loaded solid samples were dried at 100 °C for 1-2 h and then analyzed with the previously described XRD equipment.

### 3. Results and discussion

The evolution of the dye adsorption phenomenon as a function of the equilibration time for the three dye species are shown in Figure S2 in Supporting Information. In the case of MO and OG, the kinetic curves were measured for three dye initial concentrations, chosen in a way to represent the following physical situations: (i) total dye adsorption leaving a negligible quantity of the solute in the supernatant solution, (ii) adsorption system in the intermediate adsorption range, (iii) adsorption system corresponding to the plateau saturation region. It can be clearly seen that the initial rates of MO adsorption are relatively rapid and the states near to equilibrium are reached within 60 min. It should be noted that all nitrate counter-ions have been already displaced from the LDH interlayer space at the end of this stage (HPLC results not shown here). Then the adsorption phenomenon proceeds at a slower rate and the final equilibrium is totally attained after 200 min. The main hypothesis at this stage is to ascribe this decrease in the MO adsorption kinetics to the removal of carbonates from LDH; the dye species need more time to replace the carbonate anions which originate from strong interactions between CO<sub>2</sub> molecules and the strongest basic sites in the LDHs structure, and thus it takes more time to attain the adsorption equilibrium. For OG, the adsorption equilibrium is reached after 100 min and only one step can be observed in the kinetic behavior. In the case of OII, the adsorption equilibrium is reached within the first 60 min.

Three kinetic models were used to fit the kinetic data reported in Figure S3-S4. The resulting best-fit values of kinetic parameters have been collected in Table S1 in Supporting Information.

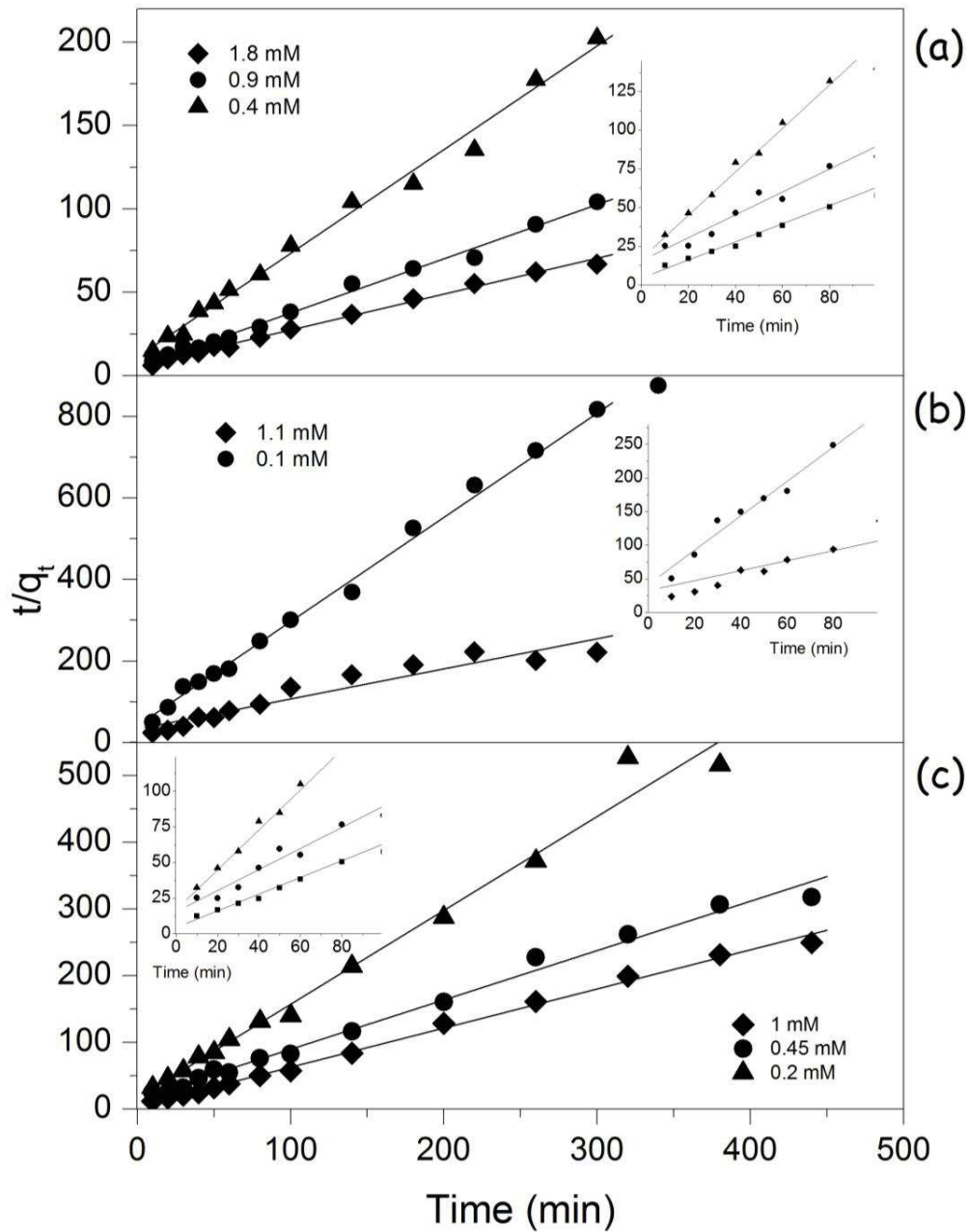


**Figure 2.** Pseudo-second order kinetics model of MO (a), OII (b) and OG (c) adsorption onto Mg-Al-LDH-NO<sub>3</sub> for different initial concentrations.

The highest goodness-of-fit is obtained with the pseudo-second order model (see **Figure 2**) in accordance with the literature of the subject [13, 14]. This means that the dye removal passes through a chemisorption stage, which constitutes the rate-limiting process. For the sorption of MO,

the rate constant  $k_2$  obtained for the pseudo-second order kinetic model (see kinetic equations in Supporting Information) decreases from 0.035 to 0.008 mmol g<sup>-1</sup> min<sup>-1</sup> with increasing the initial dye concentration.

This effect can be attributed to the increased competition for the surface active sites at higher MO concentrations [32]. It is interesting to notice that the kinetic plots following the Weber's intraparticle diffusion model do not pass through the origin. This means that the interparticle diffusion is the rate-controlling step [33, 34].

The equilibrium isotherms for the three dye molecules adsorbed onto Mg-Al-LDH-NO<sub>3</sub> are presented in **Figure 3**. For all orange-type dyes, the amount adsorbed increases with increasing the equilibrium dye concentration. The quasi-vertical portions at very low initial concentrations revealed the high affinity of the LDH host towards the three dye species. The adsorption isotherms correspond to the H2-type according to the Giles classification [35]. The amount adsorbed levels off in the plateau region and it is approximately equal to 5.5 mmol g<sup>-1</sup>, MO; 2.7 mmol g<sup>-1</sup>, OII; 1.7 mmol g<sup>-1</sup>, OG. The modification of pH during sorption is rather small. For OG and OII, the pH of the suspension does not vary a lot (0.1-0.2 pH unit, OG; 0.2 to 0.4 pH unit, OII). In the case of MO, the pH change is somewhat higher, with an increase of pH around 1 unit (between 0.6 and 1.3). The observed differences in the maximum adsorption quantities can be obviously correlated with the cross-sectional area of the dye species which increases in the order: MO < OII < OG (see **Figure 1**). Furthermore, since one OG anion bears two negative charges, the quantity adsorbed of this molecule should be smaller than those of the two others. The hydrophobic-hydrophilic character of each dye unit is another parameter to be considered when explaining the observed trends in the maximum amounts adsorbed. The MO moiety is more hydrophobic than the OII one since it contains additional terminal methyl groups, whereas the hydrophobic character of the latter is diminished by addition of a hydrophilic OH group [36]. In the case of OG, the presence of two SO<sub>3</sub><sup>-</sup> groups, together with the hydrophilic OH substituent, renders this anion the less hydrophobic among the three dyes [37].

It is worth underlying that the MO amount adsorbed is almost twice that of theoretical AEC as inferred from the chemical formula of the pristine LDH sample (see Table 1). Such an LDH performance has never been shown in the literature. Two hypotheses taken from the previous studies can be considered to rationalize this effect. MO anions may adsorb on the external surface

of LDH [25, 38]. Another possibility corresponds to the formation of some aggregates inside the LDH interlayer space due to the hydrophobic interactions of chromonic MO species between themselves [39]. In both cases, the excess of negative charge relatively to the AEC has to be neutralized by the uptake of some positively charged species.

The uptake of sodium cations during the adsorption of dye anions is illustrated in **Figure 3**. Sodium is the counter-ion with respect to the dye sulfonate moiety  $-\text{SO}_3^-$ . It is clear that  $\text{Na}^+$  ions are co-adsorbed, especially for high dye uptakes. In the case of MO, the sodium uptake curve may be divided into 2 parts. In the first part, no adsorption of  $\text{Na}^+$  can be observed. It corresponds to the vertical part of the MO adsorption isotherm, where the interaction between  $\text{MO}^-$  anions and LDH is strong and the formers exchange with the pristine  $\text{NO}_3^-$  counter-ions. Since the sulfonate moieties of MO anions compensate successively the positive charge of the brucite-like layer, the sodium co-ions cannot enter the inter-lamellar domain of the LDH host. The co-adsorption of  $\text{Na}^+$  ions begins at  $Q_{\text{ads}} > 4 \text{ mmol g}^{-1}$ , where the amount of MO exceeds the AEC of the pristine LDH sample ( $3.25 \text{ meq g}^{-1}$ ). The excess of adsorbed MO anions is likely due to hydrophobic interactions resulting in the formation of surface-bound aggregates groups [36]. The free  $-\text{SO}_3^-$  moieties are thus neutralized by the co-adsorbed  $\text{Na}^+$  ions.

In contrast, co-adsorption of sodium cations parallels the adsorption of OII anions at a constant proportion of 1:3. Therefore, there are some negative species (e.g., carbonate impurities from air and also hydroxyl groups) in the interlayer space of LDH whose charge could be partially neutralized by the co-adsorption of  $\text{Na}^+$  ions.

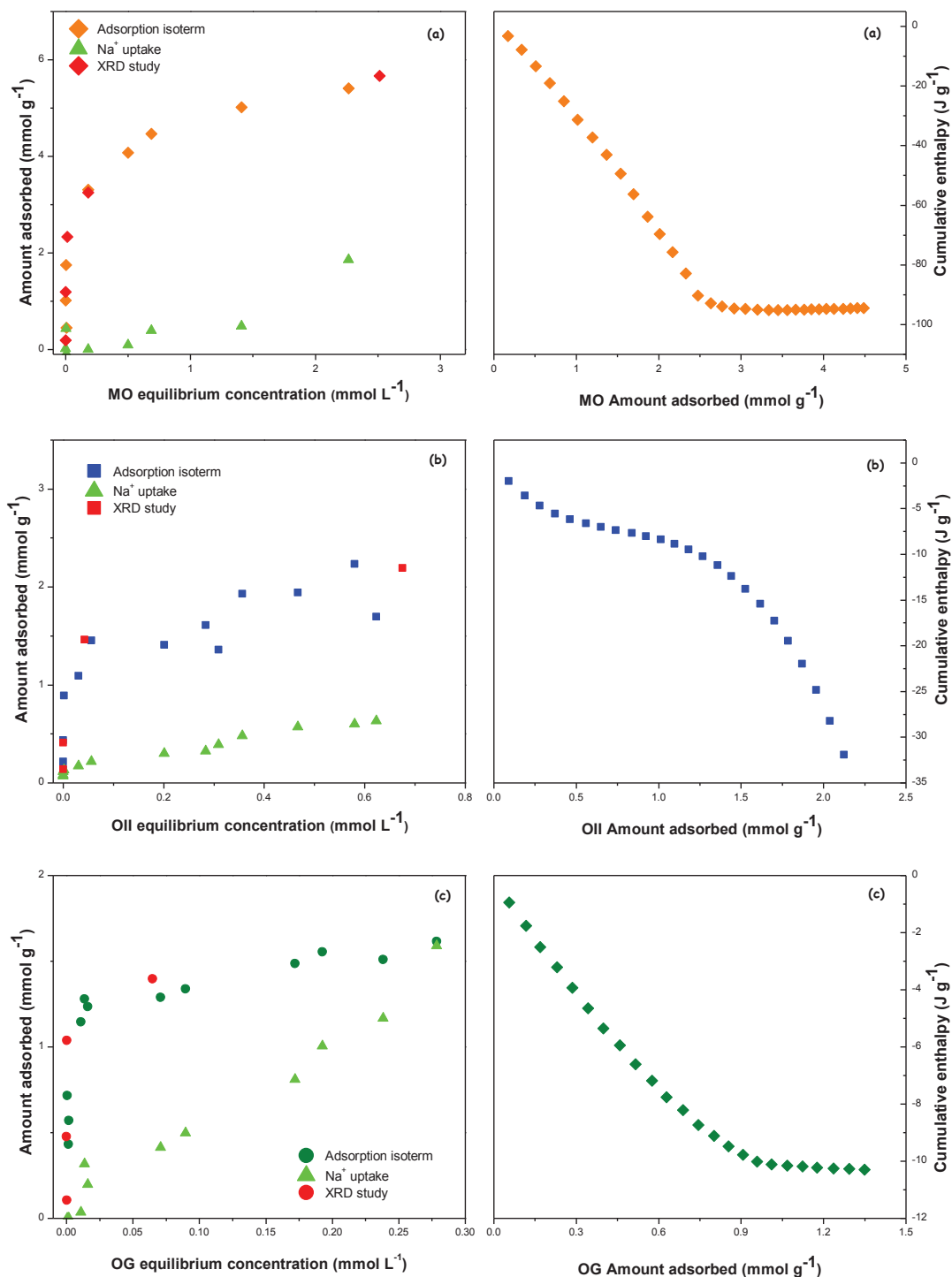


**Figure 3.** Left panels: adsorption isotherms for MO (a), OII (b), and OG (c) anions and sodium cations from aqueous solutions onto Mg-Al-LDH-NO<sub>3</sub> at 25 °C; Right panels: variations of the cumulative enthalpy of displacement as a function of the amount of dye adsorbed.

The isotherm of sodium uptake accompanying the adsorption of OG anions can be divided into 3 parts, corresponding, respectively, to zero Na<sup>+</sup> adsorption, partial Na<sup>+</sup> co-adsorption, and high Na<sup>+</sup> retention. As in the case of MO adsorption, the first part matches the vertical part of the OG adsorption isotherm. The second part falls in line with the beginning of the saturation plateau region. A plausible explanation is that some OG anions are retained only with one negatively charged center, the second one being neutralized with one sodium counter-ion. When the dye adsorption reaches its maximum value, one Na<sup>+</sup> ion adsorbs, on average, for one retained OG anion.

The above discussion indicates that the mechanism of dye removal from the aqueous phase by Mg-Al-LDH-NO<sub>3</sub> sample is a complex process passing through various stages involving a variety of species retained at the solid-liquid interface or released to the supernatant solution. The displacement is a commonly used term to designate such a process. Direct calorimetry measurements of the enthalpy changes accompanying the displacement process can shed some light on the interactions involved. The variations of the cumulative enthalpy of displacement are plotted against the amount of dye adsorbed in **Figure 3**.

Despite some marked differences between the three enthalpy curves, the general conclusion drawn from the calorimetric measurements is that the overall process of displacement has an exothermic character. This observation is at variance with the endothermicity of dye adsorption postulated in the previously published papers [14, 15, 17] describing the sorption of anionic dyes onto LDHs. It should be emphasized that, contrary to the enthalpy quantities determined previously, the direct calorimetry measurement and further data processing employed here provide estimate of the global heat effect accompanying the sorption process. Indeed, the cumulative enthalpy represents a global effect combining such contributions involved in the sorption phenomenon as the intercalation of the adsorbed species, interlayer anion displacement, swelling of the layers, hydration/dehydration effects and also the displacement of other species (such as Na<sup>+</sup> and OH<sup>-</sup>). In the case of MO and OG, the exothermic displacement continues up to the end of the vertical portion of the dye adsorption isotherm; then it levels off quite quickly and the displacement becomes almost athermal. The exothermic effect of displacement accompanying the retention of MO species is much more marked than that of OG adsorption. It decreases to about -90 J g<sup>-1</sup> in the enthalpy plateau region, contrary to the enthalpy change during OG adsorption, which diminishes only to about -10 J g<sup>-1</sup>. The enthalpy variations for OII do not follow the same

trend. The initial decrease to about  $-10 \text{ J g}^{-1}$  at the end of the vertical portion of the OII adsorption isotherms is consistent with the enthalpy curve for OG. After a short 'hesitation' interval, a new strongly exothermic contribution to the total enthalpy of displacement becomes noticeable. This trend is difficult to be explained on the basis of the results reported here.

According to the well-documented literature [3, 4, 8, 10, 16-18, 26], the intercalation of dye anions into the interlayer space of LDH materials may lead to an expansion of the interlayer distance. The results of similar XRD study made on the selected LDH samples loaded with different amounts of dye anions are reported below. For each type of dye, the quantities adsorbed are marked with red points directly on the related adsorption isotherms in **Figure 3**.

X-ray diffraction patterns of Mg-Al-LDH with increasing MO content are shown in **Figure 4**. They are compared with XRD patterns of the pristine samples containing carbonate and nitrate anions. For the first point in the adsorption isotherm (system MO-1), where there are 0.2 mmol of MO retained per gram of the pristine LDH sample, a displacement of the (003) peak from a  $2\theta$  position of  $10^\circ$  to  $11.5^\circ$  can be seen. The interlayer distance thus decreases from 0.89 to 0.77 nm. The latter value is consistent with the Mg-Al-LDH-CO<sub>3</sub> system in which the (003) peak is located at  $11.6^\circ$  with a  $d_{003}$  value of 0.765 nm. This means that there is no more NO<sub>3</sub> anions within the interlayer space of LDH even for very small MO adsorption quantities. The pristine nitrate anions are thus easily replaced by the carbonate ones, provided by dissolution of CO<sub>2</sub> in water from open system. Moreover, pristine LDHs contain already carbonate species in the structure. The latter phase cannot be observed in the XRD pattern of the pristine material because of the too small carbonate content (Table 1) and because it is masked by the presence of the nitrate phase. However, the displacement of nitrate anions by the incoming MO species makes the CO<sub>3</sub> phase distinguishable in the XRD pattern of the MO-1 system, though with a very low intensity. It is worth mentioning that there is no important narrowing of the basal spacing in the system with MO<sup>-</sup> intercalation, because of the very small quantity adsorbed  $0.2 \text{ mmol g}^{-1}$ .

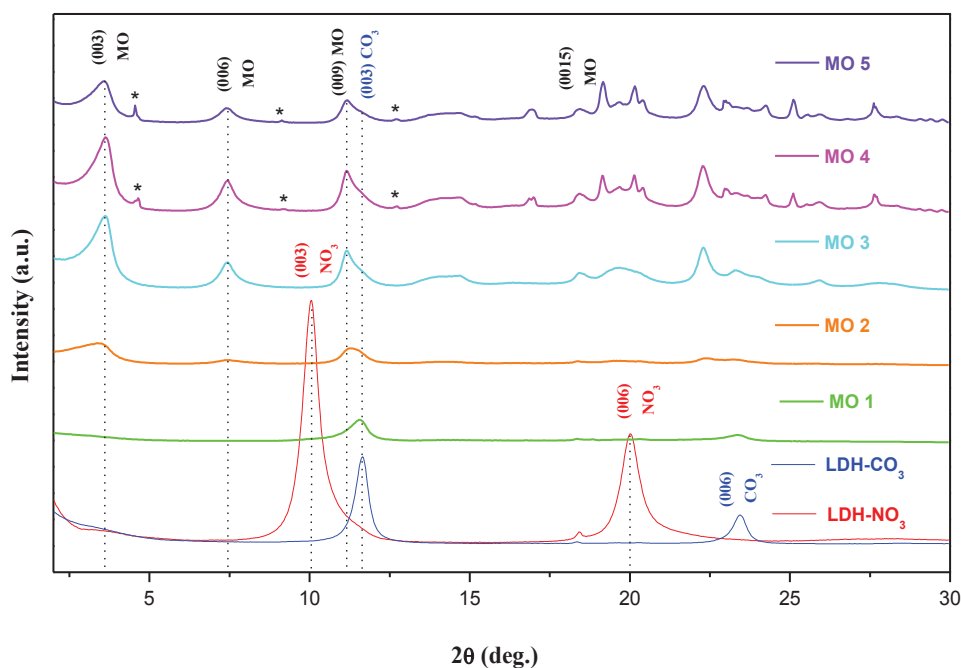


**Figure 4.** X-ray diffraction patterns in the  $2\theta$  range from  $2^\circ$  to  $30^\circ$  for the intercalation of MO in the Mg-Al-LDH-NO<sub>3</sub> structure corresponding to 5 points in the MO adsorption isotherm (as marked by crosses in **Figure 3**).

In the case of the MO-2 system ( $Q_{\text{ads}} = 1.2 \text{ mmol g}^{-1}$ ), two new harmonic peaks appear at  $2\theta$  positions of  $3.6^\circ$  and  $7.4^\circ$  corresponding to  $d$ -values of 2.42 and 1.2 nm. These new peaks are ascribed to the (003) and (006) reflections due to MO<sup>-</sup> species intercalated in the LDH host. The third (009) harmonic peak should have appeared at  $11.1^\circ$  but it is not clearly distinguishable in **Figure 4**. Nevertheless, the broadening of the carbonate peak (between  $2\theta$  positions from  $11.1$  to  $11.5^\circ$ ) may evidence for the existence of the (009) peak of MO<sup>-</sup>. These features in the XRD pattern indicate that MO and CO<sub>3</sub> containing interlayers are present in the LDH.

Further MO uptake (from MO-3 to MO-5) induces an increase of intensity of the (009) reflection with a  $d$  value of 0.8 nm. The MO phase becomes predominant already in the MO-3 system. The presence of three (001) harmonic reflections corresponding to  $d$ -values of 2.42, 1.2 and 0.8 nm is in good agreement with the previous papers reporting the intercalation patterns in Mg-Al-LDHs [7, 26] Zn-Al-LDHs [3, 13, 40], and Ca-Al-LDHs [13]. The expansion of the basal interlayer distance ( $d_{003}$ ) of the host LDH lattice from 0.89 to 2.42 nm, which parallels the MO intercalation, points toward the successful exchange with NO<sub>3</sub><sup>-</sup> anions. Furthermore, three new

sharp peaks are visible in the XRD patterns of the MO-4 and MO-5 systems (\*). According to the previous discussion, the amounts of MO retained by the LDH host (3.3 and 5.5 mmol g<sup>-1</sup>, respectively) exceed the AEC of LDH (3.25 meq g<sup>-1</sup>). The possibility of MO sorption or crystallization on the external surface was checked thoroughly by washing, prior to XRD analysis, a LDH sample previously loaded with 3.7 mmol g<sup>-1</sup> of MO. The resulting diffractogram (not shown here) exhibited only 3 harmonic peaks at 2θ positions of 3.6°, 7.4°, and 11.1°. This corroborated the starting hypothesis of interaction between dye and external surface.

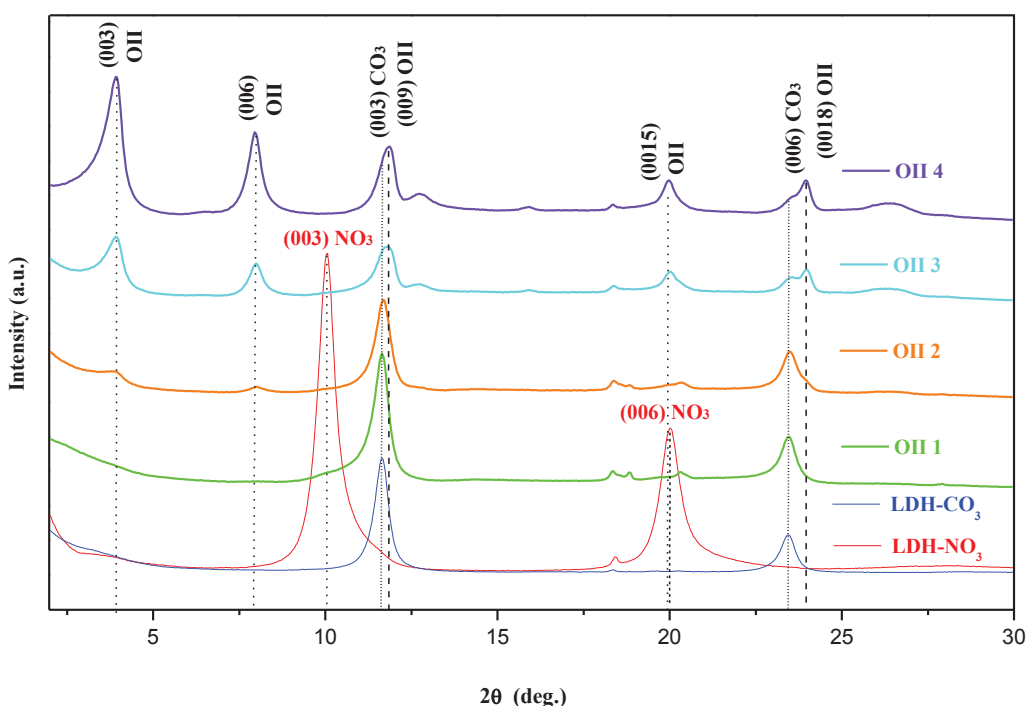


**Figure 5.** X-ray diffraction patterns in the 2θ range from 2° to 30° for the intercalation of OII in the Mg-Al-LDH-NO<sub>3</sub> structure corresponding to 4 points in the OII adsorption isotherm (as marked by crosses in **Figure 3**).

Four different points have been selected in the OII adsorption isotherm (**Figure 3** (b)) to perform XRD study on the Mg-Al-LDH-OII systems. The resulting XRD patterns are given in **Figure 5**. The diffractograms recorded on the pristine LDH-NO<sub>3</sub> and LDH-CO<sub>3</sub> samples are also included for the comparison purpose. The XRD pattern of the OII-1 system ( $Q_{\text{ads}} = 0.14 \text{ mmol g}^{-1}$ ) exhibits two harmonic peaks at 2θ positions of 11.6° and 23.4°, providing interlayer space

distances of 0.76 nm and 0.38 nm. These (003) and (006) peaks indicate the presence of CO<sub>3</sub><sup>2-</sup> species in the interlayer space. Moreover, small peaks of the nitrate phase are still present. On the contrary, there are not enough OII units for the peaks of the intercalated species to be distinguishable. With the increased amount of adsorbed OII<sup>-</sup> units in the OII-2 system ( $Q_{\text{ads}} = 0.41 \text{ mmol g}^{-1}$ ), two harmonic (003) and (006) peaks become visible at  $2\theta$  positions of 3.9° and 7.9°. These peaks corresponded to interlayer space distances of 2.22 nm and 1.11 nm and thus indicate the intercalation of OII<sup>-</sup> anions within the LDH structure. The (009) harmonic peak of OII has almost the same position as the (003) peak of the intercalated carbonate anions and, therefore, it is difficult to deduce the role of carbonate species during dye intercalation. It is useful to compare the harmonic (006) peak of carbonates with the (0018) peak of OII<sup>-</sup> so as to notice the increasing predominance of the OII<sup>-</sup> phase when passing from OII-2 to OII-4 system; the (0018) reflection becomes sharper than the (006) peak of carbonates already in the XRD pattern of the OII-3 system. The existence of the CO<sub>3</sub><sup>2-</sup> phase even in the OII plateau adsorption region confirms the previous hypothesis explaining the co-adsorption of sodium cations and OII<sup>-</sup> anions at a constant proportion of 1:3. XRD results are in agreement with those reported for OII<sup>-</sup> adsorption onto LDH [16, 41-43] and LDH-PVA [40] structures. The last unattributed peak could be explained by specific interaction of OII and LDH as observed from calorimetric results. This mechanism deserves to be studied more in details to check the hypothesis.

**Figure 6** shows XRD patterns recorded on LDH samples loaded with increasing amounts of OG units. For the OG-1 system, the corresponding diffractogram clearly indicates the presence of nitrates and carbonates ions in the interlayer space with the related (003) and (003) reflections at  $2\theta$  positions of 10° and 11.6°, respectively. The OG phase is not clearly visible probably because of the very small amount adsorbed (about 0.11 mmol g<sup>-1</sup>). The orientation of the intercalated dye units is likely parallel to the layers and the corresponding peak is hidden by the peaks of CO<sub>3</sub> and NO<sub>3</sub> phases. When one passes to the OG-2 system, a new peak appears at a  $2\theta$  position of 5.2°. It can be assigned to the (003) reflection of the OG phase in relation with the interlayer distance of 1.68 nm. Broadening the peaks corresponding, to the (003), (003), and (006) reflections of the NO<sub>3</sub>, CO<sub>3</sub> and OG phases respectively can be interpreted as the result of increased adsorption of OG units ( $Q_{\text{ads}} = 0.48 \text{ mmol g}^{-1}$ ). The NO<sub>3</sub> phase disappears in the XRD pattern recorded on the OG-3 system ( $Q_{\text{ads}} = 1.04 \text{ mmol g}^{-1}$ ). Simultaneously, the OG phase becomes predominant over the carbonates species, as inferred from the (006) reflection by OG species and the (003) by the CO<sub>3</sub><sup>2-</sup>

ones. Two new harmonic reflections of OG at 2θ positions of 15.8° and 21.1° can be found in the XRD pattern. They may be assigned as the (009) and (0012) reflections of OG species. For the last OG-5 system, no peaks characteristic of the CO<sub>3</sub> phase are visible and the intercalated OG<sup>2-</sup> species constitute the only phase present in the interlayer space. The expansion of the LDH structure by intercalation of the OG units results in an increase in the interlayer space distance from 0.89 nm to 1.68 nm. The latter is not far from the 1.77 nm [18] and 1.78 Å [40, 44] values reported previously in the literature. Furthermore, this expansion is in a good agreement with the co-adsorption of sodium cations and in line with the vertical orientation of the intercalated OG units interacting through only one -SO<sub>3</sub> moiety with the positively charged LDH layers.

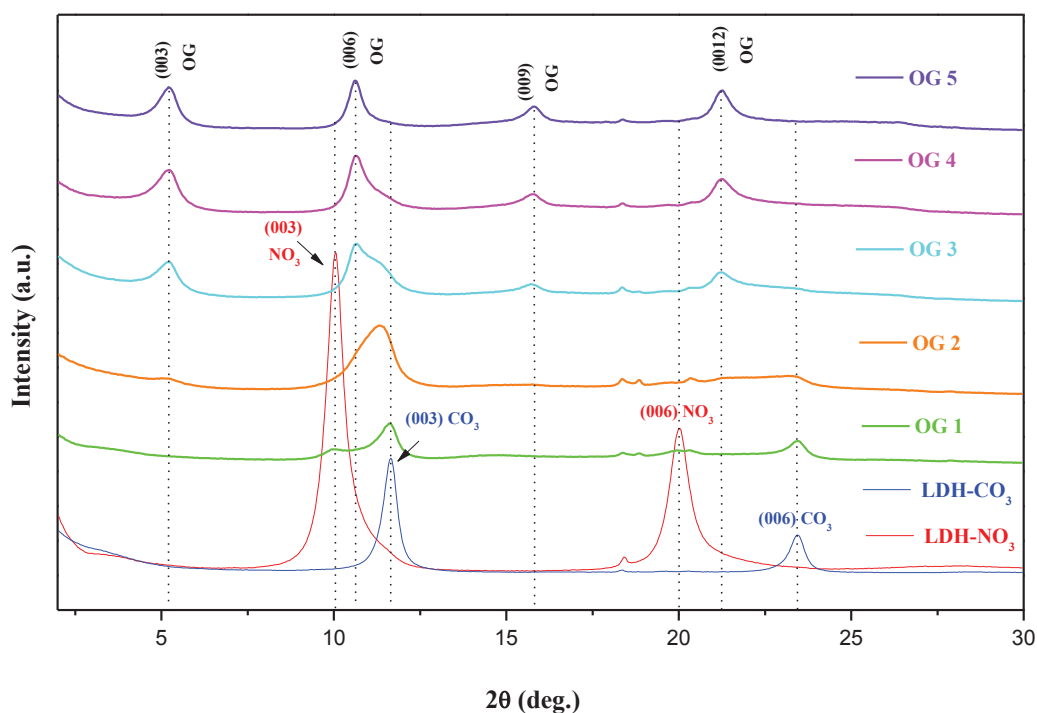


**Figure 6.** X-ray diffraction patterns in the 2θ range from 2° to 30° for the intercalation of OG in the Mg-Al-LDH-NO<sub>3</sub> structure corresponding to 5 points in the OG adsorption isotherm (as marked by crosses in **Figure 3**).

#### 4. Conclusions

The combination of various experimental techniques has been applied to study some important aspects of the adsorption of azo anionic dyes from aqueous solutions onto Mg-Al-LDH sample containing nitrate anions in the interlayer space. Despite certain differences in the kinetic behavior among Methyl Orange, Orange II, and Orange G, the adsorption equilibrium is attained after 200 min at the last; the kinetic rate is the highest for OII and the lowest for MO. The dye retention kinetics obeys the pseudo-second order kinetic model, thereby indicating a strong interaction between the dye units and the LDH host structure. The maximum amount of dye retained in the adsorption plateau region increases in the order: MO >> OII > OG. This trend can be first rationalized when taking into account the differences in the molecular sizes, electrical charges and hydrophobic character of the molecules. In the case of MO, the maximum dye adsorption exceeds the anionic exchange capacity of the pristine LDH material. The retention of the MO units on the external surface and their aggregation inside the interlayer space may be considered to explain this result, which has never been obtained before. The uptake of dye anions by the LDH material can be accompanied by the co-adsorption of Na<sup>+</sup> cations and this is a second original contribution of the present study to improve the understanding of the adsorption mechanism. For OII, the Na<sup>+</sup> co-adsorption is observed for all points in the adsorption isotherm and, on average, one sodium cation is retained per 3 OII units. In the case of the two other dyes, the co-adsorption of sodium becomes noticeable only for higher dye uptakes. The detailed analysis of XRD patterns recorded on different LDH samples loaded with varying amounts of dye species showed that MO, OII, and OG anions are intercalated into the interlayer space of the Mg-Al-LDH-NO<sub>3</sub> structure, thereby displacing nitrate anions to the supernatant aqueous phase. This intercalation step is paralleled by the expansion of the basal interlayer distance ( $d_{003}$ ) of the host LDH lattice from 0.89 nm to 2.42 nm, MO; 2.22 nm, OII; 1.68 nm, OG.

In summary, Mg-Al-LDH has been proven to be a good adsorbent for the three Orange-like dyes molecules. The results reported in the present paper indicate the complex mechanism of the adsorption phenomenon involving several species which can either compete against one another for the active sites at the LDH surface or they can give rise to a co-operative adsorption. The overall mechanism is exothermic, especially in the case of MO. This result is at variance with the endothermic character previously reported in the literature on the basis of the modeling studies.

Further study on the OII adsorption is necessary to explain the variations of the enthalpy of displacement at higher adsorbed amounts.

### Acknowledgment

The authors are grateful to Mr. Bernard Fraisse for his assistance with the XRD measurements and to Mr. Amine Geneste for his valuable help with calorimetric experiments.

### References

1. Verma, A. K.; Dash, R. R.; Bhunia, P., A review on chemical coagulation/flocculation technologies for removal of colour from textile wastewaters. *Journal of Environmental Management* **2012**, *93*, 154-168.
2. Geethakarathi, A.; Phanikumar, B. R., Industrial sludge based adsorbents/industrial by-products in the removal of reactive dyes – A review. *International Journal of Water Resources and Environmental Engineering* **2011**, *3*, 1-9.
3. Costantino, U.; Coletti, N.; Nocchetti, M.; Aloisi, G. G.; Elisei, F., Anion exchange of methyl orange into Zn-Al synthetic hydroxalite and photophysical characterization of the intercalates obtained. *Langmuir* **1999**, *15*, 4454-4460.
4. Ni, Z.-M.; Xia, S.-J.; Wang, L.-G.; Xing, F.-F.; Pan, G.-X., Treatment of methyl orange by calcined layered double hydroxides in aqueous solution: adsorption property and kinetic studies. *Journal of Colloid and Interface Science* **2007**, *316*, 284-291.
5. El Gaini, L.; Lakraimi, M.; Sebbar, E.; Bakasse, M., Removal of methyl orange dye from water to zinc-aluminium-chloride layered double hydroxides. *Journal of Optoelectronics and Advanced Materials* **2008**, *10*, 1415-1420.
6. Mandal, S.; Lerner Dan, A.; Marcotte, N.; Tichit, D., Structural characterization of azoic dye hosted layered double hydroxides. *Zeitschrift für Kristallographie International journal for structural, physical, and chemical aspects of crystalline materials*, 2009; Vol. 224, p 282.
7. Morimoto, K.; Tamura, K.; Iyi, N.; Ye, J.; Yamada, H., Adsorption and photodegradation properties of anionic dyes by layered double hydroxides. *Journal of Physics and Chemistry of Solids* **2011**, *72*, 1037-1045.
8. Zhang, P.; Wang, T.; Qian, G.; Wu, D.; Frost, R. L., Removal of methyl orange from aqueous solutions through adsorption by calcium aluminate hydrates. *Journal of Colloid and Interface Science* **2014**, *426*, 44-47.
9. Zhou, K.; Zhang, Q.; Wang, B.; Liu, J.; Wen, P.; Gui, Z.; Hu, Y., The integrated utilization of typical clays in removal of organic dyes and polymer nanocomposites. *Journal of Cleaner Production* **2014**, *81*, 281-289.

10. Zhang, P.; Qian, G.; Shi, H.; Ruan, X.; Yang, J.; Frost, R. L., Mechanism of interaction of hydrocalumites (Ca/Al-LDH) with methyl orange and acidic scarlet GR. *Journal of Colloid and Interface Science* **2012**, *365*, 110-116.
11. Li, Z.; Yang, B.; Zhang, S.; Wang, B.; Xue, B., A novel approach to hierarchical sphere-like ZnAl-layered double hydroxides and their enhanced adsorption capability. *Journal of Materials Chemistry A* **2014**, *2*, 10202-10210.
12. Zheng, Y.-M.; Li, N.; Zhang, W.-D., Preparation of nanostructured microspheres of Zn-Mg-Al layered double hydroxides with high adsorption property. *Colloids and Surfaces A: Physicochemical and Engineering Aspects* **2012**, *415*, 195-201.
13. Ai, L.; Zhang, C.; Meng, L., Adsorption of methyl orange from aqueous solution on hydrothermal synthesized Mg-Al layered double hydroxide. *Journal of Chemical & Engineering Data* **2011**, *56*, 4217-4225.
14. Zaghouane-Boudiaf, H.; Boutahala, M.; Arab, L., Removal of methyl orange from aqueous solution by uncalcined and calcined MgNiAl layered double hydroxides (LDHs). *Chemical Engineering Journal* **2012**, *187*, 142-149.
15. Monash, P.; Pugazhenth, G., Utilization of calcined Ni-Al layered double hydroxide (LDH) as an Adsorbent for removal of methyl orange dye from aqueous solution. *Environmental Progress & Sustainable Energy* **2014**, *33*, 154-159.
16. Mustapha Bouhent, M.; Derriche, Z.; Denoyel, R.; Prevot, V.; Forano, C., Thermodynamical and structural insights of orange II adsorption by Mg<sub>R</sub>AlNO<sub>3</sub> layered double hydroxides. *Journal of Solid State Chemistry* **2011**, *184*, 1016-1024.
17. Benselka-Hadj Abdelkader, N.; Bentouami, A.; Derriche, Z.; Bettahar, N.; de Ménorval, L. C., Synthesis and characterization of Mg-Fe layer double hydroxides and its application on adsorption of Orange G from aqueous solution. *Chemical Engineering Journal* **2011**, *169*, 231-238.
18. Extremera, R.; Pavlovic, I.; Pérez, M.; Barriga, C., Removal of acid orange 10 by calcined Mg/Al layered double hydroxides from water and recovery of the adsorbed dye. *Chemical Engineering Journal* **2012**, *213*, 392-400.
19. Laguna, H.; Loera, S.; Ibarra, I. A.; Lima, E.; Vera, M. A.; Lara, V., Azoic dyes hosted on hydrotalcite-like compounds: Non-toxic hybrid pigments. *Microporous and Mesoporous Materials* **2007**, *98*, 234-241.
20. Gil, A.; Assis, F. C. C.; Albeniz, S.; Korili, S. A., Removal of dyes from wastewaters by adsorption on pillared clays. *Chemical Engineering Journal* **2011**, *168*, 1032-1040.
21. Lee, S. M.; Tiwari, D., Organo and inorgano-organo-modified clays in the remediation of aqueous solutions: An overview. *Applied Clay Science* **2012**, *59-60*, 84-102.
22. Rives, V.; Angeles Ulibarri, M. a., Layered double hydroxides (LDH) intercalated with metal coordination compounds and oxometalates. *Coordination Chemistry Reviews* **1999**, *181*, 61-120.
23. Sato, T.; Fujita, H.; Endo, T.; Shimada, M.; Tsunashima, A., Synthesis of hydrotalcite-like compounds and their physico-chemical properties. *Reactivity of Solids* **1988**, *5*, 219-228.

24. Elmoubarki, R.; Mahjoubi, F. Z.; Tounsadi, H.; Moustadraf, J.; Abdennouri, M.; Zouhri, A.; El Albani, A.; Barka, N., Adsorption of textile dyes on raw and decanted Moroccan clays: Kinetics, equilibrium and thermodynamics. *Water Resources and Industry* **2015**, *9*, 16-29.
25. Rives, V., *Layered double hydroxides: present and future*; Nova Publishers, 2001.
26. Mandal, S.; Tichit, D.; Lerner, D. A.; Marcotte, N., Azoic Dye Hosted in Layered Double Hydroxide: Physicochemical Characterization of the Intercalated Materials. *Langmuir* **2009**, *25*, 10980-10986.
27. Ay, A. N.; Birgul, Z.-K., Luis, Mafra ; Mafra, L., A Simple Mechanochemical Route to Layered Double Hydroxides: Synthesis of Hydrotalcite-Like Mg-Al-NO<sub>3</sub>-LDH by Manual Grinding in a Mortar. *Zeitschrift für anorganische und allgemeine Chemie* **2009**, *635*, 1470-1475.
28. Lagergren, S., *Zur theorie der sogenannten adsorption gelöster stoffe: Kungliga Svenska Vetenskapsakademiens; Handlingar*, 1898.
29. Ho, Y.-S.; McKay, G., Pseudo-second order model for sorption processes. *Process Biochemistry* **1999**, *34*, 451-465.
30. Ho, Y.-S.; McKay, G., Kinetic models for the sorption of dye from aqueous solution by wood. *Process Safety and Environmental Protection* **1998**, *76*, 183-191.
31. Prelot, B.; Ayed, I.; Marchandea, F.; Zajac, J., On the real performance of cation exchange resins in wastewater treatment under conditions of cation competition: the case of heavy metal pollution. *Environmental Science and Pollution Research* **2014**, *21*, 9334-9343.
32. Chen, H.; Dai, G.; Zhao, J.; Zhong, A.; Wu, J.; Yan, H., Removal of copper(II) ions by a biosorbent-Cinnamomum camphora leaves powder. *Journal of Hazardous Materials*, *177*, 228-236.
33. Arami, M.; Limaee, N. Y.; Mahmoodi, N. M., Evaluation of the adsorption kinetics and equilibrium for the potential removal of acid dyes using a biosorbent. *Chemical Engineering Journal* **2008**, *139*, 2-10.
34. Poots, V. J. P.; McKay, G.; Healy, J. J., Removal of basic dye from effluent using wood as an adsorbent. *Journal (Water Pollution Control Federation)* **1978**, *926-935*.
35. Giles, C. H.; MacEwan, T.; Nakhwa, S.; Smith, D., Studies in adsorption. Part XI. A system of classification of solution adsorption isotherms, and its use in diagnosis of adsorption mechanisms and in measurement of specific surface areas of solids. *Journal of the Chemical Society* **1960**, 3973-3993.
36. Reeves, R. L.; Harkaway, S. A., Surface tensions of aqueous solutions of some azo dye sulfonates and analogs. *Journal of Colloid and Interface Science* **1978**, *64*, 342-347.
37. Madhavan, J.; Grieser, F.; Ashokkumar, M., Degradation of orange-G by advanced oxidation processes. *Ultrasonics Sonochemistry* **2010**, *17*, 338-343.
38. Châtelet, L.; Bottero, J. Y.; Yvon, J.; Bouchelaghem, A., Competition between monovalent and divalent anions for calcined and uncalcined hydrotalcite: anion exchange and adsorption sites. *Colloids and Surfaces A: Physicochemical and Engineering Aspects* **1996**, *111*, 167-175.

39. Lydon, J., Chromonic liquid crystal phases. *Current Opinion in Colloid & Interface Science* **1998**, *3*, 458-466.
40. Marangoni, R.; da Costa Gardolinski, J. E. F.; Mikowski, A.; Wypych, F., PVA nanocomposites reinforced with Zn<sub>2</sub>Al LDHs, intercalated with orange dyes. *Journal of Solid State Electrochemistry* **2011**, *15*, 303-311.
41. Géraud, E.; Bouhent, M.; Derriche, Z.; Leroux, F.; Prévot, V.; Forano, C., Texture effect of layered double hydroxides on chemisorption of Orange II. *Journal of Physics and Chemistry of Solids* **2007**, *68*, 818-823.
42. Liu, L.-Y.; Pu, M.; Yang, L.; Li, D.-Q.; Evans, D. G.; He, J., Experimental and theoretical study on the structure of acid orange 7-pillared layered double hydroxide. *Materials Chemistry and Physics* **2007**, *106*, 422-427.
43. Melánová, K.; Beneš, L.; Zima, V.; Svoboda, J., Intercalation of dyes containing SO<sub>3</sub>H groups into Zn–Al layered double hydroxide. *Journal of Inclusion Phenomena and Macrocyclic Chemistry* **2005**, *51*, 97-101.
44. Marangoni, R.; Ramos, L. P.; Wypych, F., New multifunctional materials obtained by the intercalation of anionic dyes into layered zinc hydroxide nitrate followed by dispersion into poly (vinyl alcohol)(PVA). *Journal of Colloid and Interface Science* **2009**, *330*, 303-309.

## SUPPORTING INFORMATION I

### S1. Characteristics of Mg-Al-LDH-NO<sub>3</sub> solid and dye molecules

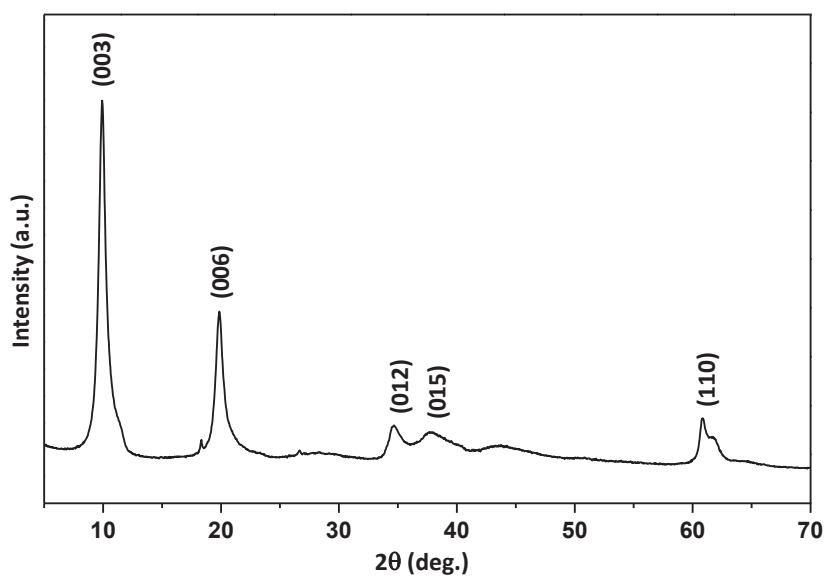
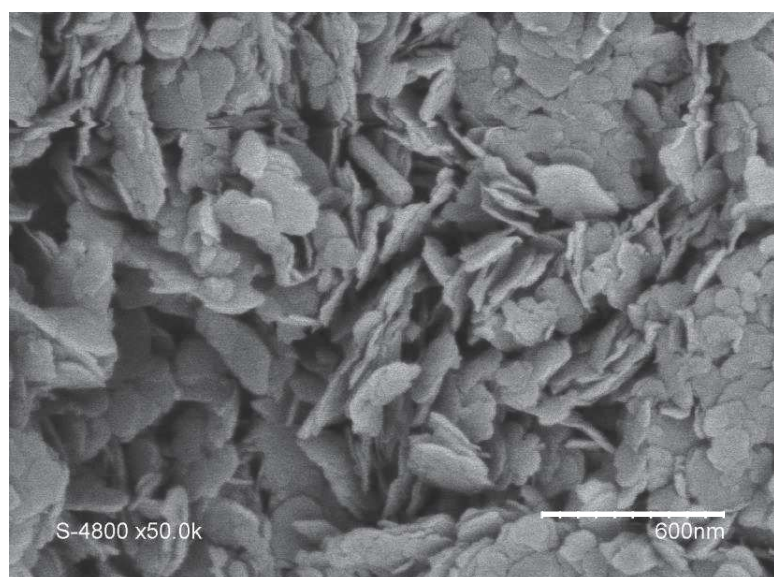


Figure S 1. SEM image (upper panel) and X-ray powder diffraction pattern (lower panel) of Mg-Al-LDH-NO<sub>3</sub>

The morphology of adsorbent was observed by scanning electron microscopy (SEM). Figure S 1 (upper panel) shows the typical SEM images of the Mg-Al-LDH-NO<sub>3</sub> with well defined layered platelets. The structure of layered double hydroxide was inferred from the XRD analysis Figure S 1 (lower panel). This type of material crystallizes in hexagonal lattice with *R-3m* rhombohedral symmetry [45, 46]. The diffractogram exhibits the structure with a series of *00l* peaks, such as (003), (006) and (009) which contains information about the cell parameters. The parameters *c* and *a* can be estimated from the (003) ( $c = 3d_{003}$ ) and (011) ( $a = 2d_{110}$ ) positions, respectively [26]. The *c* value of 2.6 nm agrees with those previously reported in literature for Mg/Al LDH [16, 25, 26]. It was used to calculate basal spacing [47] of the layered material,  $d_{003} = 0.89$  nm. The layer thickness of brucite-like minerals is 0.48 nm [46] and the interlayer spacing is therefore 0.41 nm. This is in agreement with the diameter of the nitrate anion (0.4 nm) [48].

### *S2. Repeatability and experimental uncertainties*

The repeatability and experimental uncertainties of the adsorption measurements were tested in the following manner: (1) the measurements were carried out twice by adding new points to the sorption curve obtained in a previous experiment under the same experimental conditions (such points had been selected to represent low, medium, and high concentrations and they were subsequently integrated into the sorption curves reported in the manuscript); (2) the sorption experiments were repeated independently by following the same measurement procedures. In the pre-plateau region, the greatest deviations between the corresponding adsorption curves were: 10%, MO; 17%, OII; 7%, OG. In the plateau region, these deviations were: 4%, MO; 23%, OII; 3%, OG.

### S3. Kinetic Models

For the various models, the kinetic constants of adsorption were calculated and the linear regression correlation coefficient ( $R^2$ ) values were compared to evaluate the best fit model.

The Lagergren-pseudo-first order model can be described by the following linear form:

$$\log(q_l - q_t) = \log(q_l) - \frac{k_1}{2.303} t \quad (S1)$$

where  $q_l$  and  $q_t$  are the amounts of the dye adsorbed at equilibrium and at time  $t$ , respectively;  $k_1$  is the equilibrium rate constant in the pseudo-first order model. Values of  $k_1$  and  $R^2$  were found from the linear plots of  $\log(q_l - q_t)$  vs. time.

The pseudo-second order kinetic model is expressed as follow:

$$\frac{t}{q_t} = \frac{1}{k_2 q_e^2} + \frac{1}{q_e} t \quad (S2)$$

$$h = k_2 q_e^2 \quad (S3)$$

where:

$h$  is the initial sorption rate;  $q_e$  is the amount of the dye adsorbed at equilibrium and  $k_2$  is the equilibrium rate constant in the pseudo-second order model. They can be calculated from the slope of the plot of  $t/q_t$  as a function of time.

The Weber's interparticule diffusion model equation may written as follows:

$$q_t = k_{id} t^{0.5} + C \quad (S4)$$

where:

$k_{id}$  is the equilibrium rate constant of the interparticule diffusion model. The plots of  $q_t$  as a function of  $t^{0.5}$  should represent straight lines and were used to obtain the rate constants.

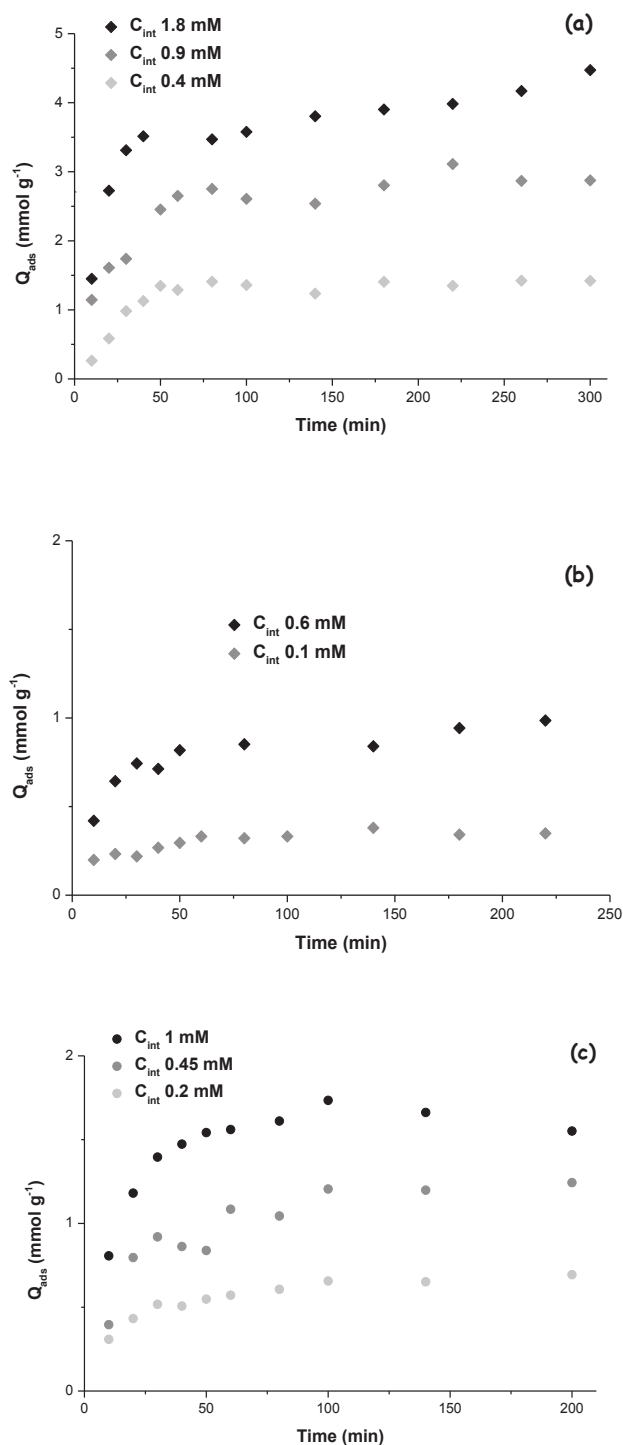


Figure S 2. Amount of MO (a), OII (b) and OG (c) adsorbed onto Mg-Al-LDH-NO<sub>3</sub> as a function of the contact time for different initial concentrations.

Table S 1. Kinetic parameters of Orange dyes adsorption onto Mg-Al LDHs for different initial dye concentrations.

C <sub>o</sub> (mM)	q <sub>exp</sub> (mmol/g)	Lagergren-first-order			Pseudo-second order			Intra-particle mass transfer diffusion	
		q <sub>l. cal</sub> (mmol g <sup>-1</sup> )	k <sub>l</sub> (min <sup>-1</sup> )	R <sup>2</sup>	q <sub>e. cal</sub> (mmol g <sup>-1</sup> )	k <sub>2</sub> (mmol g <sup>-1</sup> min <sup>-1</sup> )	R <sup>2</sup>	k <sub>id</sub> (mmol g <sup>1</sup> min <sup>-1/2</sup> )	R <sup>2</sup>
0.4	1.64	0.66	0.005583	0.9227	1.61	0.035011	0.9916	0.05353	0.7918
0.9	3.25	1.17	0.015304	0.6689	3.08	0.020739	0.9935	0.10371	0.6862
1.8	4.47	2.34	0.008041	0.9204	4.64	0.008066	0.995	0.17724	0.8841
0.1	0.39	0.15	0.00674	0.8689	0.38	0.190567	0.9964	0.01091	0.7877
1.1	1.55	0.94	0.00492	0.6274	1.48	0.457593	0.97	0.05369	0.9592
0.17	0.74	0.32	0.00919	0.9293	0.71	0.118396	0.9849	0.0185	0.6359
0.45	1.42	0.62	0.00467	0.7353	1.41	0.02727	0.9891	0.03598	0.7358
1	1.76	0.34	0.00306	0.3532	1.70	0.079305	0.996	0.02745	0.4127

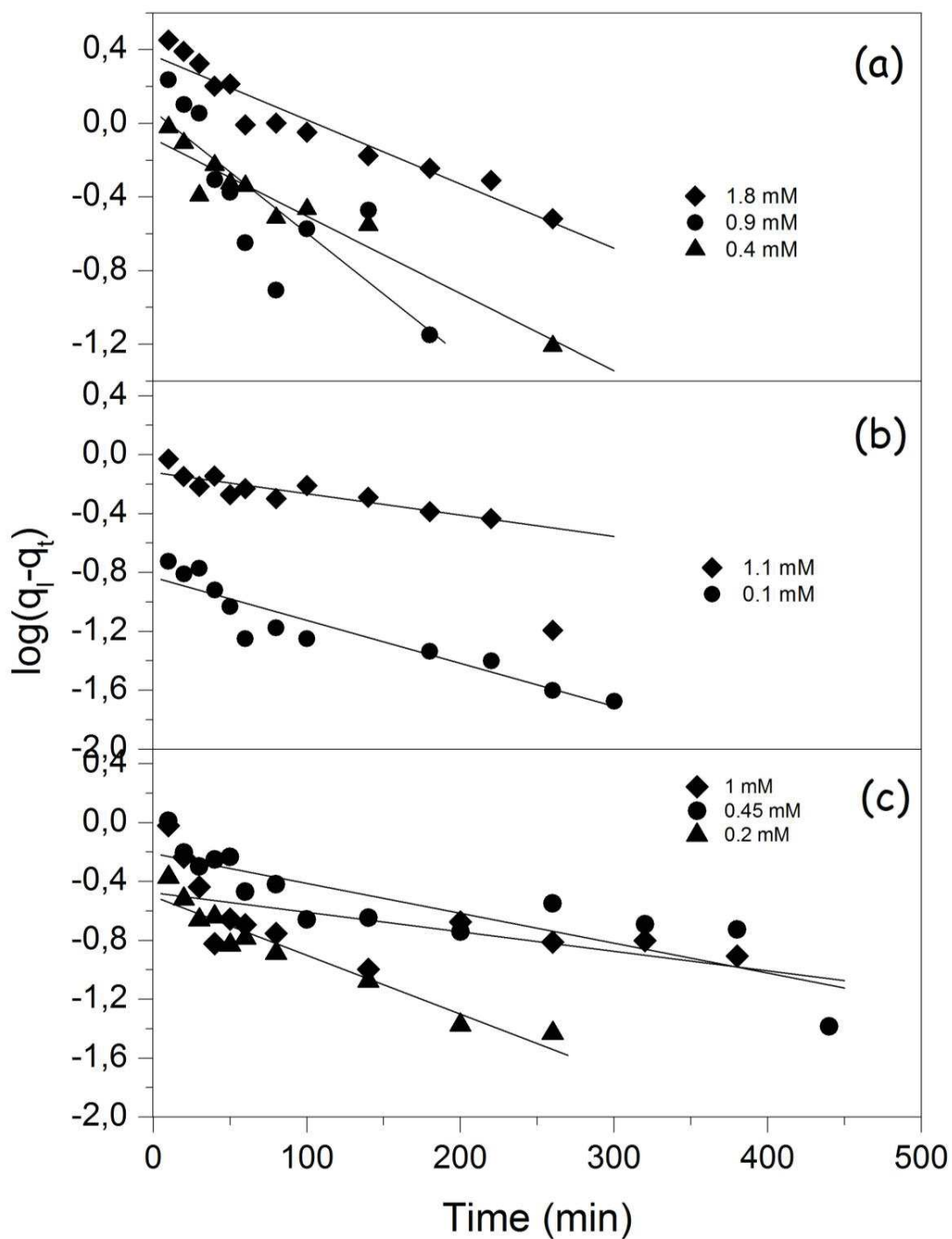


Figure S 3. First order sorption kinetics of MO (a), OII (b) and OG (c) adsorption onto Mg-Al-NO<sub>3</sub> LDH for different initial concentrations.

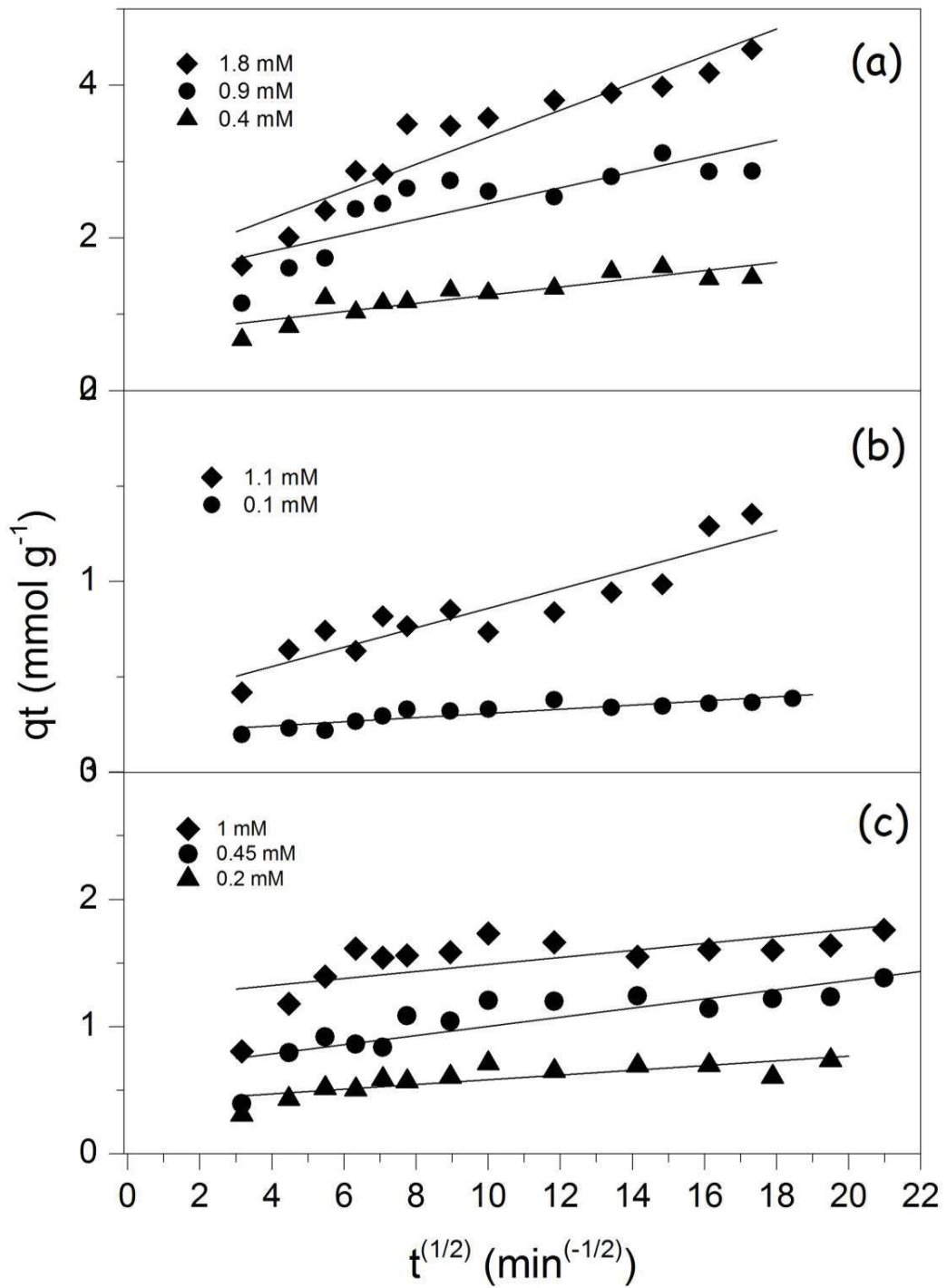


Figure S 4. Intra-particle mass transfer diffusion model for MO (a), OII (b) and OG (c) adsorption onto Mg-Al-NO<sub>3</sub> LDH for different initial dye concentrations.

1. Mandal, S.; Lerner Dan, A.; Marcotte, N.; Tichit, D., Structural Characterization of Azoic Dye Hosted Layered Double Hydroxides. In *Zeitschrift für Kristallographie*, 2009; Vol. 224, p 282.
2. Miyata, S., The Syntheses of Hydrotalcite-Like Compounds and Their Structures and Physico-Chemical Properties I: The Systems Mg<sup>2+</sup>-Al<sup>3+</sup>-NO<sub>3</sub><sup>-</sup>, Mg<sup>2+</sup>-Al<sup>3+</sup>-Cl<sup>-</sup>, Mg<sup>2+</sup>-Al<sup>3+</sup>-ClO<sub>4</sub><sup>-</sup>, Ni<sup>2+</sup>-Al<sup>3+</sup>-Cl<sup>-</sup> and Zn<sup>2+</sup>-Al<sup>3+</sup>-Cl. *Clays Clay Miner.* **1975**, 23, 369-375.
3. Mandal, S.; Tichit, D.; Lerner, D. A.; Marcotte, N., Azoic Dye Hosted in Layered Double Hydroxide: Physicochemical Characterization of the Intercalated Materials. *Langmuir* **2009**, 25, 10980-10986.
4. Rives, V., *Layered Double Hydroxides: Present and Future*; Nova Publishers, 2001.
5. Mustapha Bouhent, M.; Derriche, Z.; Denoyel, R.; Prevot, V.; Forano, C., Thermodynamical and Structural Insights of Orange I Adsorption by Mg<sub>3</sub>Al<sub>2</sub>(OH)<sub>6</sub> Layered Double Hydroxides. *J. Solid State Chem.* **2011**, 184, 1016-1024.
6. Suzuki, E.; Idemura, S.; Ono, Y., Properties of Hexacyanocobaltate (Iii)-Exchanged Hydrotalcite-Like Minerals. *Clays Clay Miner.* **1989**, 37, 173-178.
7. Ay, A. N.; Birgul, Z.-K., Luis, Mafra ; Mafra, L., A Simple Mechanochemical Route to Layered Double Hydroxides: Synthesis of Hydrotalcite-Like Mg-Al-NO<sub>3</sub>-Ldh by Manual Grinding in a Mortar. *Z. Anorg. Allg. Chem.* **2009**, 635, 1470-1475.

## II. On the origin of anomalous enthalpy effects accompanying the adsorption of Orange II onto Mg-Al Layered Double Hydroxide from aqueous solutions

*Ganna Darmograi, Benedicte Prelot\*, Amine Geneste, Jerzy Zajac*

Institut Charles Gerhardt de Montpellier, UMR-5253 CNRS-UM-ENSCM,  
C.C. 1502 Place Eugène Bataillon, F-34095 Montpellier cedex 5, France

## 1. Introduction

Understanding of the sorption mechanism is essential to improve suitable procedure for contaminant removal. Layered Double Hydroxides (LDHs) systems are well-known layered materials able to remove anionic pollutants [1-3]. Different experimental approaches are used to gain clear view on the mechanism of pollutant uptake onto various types of sorbents, together with all the related hidden contribution to the overall process. Equilibrium sorption isotherms, together with X-ray diffraction and Fourier Transform Infrared (FTIR) spectroscopy are the most widely reported techniques in the literature for the adsorption of hazardous species onto layered materials [4-6]. Effects of pHs, of temperature, of adsorbent dosage, sorption kinetics, ... are also parameters regularly used to understand the removal mechanisms from the solvent environment [7-11]. Some of these authors occasionally calculate thermodynamic parameters such as, the standard Gibbs free energy ( $\Delta G^\circ$ ), enthalpy ( $\Delta H^\circ$ ) and entropy ( $\Delta S^\circ$ ) to evaluate the thermodynamics of the pollutant uptake [9, 10, 12]. Their thermodynamic description is based on modelled isotherm, and the temperature dependence of the constants giving access to the enthalpy and entropy terms (the so-called Van't Hoff approach to evaluate  $\Delta H$  and  $\Delta S$ ). However, it is shown from previous study that estimation of the endo- or exothermicity of removal process based on simulated isotherm could give contradictory results compared to the direct experimental achievement [13]. Indeed, there are several contributions to the overall enthalpy change upon displacement. The cumulative enthalpy represents a global effect combining all various contributions involved in the sorption process. This includes such different contributions as, the intercalation of the adsorbed species, interlayer anion displacement, swelling (expansion or compression) of the layers, hydration / dehydration of the exchanged species, the displacement of other species (e.g. uptake of Na, uptake/release of protons) and the dewetting of the solid surface (sorption on external surface, etc). All these contribution are not always taken into account in the simulation of modeled isotherm. That is why ITC was used to assess the global heat effect accompanying the sorption process. The key point of this work is the use of calorimetry to measure directly the overall heat effect of displacement, combined with other experimental techniques, and to decompose the overall heat effect of sorption so as to identify these various contributions. The literature on the thermodynamic of sorption onto LDHs is not abundant. Due to the complexity of these systems, very few works

based on ITC report the pollutants uptake [14-16]. Israëli et al. were the first to report the enthalpies of anion exchange on Zn-Al-LDH-Cl using microcalorimeter titration [15]. The heats effect associated with the exchange of Cl<sup>-</sup> for F<sup>-</sup>, Br<sup>-</sup>, I<sup>-</sup>, OH<sup>-</sup>, NO<sub>3</sub><sup>-</sup> and SO<sub>4</sub><sup>2-</sup> anions were measured as well as the standard molar enthalpies of these exchange reactions. The variation of the standard molar enthalpy was found to be dependent of the nature of the anions. They demonstrate that the anions can be either weakly or strongly hydrated upon intercalation. Hence, they concluded that anion selectivity on LDHs is mainly governed by enthalpic aspect, while the exchange processes appear to be more entropy - driven. Later on, the same research group presented thermodynamic study of dicarboxylate anions exchange onto the same LDHs [14]. Four different organics anions were tested: oxalate, succinate, adipate and tartrate. Interestingly that almost for all organics moieties exchange with Cl<sup>-</sup> was endothermic process contrary to exothermic exchange of the common anions. The only exception was tartrate, bearing an -OH groups in its structure, which exhibited an exothermic behavior. This could be due to the partial dehydration of -OH upon intercalation during the uptake process as well as to the formation of hydrogen bonding between the -OH group of the tartrate anions and the CH<sub>2</sub> groups.

In our previous study [17], the exchange – adsorption from aqueous solutions of three azo dyes, Methyl Orange (MO), Orange II (OII), and Orange G (OG), onto Mg-Al-LDH-NO<sub>3</sub> Layered Double Hydroxides (LDH, molar Mg:Al ratio of 2) was investigated through monitoring all retained and removed species in combination with direct calorimetry and X-ray diffraction measurements. Despite some marked differences between the three enthalpy curves, the general conclusion drawn from the calorimetric measurements is that the overall process of displacement has an exothermic character. However, in the particular case of the OII sorption onto LDH at high surface coverage, a new strongly exothermic contribution to the total enthalpy of displacement became noticeable, whose trend was difficult to explain on the basis of the obtained results. The objective of the present work is to describe in details the anomalous enthalpy effects accompanying the adsorption of Orange II onto Mg-Al Layered Double Hydroxide from aqueous solutions using mainly Isotherm Titration Calorimetry (ITC).

## ***2. Materials and methods***

All experiments were performed on the as-prepared Mg-Al-LDH-NO<sub>3</sub>. The synthesis and characterization of adsorbent were described previously [17]. Except for titration calorimetry, the detailed descriptions of the experimental procedure are given in the Supporting Information. A differential TAM III microcalorimeter combined with titration cell was used to measure the enthalpy changes accompanying the removal of dye species from aqueous solutions Mg-Al-LDH-NO<sub>3</sub> materials or their interaction with species in solution. Prior to each calorimetric run, for the experiment in suspension with the presence of LDH particles, a sample of about 1-2 mg of LDH powder was suspended in 0.8 mL of distilled water in the calorimetric cell. For experiments in solution, 0.8 mL of Mg(NO<sub>3</sub>)<sub>2</sub> or Al(NO<sub>3</sub>)<sub>3</sub> (7 mmol L<sup>-1</sup>) was placed in the measuring cell. A second cell containing only the solvent is used as a reference. Then, both cells were placed inside the microcalorimeter and the thermal equilibrium was reached after 2-4 h. The injection system was equipped with a syringe filled with the appropriate stock solution of 14 mmol L<sup>-1</sup> OII dye. For the interaction of OII with Mg(II) or Al(III), syringe was filled with 5 mmol L<sup>-1</sup> OII solution. Successive injections of the 10 μL aliquots of a given stock solution during 10 sec resulted in an electric signal directly fed into a computer; the digitized signal representing the related thermal peaks was recorded with an equilibration time of 45 min applied between 2 injections. Integration of the areas under the thermal peaks was performed and the resulting enthalpy values were related to the mass of LDH in the cell or the molar ratio. For the sorption experiments, similar procedures were applied to evaluate the effects of dilution and to correct the enthalpy values accordingly [13]. The same type of procedure was used for the experiment in solution. Agitation in the cell was ensured using home-made Teflon or commercial gold stirrer, with 120 or 90 tpm for suspension or solution measurements respectively. Heat flow measured at 25 °C.

### 3. Results and Discussion

The capacity of Mg-Al-LDH-NO<sub>3</sub> to remove the dyes from aqueous solutions was followed by sorption isotherms. In the previous work [17] we reported that dye adsorption isotherms (H2-type) showed some differences in the maximum adsorption quantity (5.5 mmol g<sup>-1</sup>, MO; 2.7 mmol g<sup>-1</sup>, OII; 1.7 mmol g<sup>-1</sup>, OG), consistent with anionic exchange capacity and sorption on the external surface, depending on the cross-sectional area of the dye species and with their hydrophobic-hydrophilic character. MO and OG sorption isotherms exhibit higher affinity, with sharp slope at low initial concentrations. For OII, there is also high interaction for amount adsorbed lower than 1 meq g<sup>-1</sup>, and then the slope decreases, meaning lower interactions and modifications of the sorption process before complete exchange (AEC). Further XRD analysis has shown the presence of one unattributed peak that was probably related to specific interactions between OII and LDH. The cumulative enthalpy of displacement was negative in conformity with the exothermic character of the overall process. The exothermic effect of displacement accompanying the retention of MO species is much more marked than that of OG adsorption, with decrease and stabilization after completing the exchange to about -90 J g<sup>-1</sup> and -10 J g<sup>-1</sup> respectively. This is correlated with the less hydrophobic nature of OG in comparison to MO [18, 19]. However, the enthalpy variations for OII do not follow the same trend.

As observed on the Figure 7, for OII sorption, after a short ‘hesitation’ interval, a new strongly exothermic contribution to the total enthalpy of displacement becomes significant. This modification of the enthalpy curve is consistent with the change of the shape of the sorption isotherm. In order to compare two analysis, isothermal and enthalpy plots were divided on the zones. Zone I is attributed to the low values of OII amount adsorbed (<1 meq g<sup>-1</sup>), while Zone II for higher values of amount adsorbed (>1 meq g<sup>-1</sup>). In Zone I, the sharp slope, which indicates the high affinity between OII and LDH (upper panel), characterizes adsorption phenomenon and this adsorbent-adsorbate interactions are described by exothermic effect (lower panel). In addition, the end of the sharp slope occurs when the cumulative enthalpy curve reaches its pseudo-plateau.

In Zone II the sorption isotherm exhibits an inflexion, however OII continue to adsorb ‘slowly’ with the increase in its equilibrium concentration. Moreover, the enthalpy curve is no more stable in this zone, and can be characterized by the monotonous decrease in the values of

cumulative enthalpy from -10 to -25 J g<sup>-1</sup>. The results obtained in the first Zone I for both plots are consistent with the enthalpy curve for two another dyes (i.e. MO and OG) [17]. However, the results reported in the second Zone II, are unusual because of the two main reasons: no stabilization of isothermal plateau and no level off of the thermal effect of OII displacement are observed.

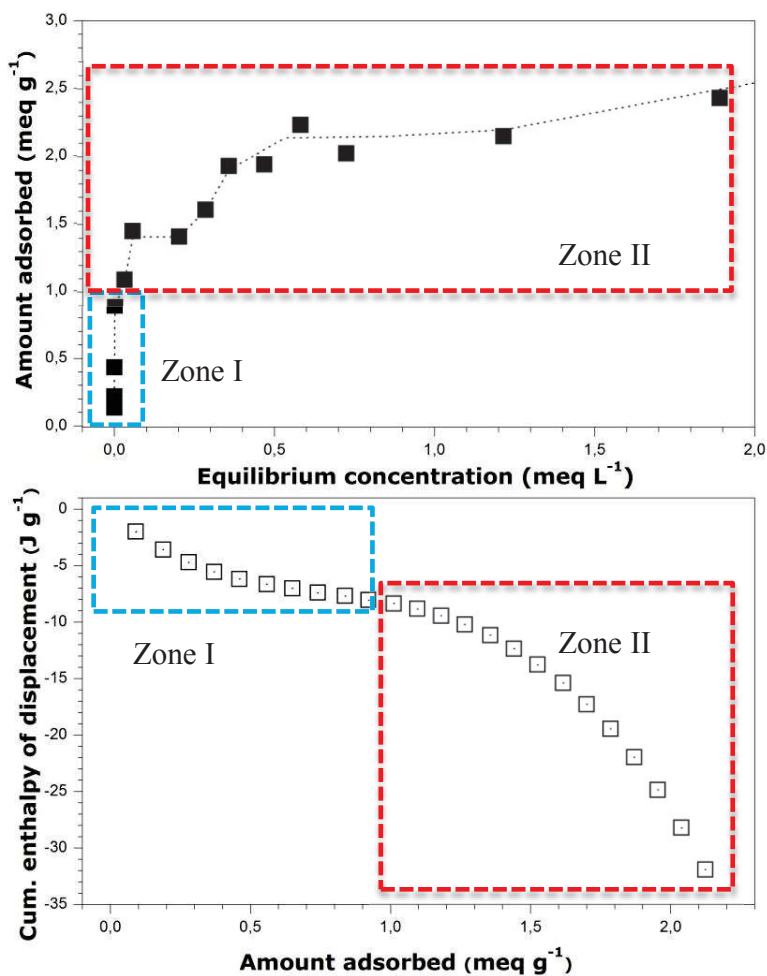


Figure 7. Sorption isotherm of OII on Mg-Al-LDH-NO<sub>3</sub> from aqueous solution (upper panel) and calculated cumulative enthalpies of displacement as a function of the OII amount adsorbed (lower panel).

Additional information have been obtained from the macroscopic observation of OII-LDH suspensions at bottom of the tubes. Hence, they exhibit cloudy supernatant, together with mixture of well-defined particles and sticky fibers (Figure S5 in Supporting Information). To have a

microscopic view of these newly formed aggregates, the LDH sample after adsorption of OII at high equilibrium concentration has been analyzed with TEM microscopy. To that purpose, small amount of particles have been removed from the bottom of the tube. Figure 8 (A, B) displays the fibers with 2D structure, formed during OII retention onto LDHs, together with LDHs particles beaded on the OII-fibers.

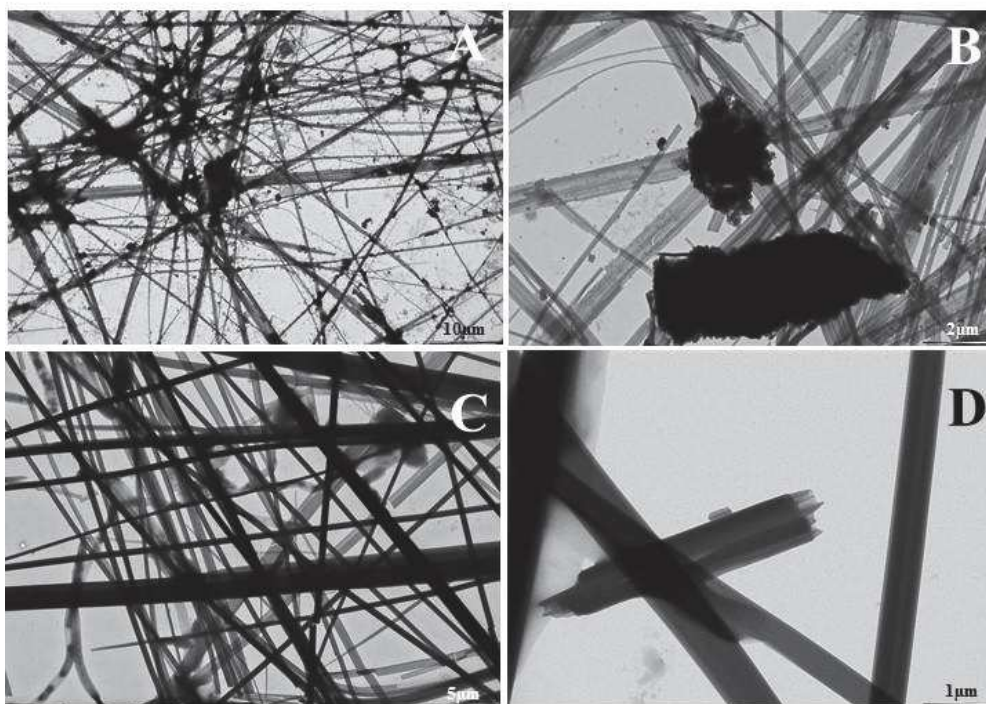


Figure 8. TEM images of fibers formed during adsorption onto LDHs (A, B) and by direct contact between OII Mg(NO<sub>3</sub>)<sub>2</sub> solution (C, D). In the presence of LDH (A, B), only a small part of the LDH solid particles was taken from in the base of the tube, with the aim to avoid too high number of particles and keep better image quality.

To have a further insight in this unexpected behavior, the supernatants after OII sorption onto LDH are carefully studied. Taking into account the composition of Mg-Al-LDH sorbent, free Mg(II) in the supernatant have been analyzed using Ionic chromatography (See Supporting Information). Points with different OII equilibrium concentrations between 1.4 to 2 mM have shown free Mg(II), with 0.09 mM, i.e. about 0.35 mmol released per gram of LDH. In addition, the same analysis was performed for MO dye and no free Mg(II) was observed after this dye uptake (results are not reported here). This indicates that in the presence of OII species Mg-Al-LDH adsorbent is partially dissolved. This is in contrast with MO, for which no dissolution occurs. This

could be explained by the ability of OII to interact strongly with Mg(II) cations, even with those presented inside the LDHs, leading to the partial dissolution of LDH, and the interaction between Mg(II) and OII.

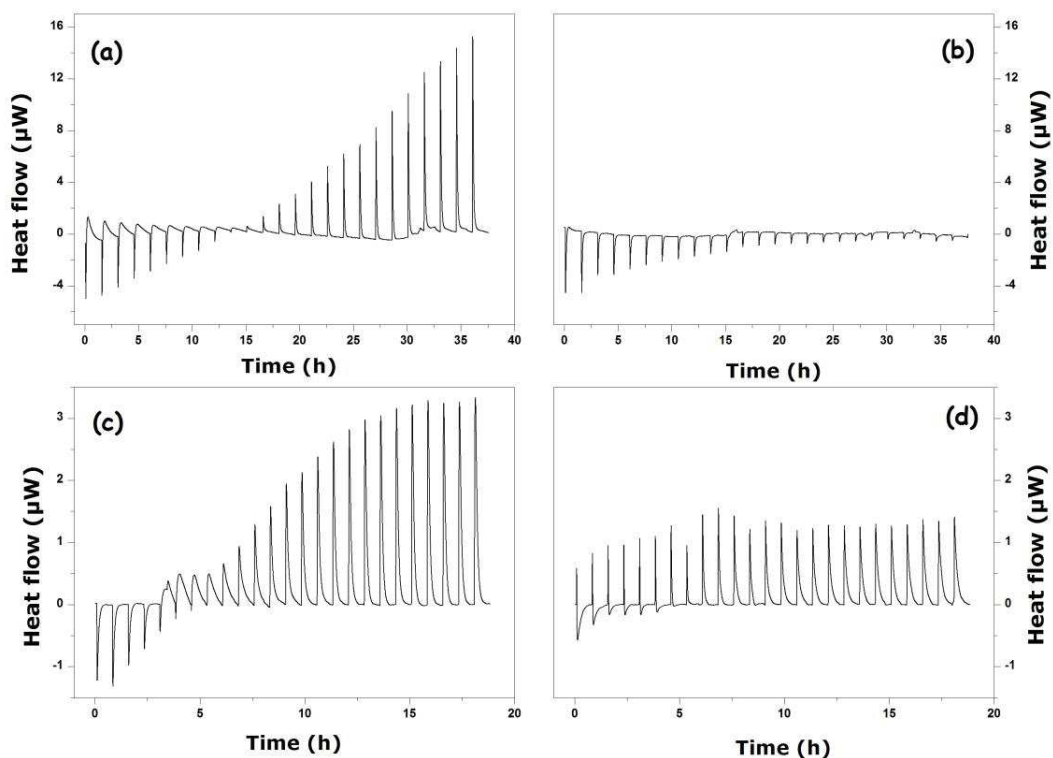


Figure 9. Thermograms for OII adsorption onto Mg-Al-LDH-NO<sub>3</sub> (a), OII dilution in water (under the same conditions as for sorption onto Mg-Al-LDH-NO<sub>3</sub>) (b), OII interaction with Mg(NO<sub>3</sub>)<sub>2</sub> (c) and with Al(NO<sub>3</sub>)<sub>3</sub> (d) solutions.

To have the information about thermal effect of the implying interaction between OII with Mg(II) as well as Al(III) to compare with those of OII adsorption onto LDH, calorimetric measurements were investigated and reported in Figure 9. In addition, thermal effect of OII dilution in ultrapure water was also reported in this figure. As observed, all the thermograms inhibit similar parts of the thermal effect curves.

For sorption experiments, the shape of thermograms is considered as conventional if the signal observed is due to the solute dilution, after the end of the sorption process and the saturation

plateau is reached. However, the profile of enthalpy curve is different for OII retention by LDH Figure 9 (a). For the first ten injections (OII amount adsorbed is around 1 meq g<sup>-1</sup>) performed during first 15 hours, two contributions are distinguished for each injection. The first one is the sharp endothermic effect that was correlated with OII dilution in water (see Figure 9 (b)). The second contribution is an exothermic broad signal that is probably the heat effect due to OII sorption onto LDH.

The global heat effect tends to zero when the sorption reaches 1 meq g<sup>-1</sup>, that is the part where the cumulative enthalpy of displacement is stabilized around -10 J g<sup>-1</sup>, i.e. Zone I, mentioned above. However, for the following injections the heat effect continues to grow, with the only visible exothermic contribution. Moreover, it becomes greater than expected heat effect due to OII dilution (endothermic effect). The profile of the thermogram obtained for OII in the presence of Mg(II) in solution Figure 9 (c) seems to be similar to that obtained for the complexation between organic molecules and cations. Hereafter, two different mechanisms were revealed for OII retained by LDH. Thus, the first exchange mechanism is followed by the aggregation of the molecules with the Mg(II) release during the LDH dissolution. From the ITC raw data obtained on OII dilution in Mg(II) solution, the following thermodynamic parameters have been calculated:  $n = 0,037$ ,  $\Delta H = 23,17 \text{ kJ mol}^{-1}$ .

To confirm the particular behavior of Mg(II) with OII, this newly formed phase has been visually observed in solution containing both Mg(II) and OII. Furthermore, their shapes were compared with particles and fibers obtained with LDHs contacted with OII with TEM (Figure 8 (C, D)). The observed particles formed during OII dilution in Mg(II) (Mg(NO<sub>3</sub>)<sub>2</sub>) solution presents the same shape and seems to have the same 2D dimensional structure. Their structural characterization has been performed using XRD analysis.

Figure 10 shows the XRD patterns of the LDH samples loaded with OII (1), fibers collected around the LDHs after sorption (2) together with the fibers / particles formed after during OII dilution in Mg(NO<sub>3</sub>)<sub>2</sub> solution (3). For Mg-Al-LDH-OII powder, the XRD patterns shows a typical character of OII dye intercalated in LDH structure with three harmonic peaks at (003), (006) and (009) corresponding to distances of 22.2, 11.1 and 7.4 Å [17]. The broad peak observed at 13° 2θ position appears at similar position compared to the one observed one pure fibers (see curve (3) on Figure 10). The diffractogram (2) presents the fibers, cautiously taken after the adsorption

experiment in order to avoid the presence of LDH, but a small quantity of LDHs particles are present in the OII aggregates and visible on the diffraction patterns (presence of harmonic peaks). At the same time, it can be observed that a highly pronounced sharp peak of OII aggregates at the same 13° 2θ position. This peak, together with those observed at 7, 9.8 and 14.5 ° 2θ positions are characteristic and are attributed to the formation of the fibers (see curve (3) on Figure 10).

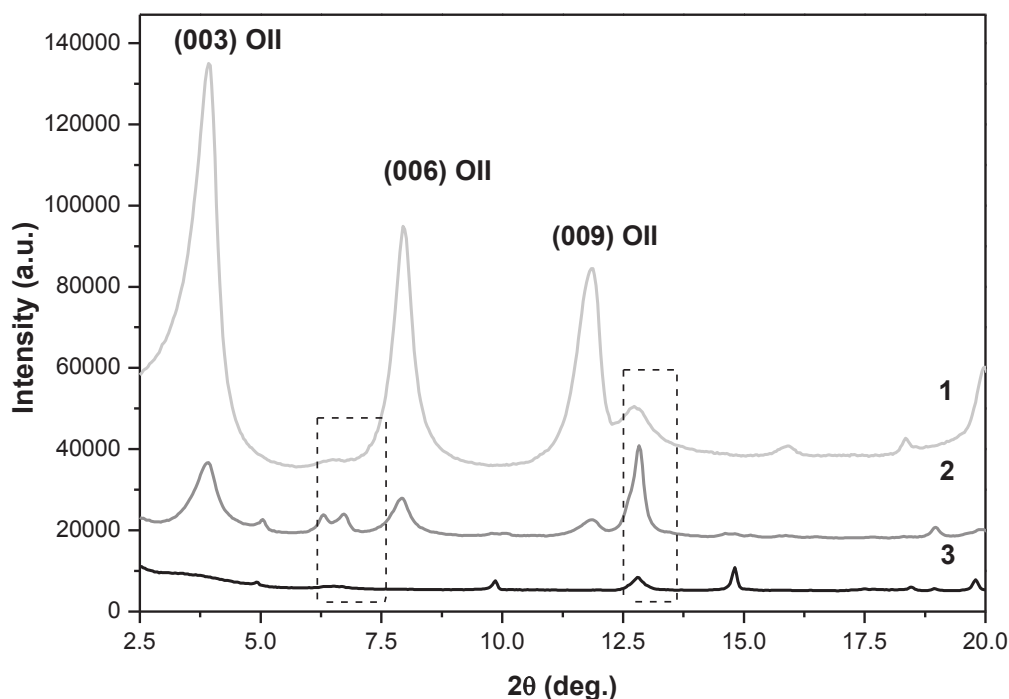


Figure 10. XRD patterns of Mg-Al-LDH-OII (1), fibers OII-LDH (2) and of fibers / particles formed during OII dilution in Mg(NO<sub>3</sub>)<sub>2</sub> (3).

## 5. Conclusion

Various contributions of the interactions between azo dyes OII in suspension with Mg-Al-LDH-NO<sub>3</sub> particles have been analyzed using Isothermal Titration Calorimetry. Adsorption exhibits an ionic exchange below 1 meq g<sup>-1</sup>, with cumulative enthalpy of displacement about -10 J g<sup>-1</sup>. For high OII equilibrium concentration, the reaction is still under process, and Mg(II) released from the LDHs have been evidenced. The free ions exhibit strong interactions with OII, which were characterized in solution to determine their thermodynamic parameters. The presence of the

aggregated OII fibers in solution or around the LDHs was confirmed by XRD and TEM microscopy.

### *Acknowledgements*

The authors greatly acknowledge the financial support of this work by the French Ministry of National Education, Higher Education and Research.

### *References*

- [1] X. Lei, M. Jin, G.R. Williams, Layered Double Hydroxides in the Remediation and Prevention of Water Pollution, *Energy and Environment Focus*, 3 (2014) 4-22.
- [2] F.L. Theiss, S.J. Couperthwaite, G.A. Ayoko, R.L. Frost, A review of the removal of anions and oxyanions of the halogen elements from aqueous solution by layered double hydroxides, *J. Colloid Interface Sci.*, 417 (2014) 356-368.
- [3] S.P. Newman, W. Jones, Synthesis, characterization and applications of layered double hydroxides containing organic guests, *New J. Chem.*, 22 (1998) 105-115.
- [4] X. Ruan, P. Sun, X. Ouyang, G. Qian, Characteristics and mechanisms of sorption of organic contaminants onto sodium dodecyl sulfate modified Ca-Al layered double hydroxides, *Chin. Sci. Bull.*, 56 (2011) 3431-3436.
- [5] P. Zhang, G. Qian, H. Shi, X. Ruan, J. Yang, R.L. Frost, Mechanism of interaction of hydrocalumites (Ca/Al-LDH) with methyl orange and acidic scarlet GR, *J. Colloid Interface Sci.*, 365 (2012) 110-116.
- [6] U. Costantino, N. Coletti, M. Nocchetti, G.G. Aloisi, F. Elisei, Anion exchange of methyl orange into Zn-Al synthetic hydrotalcite and photophysical characterization of the intercalates obtained, *Langmuir*, 15 (1999) 4454-4460.
- [7] T. Xue, Y. Gao, Z. Zhang, A. Umar, X. Yan, X. Zhang, Z. Guo, Q. Wang, Adsorption of acid red from dye wastewater by Zn<sub>2</sub>Al-NO<sub>3</sub> LDHs and the resource of adsorbent sludge as nanofiller for polypropylene, *J. Alloys Compd.*, 587 (2014) 99-104.
- [8] F.P. de Sá, B.N. Cunha, L.M. Nunes, Effect of pH on the adsorption of Sunset Yellow FCF food dye into a layered double hydroxide (CaAl-LDH-NO<sub>3</sub>), *Chem. Eng. J.*, 215 (2013) 122-127.
- [9] H. Zaghouane-Boudiaf, M. Boutahala, L. Arab, Removal of methyl orange from aqueous solution by uncalcined and calcined MgNiAl layered double hydroxides (LDHs), *Chem. Eng. J.*, 187 (2012) 142-149.
- [10] M.C. Alexandrica, M. Silion, D. Hritcu, M.I. Popa, Layered Double Hydroxides as adsorbents for anionic dye removal from aqueous solutions *Environmental Engineering and Management Journal*, 14 (2015) 381-388.

- [11] N.I. Taib, N. Kantasamy, S.M. Sumari, N.M. Rafi, Adsorption of arsenic (V) and phosphate onto MgAlNO<sub>3</sub>-LDHs, Humanities, Science and Engineering Research (SHUSER), 2012 IEEE Symposium IEEE, 2012, pp. 333-338.
- [12] P. Monash, G. Pugazhenti, Utilization of calcined Ni-Al layered double hydroxide (LDH) as an Adsorbent for removal of methyl orange dye from aqueous solution, Environmental Progress & Sustainable Energy, 33 (2014) 154-159.
- [13] B. Prelot, I. Ayed, F. Marchandea, J. Zajac, On the real performance of cation exchange resins in wastewater treatment under conditions of cation competition: the case of heavy metal pollution, Environmental Science and Pollution Research, 21 (2014) 9334-9343.
- [14] N. Morel-Desrosiers, J. Pisson, Y. Israëli, C. Taviot-Guého, J.-P. Besse, J.-P. Morel, Intercalation of dicarboxylate anions into a Zn-Al-Cl layered double hydroxide: microcalorimetric determination of the enthalpies of anion exchange, J. Mater. Chem., 13 (2003) 2582-2585.
- [15] Y. Israëli, C. Taviot-Guého, J.-P. Besse, J.-P. Morel, N. Morel-Desrosiers, Thermodynamics of anion exchange on a chloride-intercalated zinc-aluminum layered double hydroxide: a microcalorimetric study, J. Chem. Soc., Dalton Trans., DOI (2000) 791-796.
- [16] J. Zhu, Q. Huang, M. Pigna, A. Violante, Immobilization of acid phosphatase on uncalcined and calcined Mg/Al-CO<sub>3</sub> layered double hydroxides, Colloids and Surfaces B: Biointerfaces, 77 (2010) 166-173.
- [17] G. Darmograi, B. Prelot, G. Layrac, D. Tichit, G. Martin-Gassin, F. Salles, J. Zajac, Study of Adsorption and Intercalation of Orange-Type Dyes into Mg-Al Layered Double Hydroxide, Journal of Physical Chemistry C, Just Accepted September 22, doi : 10.1021/acs.jpcc.5b05510.
- [18] R.L. Reeves, S.A. Harkaway, Surface tensions of aqueous solutions of some azo dye sulfonates and analogs, J. Colloid Interface Sci., 64 (1978) 342-347.
- [19] J. Madhavan, F. Grieser, M. Ashokkumar, Degradation of orange-G by advanced oxidation processes, Ultrason. Sonochem., 17 (2010) 338-343.

## SUPPORTING INFORMATION II

### *Experimental*

#### *1.1. Materials*

All experiments were performed on the as-prepared Mg-Al-LDH-NO<sub>3</sub>. The synthesis and characterization of adsorbent were described previously<sup>1</sup>. Methyl Orange, Orange II (Acid Orange 7) and Orange G (Acid Orange 10) were supplied by Sigma-Aldrich, and labelled MO, OII and OG, respectively. All the dyes have high purity > 99% and were used as received. The maximum adsorption ( $\lambda$ ) is 466 nm for MO, 483 nm for OII and 480 nm for OG. All aqueous solutions were prepared in distilled MQ-water from integral water purification system PURELAB Classic.

#### *1.2. Adsorption studies*

Classical batch adsorption studies were carried out to evaluate retention properties. Series of 30 ml Nalgene™ tubes were prepared. In each tube, a solid sample of LDH (2.5 mg) was dispersed in 10 ml of dye solution of known initial concentration. Concentration of OII in the tubes was varied from 0.02 – 5 mmol L<sup>-1</sup>. The pHs of the suspensions were carefully checked before and after adsorption experiment. The tubes were stirred overnight at 298 K. The separation of solid phase from the liquid was achieved by centrifugation at 10 000 rpm for 12 min. The supernatant was then analyzed by using V-670 UV-Vis Spectrophotometer (interval of wavelength 350 – 550 nm) to determine the equilibrium concentration of dye. The adsorption capacity ( $Q_{ads}$ , meq g<sup>-1</sup>) was calculated as followed in equation 1, and displayed as function of equilibrium concentration.

$$Q_{ads} = \frac{V_0 (C_i - C_{eq})}{m_s}$$

---

<sup>1</sup> G. Darmograi, B. PreLOT, G. Layrac, D. Tichit, G. Martin-Gassin, F. Salles, J. Zajac, Study of Adsorption and Intercalation of Orange-Type Dyes into Mg-Al Layered Double Hydroxide, Journal of Physical Chemistry C, Just Accepted September 22, doi : 10.1021/acs.jpcc.5b05510.

$C_i$  and  $C_{eq}$  are respectively the initial and final (equilibrium) concentration of Orange dyes expressed in  $\text{mmol L}^{-1}$ ,  $V_o$  (L) is the initial volume of the sample solution, and  $m_s$  are the weight (in g) of the adsorbent.

### ***2.3. Ionic chromatography of the supernatant***

Mg(II) were analyzed using ion chromatography (HPLC Shimadzu HPLC) apparatus. A Shim-Pack IC-C1 column (with an IC-GC1 precolumn) and a conductivity detector were employed and the mobile phase was a mixture of 4  $\text{mmol L}^{-1}$  tartaric acid and 1.4  $\text{mmol L}^{-1}$  ethylenediamine. The following parameters were used: a flow rate of  $1.5 \text{ mL min}^{-1}$ , an injection volume of 45  $\mu\text{L}$ , a column temperature of 40 °C.

### ***2.4. XRD and TEM analysis***

Adsorption experiment of OII was performed with 5 mg of LDH dispersed in 20 ml of dye solution at known initial concentration. The analysis of supernatant was performed to find out the equilibrium concentration and adsorbed quantity. The solid samples after adsorption were dried at 80 °C during 1-2h and then analyzed with XRD equipment. For fibers, solid dye aggregates were removed from the supernatant after adsorption or calorimetric experience and placed on sample holder to dry at the same condition described above. Zero background sample holder was used for XRD study. Powder pattern were recorded on a PHILIPS X'Pert MPD  $\theta$ - $\theta$  diffractometer equipped with the X'Celerator detector with Cu K $\alpha$  radiation and nickel filter. Data were collected over the  $2\theta$  range from 2° to 30° at 30 mA, 45 kV, with scan speed 0.003°/min and using incident beam mask 10 mm.

To characterize the OII fibers, transmission electron microscopy (TEM) was performed with a JEOL 1200 EXII (operated at 120 kV) microscope. The fibers were pipetted onto 200 square mesh copper grids and dried at room temperature under protection.

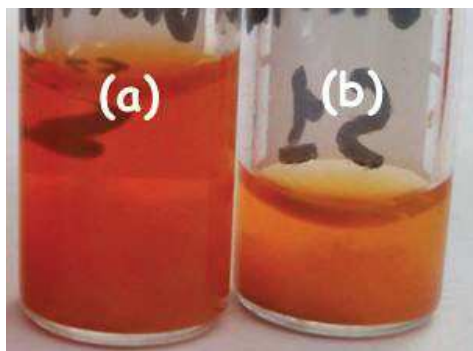


Figure S 5. The following tubes contain the solid particles removed from supernatant after sorption process for HPLC analysis. The tube (a) contains 0.35 mmol g<sup>-1</sup> released Mg and 2.78 mmol g<sup>-1</sup> adsorbed OII; (b) contains 0.36 mmol g<sup>-1</sup> of Mg and 2.38 mmol g<sup>-1</sup> OII.

## **CONCLUSIONS**

Mg-Al-NO<sub>3</sub> showed good adsorbing properties for Orange-type dyes Methyl Orange (MO), Orange II (OII) and Orange G (OG). Nitrates anions, which are present in the interlayers of the LDH, were easily replaced by the dyes molecules. The kinetic of adsorption was shown to be fast for all three dyes and can be modeled by the pseudo-second order kinetic model. The maximum amount of dye retained in the adsorption plateau region increases in the order: MO >> OII > OG. This trend can be rationalized to the differences in molecular sizes, electrical charges and hydrophobic character of the molecules.

Analysis of all the species present in the system showed simultaneous adsorption of the dyes' counter-ion sodium. XRD analysis of the dye-loaded samples confirmed the co-adsorption of carbonates ions, which intercalate at the same time with the dyes. All these important contributions were helpful to understand the mechanism of dye adsorption. For example, MO uptake from the bulk occurs by exchange into the layer i.e. with expansion of the layers and by sorption onto LDH's external surface. These results were confirmed by XRD patterns and co-adsorption of Sodium (neutralization of the MO molecules on the surface). The mechanism of OG uptake onto the LDH is an anion exchange process. In addition, co-adsorption of counter-ions signified that OG uses only one negative charge for the exchange.

The mechanisms of MO and OG dyes retention were in good agreement with the results obtained by ITC analysis. The signal of the thermic effect was further attenuated at the end of the dye exchange into LDH. While the adsorption of OII molecule has two combined sorption mechanisms: the first one is the exchange in the interlayer followed by the complexation of Orange II on the interface of the LDH structure.



**Chapter III:**  
**Competitive adsorption of Dyes  
and Inorganic divalent anions  
onto Mg-Al-NO<sub>3</sub> Layered  
Double Hydroxide**



## ***INTRODUCTION***

This Chapter summarizes the investigation of multi-component adsorption of Orange type dyes onto Mg-Al-LDH-NO<sub>3</sub>. The results obtained using the single component system will be used to evaluate either the positive influence in case of synergy or negative in the case of competition in the presence of the negatively charged inorganic ions. Multi-component adsorption will also be presented for the three dyes with the inorganic anions for different molar ratios so as to have an idea about the influence of this parameter on the competing species uptake.

As main competing species these inorganic anions will be used: sulfates, phosphates and chromates (Cr(VI)). These ions were selected because of the abundant presence of these species in the wastewaters from the textile industries. During the adsorption from the bi-solute component systems, the amount adsorbed will be evaluated for both competing species i.e. the dye and oxyanion. This will permit the understanding of the nature of interactions between adsorbing species.

The competitive adsorption will be also investigated for these dyes in the presence of carbonate ions because the results in Chapter II showed that these anions, which are present, even in small contents (provided from atmosphere) are able to occupy the interlayer space of the LDH. Therefore, the influence of the specially added carbonates will be studied on the dye uptake.

During the multi-component adsorption complementary analysis such as XRD and ITC were used. Thus, XRD patterns of the adsorbent loaded with the competitive mixture will give information about which anions occupied the interlayer spacing. The comparison of the cumulative enthalpies of displacement of these species from the single-solute solutions would help to understand the behavior of the competing anions during multi-component adsorption.

# Competitive adsorption of anionic Orange-type dyes and inorganic divalent anions onto Mg-Al Layered Double Hydroxide from bi-solute aqueous solutions

*Ganna Darmograi, Bénédicte Prelot, Amine Geneste, Gaëlle Martin-Gassin, Fabrice  
Salles, Jerzy Zajac*

Institut Charles Gerhardt de Montpellier, UMR-5253 CNRS-UM-ENSCM,  
C.C. 1502 Place Eugène Bataillon, F-34095 Montpellier cedex 5, France

## 1. Introduction

The co-occurrence of various contaminants and pollutants in industrial effluents is one of the most difficult problems the researchers have to face in the field of Environmental Remediation. Textile industry is a very good illustration of this problem since the various stages of textile processing generate wastewater of a complex composition, thereby leading to a potentially disastrous contamination of drinking water. If the sorption-based process is to be used in dye wastewater treatment [1-5], there is a need for fundamental studies of the competition between the dyes and other dissolved species for binding at the Solid-Liquid interface, phenomenon that may constitute the principal limitation to the effectiveness of the dyes removal technology. In such fundamental studies, the choice of co-existing substances to compete with the dye components should be decided on the basis of surface properties of the adsorbent and molecular structure of the dye studied.

In several papers that have been published up to nowadays regarding the retention of acid or basic dyes by various inorganic or carbonaceous solid substrates from multi-solute solutions [6-15], the competition is chiefly viewed between the negatively or positively charged dye and inorganic species. The retention performance towards a given dye in the mixed dye solutions was generally found to be decreased as compared to the single-solute systems [6-9]. Furthermore, the impact of competition on individual sorption quantities was demonstrated to depend on both the individual affinity of each dye for the solid surface and the composition of the aqueous phase. Similar conclusions were drawn by Wang *et al.* [10] from their study of the competitive adsorption of Malachite green and Pb<sup>2+</sup> onto natural zeolite: in the binary system, the individual amounts adsorbed of the dye and heavy metal cation were depressed, respectively, to about 80 and 90% of the single-solute adsorption values. It is worth noting that the overall adsorption (i.e., the sum of the individual adsorption quantities) was greatly increased. The adsorption of acid and basic dyes (Blue 25, Blue 9, and Violet 3), as well as heavy metal cations (Pb<sup>2+</sup>, Ni<sup>2+</sup>, Zn<sup>2+</sup>, and Cd<sup>2+</sup>) was investigated making use of two zeolite samples: Erionite with a higher specific surface area and an acidic surface character and a low-surface and basic Clinoptilolite [11]. No fundamental differences in the dye removal performance as a function of the surface properties of the two

zeolites were observed, always with the preferential retention of the basic dyes. Erionite was more selective towards the heavy metal cations, thus showing a selectivity order as follows:  $\text{Pb}^{2+} > \text{Ni}^{2+} > \text{Zn}^{2+} > \text{Cd}^{2+}$ . In the dye-metal binary solutions, an antagonistic effect was observed in the removal of basic dyes and heavy metals. Visa *et al.* [12] monitored the impact of the addition of Methylene blue (at a fixed concentration) to equimolar multi-cation solutions of  $\text{Cd}^{2+}$ ,  $\text{Cu}^{2+}$ , and  $\text{Ni}^{2+}$  on the adsorption efficiency and kinetics onto fly ash representing a complex mixture of silica, alumina, iron oxide and un-burned carbon. The observed enhancement in the retention of metal cations was ascribed to the formation of new surface sites as a result of the dye pre-adsorption; copper showed higher affinity for such sites, as compared to cadmium and nickel. The use of a composite material based on lignocellulose and montmorillonite clay was also considered for the removal of Methyl Orange,  $\text{Pb}^{2+}$ , and  $\text{Cd}^{2+}$  from binary aqueous solutions [13]. Firstly, the composite substrate showed increased adsorption of Methyl Orange in comparison with those obtained when using the two constituents separately. Secondly, this retention performance towards the dye species was further increased upon addition of heavy metal cations to the aqueous phase. The effect of different inorganic anions on the adsorption of acid Flavine 2G was studied using a composite material made from Mg-Al Layered Double Hydroxide (LDH) and magnetic iron oxide [14]. The X-ray Diffraction (XRD) patterns of the dye-loaded samples indicated that the dye anions were unable to compete with pristine carbonates and thus difficult to intercalate within the interlayer LDH space. The order of effectiveness in decreasing the dye adsorption by the co-existing inorganic anions was as follows:  $\text{CO}_3^{2-} > \text{SO}_4^{2-} > \text{HPO}_4^{2-} > \text{Cl}^- > \text{NO}_3^-$ . The uptake of Methyl Orange by a calcined Zn-Al LDH was postulated to follow the structural reconstruction pathway after rehydration and intercalation of the dye and carbonate anions within the interlayer space, as evidenced by XRD and inductively coupled plasma (ICP) emission spectroscopy [15]. In the equimolar dye-anion solutions, phosphate ( $\text{PO}_4^{3-}$ ) and carbonate ions were demonstrated to depress the dye retention by the sorbent to a much greater extent than sulfates, chlorides and nitrates did, in accordance with a greater affinity of the LDH surface for multivalent anions. Since no clear trends with respect to the general impact of competition emerge from these studies, it is clear that the problem should be investigated in reference to the retention mechanism involved in a particular sorption system.

In the previous paper [16], the mechanism of individual sorption of three azo dyes with varying anionic charge and hydrophobic-hydrophilic character (Methyl Orange, Orange II, and Orange G) from single-component solutions onto non-calcined Mg-Al-LDH-NO<sub>3</sub> (molar Mg:Al ratio of 2) was elucidated in open systems exposed to the ambient atmosphere (without pH re-adjustment and in the presence of carbonates coming from air). The exchange of anionic dye species, pristine NO<sub>3</sub><sup>-</sup> anions, carbonates, and sodium counter-ions between the LDH structure and the aqueous solution was monitored through the determination of equilibrium adsorption isotherms, kinetic curves, or the analysis of XRD patterns recorded on the dye-loaded samples. The dye uptake by the LDH sample was accompanied by the intercalation of the organic species into the interlayer space as well as their adsorption on the external surface, with the global effect being dependent on the dye type and overall exchange balance in relation with the anionic exchange capacity (AEC) of the solid material. The cumulative enthalpy of displacement, as measured directly by Isothermal Titration Calorimetry (ITC), pointed out the exothermic character of the complex exchange process.

The objective of the present work was to quantify the mutual effect of the three anionic dye species and inorganic divalent HPO<sub>4</sub><sup>2-</sup>, SO<sub>4</sub><sup>2-</sup>, CrO<sub>4</sub><sup>2-</sup>, and carbonate anions, coexisting in bi-solute dye-inorganic anion solutions, on their individual retention propensities by the same pristine LDH sample. The previously established research strategy based on the combined adsorption isotherm and XRD studies on the well-defined sorption systems was employed here. Three different values for the molar ratio between the dye and inorganic anion (i.e., 2:1, 1:1, and 1:2) were considered in view of increasing the efficiency of dyes removal by optimizing experimental conditions. The dye uptake schemes in the presence of inorganic anions were categorized in regards with the shape of the experimental adsorption isotherms and correlated with the individual adsorbate affinities for the LDH sample, as inferred from the calorimetry measurements of the cumulative enthalpy of displacement in single-solute systems.

## 2. Experimental

### 2.1. Materials

The preparation and structural properties of the non-calcined Mg-Al-LDH-NO<sub>3</sub> used in the present study was detailed previously [16]. The solid substrate, represented by an empirical formula of Mg<sub>0.67</sub>Al<sub>0.33</sub>(OH)<sub>2</sub>[(CO<sub>3</sub>)<sub>0.027</sub>•(NO<sub>3</sub>)<sub>0.276</sub>•1.32H<sub>2</sub>O], had an anionic exchange capacity (AEC) of 3.2 meq g<sup>-1</sup>. The three Orange-type dyes of high purity (dye content > 99%) were purchased from Sigma-Aldrich and used without further purification. They are further designated as follows: MO = Methyl Orange, OII = Orange II or Acid Orange 7, OG = Orange G or Acid Orange 10. The maximum absorbance in the ultraviolet (UV) spectra was observed at a wavelength of 466 nm, MO; 483 nm, OII; and 480 nm, OG. The co-existing inorganic anions were provided with aqueous solutions of potassium chromate (K<sub>2</sub>CrO<sub>4</sub>, Sigma-Aldrich), sodium carbonate (Na<sub>2</sub>CO<sub>3</sub>, Sigma-Aldrich), sodium sulfate (Na<sub>2</sub>SO<sub>4</sub>, Merck), and sodium hydrogen phosphate (Na<sub>2</sub>HPO<sub>4</sub>, Sigma-Aldrich). These salts were employed as received. The 18.2 MΩ cm water used in all experiments was obtained with the aid of a combined Purite Select Analyst (France Eau) and PURELAB<sup>®</sup> Classic (ELGA LabWater, France) water purification system.

### 2.2. Measurements of the cumulative enthalpy of displacement in single-solute systems by isothermal titration calorimetry (ITC)

The overall enthalpy change upon the displacement process accompanying the retention of dye or inorganic anions from single-solute solutions onto Mg-Al-LDH-NO<sub>3</sub> at 298 K was measured using a differential TAM III microcalorimeter operating in a heat flow mode. A high precision liquid thermostat (oil heat exchanger with Peltier coolers) maintained the temperature constant within ± 0.0001 deg. The experimental setup was equipped with a computer-controlled micro-syringe injection device allowing small aliquots of a stock solution at a given molality to be injected into a 1 mL glass ampoule. More details about the operating procedures and data processing can be found elsewhere [16]. Prior to measurements, about 1-2 mg of the LDH powder was suspended in 0.8 mL of ultrapure water in the measuring ampoule. The same amount of water was introduced into another 1 mL glass ampoule placed on the reference side. The two ampoules

were subsequently returned to the microcalorimeter and equilibrated thermally during 2 h. The homogeneity of the solid suspension was maintained by means of an agitation system equipped with a Teflon paddle stirrer. The concentration of the stock solution injected into the measuring ampoule was optimized to make the resulting plot of the heat flow,  $W$ , against time,  $\tau$ , easier to be recorded and further processed: 8.5 mmol L<sup>-1</sup>, MO and SO<sub>4</sub><sup>2-</sup>; 14 mmol L<sup>-1</sup>, OII and HPO<sub>4</sub><sup>2-</sup>; 12 mmol L<sup>-1</sup>, OG; 9 mmol L<sup>-1</sup>, CrO<sub>4</sub><sup>2-</sup>; 8.5 mmol L<sup>-1</sup>. Other experimental parameters (i.e., number of injections, injection volume and speed, agitation speed and equilibration time applied between two successive injections) have been collected in Table S1 in Supporting Information. Integration of the thermal peaks appearing in the thermogram recorded for each series of successive injections resulted in discrete  $\Delta_{inj}H_i$  enthalpy values related to the mass of solid in the measuring ampoule and expressed in J g<sup>-1</sup>. The thermal effects of injections were corrected for dilution effects. For this purpose, analogous dilution experiments were carried out under exactly the same experimental conditions but without introducing a solid sample into the measuring ampoule. The resulting enthalpy values were summed up to obtain the cumulative enthalpy of displacement,  $\Delta_{dpl}H_{cum}$ , per unit mass of the LDH sample. The  $\Delta_{dpl}H_{cum}$  values were plotted as a function of the amount of a given species retained by LDH over an adsorption range matching with the quasi-vertical portion on the adsorption isotherm. The repeatability of the calorimetry measurements was assessed by carrying out two simultaneous experiments with the use of two microcalorimeters working under the same conditions; it was within 6%, MO; 17%, OII; 4%, OG; 23%, CrO<sub>4</sub><sup>2-</sup>; 20%, HPO<sub>4</sub><sup>2-</sup>; 7%, SO<sub>4</sub><sup>2-</sup>. Nevertheless, the same trends in  $\Delta_{dpl}H_{cum}$  with the quantity of adsorption were recorded in in the two calorimetric runs.

### ***2.3. Measurements of the adsorption isotherms in single-solute and bi-solute systems***

The solution depletion method was used to determine the individual adsorption isotherms of the adsorbing organic and inorganic anions. The individual points on the adsorption isotherms were obtained by equilibrating about 2.5 mg of the solid sample with 10 ml of solution at a given concentration in 30 ml Nalgene® reactors. In the single-solute systems, the solute concentrations were varied within the following range: 0.02 – 5 mmol L<sup>-1</sup>, MO and OII; 0.02 – 3 mmol L<sup>-1</sup>, OG, 0.03 – 1.2 mmol L<sup>-1</sup>, HPO<sub>4</sub><sup>2-</sup>; 0.03 – 0.7 mmol L<sup>-1</sup>, SO<sub>4</sub><sup>2-</sup> and CrO<sub>4</sub><sup>2-</sup>. Note that the three adsorption

isotherms for dyes had been reported previously [16]. To determine the individual adsorption isotherms of the two anionic species from bi-solute solutions, mixed stock solutions were prepared at three molar ratios between the dye and inorganic anion of (2:1), (1:1), (1:2) and each stock solution was used to obtain appropriate diluted solutions to be poured into Nalgene® tubes. In the equimolar dye-inorganic anion solutions, the dye concentration was as follows: 4 mmol L<sup>-1</sup>, MO; 1.2 mmol L<sup>-1</sup>, OII and OG. For comparison purposes, the dilution schemes were designed to generate the individual adsorption isotherms for the dye species covering ranges of the equilibrium dye concentration similar to those obtained in the single-solute systems. The pH of the solid suspension in single-solute and bi-solute solutions was carefully checked before and after the attainment of the adsorption equilibrium. From the point of view of methodology, no effort was made to re-adjust this parameter to its initial value or minimize contact with atmospheric air during solution preparation. The initial pH of the solid suspension was around 7.5-8, owing to the intrinsic basic character of the Mg-Al-LDH-NO<sub>3</sub> sample. Then, some increase in the pH was observed with the progress of adsorption depending on the system components and the composition of the aqueous phase. The equilibrium pH value also increased along the adsorption isotherm and was greatest in the case of Methyl Orange but always within 1.5 pH unit.

Taking into account the fast kinetics of dye sorption demonstrated previously [16], the Nalgene® reactors were shaken overnight in a thermostated cage ( $\pm 0.1$  deg) at 298 K. Then the solid phase was separated from the supernatant solution by centrifugation at 10 000 rpm for 10 min and the equilibrium concentration of a selected species in the bulk phase was determined either by UV-Vis spectroscopy (Jasco V-670 UV-Vis Spectrophotometer operating in the wavelength range from 350 to 550 nm) or by ion chromatography (Shimadzu HPLC apparatus equipped with a Shim-pack IC-A1 column and a conductivity detector; a flow rate of 1.5 mL min<sup>-1</sup>, an injection volume of 45  $\mu$ L, a column temperature of 40 °C; with the mobile phase depending on the nature of inorganic anion: 2 mmol L<sup>-1</sup> potassium hydrogen phthalate (pH 4.2), NO<sub>3</sub><sup>-</sup> and SO<sub>4</sub><sup>2-</sup>; 4 mmol L<sup>-1</sup> sodium carbonate, CrO<sub>4</sub><sup>2-</sup>; a mixture of 1.5 mmol L<sup>-1</sup> phthalic acid and 0.7 mmol L<sup>-1</sup> diethylenetriamine, HPO<sub>4</sub><sup>2-</sup>. The amount adsorbed of a selected species was calculated from the following formula:

$$Q_{ads} = \frac{V_o(C_i - C_{eq})}{m_s}$$

where  $C_i$  and  $C_{eq}$  represent, respectively, the initial and final (after attaining the equilibrium) concentrations of the adsorbed species,  $V_0$  is the initial volume of the aqueous solution, and  $m_s$  is the mass of the adsorbent. The methodology applied to evaluate the repeatability and experimental uncertainties of the adsorption experiments was described previously [16].

#### *2.4. X-ray diffraction (XRD) study of the LDH samples loaded with the adsorbate*

Some solid samples collected after their separation from the supernatant solution in the adsorption experiments were subsequently analyzed by X-ray diffraction so as to monitor changes in the layered structure induced by the incorporation of the adsorbed species. The choice of the samples for such studies was made in a way to represent 2-3 points on the adsorption isotherms localized within characteristic adsorption regions. Prior to XRD experiment, the powdered solid sample was dried at 373 K during 1-2 h. The XRD patterns were collected on a PHILIPS X'Pert MPD  $\theta$ - $\theta$  diffractometer (X'Celerator detector, Cu K $\alpha$  radiation  $\lambda = 1.5418 \text{ \AA}$ , nickel filter) over the  $2\theta$  range from  $2^\circ$  to  $30^\circ$  at 30 mA, 45 kV, with a scan speed of  $0.003^\circ \text{ min}^{-1}$  and using an incident beam mask of 10 mm.

### *3. Results and discussion*

The actual pH of the aqueous suspension of LDH particles is of crucial importance to decide the chemical form of the adsorbing species, especially when this physical factor changes upon adsorption. In the single-solute solutions of inorganic anions, the pH of the solid suspension changed only a little along the adsorption isotherms and was always between 8 and 9. The  $\text{SO}_4^{2-}$ ,  $\text{CrO}_4^{2-}$ , and  $\text{HPO}_4^{2-}$  anions were the predominant species in the aqueous phase before and after the attainment of the adsorption equilibrium. In the systems containing dyes, the minimum pH value was about 8, whereas the maximum value was as follows: 10.0, MO; 8.6, OII; 8.8, OG. Under such conditions, the sulfonate groups of the dye units should be deprotonated [17] but the pH of the suspension was too low for the R-N-NH-R group to be additionally ionized [18, 19]. Therefore, only the following anionic species were present in the single-solute or bi-solute solutions: MO<sup>-</sup>, OII<sup>-</sup>, OG<sup>2-</sup>,  $\text{SO}_4^{2-}$ ,  $\text{CrO}_4^{2-}$ , and  $\text{HPO}_4^{2-}$ .

In the first stage of the present study, it was necessary to shed more light on the individual affinity of each anionic species for the Mg-Al-LDH-NO<sub>3</sub> surface under conditions of exposure to the ambient atmosphere. One should be aware that the retention of dye or inorganic anions in such ‘open’ systems may be a complex outcome of several ‘primary’ processes involving ion exchange with the pristine compensating anions (i.e., NO<sub>3</sub><sup>-</sup> or OH<sup>-</sup>) or secondary species coming from ambient air (e.g., carbonates), intercalation of the adsorbed species within the interlayer space or their localization on the external surface, co-adsorption of counter-ions, surface dewetting, partial dehydration of the retained and re-hydration of the released substances, as well as mutual interactions among all solution components (especially those operating in the interfacial region) [16]. On the other hand, such conditions are close to those encountered in real applications for Environmental Remediation. Therefore, this has been the main motivation for the choice of the working system in the present study.

Considering the probability of ion exchange as the main mechanism for anion retention by LDH and given the differences in the number of charges among the anions studied, the amount adsorbed and concentration will be further expressed in *milliequivalents* instead of *millimoles* for comparative purposes. The individual adsorption isotherms for the three dyes (as determined previously [16]) and three inorganic anions from single-solute solutions are reported in Figures S1 and S2 in Supporting Information. All adsorption curves have a characteristic shape representing a very steep initial portion at low equilibrium concentrations and an adsorption plateau at higher values. In general, the inorganic anions adsorb onto Mg-Al-LDH-NO<sub>3</sub> to a lower extent than the three dyes do, with the maximum adsorption capacity,  $Q_{max}$ , being always smaller than the AEC of the adsorbent (see Table 1). It worth noting that the present results are in good agreement with those reported on the retention of SO<sub>4</sub><sup>2-</sup> and CrO<sub>4</sub><sup>2-</sup> anions by Mg-Al-LDH-CO<sub>3</sub> [17], Mg-Al-LDH-Cl [18, 19]. On the contrary, maximum retention capacities of various Mg-Al-LDHs containing CO<sub>3</sub><sup>2-</sup> and Cl<sup>-</sup> as interlayer anions towards HPO<sub>4</sub><sup>2-</sup> ranging between 0.6 and 3.7 meq g<sup>-1</sup> were published in literature [20-26].

Since the quasi-vertical portion on the adsorption isotherm corresponds to an adsorption range of the strongest affinity between the adsorbed species and the LDH structure under given experimental conditions, estimates of the retention performance in terms of quantity and energetics are further analyzed only within this particular  $Q_{ads}$  -interval (i.e., up to an amount adsorbed of

$Q_{ads}^*$ . Variations of the cumulative enthalpy of displacement as a function of the amount adsorbed onto Mg-Al-LDH-NO<sub>3</sub> are illustrated in Fig. S3 in Supporting Information. Generally speaking, the overall displacement process is exothermic for all organic and inorganic species, thereby indicating that the anion retention by Mg-Al-LDH-NO<sub>3</sub> under the experimental conditions employed is at least enthalpy-driven. For Methyl Orange, sulfates, and chromates, the quasi-linearity of the  $\Delta_{dpl}H_{cum}$  vs.  $Q_{ads}$  plot indicates that the enthalpy balance for displacement does not change as the sorption progresses. Therefore, the molar enthalpy effect,  $\Delta_{dpl}h_{cum}$ , is a constant function of the amount adsorbed and a unique mechanism of displacement may be postulated on this basis. If the displacement process yields concave enthalpy curves, like those obtained for OII, OG, and hydrogen phosphates, the decreasing exothermicity evidences potential changes in the mechanism; this effect is particularly marked near the end of the vertical portion of the adsorption isotherm, where the displacement becomes athermal and thus entropy-driven. In this case, the average value of the molar enthalpy of displacement over this vertical isotherm portion,  $\overline{\Delta_{dpl}h_{cum}}$ , will be taken as an estimate of the surface affinity of the adsorbing anion. The enthalpy parameters inferred from this analysis are given in Table 1. The values of  $Q_{ads}^*$  in Table 1 have been obtained from a simultaneous analysis of the corresponding adsorption isotherms and enthalpy curves for each anion.

Table 1. Maximum retention capacity,  $Q_{max}$ , and average affinity,  $\overline{\Delta_{dpl}h_{cum}}$ , of Mg-Al-LDH-NO<sub>3</sub> toward various dye and inorganic anions when adsorbed from single-solute solutions under conditions of exposure to the ambient atmosphere employed in the present study; the  $\Delta_{dpl}H_{cum}^*$  represents the value of the cumulative enthalpy of displacement at the end of the initial vertical portion on the adsorption isotherm (i.e.,  $Q_{ads}^*$  at).

Adsorbing anionic species	$Q_{max}$ ( $meq\ g^{-1}$ )	vertical portion of the isotherm		$\overline{\Delta_{dpl}h_{cum}}$ ( $kJ\ eq^{-1}$ )
		$\Delta_{dpl}H_{cum}^*$ ( $J\ g^{-1}$ )	$Q_{ads}^*$ ( $meq\ g^{-1}$ )	
Methyl Orange	5.5±0.3	-93±6	2.6±0.3	-35.8±6.4
Orange II	2.7±0.6	-8.6±1.5	1.0±0.2	-8.6±3.2
Orange G	3.2±0.3	-10.2±0.4	2.1±0.2	-4.9±0.7
HPO <sub>4</sub> <sup>2-</sup>	2.7±0.7	-7.4±1.5	1.4±0.3	-5.3±2.2
SO <sub>4</sub> <sup>2-</sup>	2.5±0.2	-0.27±0.01	2.1±0.2	0.13±0.01

CrO <sub>4</sub> <sup>2-</sup>	2.1±0.2	-0.31±0.02	1.7±0.2	0.18±0.01
--------------------------------	---------	------------	---------	-----------

The results from Table 1 allow the adsorbing anions to be ranked in increasing affinity order with regard to their capacity of interacting with Mg-Al-LDH-NO<sub>3</sub> *under the experimental conditions employed in the present work*: CrO<sub>4</sub><sup>2-</sup> ≈ SO<sub>4</sub><sup>2-</sup> < OG<sup>2-</sup> ≈ HPO<sub>4</sub><sup>2-</sup> < OII<sup>-</sup> < MO<sup>-</sup>. This affinity order, *on a per-equivalent basis*, clearly indicates that the charge number is not the only parameter on which to judge the retention performance of the LDH sample toward various anionic species; the hydrophobic-hydrophilic character of the anion, its size, hydration parameters, and capacity of generating lateral interactions with the other adsorbed species within the LDH structure should be also taken into account. With the use of a chloride-intercalated Zn-Al LDH, Israëli *et al.* studied thermodynamics of anion exchange between the pristine Cl<sup>-</sup> counter-ions and a series of anions [27]. Negative values of *standard molar enthalpy* ranging between -7.3±0.2 and -0.44±0.02 kJ mol<sup>-1</sup> were measured by isothermal titration calorimetry for each anion-exchange process and the order of *increasing enthalpy was as follows*: SO<sub>4</sub><sup>2-</sup> < OH<sup>-</sup> < F<sup>-</sup> < NO<sub>3</sub><sup>-</sup> < Br<sup>-</sup> < I<sup>-</sup>. These trends were correlated with the enthalpy effects related to dehydration-rehydration phenomena accompanying ion exchange, in line with the strength and specificity of interactions between the intercalated anion and water molecules present in large quantities within the interlayer domain of LDH. Afterwards, Morel-Desrosiers and collaborators reported endothermic ion exchange between Cl<sup>-</sup> and divalent oxalate, succinate or adipate anions intercalated perpendicularly within the layers of a similar LDH sample [28]. This was considered to be consistent with partial dehydration of the methylene groups upon intercalation. On the contrary, the exothermic exchange of chloride for L(1)-tartrate anion was interpreted as a result of hydrogen bonding between the neighboring organic species within the interlayer domain, due to the presence of OH groups in tartrate units.

In the present work, monovalent Methyl Orange is the most hydrophobic and the smallest anion (1.5 nm × 0.55 nm), as compared with monovalent Orange II (1.33 nm × 0.68 nm) or divalent Orange G (1.34 nm × 0.83 nm) [16]. Hydrophobic interactions between the aromatic rings of the adsorbed dye units may lead to a π-π stacking phenomenon, thereby reinforcing their propensity to adsorb beyond the ion-exchange pathway due to their electric charge. Divalent inorganic anions are much smaller and more hydrated than the dye ones, with the radius, *r*, of the bare anion, average

number,  $n$ , of water molecules in the hydration shell, and enthalpy of hydration,  $\Delta_{\text{hyd}}H$ , being as follows:  $r = 0.238$  nm,  $n = 3$ ,  $\text{HPO}_4^{2-}$ ;  $r = 0.240$  nm,  $n = 3$ ,  $\Delta_{\text{hyd}}H = -1035$  kJ mol<sup>-1</sup>,  $\text{SO}_4^{2-}$ ;  $r = 0.255$  nm,  $n = 2.8$ ,  $\Delta_{\text{hyd}}H = -1010$  kJ mol<sup>-1</sup>,  $\text{CrO}_4^{2-}$  [29]. Hydrogen phosphate anion can additionally act as a hydrogen bonding donor [30], which likely contributes to its stronger interaction within the LDH structure.

The adequacy of the above anion ranking to explain the sorption behavior in bi-solute solution systems will be checked in the next paragraphs. The *individual adsorption isotherms* for all systems studied in the present work are given in Figures S4-S12 in Supporting Information. Moreover, variations of the total amount of adsorption are illustrated by the sum of the individual quantities of adsorption and plotted as a function of the equilibrium concentration of the dye component in the bulk solution, thereby producing the so-called *composite isotherms*.

### 3.1. Competitive adsorption of dye and inorganic anions from equimolar bi-solute solutions

In the adsorption systems containing equimolar bi-solute solutions of organic and inorganic anions, the driving force for adsorption should depend chiefly on the difference of surface affinities between the two adsorbing species. For monovalent dye anions, i.e., Methyl Orange and Orange II, this driving force will be additionally influenced by the unequal equivalent concentrations of both anions in the initial bulk phase. The detailed analysis of the corresponding experimental curves in Figures S4-S12, as well as their comparison with those obtained in the single-solute systems, has led to the identification of three different competition schemes, which are exemplified in Fig. 1. For comparative purposes, the individual and composite adsorption isotherms for the bi-solute systems have been plotted against the concentration of the dye component in the equilibrium bulk solution. To further assist the analysis of these cases, X-ray diffraction patterns of the LDH sample equilibrated with various single-solute and bi-solute solutions are given in Figures 2-4.

The competition scheme of Type I is encountered in the bi-solute systems where the surface affinities of the two components differ by roughly two orders of magnitude, i.e., in equimolar mixtures of Methyl Orange and sulfates or chromates (Fig. 1a). Only a small decrease in the amount of dye retained by the LDH sample is observed, whereas the adsorption of the competing

inorganic anion is depressed to a very great extent. As a result, the sum of the individual amounts adsorbed is close to the quantity of dye adsorbed from the single-solute solutions, especially at higher dye concentrations. When adsorption is performed from very dilute solutions, the two anionic species seem retained strongly by LDH and these effects manifest themselves through steep initial portions on the individual adsorption isotherms. The adsorption quantity of SO<sub>4</sub><sup>2-</sup> attains its maximum value of about 1.3 meq g<sup>-1</sup> and then it decreases monotonously. In the adsorption range up to 1.3 meq g<sup>-1</sup>, the adsorption of the inorganic anion is twice that of the dye one. Here the competition seems to be also affected by the equivalent concentrations of both anions in addition to their individual affinities (Table 1). In the analogous adsorption range of the MO+CrO<sub>4</sub><sup>2-</sup> system, this proportion is reversed – there are more dye units (1.4 meq g<sup>-1</sup>) than chromate anions (1 meq g<sup>-1</sup>) retained by Mg-Al-LDH-NO<sub>3</sub>. This means that there are some quantitative differences between two systems belonging to the same category. It is very important to emphasize that the composite adsorption in the MO+SO<sub>4</sub> and MO+CrO<sub>4</sub> systems exceeds the AEC of the LDH sample.

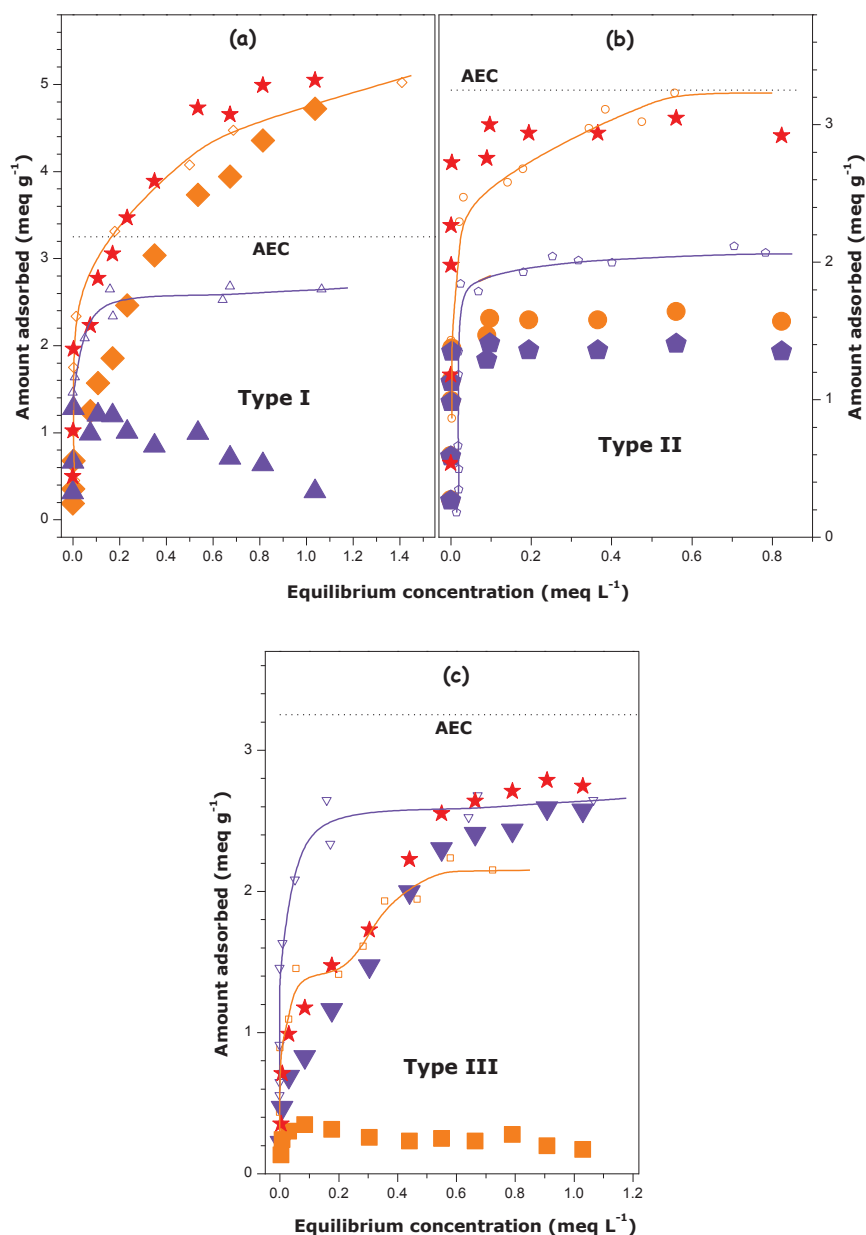


Figure 1. Three different competition schemes exemplified by the individual adsorption isotherms for dye anions (big orange symbols) and inorganic anions (big violet symbols), as well as the composite adsorption isotherm (red stars) plotted as a function of the concentration of the dye component in the equilibrium bulk solution: (a) MO + SO<sub>4</sub><sup>2-</sup> system (Type I), (b) OG + CrO<sub>4</sub><sup>2-</sup> system (Type II), (c) OII + HPO<sub>4</sub><sup>2-</sup> system (Type III). The solid (with small orange symbols) and dashed lines (with small violet symbols) represent the adsorption isotherms of the dye and inorganic ion, respectively, as determined in the separate single-solute systems (as a function of the equilibrium concentration of the corresponding solute). The vertical dotted line is used to indicate the theoretical anion exchange capacity (AEC) of LDH.

The corresponding XRD patterns evidence the intercalation of dye and inorganic anions within the interlayer space of LDH (Fig. 2 and Fig. S13 in Supporting Information).

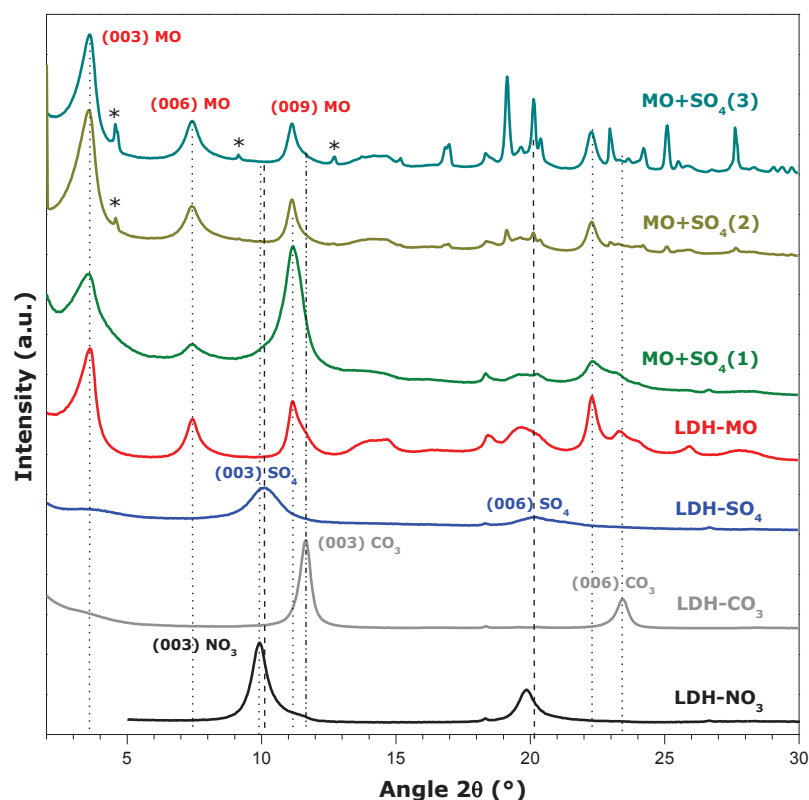


Figure 2. X-ray diffraction patterns in a  $2\theta$  range from  $2^\circ$  to  $30^\circ$  for Mg-Al-LDH-NO<sub>3</sub> loaded with various anionic species from single- and bi-solute equimolar solutions. For the three mixtures of MO and sulfate anions, the amounts adsorbed are as follows: (1)  $0.65 \text{ meq g}^{-1}$ , MO;  $1.29 \text{ meq g}^{-1}$ , SO<sub>4</sub><sup>2-</sup>; (2)  $2.69 \text{ meq g}^{-1}$ , MO;  $0.96 \text{ meq g}^{-1}$ , SO<sub>4</sub><sup>2-</sup>; (3)  $3.93 \text{ meq g}^{-1}$ , MO;  $0.68 \text{ meq g}^{-1}$ , SO<sub>4</sub><sup>2-</sup>.

In Fig. 2, the XRD pattern recorded on the MO+SO<sub>4</sub>(1) sample shows three harmonic reflections at  $2\theta$  positions of  $3.6^\circ$ ,  $7.4^\circ$  and  $11.1^\circ$ , which correspond to interlayer distances,  $d$ , 2.42, 1.2 and 0.8 nm of the intercalated MO phase. The third broad asymmetric peak is attributable to the presence of a mixture of dye, sulfate, and carbonate species within the LDH structure. For the second and third points analyzed on the adsorption isotherm, the absence of the carbonate phase can be noticed. Large amounts of MO adsorbed mask the SO<sub>4</sub><sup>2-</sup> peaks in the diffraction pattern and only the asymmetric shape of the third peak provides some indication of the presence of

intercalated sulfate species. Peaks marked with asterisks (\*) can be ascribed to the dye crystallized on the surface of LDH when its adsorption quantity goes beyond the AEC of LDH.

Similar conclusions can be drawn from the analysis of the XRD patterns recorded on the MO+CrO<sub>4</sub><sup>2-</sup> system (see Fig. S13 in Supporting Information). Again, the (009) MO peak is broad and includes the contribution of the intercalated CrO<sub>4</sub><sup>2-</sup> species. It becomes narrower with increasing the amount of MO intercalated, thus indicating a marked decrease in the chromate phase (the isotherm of chromate adsorption in Fig. S6b goes down to zero at higher equilibrium concentrations). The rest of the initial nitrate phase can be found at a 2θ position of 10° still for the MO+CrO<sub>4</sub>(1) sample, whereas it disappears completely from the diffraction patterns of the two other samples. This points to the composition of the intercalated phase being very complex in the systems studied in the present work: it can also contain pristine nitrates or carbonates coming from air.

Chromate or sulfate anions compete with Orange II or Orange G in a somewhat different manner, following the competition scheme of Type II (Fig. 1b). Although the difference between the component affinities (Table 1) diminishes in comparison with those characterizing the previous category, the dye still interacts more strongly with the LDH structure. The individual adsorption isotherm of each anion resembles that determined from the corresponding single-solute solution: it has a very steep initial portion and an adsorption plateau. The only difference is that the 'height' of the vertical portion and the plateau value are decreased in the bi-solute system. The ratio between the two amounts adsorbed in the initial range depends on the proportion between the equivalent concentrations in the initial solution. The composite adsorption isotherm rests always below the AEC value.

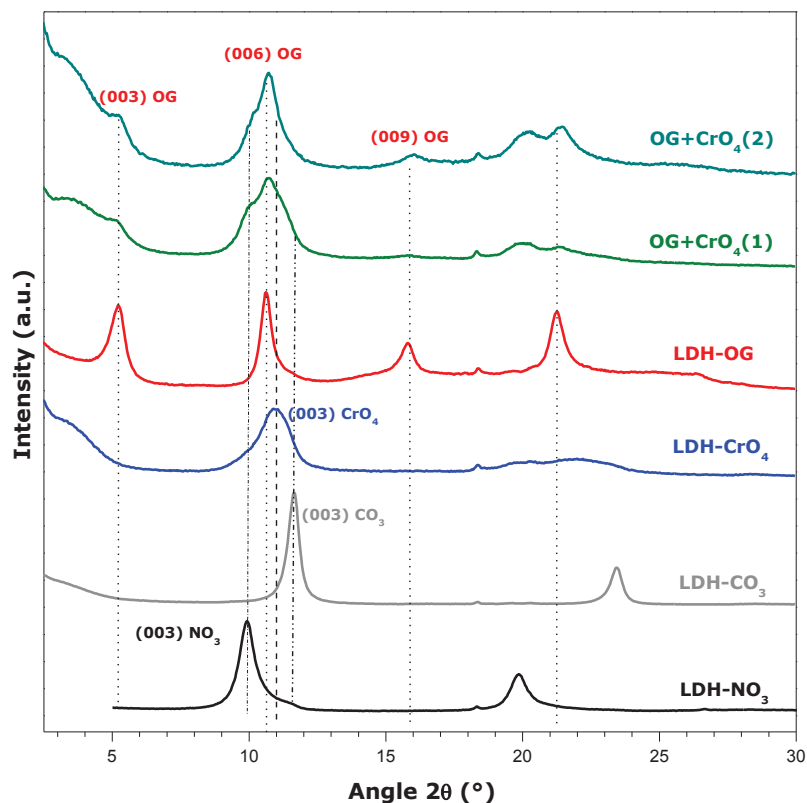


Figure 3. X-ray diffraction patterns in a  $2\theta$  range from  $2^\circ$  to  $30^\circ$  for Mg-Al-LDH-NO<sub>3</sub> loaded with various anionic species from single- and bi-solute equimolar solutions. For the two mixtures of OG and chromate anions, the amounts adsorbed are as follows: (1) 1.01 meq g<sup>-1</sup>, OG; 0.99 meq g<sup>-1</sup>, CrO<sub>4</sub><sup>2-</sup>; (2) 1.57 meq g<sup>-1</sup>, OG; 1.42 meq g<sup>-1</sup>, CrO<sub>4</sub><sup>2-</sup>.

The XRD patterns for the OG+CrO<sub>4</sub><sup>2-</sup> mixture are shown in Fig. 3. For the first point localized on the vertical portion of the adsorption isotherm, i.e., OG+CrO<sub>4</sub>(1) sample, the broad peak between 8 and 13°  $2\theta$  position contains contributions from the (003) CO<sub>3</sub>, (003) CrO<sub>4</sub>, (006) OG, and (003) NO<sub>3</sub> reflections. When the system composition passes to the adsorption plateau regions, i.e., OG+CrO<sub>4</sub>(2) sample, the intercalated carbonates disappear but the three other phases still remain within the interlayer space of LDH. The analysis of Figures S14, S15, and S16 in Supporting Information also indicates simultaneous intercalation of carbonates coming from air, OII or OG, and sulfonates or chromates for OG+SO<sub>4</sub>(1), OII+SO<sub>4</sub>(1), and OII+CrO<sub>4</sub>(1) samples. In the case of OII+CrO<sub>4</sub>(2) sample, some re-adsorption of nitrate species is to be noticed (Fig. S15).

The competition between hydrogen phosphate anion and Methyl Orange may be reckoned to the same category (Type II), although the isotherm of dye adsorption contains a very short vertical portion and that of inorganic anion is only to a small extent affected by the presence of dye species. From the diffraction patterns in Fig. S17 in Supporting Information, it can be concluded that the interlayer space is mainly occupied by HPO<sub>4</sub><sup>2-</sup> anions and a small amount of intercalated MO species. The intercalated carbonates are detectable already for the first analyzed adsorption point, i.e., MO+HPO<sub>4</sub>(1) sample. When the composite adsorption exceeds the AEC value, small peaks marked with asterisks (\*) appear in the diffraction patterns of MO+HPO<sub>4</sub>(2) and MO+HPO<sub>4</sub>(3) samples.

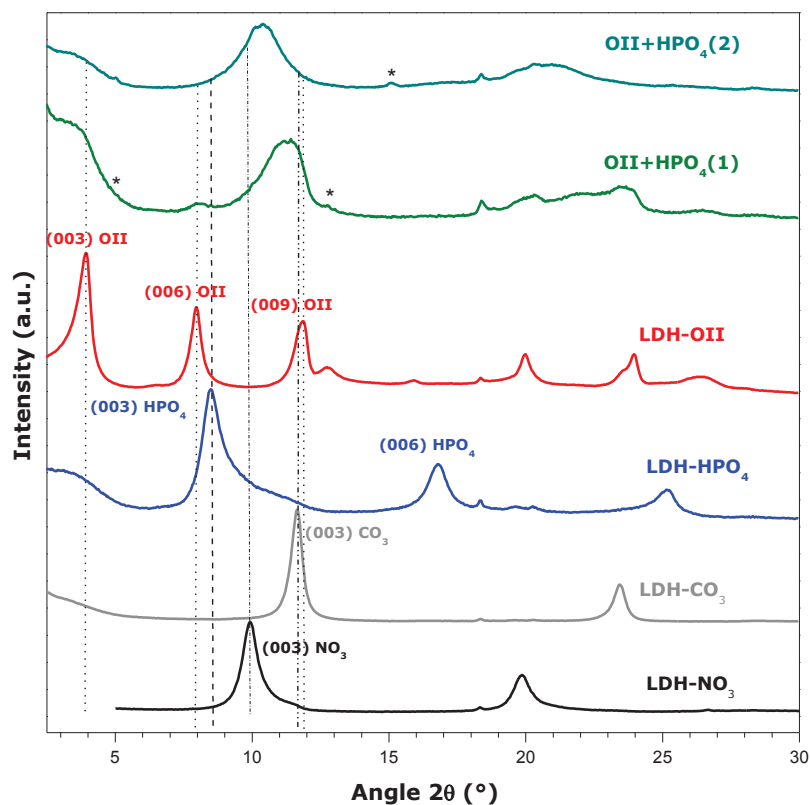


Figure 4. X-ray diffraction patterns in a  $2\theta$  range from  $2^\circ$  to  $30^\circ$  for Mg-Al-LDH-NO<sub>3</sub> loaded with various anionic species from single- and bi-solute equimolar solutions. For the two mixtures of OII and hydrogen phosphate anions, the amounts adsorbed are as follows:  
(1)  $0.27 \text{ meq g}^{-1}$ , OII;  $0.83 \text{ meq g}^{-1}$ , HPO<sub>4</sub><sup>2-</sup>; (2)  $0.20 \text{ meq g}^{-1}$ , OII;  $2.56 \text{ meq g}^{-1}$ , HPO<sub>4</sub><sup>2-</sup>.

The competition scheme of Type III has been observed for inorganic anions and dye species with comparable affinities for LDH, namely HPO<sub>4</sub><sup>2-</sup> in competition with OII or OG (see Fig. 1c). The adsorption of the inorganic anion is depressed in the vertical part of the isotherm and over the interval of moderate dye concentrations in the equilibrium bulk solution. In the case of dye, the extent of adsorption is reduced to a large extent; it can even decrease monotonously after having reached a maximum value at very low concentrations. The XRD diffraction patterns of OII+HPO<sub>4</sub>(1) and OG+HPO<sub>4</sub>(1) samples reported, respectively, in Fig. 4 and Fig. S18 in Supporting Information reveal the presence of intercalated carbonates within the LDH structure. It should be underlined that no expansion of the interlayer space is detected in the XRD diffraction patterns OII+HPO<sub>4</sub>(2) and OG+HPO<sub>4</sub>(2) samples. This means that such dyes do not form the intercalated species and their adsorption probably occurs on the external surface of LDH.

### *3.2. Effects of the molar ratio between the dye and inorganic anion on their competitive adsorption from bi-solute solutions*

When the molar ratio of dye to inorganic anion in the adsorption system is modified, the driving force for adsorption will undergo changes depending on the proportion between the equivalent concentrations of the two solutes in the aqueous phase and their evolution with time. Three molar ratios chosen for the purpose of the present work are as follows (dye : inorganic anion): 2:1, 1:1, and 1:2. The question arises as to whether the competition scheme remains the same when this ratio changes. A careful review of the adsorption isotherms reported in Figures S4-S12 in Supporting Information has resulted in Table 2, which shows the affiliation of all systems studied to one of the three types defined in Fig. 1.

It is worth noting that, with a few notable exceptions, modifying the molar ratio makes the quantitative differences to be amplified in one direction or another, though the general competition scheme does not change. The behavior of the MO+HPO<sub>4</sub><sup>2-</sup>(2:1), OII+CrO<sub>4</sub><sup>2-</sup>(2:1), OG+CrO<sub>4</sub><sup>2-</sup>(2:1) systems represents an exception to this rule: when the greater surface affinity of dye (as compared to that of inorganic anion) is reinforced by the increased dye content in the system, the competition scheme shifts to Type I. Here the individual adsorption of the inorganic anion from bi-solute solutions is greatly depressed and it decreases constantly as the dye adsorption progresses. With

the systems belonging to Type I, the composite adsorption isotherms either are similar to or lie below the corresponding isotherm of dye adsorption from the single-solute solution. In conclusion, the retention of inorganic anion by Mg-Al-LDH-NO<sub>3</sub> does not always compensate for the decrease in the dye uptake. Within Type III, the composite adsorption of both solutes may exceed the amount of dye adsorbed in the single-solute system. This is possible because the OII and OG units are adsorbed mostly on the external surface and HPO<sub>4</sub><sup>2-</sup> anions with a smaller molecular size are intercalated within the interlayer space. No such steady trends in the composite isotherms are observed for systems belonging to Type II.

Table 2. Affiliation of the bi-solute systems studied in the present work to one of the four types of the competition scheme, as defined in Fig. 2 (the molar ratio of dye to inorganic anion is specified in the brackets)

Competition scheme	Affiliated systems
Type I	MO+CrO <sub>4</sub> <sup>2-</sup> (all ratios); MO+SO <sub>4</sub> <sup>2-</sup> (all ratios); OG+HPO <sub>4</sub> <sup>2-</sup> (all ratios)
Type II	OII+CrO <sub>4</sub> <sup>2-</sup> (1:1,1:2); OG+CrO <sub>4</sub> <sup>2-</sup> (1:1,1:2); OII+SO <sub>4</sub> <sup>2-</sup> (1:1, 2:1); OG+SO <sub>4</sub> <sup>2-</sup> (all ratios); MO+HPO <sub>4</sub> <sup>2-</sup> (1:1)
Type III	OII+CrO <sub>4</sub> <sup>2-</sup> (2:1); OG+CrO <sub>4</sub> <sup>2-</sup> (2:1); OII+HPO <sub>4</sub> <sup>2-</sup> (all ratios); MO+HPO <sub>4</sub> <sup>2-</sup> (2:1,1:2); OII+SO <sub>4</sub> <sup>2-</sup> (1:2);

To better illustrate the quantitative effects of the addition of inorganic anion on the individual adsorption of the dye component, the maximum amount of dye adsorbed from a given bi-solute solution onto Mg-Al-LDH-NO<sub>3</sub> was compared to the AEC of LDH and plotted in form of histograms as a function of the type of inorganic anion and molar ratio between the two components. In the case of systems following the Type III competition scheme, the maximum adsorption value was not taken from the adsorption plateau region but from the initial ascending part of the individual adsorption isotherm of this component. These general trends are presented in Fig. 5.

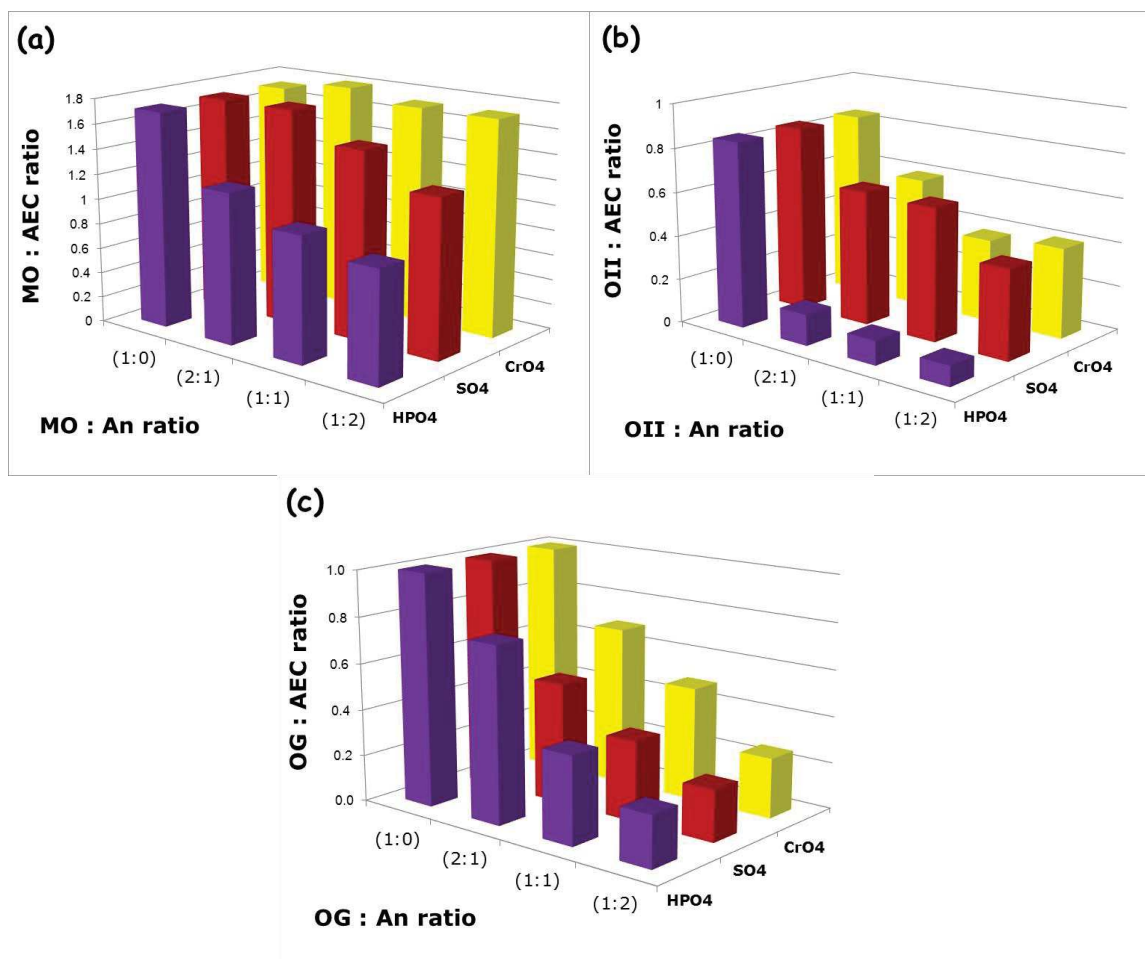


Figure 5. Effect of the addition of inorganic anions on the retention capacity of Mg-Al-LDH-NO<sub>3</sub> towards Methyl Orange (panel a), Orange II (panel b), and Orange G (panel c) from bi-solute solutions at different molar ratios between dye and inorganic anion.

For a given mixture of anions, the maximum quantity of dye adsorption decreases upon increasing the content of inorganic anion in the system; the addition of hydrogen phosphate anions to the aqueous phase causes a marked depression, whereas the presence of chromate or sulfate anions has little influence. As mentioned in the previous Section, the retention capacity of Mg-Al-LDH-NO<sub>3</sub> towards MO exceeds the AEC value both in single- and bi-solute systems, which means that the adsorption mechanism is not limited only to the ion-exchange pathway. The value of MO:AEC ratio corresponding to a MO:HPO<sub>4</sub><sup>2-</sup> proportion of 1:2 is halved in comparison with its value attained in the single-component system. The HPO<sub>4</sub><sup>2-</sup> anion is demonstrated to have the

biggest impact on the adsorption of OII: the maximum amount of dye adsorbed from such bi-solute solutions is always below 15% of AEC.

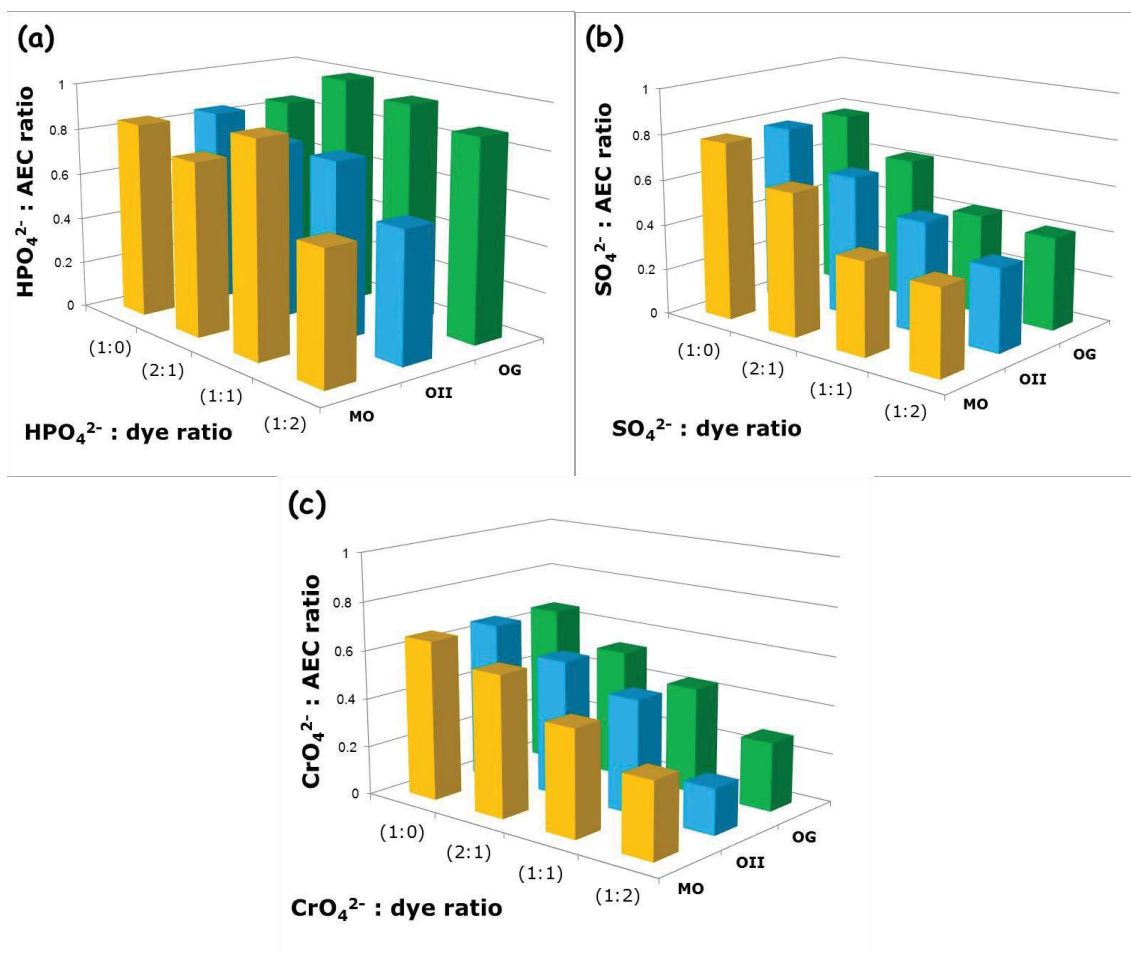


Figure 6. Effect of the addition of dye anions on the retention capacity of Mg-Al-LDH-NO<sub>3</sub> towards divalent hydrogen phosphate (panel a), sulfate (panel b), and chromate (panel c) anions from bi-solute solutions at different molar ratios between inorganic anion and dye.

The retention capacity of Mg-Al-LDH-NO<sub>3</sub> towards OG is affected also by the presence of CrO<sub>4</sub><sup>2-</sup> and SO<sub>4</sub><sup>2-</sup>: the greatest dye contribution to the anion exchange process is only 30% of AEC in the presence of chromates and around 20 % in the presence of phosphate and sulfate anions.

Similar histograms showing a mirror effect of the dye addition on the retention capacity of Mg-Al-LDH-NO<sub>3</sub> towards divalent inorganic anions from bi-solute solutions are presented in Fig. 6. For the systems within Type I, the maximum uptake of an inorganic anion was taken from the initial ascending part of the individual adsorption isotherm of this component. It is interesting to notice that the maximum amount of HPO<sub>4</sub><sup>2-</sup> adsorbed in the presence of MO or OG may be even increased in comparison with that attained in the single-solute systems. On the contrary, the retention capacity towards SO<sub>4</sub><sup>2-</sup> and CrO<sub>4</sub><sup>2-</sup> anions is always depressed upon dye addition. The biggest depression by 70% has been observed for the 2:1 OII+ CrO<sub>4</sub><sup>2-</sup> system.

### *3.3. Effects of the controlled carbonate addition to the aqueous phase on the dye adsorption from bi-solute carbonate-dye solutions*

The XRD diffraction patterns recorded on LDH samples loaded with various dye and inorganic anions in open systems evidence the complex composition of the intercalated phase which can contain carbonate species present in the initial LDH structure or coming from air [16]. Since carbonate anions are known to have a strong affinity for LDH materials [31-33], they represent additional competitors in the bi-solute systems studied here. Given the diversity of carbonate sources, the quantification of carbonates retained by the LDH sample is not very easy. To overcome this difficulty, the presence of carbonates should be controlled. For the purpose of the present work, carbonate ions have been added to the aqueous phase so as to obtain molar ratios between a given dye and carbonate species similar to those used for other inorganic anions.

The individual adsorption isotherms for Methyl Orange, Orange II, and Orange G in the presence of carbonates are given in Fig. S19 in Supporting Information. Carbonate anions clearly have a downward effect on dye adsorption from bi-solute solutions, especially for higher carbonate contents (i.e., molar dye : carbonate ratio of 1:2).

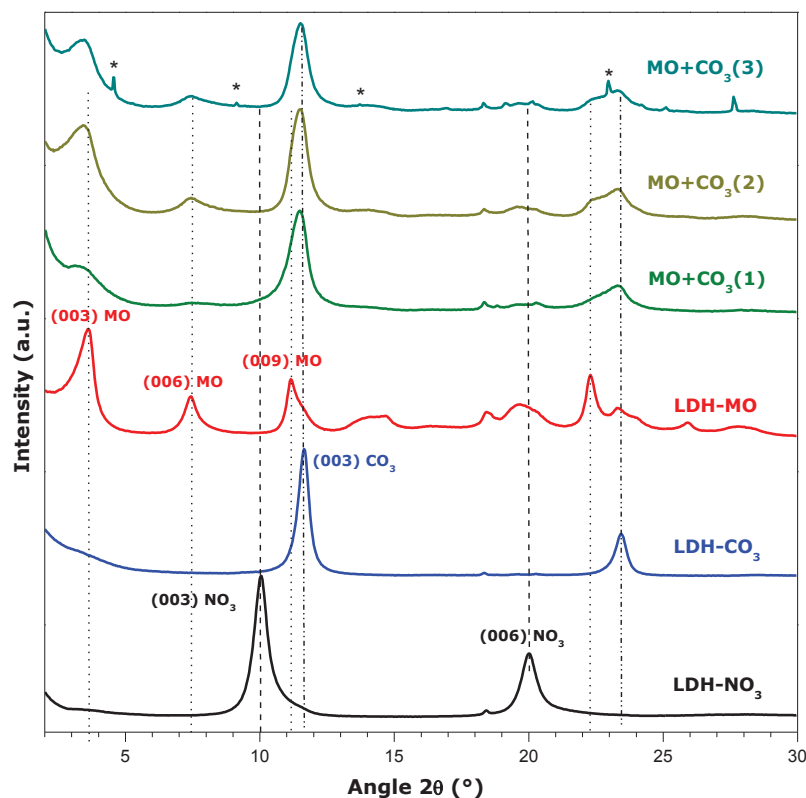


Figure 7. X-ray diffraction patterns in a  $2\theta$  range from  $2^\circ$  to  $30^\circ$  for Mg-Al-LDH-NO<sub>3</sub> loaded with various anionic species from single- and bi-solute equimolar solutions. For the three mixtures of MO and carbonate anions, the amounts of dye adsorbed are as follows: (1)  $0.48 \text{ meq g}^{-1}$ , (2)  $0.97 \text{ meq g}^{-1}$ , (3)  $1.2 \text{ meq g}^{-1}$ .

The intercalation of MO and OII units within the interlayer space of Mg-Al-LDH-NO<sub>3</sub> is confirmed in Fig. 7 and Fig. S20 (Supporting Information), where the XRD patterns of few LDH samples loaded with dye and carbonate anions from equimolar bi-solute solutions are reported. The co-insertion of organic and inorganic phases into the LDH structure is accompanied by a visible expansion of the interlayer distance from 0.88 to 2.42 nm, MO; or 2.22 nm, OII. In addition, the adsorption of MO species on the external surface leads to the formation of a new phase which is identified by small peaks marked with asterisks (\*) in the XRD pattern of the MO+CO<sub>3</sub>(3) sample (Fig. 7).

The adsorption behavior of the OG+CO<sub>3</sub><sup>2-</sup> system is somewhat different, as exemplified by the XRD patterns in Fig. 8. For the first point analyzed on the adsorption isotherm, i.e.,

OG+CO<sub>3</sub>(1) sample, some expansion of the interlayer distance to 1.68 nm can be inferred from the small peak localized at a 2θ position of 5.2°. However, such an expansion is no more observed for the OG+CO<sub>3</sub>(2) sample. In both cases, the appearance of a broad peak between 10 and 13° indicates possible co-occurrence of the OG and carbonate phases.

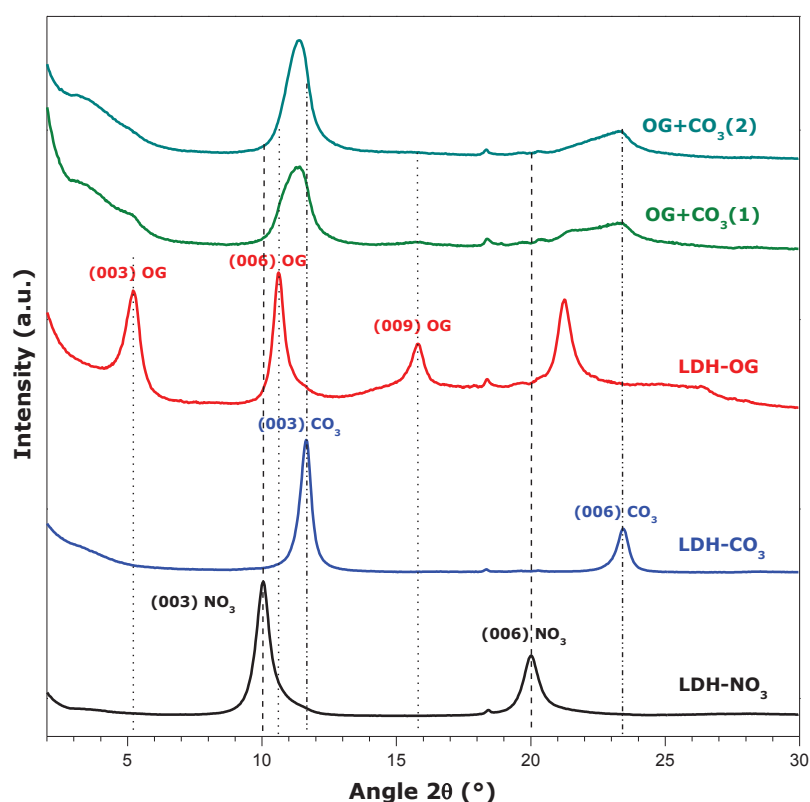


Figure 8. X-ray diffraction patterns in a 2θ range from 2° to 30° for Mg-Al-LDH-NO<sub>3</sub> loaded with various anionic species from single- and bi-solute equimolar solutions. For the two mixtures of OG and carbonate anions, the amounts of dye adsorbed are as follows: (1) 1.12 meq g<sup>-1</sup>, (2) 1.17 meq g<sup>-1</sup>.

The effects of the controlled carbonate addition to the aqueous phase on the retention capacity of Mg-Al-LDH-NO<sub>3</sub> towards the three dyes are illustrated in Figure 9. As in Figures 5 and 6, this retention capacity is compared with the AEC of LDH. For each type of dye, its maximum amount adsorbed is diminished more when more carbonate ions are introduced to the

bi-solute system. CO<sub>3</sub><sup>2-</sup> is the smallest and the most hydrated among the inorganic anions used in the present study (i.e.,  $r = 0.178$  nm,  $n = 4$ ,  $\Delta_{\text{hyd}}H = -1395$  kJ mol<sup>-1</sup>, [29]). It will be probably retained by the LDH structure preferentially over HCO<sub>3</sub><sup>-</sup>, which is a little greater and particularly less hydrated ( $r = 0.185$  nm,  $n = 2$ ,  $\Delta_{\text{hyd}}H = -380$  kJ mol<sup>-1</sup> [29]). When the most hydrophobic among the three dyes (i.e., Methyl Orange) is mixed with carbonate species to obtain molar ratios of 2.1, 1:1, and 1:2, the maximum dye adsorption is decreased by about 50%, 75%, and 85%, respectively.

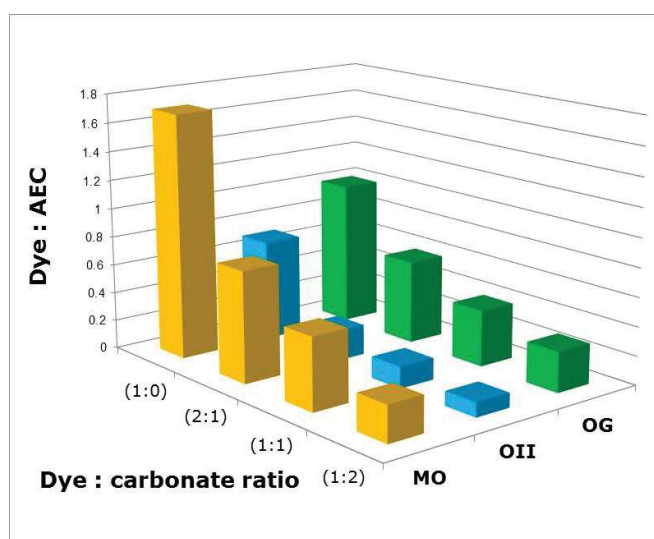


Figure 9. Effect of the addition of carbonate anions to the aqueous phase on the retention capacity of Mg-Al-LDH-NO<sub>3</sub> towards Methyl Orange (MO), Orange II (OII), and Orange G (OG) from bi-solute solutions at different molar ratios between dye and carbonate species. AEC refers to the anion exchange capacity of the LDH sample.

With less hydrophobic and divalent OG anions, carbonates become less efficient in reducing the maximum quantity of dye adsorption since the corresponding reduction rates are 48%, 58%, and 70%. When the molar ratio between OII and carbonates is equal to 2:1 (the same equivalent concentrations of both solutes), the retention capacity of the LDH sample towards OII is lowered by 77%. Further carbonate addition has less influence on the OII retention performance: the reduction rate increases to 83% and 87 % when the dye : carbonate ratio passes to 1:1 and 1:2, respectively.

When confronted with the results reported in Fig. 5, the classification of inorganic anions in order of their ability to decrease the retention capacity of Mg-Al-LDH-NO<sub>3</sub> towards the three dyes depends not only on the type of dye but also on the molar ratio between dye and inorganic anion. For comparative purposes, the equivalent concentration of inorganic anion being twice that of dye is taken as reference: the monovalent MO and OII anions are thus analyzed for a dye : An ratio of 1:1, whereas the maximum adsorption of divalent OG is provided for a dye : An ratio of 1:2. On this basis, the order of decreasing effectiveness of the inorganic anion in depressing the maximum quantity of dye adsorption is: CO<sub>3</sub><sup>2-</sup> >> HPO<sub>4</sub><sup>2-</sup> > SO<sub>4</sub><sup>2-</sup> ≈ CrO<sub>4</sub><sup>2-</sup>, Methyl Orange; HPO<sub>4</sub><sup>2-</sup> ≈ CO<sub>3</sub><sup>2-</sup> > CrO<sub>4</sub><sup>2-</sup> > SO<sub>4</sub><sup>2-</sup>, Orange II; HPO<sub>4</sub><sup>2-</sup> ≈ SO<sub>4</sub><sup>2-</sup> > CO<sub>3</sub><sup>2-</sup> ≈ CrO<sub>4</sub><sup>2-</sup>, Orange G.

#### 4. Conclusion

The competitive adsorption of anionic Orange-type dyes and inorganic divalent anions onto Mg-Al Layered Double Hydroxide from bi-solute aqueous solutions in open systems was demonstrated to follow a complex mechanism involving an ion exchange with the pristine nitrates and carbonates coming from air, which led to the intercalation of various adsorbed species within the interlayer space of LDH or their adsorption on the external surface. Based on the shape of the individual adsorption isotherms for a dye and inorganic anion, it was possible to distinguish three different competition schemes: when the reduction in adsorption extent concerns mainly one of the solutes (Type I and Type III) or when this reduction applies to both solutes (Type II). The bi-solute systems studied in the present work were ascribed to one of these categories depending on the individual solute affinities for the LDH sample, as inferred from the calorimetry measurements of the cumulative enthalpy of displacement in single-solute systems, and their overall contents in the system, as expressed by the molar ratio between dye and inorganic anion. The order of decreasing effectiveness of the inorganic anion in depressing the retention capacity of Mg-Al-LDH-NO<sub>3</sub> towards a given dye, *on a per-equivalent basis*, was as follows: CO<sub>3</sub><sup>2-</sup> >> HPO<sub>4</sub><sup>2-</sup> > SO<sub>4</sub><sup>2-</sup> ≈ CrO<sub>4</sub><sup>2-</sup>, Methyl Orange; HPO<sub>4</sub><sup>2-</sup> ≈ CO<sub>3</sub><sup>2-</sup> > CrO<sub>4</sub><sup>2-</sup> > SO<sub>4</sub><sup>2-</sup>, Orange II; HPO<sub>4</sub><sup>2-</sup> ≈ SO<sub>4</sub><sup>2-</sup> > CO<sub>3</sub><sup>2-</sup> ≈ CrO<sub>4</sub><sup>2-</sup>, Orange G.

#### Acknowledgment

The authors are grateful to Mr. Bernard Fraisse for his assistance with XRD measurements.

## References

1. Geethakarathi, A. and B.R. Phanikumar, *Industrial sludge based adsorbents/industrial by-products in the removal of reactive dyes – A review*. International Journal of Water Resources and Environmental Engineering, 2011. **3**(1): p. 1-9.
2. Wei, Y.-P., D.-Q. Wei, and H.-W. Gao, *Treatment of dye wastewater by in situ hybridization with Mg–Al layered double hydroxides and reuse of dye sludge*. Chemical Engineering Journal, 2011. **172**(2–3): p. 872-878.
3. Gil, A., et al., *Removal of dyes from wastewaters by adsorption on pillared clays*. Chemical Engineering Journal, 2011. **168**(3): p. 1032-1040.
4. Crini, G., *Non-conventional low-cost adsorbents for dye removal: A review*. Bioresource Technology, 2006. **97**(9): p. 1061-1085.
5. Yesi, F.P.S., et al., *Clays and its Modified Forms for Removal of Dyes from Aqueous Solution in Clay: Types, Properties and Uses*, J.P. Humphrey and D.E. Boyd, Editors. 2011, Nova Science Publishers p. 301-320.
6. Chiou, M.-S. and G.-S. Chuang, *Competitive adsorption of dye metanil yellow and RB15 in acid solutions on chemically cross-linked chitosan beads*. Chemosphere, 2006. **62**(5): p. 731-740.
7. Al-Degs, Y., et al., *Competitive adsorption of reactive dyes from solution: Equilibrium isotherm studies in single and multisolite systems*. Chemical Engineering Journal, 2007. **128**(2–3): p. 163-167.
8. Turabik, M. and B. Gozmen, *Removal of Basic Textile Dyes in Single and Multi-Dye Solutions by Adsorption: Statistical Optimization and Equilibrium Isotherm Studies*. CLEAN – Soil, Air, Water, 2013. **41**(11): p. 1080-1092.
9. Shen, D., et al., *Adsorption kinetics and isotherm of anionic dyes onto organo-bentonite from single and multisolite systems*. Journal of Hazardous Materials, 2009. **172**(1): p. 99-107.
10. Wang, S. and E. Ariyanto, *Competitive adsorption of malachite green and Pb ions on natural zeolite*. Journal of Colloid and Interface Science, 2007. **314**(1): p. 25-31.
11. Hernández-Montoya, V., et al., *Competitive adsorption of dyes and heavy metals on zeolitic structures*. Journal of Environmental Management, 2013. **116**: p. 213-221.
12. Visa, M., C. Bogatu, and A. Duta, *Simultaneous adsorption of dyes and heavy metals from multicomponent solutions using fly ash*. Applied Surface Science, 2010. **256**(17): p. 5486-5491.
13. Bunhu, T. and L. Tichagwa, *Adsorption of Methyl Orange, Pb<sup>2+</sup> and Cd<sup>2+</sup> from Aqueous Solution by Composites of Lignocellulose-Montmorillonite Modified with Methacryloxypropyl Trimethoxysilane*. Macromolecular Symposia, 2012. **313-314**(1): p. 146-156.

14. Jiao, F.P., et al., *Excellent adsorption of Acid Flavine 2G by MgAl-mixed metal oxides with magnetic iron oxide*. Applied Clay Science, 2014. **101**: p. 30-37.
15. Ni, Z.-M., et al., *Treatment of methyl orange by calcined layered double hydroxides in aqueous solution: Adsorption property and kinetic studies*. Journal of Colloid and Interface Science, 2007. **316**(2): p. 284-291.
16. Darmograi, G., et al., *Study of Adsorption and Intercalation of Orange-Type Dyes into Mg-Al Layered Double Hydroxide*. Journal of Physical Chemistry.
17. Rosano-Ortega, G., et al., *Green Cycle: Sulfate Sorption from Natural Water on Anionic Clay Compound Obtained from Industry Wastewater*. Green and Sustainable Chemistry, 2013. **3**(2): p. 48-55.
18. Tsujimura, A., M. Uchida, and A. Okuwaki, *Synthesis and sulfate ion-exchange properties of a hydrotalcite-like compound intercalated by chloride ions*. Journal of hazardous materials, 2007. **143**(1-2): p. 582-586.
19. Hourri, B., et al., *Removal of Chromate Ions from Water by Anionic CLAYS*. Journal de Chimie Physique et de Physico-Chimie Biologique, 1999. **96**(3): p. 455-463.
20. Badreddine, M., et al., *Ion exchange of different phosphate ions into the zinc-aluminium-chloride layered double hydroxide*. Materials Letters, 1999. **38**(6): p. 391-395.
21. Cai, P., et al., *Competitive adsorption characteristics of fluoride and phosphate on calcined Mg-Al-CO<sub>3</sub> layered double hydroxides*. Journal of hazardous materials. **213-214**(0): p. 100-108.
22. Frost, R.L., et al., *Raman spectroscopy of hydrotalcites with phosphate in the interlayer: implications for the removal of phosphate from water*. Journal of Raman Spectroscopy, 2006. **37**(7): p. 733-741.
23. Kuzawa, K., et al., *Phosphate removal and recovery with a synthetic hydrotalcite as an adsorbent*. Chemosphere, 2006. **62**(1): p. 45-52.
24. Lazaridis, N.K., *Sorption Removal of Anions and Cations in Single Batch Systems by Uncalcined and Calcined Mg-Al-CO<sub>3</sub> Hydrotalcite*. Water, Air, and Soil Pollution, 2003. **146**(1-4): p. 127-139.
25. Ookubo, A., K. Ooi, and H. Hayashi, *Preparation and phosphate ion-exchange properties of a hydrotalcite-like compound*. Langmuir, 1993. **9**(5): p. 1418-1422.
26. Shin, H.-S., et al., *Phosphorus removal by hydrotalcite-like compounds (HTLcs)*. Water Science and Technology, 1996. **34**(1-2): p. 161-168.
27. Israeli, Y., et al., *Thermodynamics of anion exchange on a chloride-intercalated zinc-aluminum layered double hydroxide: a microcalorimetric study*. Journal of the Chemical Society, Dalton Transactions, 2000(5): p. 791-796.
28. Morel-Desrosiers, N., et al., *Intercalation of dicarboxylate anions into a Zn-Al-Cl layered double hydroxide: microcalorimetric determination of the enthalpies of anion exchange*. Journal of Materials Chemistry, 2003. **13**(10): p. 2582-2585.

29. Marcus, Y., *A simple empirical model describing the thermodynamics of hydration of ions of widely varying charges, sizes, and shapes*. Biophysical Chemistry, 1994. **51**(2-3): p. 111-127.
30. Saha, A., et al., *Stability of metal ion complexes formed with methyl phosphate and hydrogen phosphate*. JBIC Journal of Biological Inorganic Chemistry, 1996. **1**(3): p. 231-238.
31. Miyata, S., *Anion-exchange properties of hydrotalcite-like compounds*. Clays Clay Miner, 1983. **31**(4): p. 305-311.
32. Schöllhorn, R. and B. Otto, *Co-operative anion exchange mechanism of layered transition metal hydroxide systems*. Journal of the Chemical Society, Chemical Communications, 1986(15): p. 1222-1223.
33. Schöllhorn, R. and B. Otto, *Layer charge sign transition  $[Z]^- \rightarrow [Z]^+$  of lamellar metal oxides*. Journal of the Chemical Society, Chemical Communications, 1987(20): p. 1559-1560.

## SUPPORTING INFORMATION

### I. Adsorption isotherms for dye or inorganic anions from single-solute solutions onto Mg-Al-LDH-NO

#### Dye anions:

MO = Methyl Orange [C<sub>14</sub>H<sub>14</sub>N<sub>3</sub>SO<sub>3</sub>]<sup>-</sup>

OII = Orange II (Acid orange 7) [C<sub>16</sub>H<sub>11</sub>N<sub>2</sub>SO<sub>4</sub>]<sup>-</sup>

OG = Orange G [C<sub>16</sub>H<sub>10</sub>N<sub>2</sub>S<sub>2</sub>O<sub>7</sub>]<sup>2-</sup>

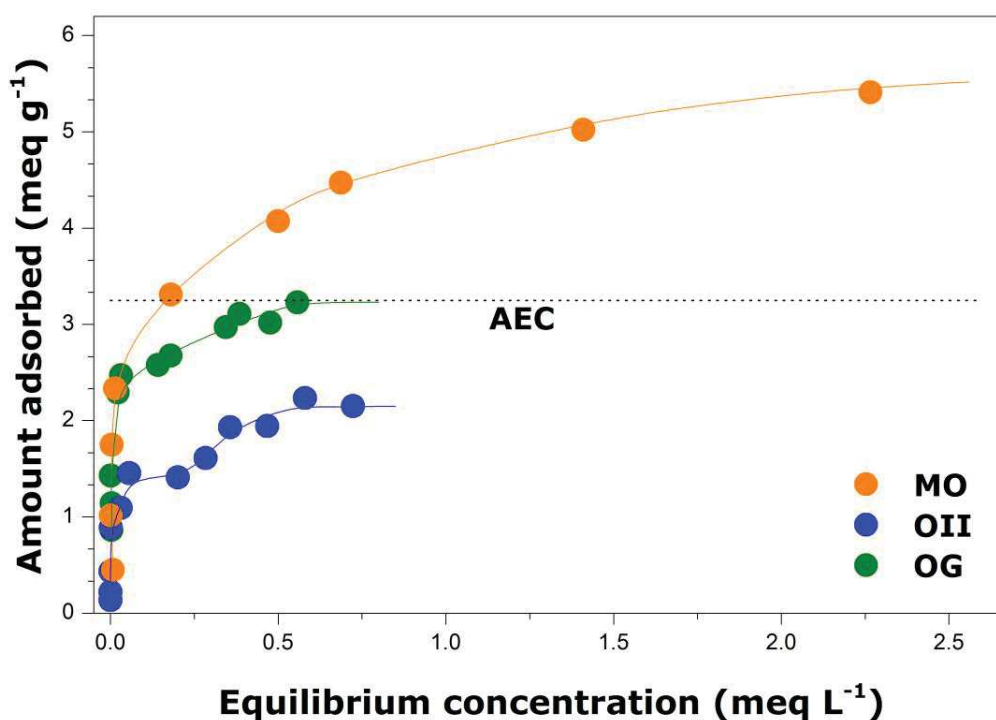


Figure S 1. Isotherms of dye adsorption from single-solute solutions onto Mg-Al-LDH-NO<sub>3</sub> at 298 K. The solid lines represent the smoothed isotherms constructed on the basis of the results of repeated adsorption experiments. The vertical dotted line is used to indicate the theoretical anion exchange capacity (AEC) of LDH. Adapted from G. Darmograi et al., *Study of Adsorption and Intercalation of Orange-Type Dyes into Mg-Al Layered Double Hydroxide*, *Journal of Physical Chemistry*, DOI: 10.1021/acs.jpcc.5b05510

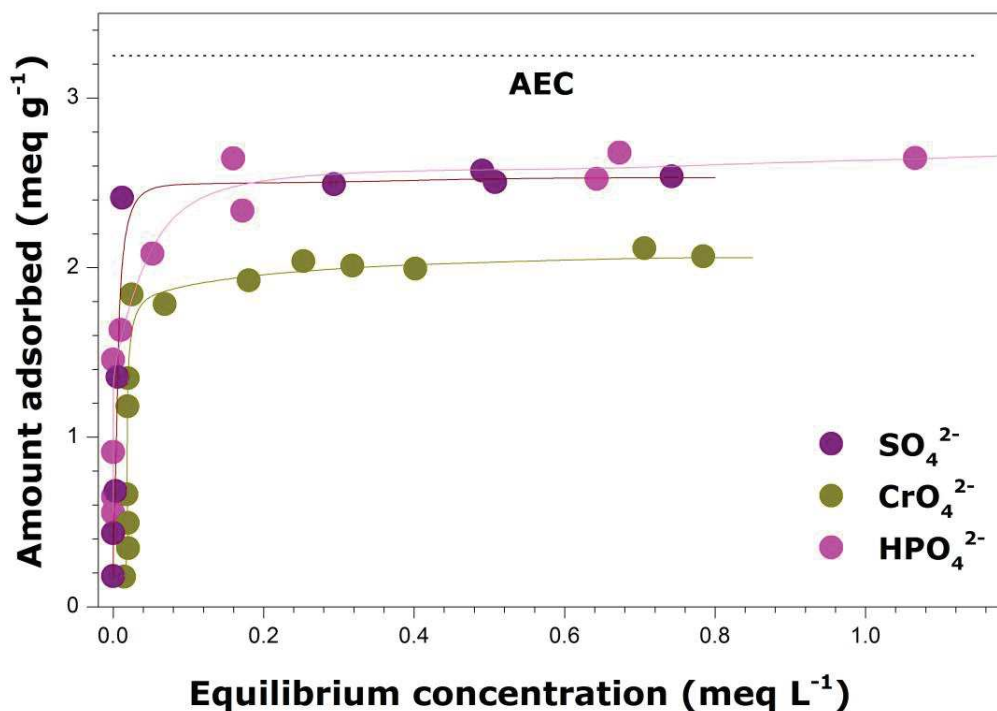


Figure S 2. Adsorption isotherms for inorganic anions from single-solute solutions onto Mg-Al-LDH-NO<sub>3</sub> at 298 K. The solid lines represent the smoothed isotherms constructed on the basis of the results of repeated adsorption experiments. The vertical dotted line is used to indicate the theoretical anion exchange capacity (AEC) of LDH.

### III. Calorimetry measurements of the enthalpy of displacement accompanying the adsorption of dye or inorganic anions from single-solute solutions onto Mg-Al-LDH-NO<sub>3</sub> at 298 K

Table S 1. Operating parameters used in the adsorption experiments carried out with the aid of isothermal titration calorimeter TAM III

Adsorbed species	Number of injections	Injection volume (μL)	Injection speed (sec)	Agitation speed (rpm)	Equilibration time between two successive injections (min)
Methyl Orange	33	30	30	120	90
Orange II	25	10	10	90	90
Orange G	25	10	10	120	180
Sulfates	25	10	10	90	90
Chromates	25	10	10	90	90
Hydrogen phosphates	25	10	10	90	90

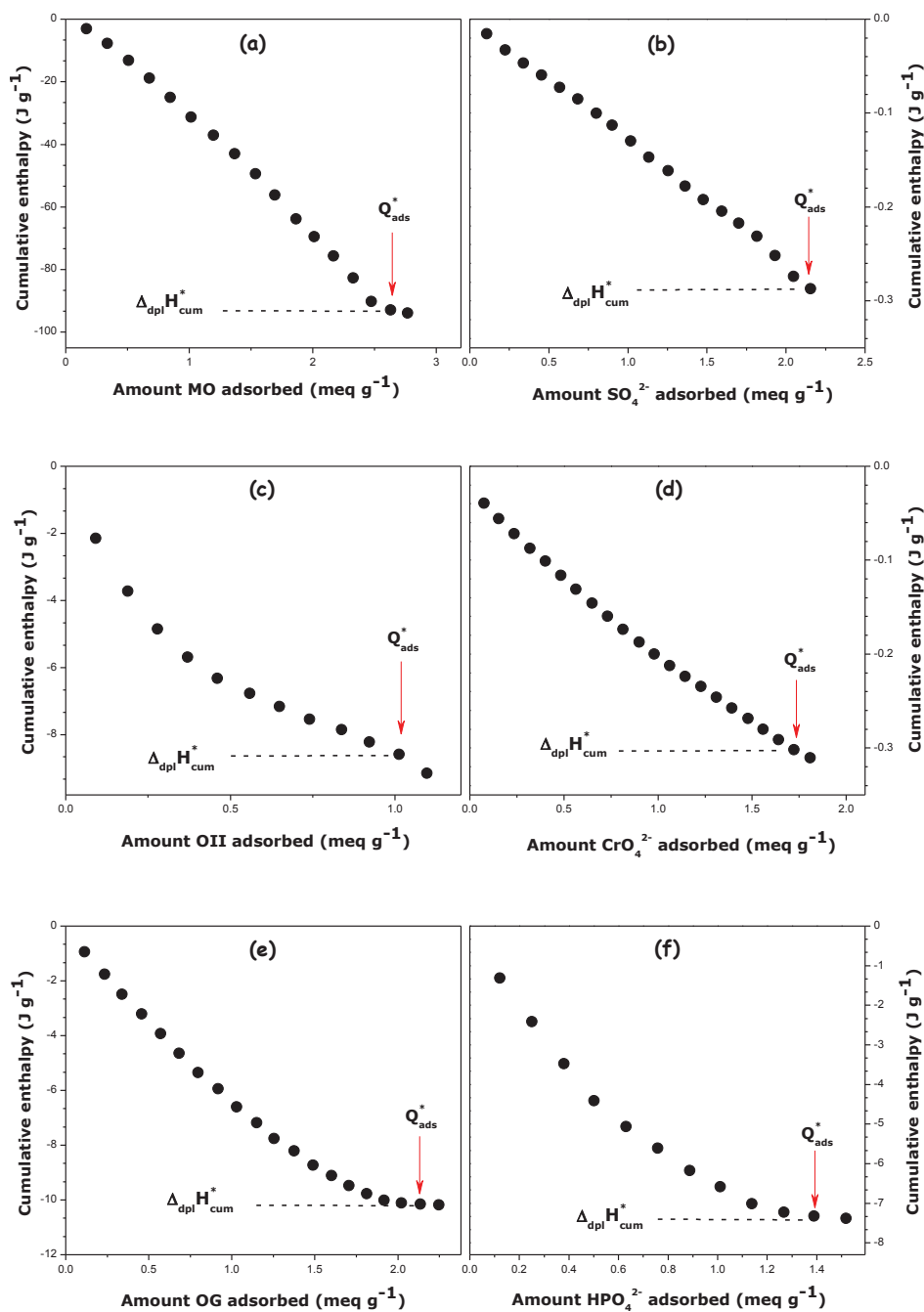


Figure S 3. Variations of the cumulative enthalpy of displacement accompanying adsorption of dye and inorganic anions from single-solute solutions onto Mg-Al-LDH-NO<sub>3</sub> at 298 K as a function of the amount of a given species retained by the solid sample, as plotted in an adsorption range corresponding to the initial quasi-vertical portion on the adsorption isotherm, i.e., up to  $Q_{ads}^*$ ;  $\Delta_{dpl}H_{cum}^*$  represents the enthalpy value at the end of this interval: (a) Methyl Orange, (b) SO<sub>4</sub><sup>2-</sup>, (c) Orange II, (d) CrO<sub>4</sub><sup>2-</sup>, (e) Orange G, (f) HPO<sub>4</sub><sup>2-</sup>.

#### IV. Results of adsorption studies on systems containing bi-solute solutions of dye and inorganic anions

The results of adsorption studies made on systems containing bi-solute solutions have been collected below. Each figure shows a set of adsorption isotherms obtained for a given solute mixture and three molar ratios between dye and inorganic anion: (2:1), (1:1), (1:2). To construct the composite adsorption isotherm, the sum of the two amounts adsorbed has been plotted as a function of the dye concentration in the equilibrium bulk solution.

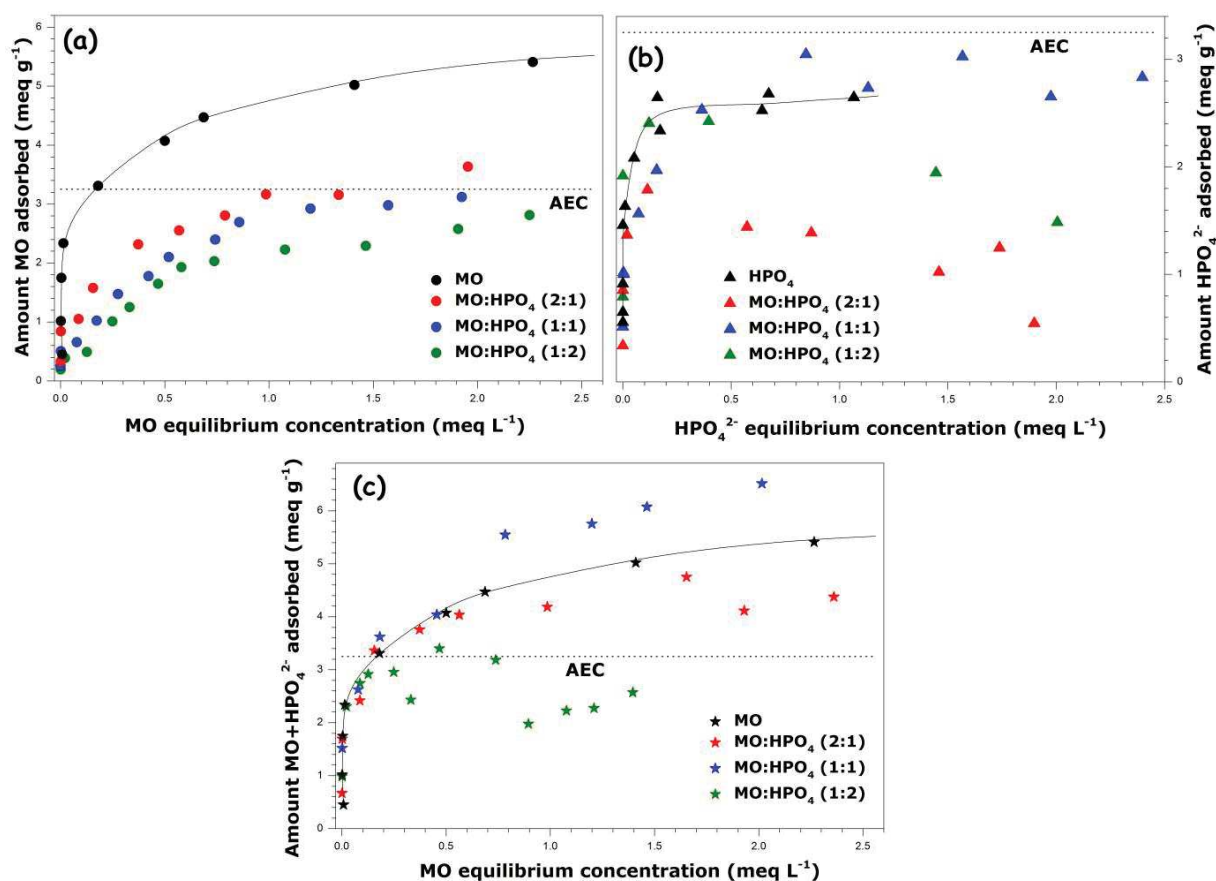


Figure S 4. Individual (panels a and b) and composite (panel c) adsorption isotherms for Methyl Orange and hydrogen phosphate anions adsorbed at 298 K onto Mg-Al-LDH-NO<sub>3</sub> from bi-solute solutions at different molar ratios between dye and inorganic anion under conditions of exposure to the ambient atmosphere employed in the present study. The dotted lines are used to indicate the anion exchange capacity (AEC) of the LDH sample.

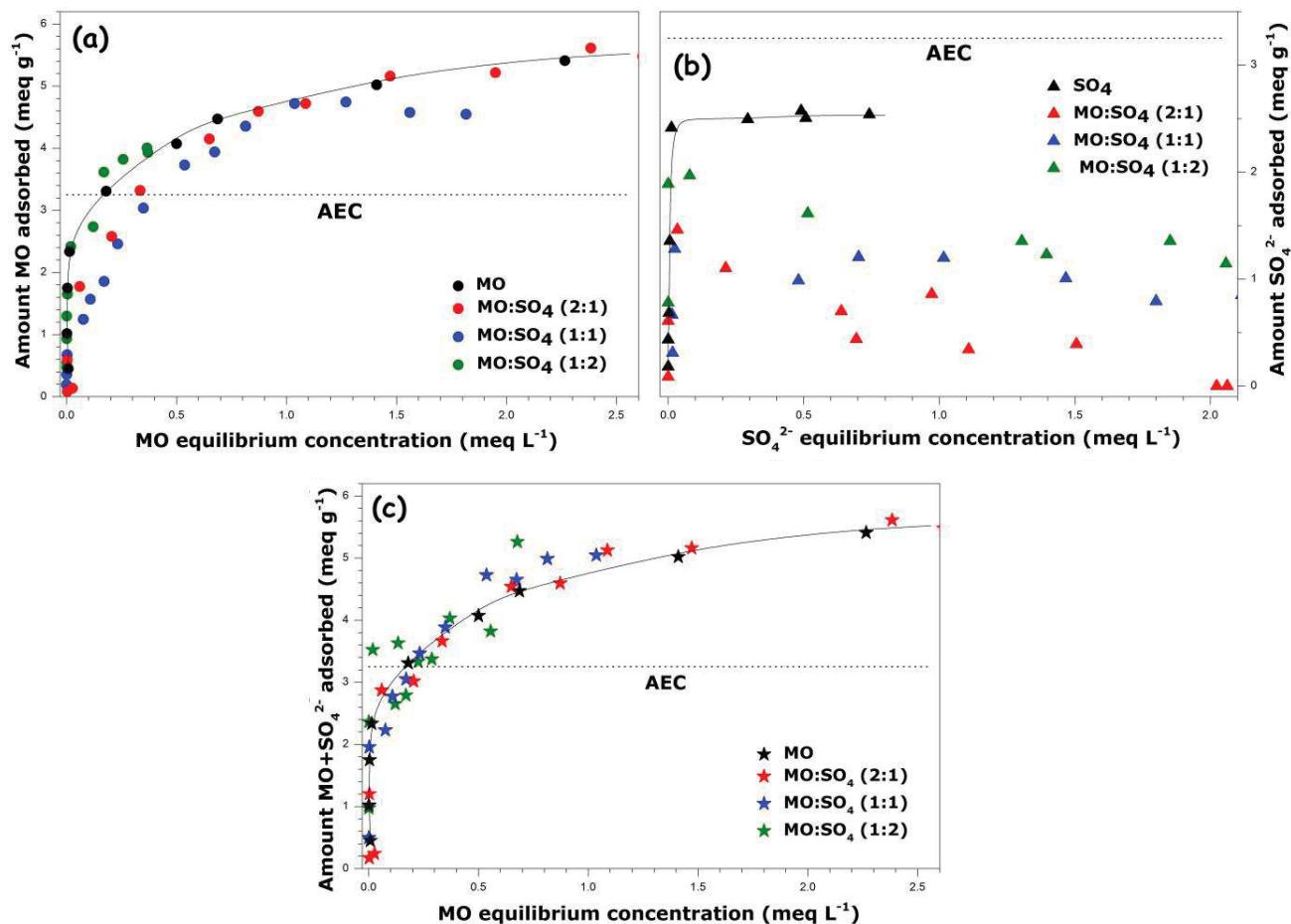


Figure S 5. Individual (panels a and b) and composite (panel c) adsorption isotherms for Methyl Orange and sulfate anions adsorbed at 298 K onto Mg-Al-LDH-NO<sub>3</sub> from bi-solute solutions at different molar ratios between dye and inorganic anion under conditions of exposure to the ambient atmosphere employed in the present study. The dotted lines are used to indicate the anion exchange capacity (AEC) of the LDH sample.

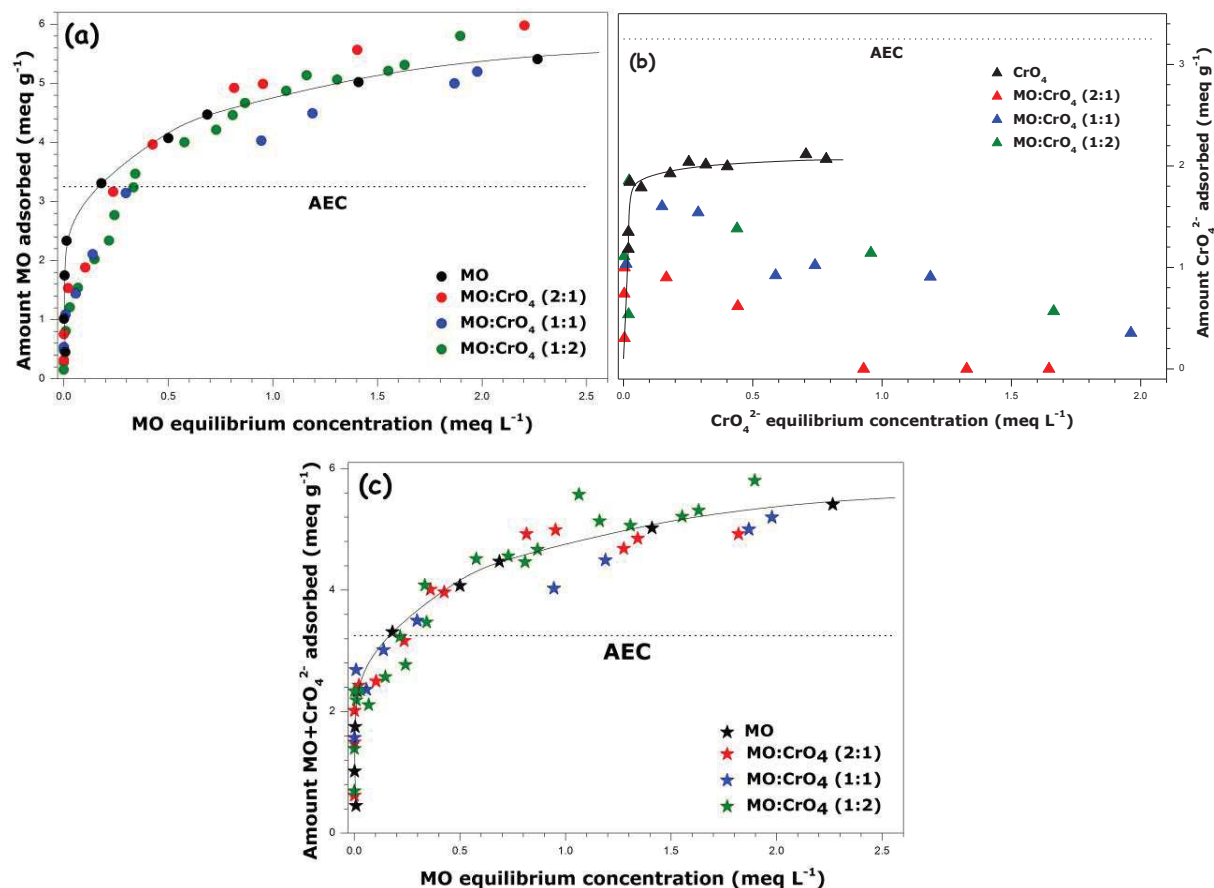


Figure S 6. Individual (panels a and b) and composite (panel c) adsorption isotherms for Methyl Orange and chromate anions adsorbed at 298 K onto Mg-Al-LDH-NO<sub>3</sub> from bi-solute solutions at different molar ratios between dye and inorganic anion under conditions of exposure to the ambient atmosphere employed in the present study. The dotted lines are used to indicate the anion exchange capacity (AEC) of the LDH sample.

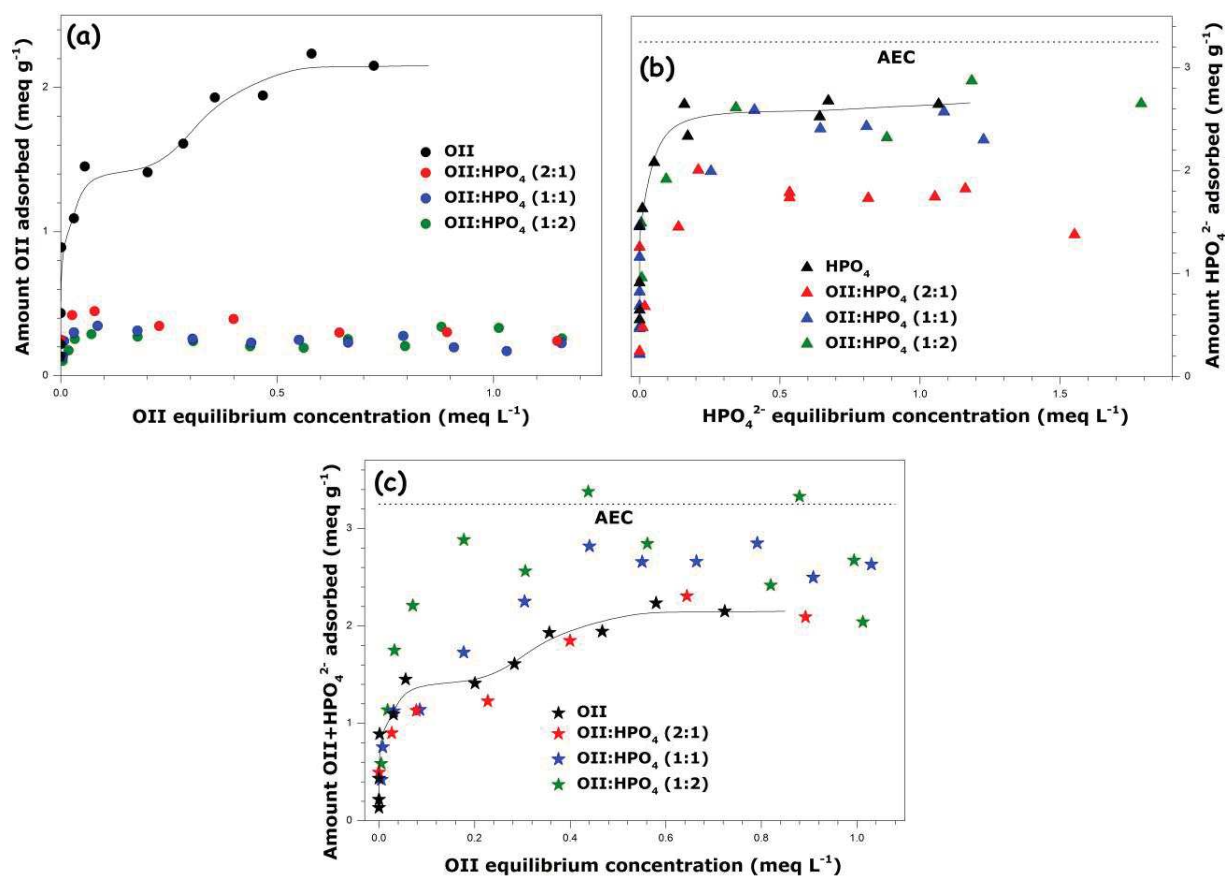


Figure S 7. Individual (panels a and b) and composite (panel c) adsorption isotherms for Orange II and hydrogen phosphate anions adsorbed at 298 K onto Mg-Al-LDH-NO<sub>3</sub> from bi-solute solutions at different molar ratios between dye and inorganic anion under conditions of exposure to the ambient atmosphere employed in the present study. The dotted lines are used to indicate the anion exchange capacity (AEC) of the LDH sample.

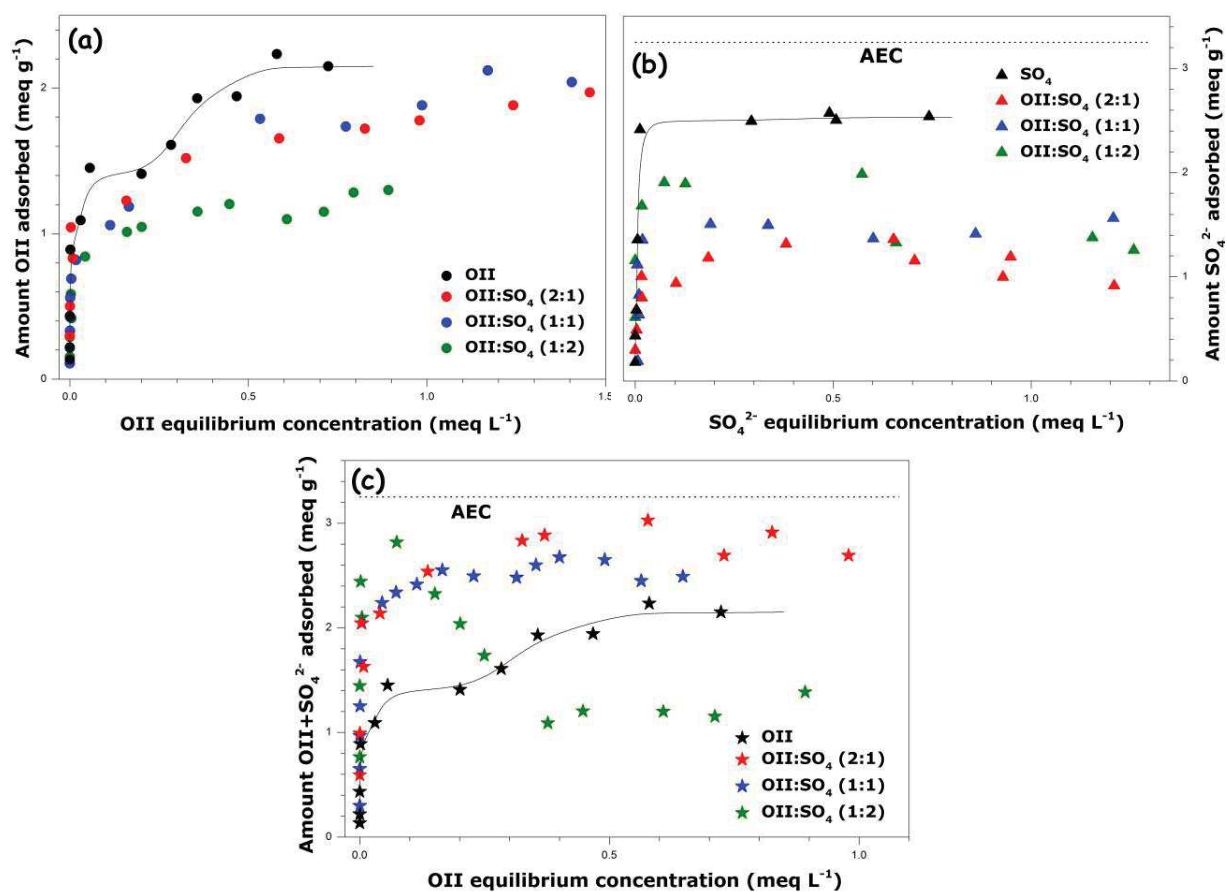


Figure S 8. Individual (panels a and b) and composite (panel c) adsorption isotherms for Orange II and sulfate anions adsorbed at 298 K onto Mg-Al-LDH-NO<sub>3</sub> from bi-solute solutions at different molar ratios between dye and inorganic anion under conditions of exposure to the ambient atmosphere employed in the present study. The dotted lines are used to indicate the anion exchange capacity (AEC) of the LDH sample.

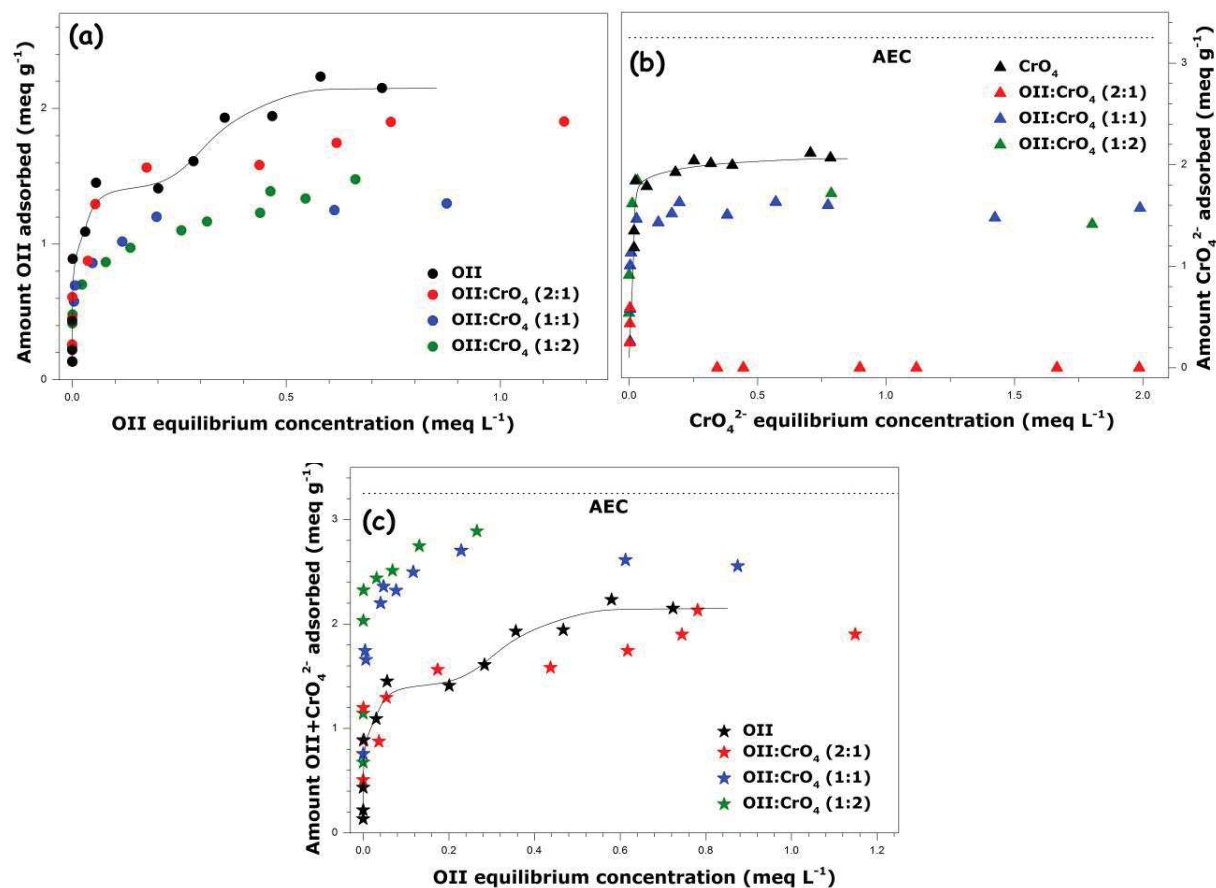


Figure S 9. Individual (panels a and b) and composite (panel c) adsorption isotherms for Orange II and chromate anions adsorbed at 298 K onto Mg-Al-LDH-NO<sub>3</sub> from bi-solute solutions at different molar ratios between dye and inorganic anion under conditions of exposure to the ambient atmosphere employed in the present study. The dotted lines are used to indicate the anion exchange capacity (AEC) of the LDH sample.

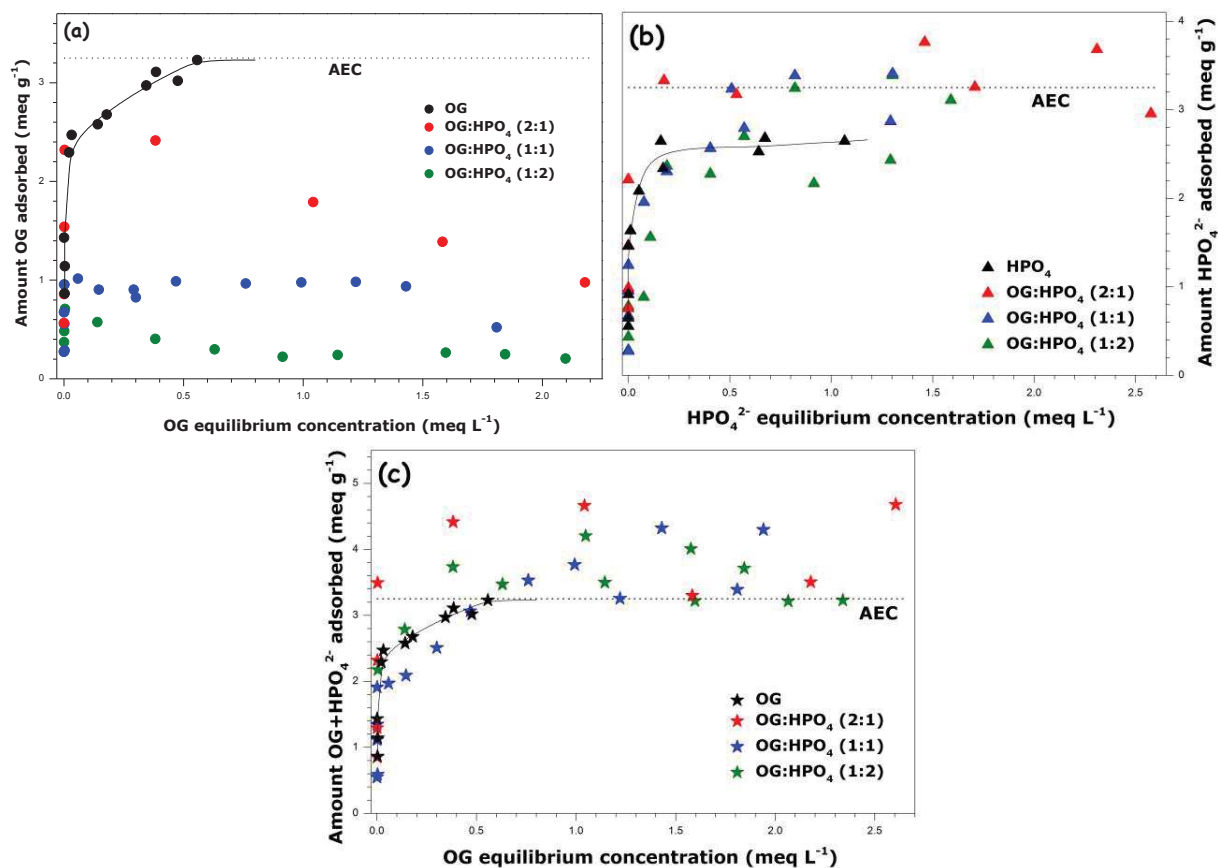


Figure S 10. Individual (panels a and b) and composite (panel c) adsorption isotherms for Orange G and hydrogen phosphate anions adsorbed at 298 K onto Mg-Al-LDH-NO<sub>3</sub> from bi-solute solutions at different molar ratios between dye and inorganic anion under conditions of exposure to the ambient atmosphere employed in the present study. The dotted lines are used to indicate the anion exchange capacity (AEC) of the LDH sample.

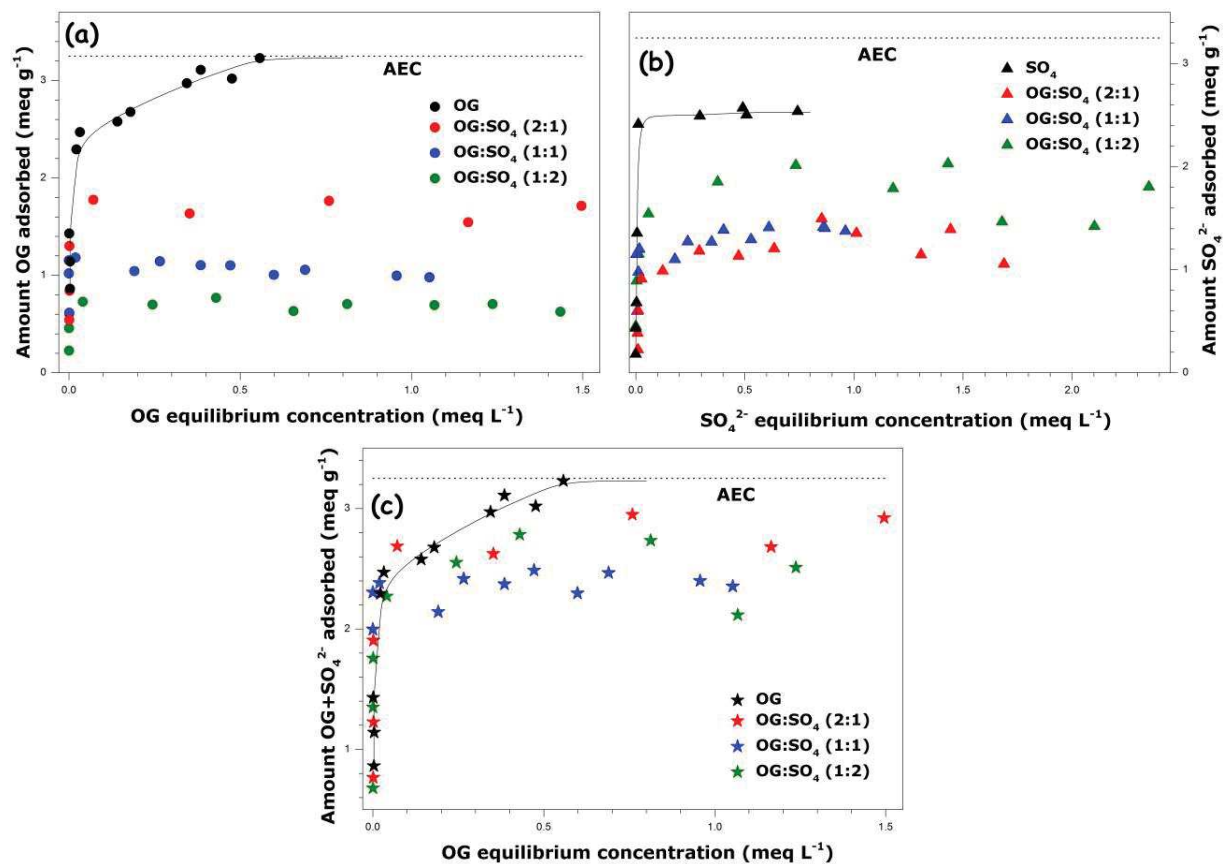


Figure S 11. Individual (panels a and b) and composite (panel c) adsorption isotherms for Orange G and sulfate anions adsorbed at 298 K onto Mg-Al-LDH-NO<sub>3</sub> from bi-solute solutions at different molar ratios between dye and inorganic anion under conditions of exposure to the ambient atmosphere employed in the present study. The dotted lines are used to indicate the anion exchange capacity (AEC) of the LDH sample.

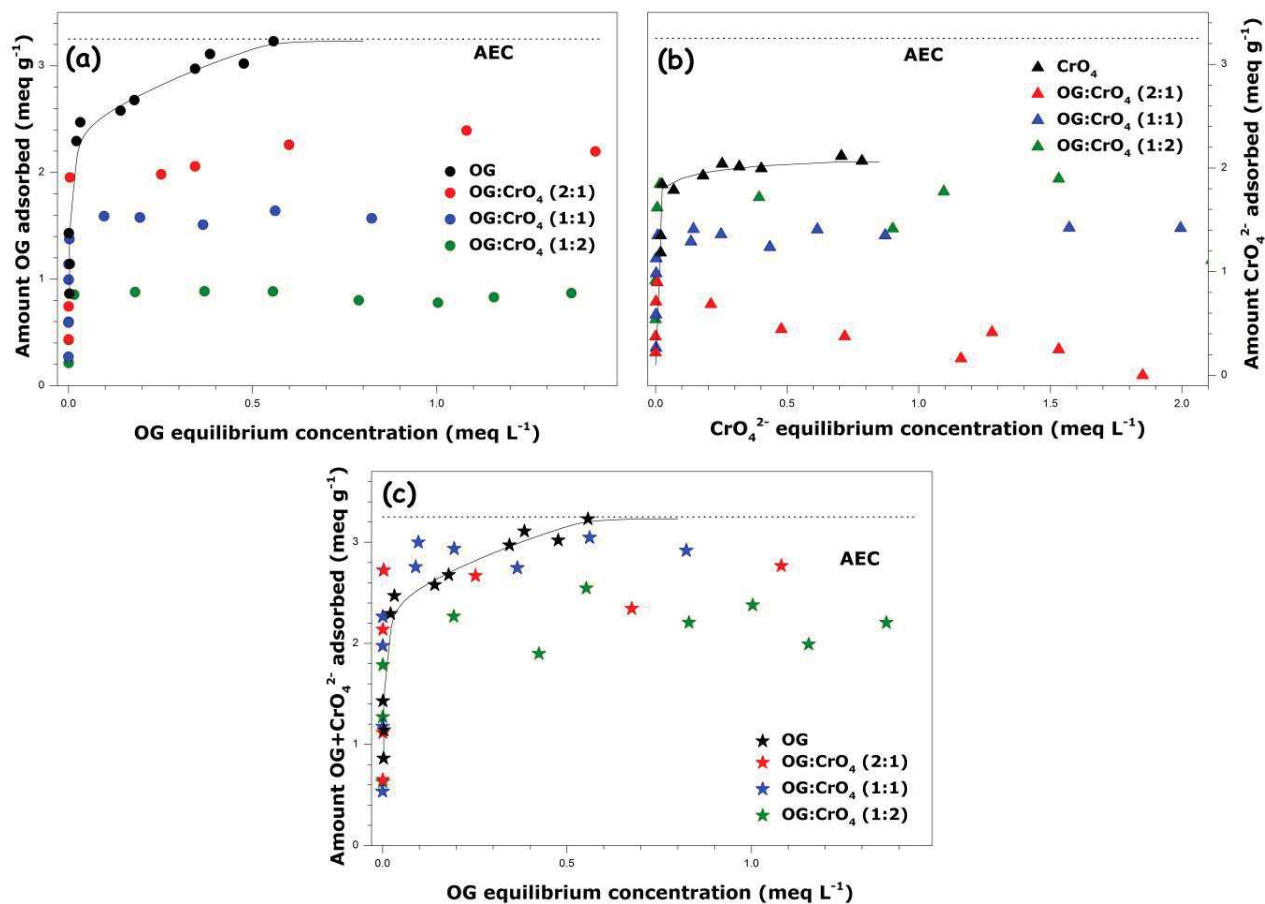


Figure S 12. Individual (panels a and b) and composite (panel c) adsorption isotherms for Orange G and chromate anions adsorbed at 298 K onto Mg-Al-LDH-NO<sub>3</sub> from bi-solute solutions at different molar ratios between dye and inorganic anion under conditions of exposure to the ambient atmosphere employed in the present study. The dotted lines are used to indicate the anion exchange capacity (AEC) of the LDH sample.

**V. XRD diffraction patterns recorded on Mg-Al-LDH-NO<sub>3</sub> loaded with different species adsorbed from equimolar bi-solute solutions of dye and inorganic anions**

The LDH samples loaded with different anions for XRD studies have been chosen such that they represent some specific portions of the corresponding adsorption isotherms. For example, the first sample denoted by ‘dye+inorganic anion (1)’ corresponds to the quasi-vertical portions of the adsorption curves, whereas the last one usually refers to the plateau adsorption regions.

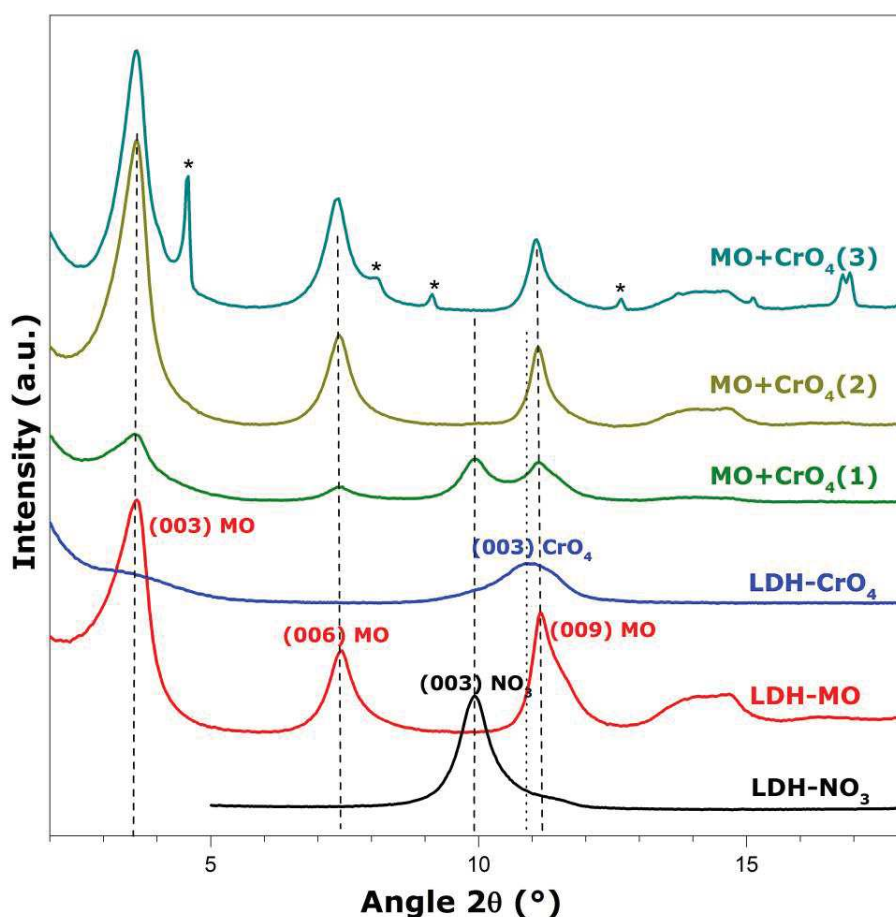


Figure S 13. X-ray diffraction patterns in a  $2\theta$  range from  $2^\circ$  to  $18^\circ$  for Mg-Al-LDH-NO<sub>3</sub> loaded with various anionic species from single- and bi-solute equimolar solutions. For the three mixtures of MO and chromate anions, the amounts adsorbed are as follows:  
(1)  $0.99 \text{ meq g}^{-1}$ , MO;  $1.86 \text{ meq g}^{-1}$ , CrO<sub>4</sub><sup>2-</sup>; (2)  $2.95 \text{ meq g}^{-1}$ , MO;  $1.53 \text{ meq g}^{-1}$ , CrO<sub>4</sub><sup>2-</sup>;  
(3)  $5.72 \text{ meq g}^{-1}$ , MO;  $0 \text{ meq g}^{-1}$ , CrO<sub>4</sub><sup>2-</sup>.

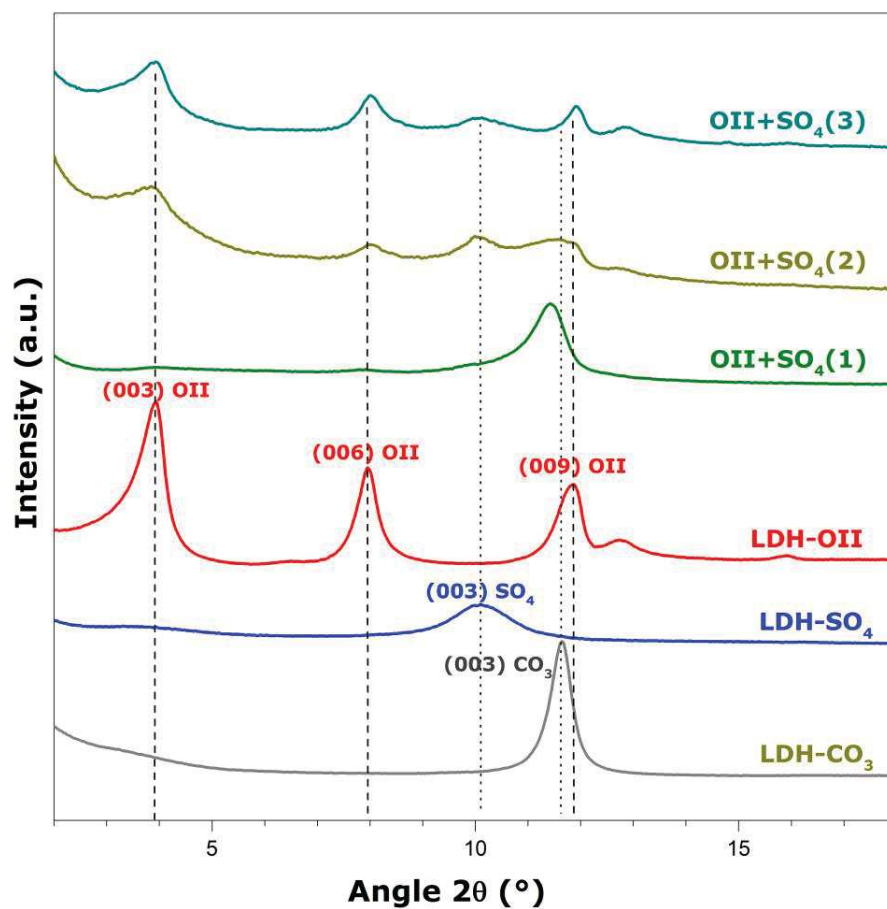


Figure S 14. X-ray diffraction patterns in a  $2\theta$  range from  $2^\circ$  to  $18^\circ$  for Mg-Al-LDH-NO<sub>3</sub> loaded with various anionic species from single- and bi-solute equimolar solutions. For the three mixtures of OII and sulfate anions, the amounts adsorbed are as follows: (1)  $0.25 \text{ meq g}^{-1}$ , OII;  $0.52 \text{ meq g}^{-1}$ , SO<sub>4</sub><sup>2-</sup>; (2)  $0.70 \text{ meq g}^{-1}$ , OII;  $1.41 \text{ meq g}^{-1}$ , SO<sub>4</sub><sup>2-</sup>; (3)  $0.94 \text{ meq g}^{-1}$ , OII;  $1.61 \text{ meq g}^{-1}$ , SO<sub>4</sub><sup>2-</sup>.

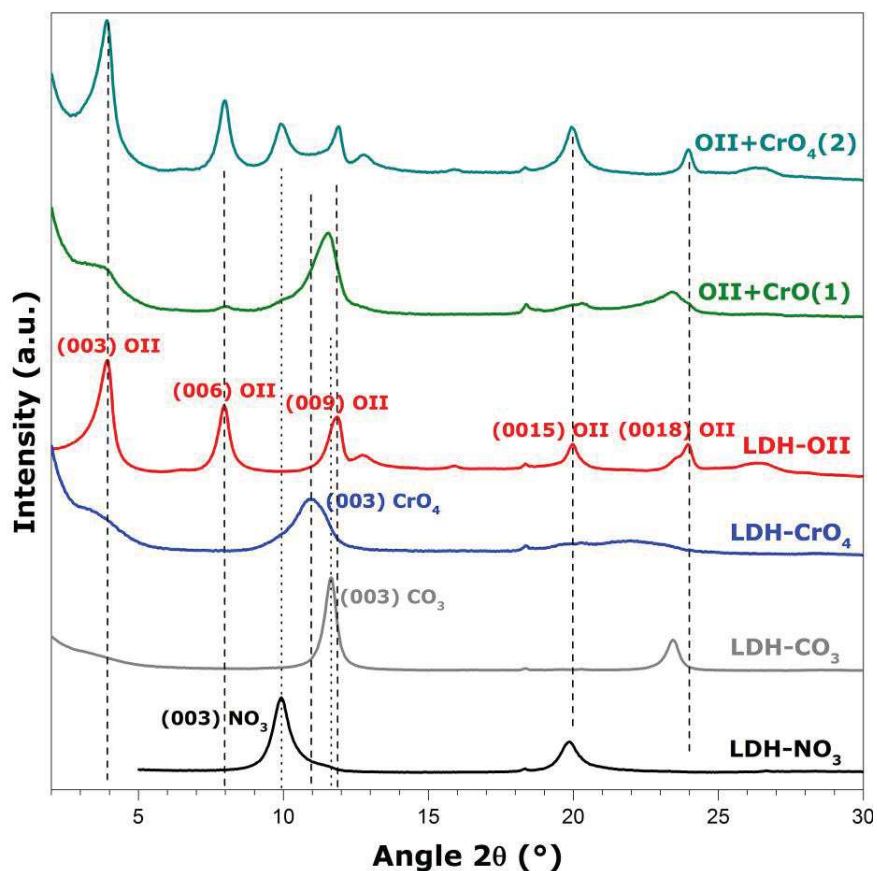


Figure S 15. X-ray diffraction patterns in a  $2\theta$  range from  $2^\circ$  to  $30^\circ$  for Mg-Al-LDH-NO<sub>3</sub> loaded with various anionic species from single- and bi-solute equimolar solutions. For the two mixtures of OII and chromate anions, the amounts adsorbed are as follows: (1)  $0.58 \text{ meq g}^{-1}$ , OII;  $1.14 \text{ meq g}^{-1}$ , CrO<sub>4</sub><sup>2-</sup>; (2)  $1.15 \text{ meq g}^{-1}$ , OII;  $1.34 \text{ meq g}^{-1}$ , CrO<sub>4</sub><sup>2-</sup>.

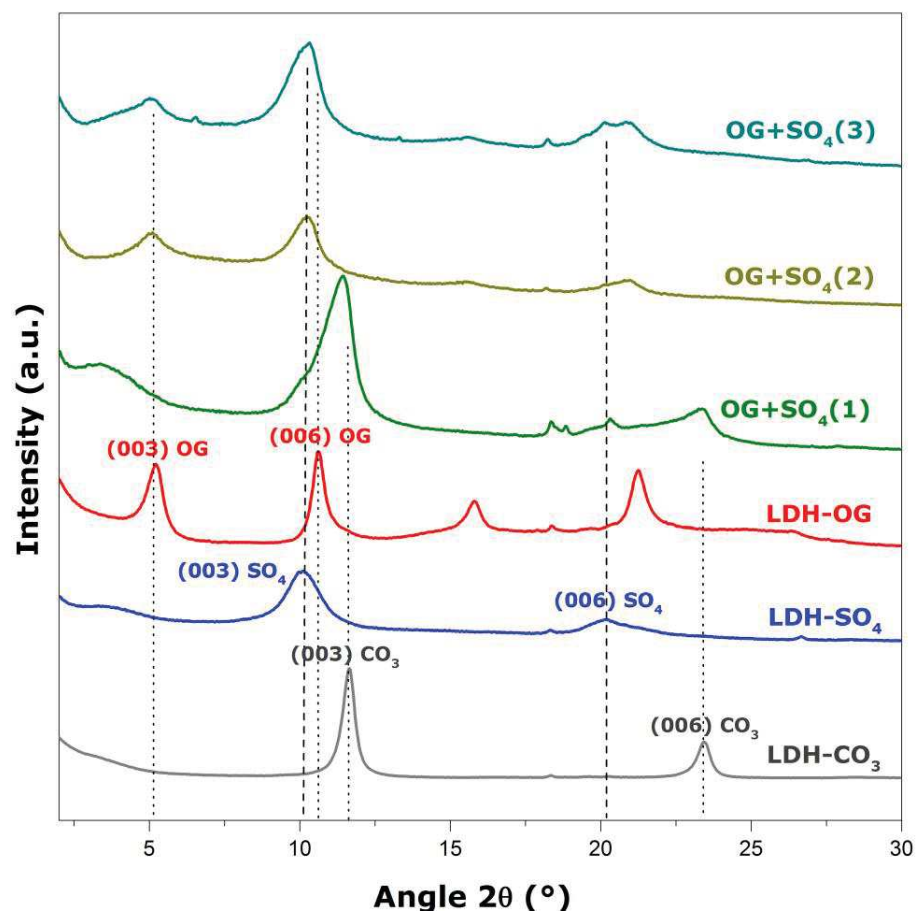


Figure S 16. X-ray diffraction patterns in a  $2\theta$  range from  $2^\circ$  to  $30^\circ$  for Mg-Al-LDH-NO<sub>3</sub> loaded with various anionic species from single- and bi-solute equimolar solutions. For the three mixtures of OG and sulfate anions, the amounts adsorbed are as follows: (1)  $0.93 \text{ meq g}^{-1}$ , OG;  $0.95 \text{ meq g}^{-1}$ , SO<sub>4</sub><sup>2-</sup>; (2)  $1.05 \text{ meq g}^{-1}$ , OG;  $1.18 \text{ meq g}^{-1}$ , SO<sub>4</sub><sup>2-</sup>; (3)  $0.92 \text{ meq g}^{-1}$ , OG;  $1.46 \text{ meq g}^{-1}$ , SO<sub>4</sub><sup>2-</sup>.

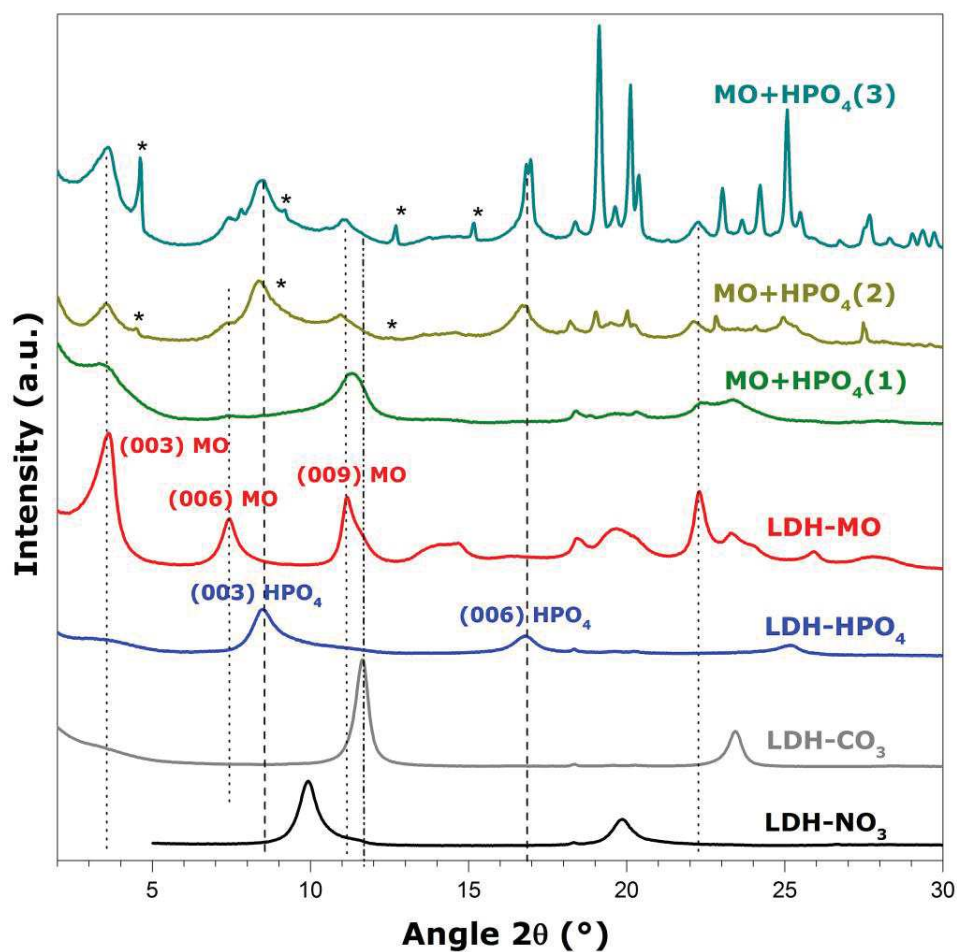


Figure S 17. X-ray diffraction patterns in a 2θ range from 2° to 30° for Mg-Al-LDH-NO<sub>3</sub> loaded with various anionic species from single- and bi-solute equimolar solutions. For the three mixtures of MO and hydrogen phosphate anions, the amounts adsorbed are as follows: (1) 0.40 meq g<sup>-1</sup>, MO; 0.81 meq g<sup>-1</sup>, HPO<sub>4</sub><sup>2-</sup>; (2) 1.33 meq g<sup>-1</sup>, MO; 2.54 meq g<sup>-1</sup>, HPO<sub>4</sub><sup>2-</sup>; (3) 2.6 meq g<sup>-1</sup>, MO; 2.11 meq g<sup>-1</sup>, HPO<sub>4</sub><sup>2-</sup>.

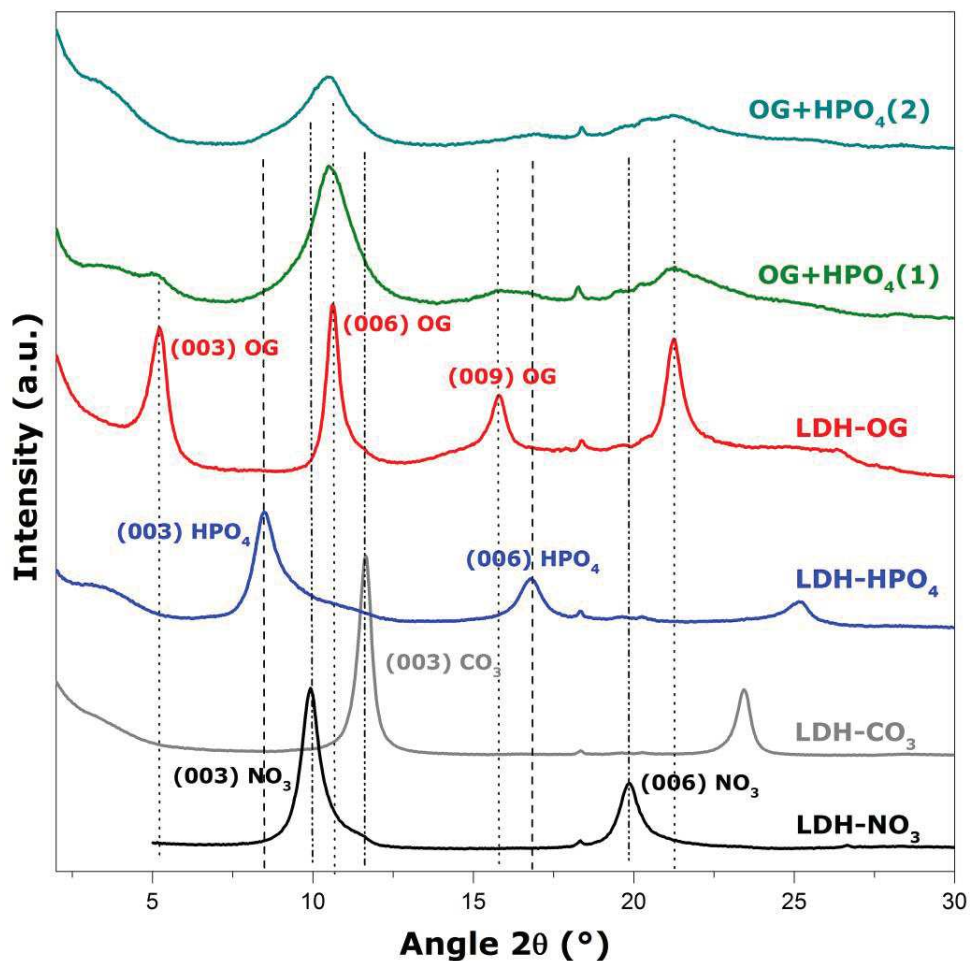


Figure S 18. X-ray diffraction patterns in a  $2\theta$  range from  $2^\circ$  to  $30^\circ$  for Mg-Al-LDH-NO<sub>3</sub> loaded with various anionic species from single- and bi-solute equimolar solutions. For the two mixtures of OG and hydrogen phosphate anions, the amounts adsorbed are as follows:

(1)  $0.70 \text{ meq g}^{-1}$ , OG;  $2.01 \text{ meq g}^{-1}$ , HPO<sub>4</sub><sup>2-</sup>; (2)  $0.28 \text{ meq g}^{-1}$ , OG;  $2.95 \text{ meq g}^{-1}$ , HPO<sub>4</sub><sup>2-</sup>.

## VI. Results of adsorption and XRD studies on systems containing bi-solute solutions of dye and carbonate anions

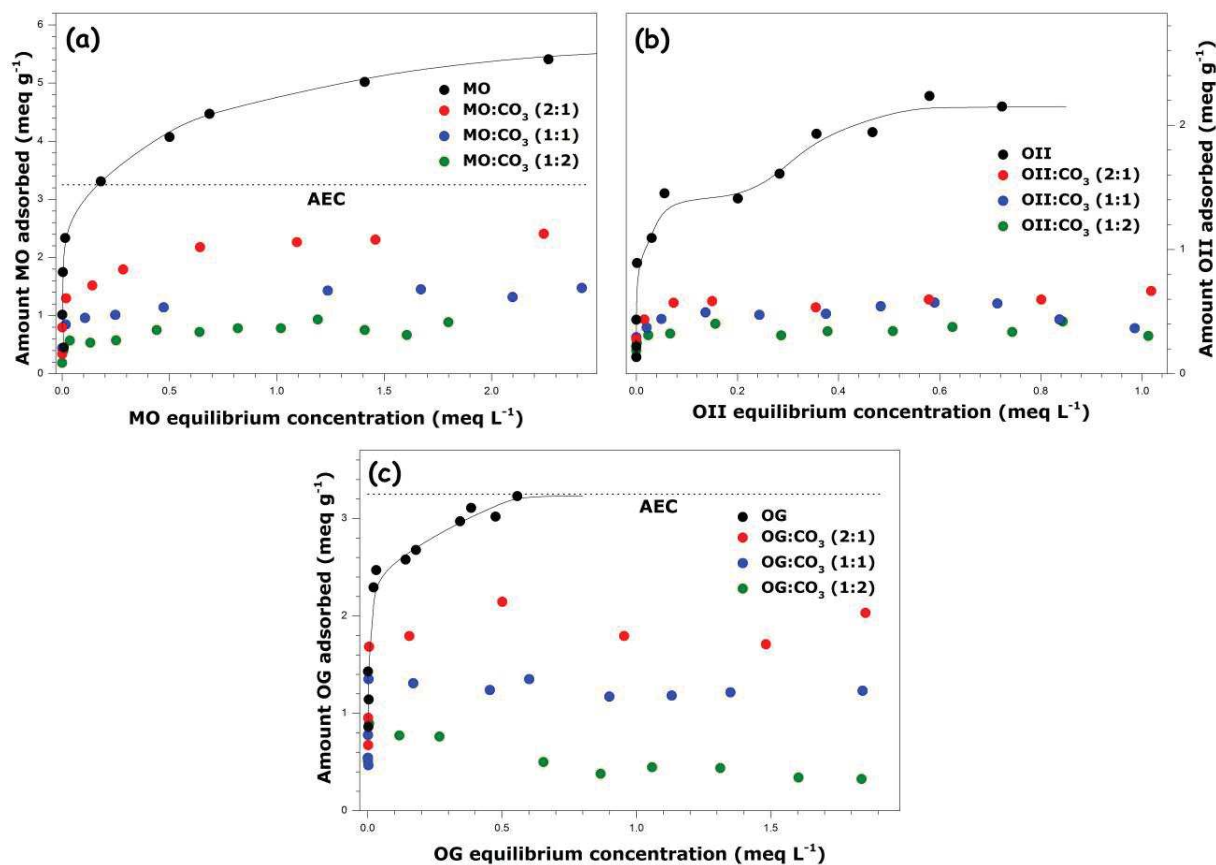


Figure S 19. Effect of the addition of carbonate anions to the aqueous phase on the adsorption of Methyl Orange (panel a), Orange II (panel b), and Orange G (panel c) at 298 K onto Mg-Al-LDH-NO<sub>3</sub> from bi-solute solutions at different molar ratios between dye and carbonate species. The dotted lines are used to indicate the anion exchange capacity (AEC) of the LDH sample.

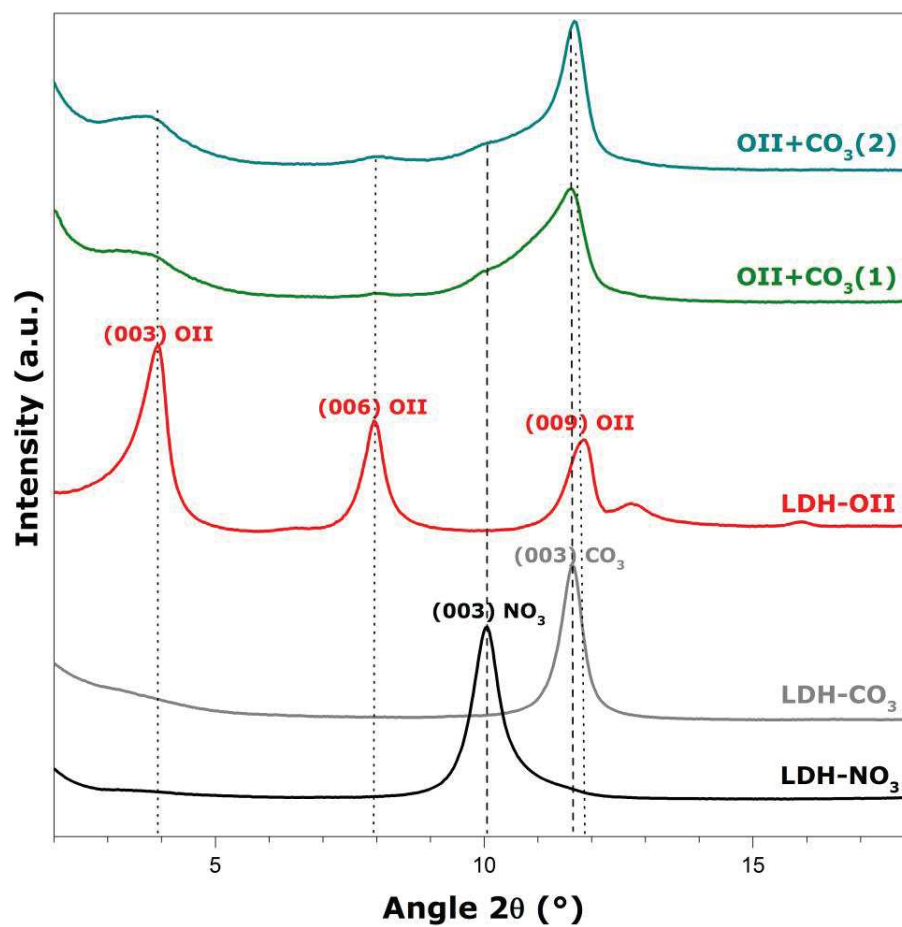


Figure S 20. X-ray diffraction patterns in a  $2\theta$  range from  $2^\circ$  to  $18^\circ$  for Mg-Al-LDH-NO<sub>3</sub> loaded with various anionic species from single- and bi-solute equimolar solutions. For the two mixtures of OII and carbonate anions, the amounts of dye adsorbed are as follows:

(1)  $0.23 \text{ meq g}^{-1}$ , (2)  $0.49 \text{ meq g}^{-1}$ .

## **CONCLUSIONS**

In this chapter the results for the multi-component adsorption of Orange-type dyes and inorganic oxyanions (sulfates, chromates, phosphates) from the bi-solute component solutions onto the Mg-Al-LDH-NO<sub>3</sub> are presented.

From the results obtained for equimolar concentrations it can be concluded that Methyl Orange, the most hydrophobic molecule has the least influence in the presence of the competing species. No influence was observed in the presence of sulfates and chromates ion and a small and insignificant effect was observed for the phosphates ions. This can be explained by the MO sorption onto the external surface of the LDH. In the case of Orange II and Orange G, both dyes have similar adsorbing properties in the presence of the inorganic anions. The amounts of dyes adsorbed are decreased in the presence of the competing inorganic ions. Moreover, these dyes are highly influenced by the presence of phosphates (OII) and sulfates (OG) ions. Multi-component adsorption measurement performed for the different organic and inorganic anions ratios showed that the removal of the dye and that of the inorganic anion is affected by both the type and the concentration of the co-existing competing species.

The multi-component adsorption in the presence of specially added carbonates showed a negative impact on the dye adsorption onto the LDH. This is due to the fact that the carbonates ions occupied all the interlayer space of the LDH as shown on the XRD pattern.

To conclude, Mg-Al-LDH-NO<sub>3</sub> can be a very good potential adsorbent for Orange - type dye adsorption. However, in the presence of competing inorganic anions, special care should be taken into consideration as possible inhibition of dye amount adsorbed in the presence of carbonates and phosphates for MO and OII and the presence of carbonates and sulfates for OG can occurred. Only chromate anions do not significantly decrease the retention of the dyes, thus potentially not dangerous for adsorption results.

**Chapter IV:**  
**Single-component and**  
**competitive adsorption of Dyes**  
**and inorganic anions on**  
**Mg-Al-LDH-Cl**



## **1. INTRODUCTION**

Layered Double Hydroxide (LDH) or anionic clays possess very good adsorptive properties mainly because of their high density of layer charge, which can accommodate various negatively charged organic and inorganic contaminants [1].

In the previous chapters, we reported the adsorption of Orange-type dyes (Methyl Orange, Orange II and Orange G) and different divalent inorganic anions from mono- and bi-solute solutions. An uncalcined LDH sample containing nitrate species as the pristine compensating anions was used there as the adsorbent material. The first objective of these chapters was to evaluate the mechanism of azo-dye intercalation into the LDH structure. Secondly, our intention was to understand the action of more complex systems by studying the competitive adsorption of these dyes from bi-component dye-inorganic ion systems. The pristine LDH sample containing nitrate interlayer anions was the best candidate to perform such studies, because nitrates may be very easily exchanged by other species [2]. Since the sorption of pollutants by LDH materials is based on anion exchange [3], the toxicity of the initial interlayer anion should be also taken into account. Even if nitrate is considered to be relatively non-toxic to adults, concentrations greater than 50 ppm can be fatal to infants under six months of age [4]. Therefore, in the present chapter an investigation of the single-component and competitive adsorption of the same dyes has been described onto LDH sample containing another interlayer anion, which has no deleterious impact on nature and human health. For this purpose, Mg-Al-LDH sample with interlayer chloride anions was selected.

This contribution to the understanding of adsorption mechanism onto LDH materials gave new results to compare the dye removal process as a function of the compensating anion. The adsorption of MO, OII and OG onto Mg-Al-LDH-Cl has never been reported earlier in the literature. The competitive adsorption was studied from bi- and tri- component systems. The bi-component systems contained azo dye with one inorganic ion (phosphate or carbonate), whereas the tri-component one was composed of one dye and two inorganic ions. As in the previous cases the Isotherm Titration Calorimetry was additionally used to date in the case of single-solute

systems and the XRD analysis of samples exchanged with dye gave indication for the dye intercalation in the LDH interlayer.

## 2. Characterization of uncalcined Mg-Al-LDH-Cl adsorbent

Thermogravimetric analysis of the Mg-Al-LDH-Cl material synthesized by coprecipitation method is shown in Figure 1. As can be seen in the TG - DTA plot, three regions of the weight loss can be distinguished in the temperature ranges: 25 - 220, 220 - 470 and 470 - 700°C. The weight loss in the first region (25 - 220°C) is about 14.5%, which is characteristic of the removal of physisorbed and interlayer water molecules from layered materials [5]. The 57% weight loss in the temperature range of 220 - 470°C corresponds to the release of the hydroxyl groups from brucite layers [6]. The last region represents the continuous dehydroxylation and formation of metal oxides. The conclusion regarding the water content in the LDH is inferred from the number of molecules based on the theoretical formula of the layered material:  $\text{Mg}_{0.67}\text{Al}_{0.33}(\text{OH})_2\text{Cl}_{0.33} \cdot 0.67 \text{H}_2\text{O}$  (the details of the calculations are included in Appendix II, section II).

The X-ray Diffraction analysis was performed to confirm the layered structure of Mg-Al-LDH-Cl material with chloride anions in the interlayer gallery (Figure 2). The diffraction pattern shows a series of peaks corresponding to rhombohedral symmetry of the layered material. Two harmonic peaks, (003) and (006), which are located respectively at 11.5 and 23° 2θ positions give information about the interlayer dimensions (parameter *c*) and confirm the presence of the desired interlayer anion. Thus, the positions at 7.724 and 3.854 Å are attributed to harmonic reflections of chloride anions in the layer of LDH. The value of parameter *c* is found to be 23.172 Å. The parameter *a* is found from (110) reflection and is equal to 3.048 Å. These values are in good agreement with those reported in the literature for Mg<sup>II</sup>/Al<sup>III</sup> layered structures, containing chloride anions [7-9].

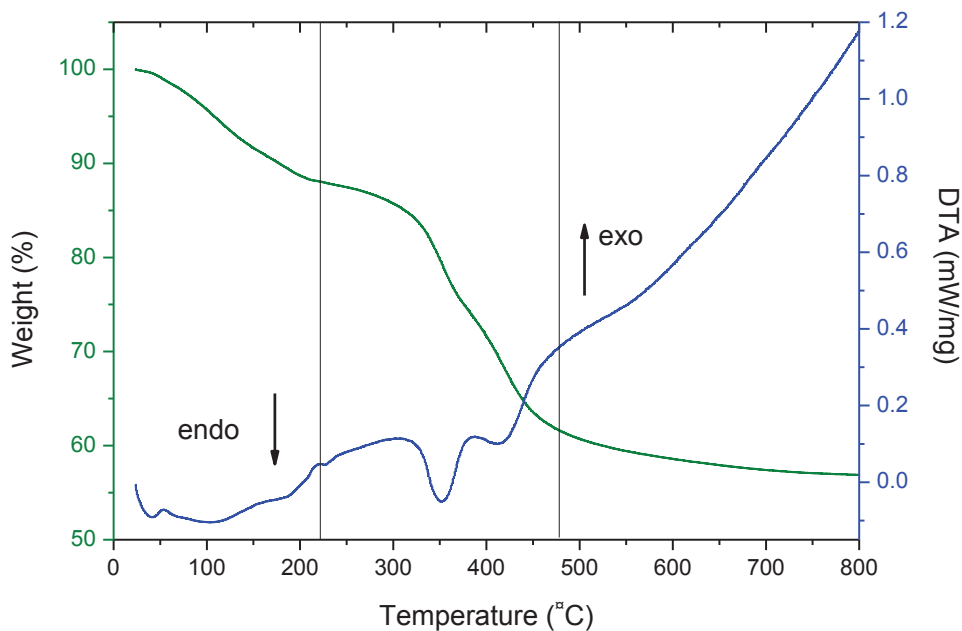


Figure 1. TG - DTA plots of uncalcined Mg-Al-LDH-Cl.

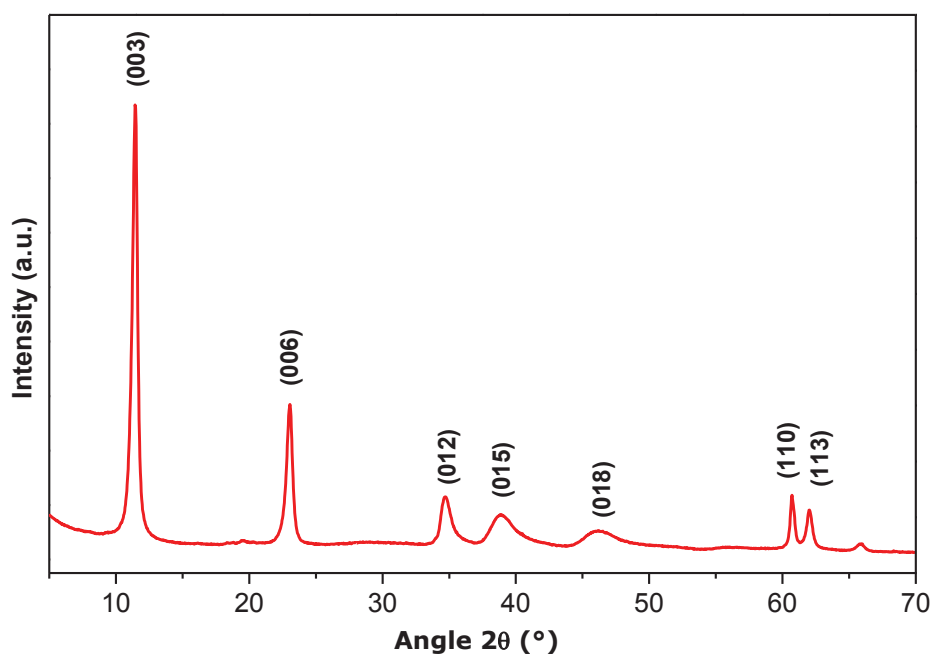


Figure 2. XRD pattern of Mg-Al-LDH-Cl adsorbent.

### 3. Adsorption of dyes from single-component aqueous solutions

In the first section of this chapter, we shall investigate the adsorption of the three azo dyes MO, OII and OG onto Mg-Al-LDH-Cl from single-component solutions. Sorption experiments are performed by following a procedure described in Appendix II, section I. The adsorption isotherms for all dyes are presented in Figure 3. For MO and OG, the amounts adsorbed attained in the plateau region are approximately equal to  $4.7 \text{ mmol g}^{-1}$  and  $0.6 \text{ mmol g}^{-1}$ , respectively. OII reaches a pseudo-plateau value of  $2.7 \text{ mmol g}^{-1}$ .

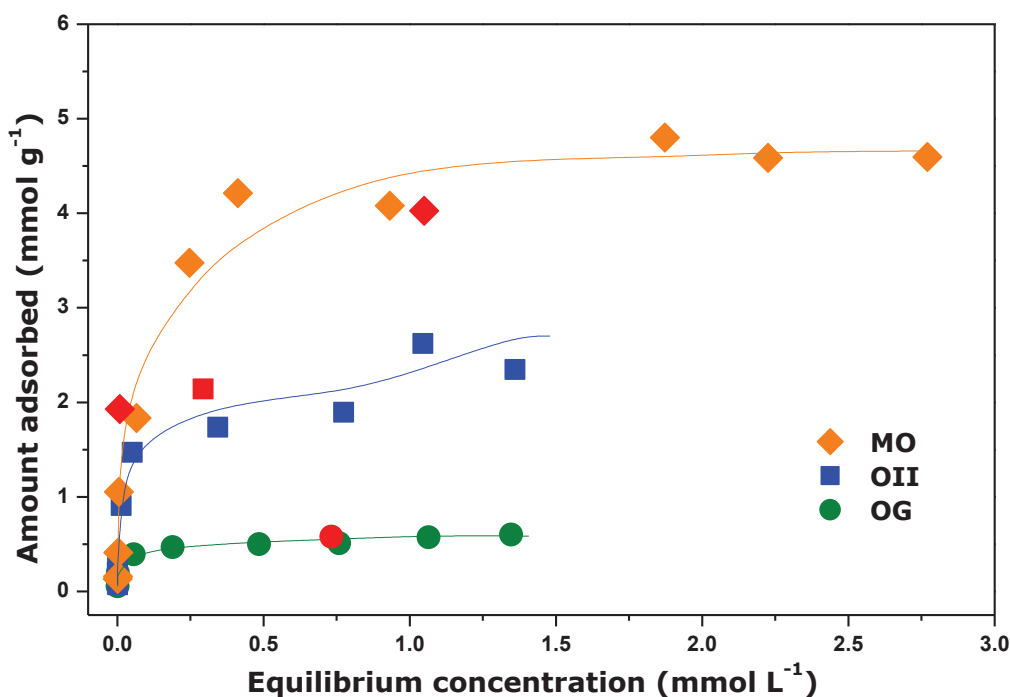


Figure 3. Isotherms of dye adsorption from single-component solutions onto Mg-Al-LDH-Cl at 298 K. The solid lines represent the smoothed isotherms constructed on the basis of the results of repeated adsorption experiments. Red points represent the dye loaded LDH samples taken for XRD.

The results obtained for LDH-Cl can be compared with those previously reported in Chapter II for LDH-NO<sub>3</sub>. The amount of MO adsorbed onto the Mg-Al-LDH-NO<sub>3</sub> ( $5.5 \text{ mmol g}^{-1}$ ) is only slightly higher than the amount of the same dye adsorbed onto the Mg-Al-LDH-Cl. On the

contrary, the quantity of OG adsorption onto Mg-Al-NO<sub>3</sub> (1.7 mmol g<sup>-1</sup>) is at least three times higher than that obtained with Mg-Al-Cl. This difference could be ascribed to the affinity of the interlayer anions towards LDH material and their ability to be exchanged. According to Miyata [2], the selectivity of inorganic monovalent anion increases in the order: OH<sup>-</sup> > F<sup>-</sup> > Cl<sup>-</sup> > Br<sup>-</sup> > NO<sub>3</sub><sup>-</sup> onto hydrotalcite-like materials. It can be considered that it is easier for NO<sub>3</sub><sup>-</sup> to leave the interlayer structure in comparison with Cl<sup>-</sup> anions, which have higher affinity for the LDH material. According to the literature [10], divalent inorganic species should have much more affinity towards LDH structure than monovalent ions have. On the contrary, our results indicate that OG<sup>2-</sup> anion is not able to replace all Cl<sup>-</sup> anion from the interlayer region. To confirm the exchange balance between the adsorbing and desorbing species, the supernatant was also analyzed by HPLC to quantify the amount of chloride anions removed from the solid. Figure 4 shows the resulting plots of dye retention as a function of the amount of Cl<sup>-</sup> released from the interlayer during the sorption experiment.

Generally, the amount of interlayer released ions in the ion exchange process should be equal to the amount of the equivalent species adsorbed from solution. However, as observed, already for the first points on the sorption isotherms an excess of chloride interlayer anions is removed from the solid into solution, at variance with straight lines, which have been expected to characterize quantitatively the phenomenon (representation of equivalent exchange). The effect is similar for the three dyes. However, with the increased amount of dye adsorbed, only MO is able to displace the equivalent amount of chloride ion.

During the OII sorption, the amount of chloride displaced from the interlayer progressively increases and the proportion between the dye and chloride in the supernatant remains the same when increasing the amount of dye adsorbed. This information points to the 1:2 stoichiometry of the OII:Cl exchange, which suggests that there is another anionic species entering the interlayer simultaneously with OII to preserve the electroneutrality of the layer. These anionic species may correspond to carbonates, coming from ambient air (see Chapter II) or hydroxide anions present in the aqueous solutions. However, the increase in the pH from the values measured in the beginning of adsorption experiment and those recorded at equilibrium indicates the release of -OH<sup>-</sup> species into the solution during adsorption (an increase of around 1.4 pH unit for MO; 2-3 pH

units for OII; 3 units for OG; see Figure AII-1 in Appendix II). This argues against the  $\text{-OH}^-$  ions co-adsorption together with the dye species.

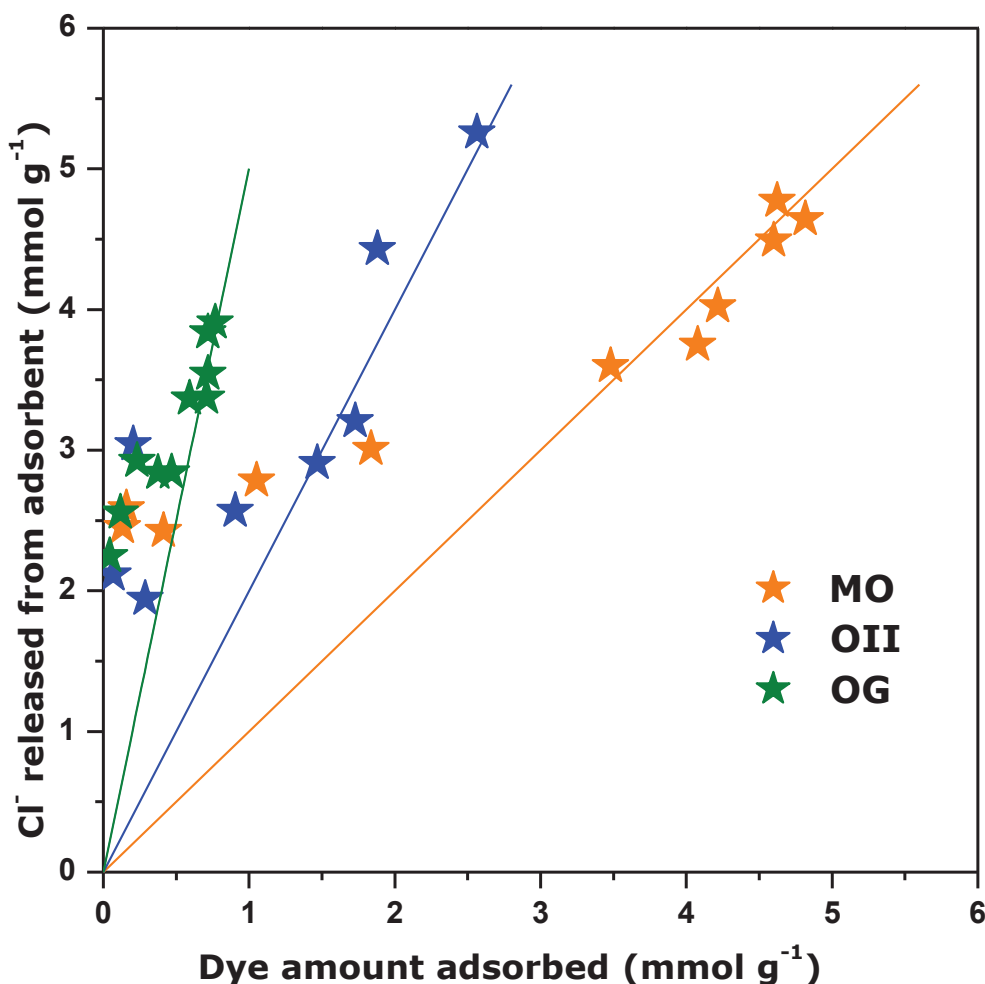


Figure 4. Dye adsorbed onto LDH as a function of chloride leached during exchange. Straight lines represent an expected equivalent exchange.

As for as OG is concerned, the amount of chloride removed from the adsorbent is about five times greater than the amount of OG removed from the solution. This could be ascribed to the greater charge of OG molecules since each OG molecule is bi-valent. However, the difference still remains great, i.e. for  $0.57 \text{ mmol g}^{-1}$  of OG adsorbed  $3.04 \text{ mmol g}^{-1}$  of Cl ions are released. Moreover, the analysis of sodium co-adsorption during the OG uptake (Figure AII-2 (c) and Figure

AII-3 in Appendix II) indicates that, after the third point on the adsorption curve, OG probably uses only one charge to neutralize the interlayer charge. Therefore, a great part of the interlayer charge freed from the released chloride ions (around 5.6) is compensated by another species present in the solution (see Table AII-1 in Appendix II).

It has been already mentioned in the previous chapters, that XRD analysis can give us valuable information about the interlayer spacing of layered double hydroxides. The same experimental analysis was performed for the present Mg-Al-LDH-Cl system. The XRD patterns shown on Figures 5-7 were recorded on the samples loaded with dyes for various points located on the adsorption curves (see Figure 3).

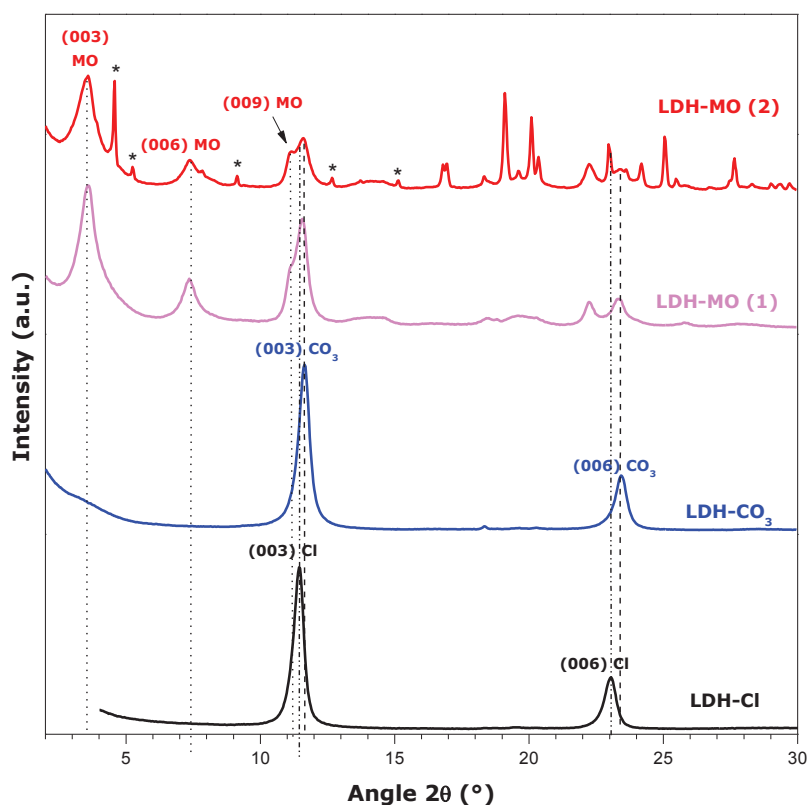


Figure 5. X-ray diffraction patterns in the  $2\theta$  range from  $2^\circ$  to  $30^\circ$  for the intercalation of MO in the Mg-Al-LDH-Cl structure corresponding to 2 selected points at  $Q_{\text{ads}} = 1.9$  and  $4.0 \text{ mmol g}^{-1}$  on the MO adsorption isotherm (as marked by crosses in Figure 3).

Two different points were chosen for MO and one for OII and OG samples. In the case of the first point at  $Q_{\text{ads}} = 1.93 \text{ mmol g}^{-1}$  where the sample is referred to as and labeled LDH-MO(1), three harmonic reflections are observed at  $3.6^\circ$ ,  $7.4^\circ$  and  $11.5^\circ$   $2\theta$  positions. The first two peaks are attributed to the MO intercalated into LDH accompanied by an increase of the interlayer distance up to 2.42 nm (assigned a MO(003) and MO(006)). The last broad peak is ascribed to the mixture of phases: MO and chlorides or carbonates. The (003) reflections of both  $\text{CO}_3$  and Cl phases are too close to each other to decide which of these anions really co-exist with MO within the layer. In consequence, the (006) reflections of these two inorganic ions can be compared. The carbonate anions appear to constitute the predominant co-adsorbed species within the increased amount of MO in the solid. For the second sample loaded with MO, i.e. LDH-MO(2) a decrease of the carbonate phase can be noted (i.e. (003)  $\text{CO}_3$ ); the broad peak at  $11.5^\circ$   $2\theta$  position is attributed to the mixture of two almost equal reflections of the (009) MO and (003)  $\text{CO}_3$ . In analogy with the results obtained for LDH containing nitrates, the sorption of MO on the external surface of Mg-Al-LDH-Cl takes place, giving rise to small sharp peaks, marked with asterisks [11].

One point was selected for LDH loaded with OII (see Figure 3), localized in the beginning of the saturation plateau ( $Q_{\text{ads}} = 2.14 \text{ mmol g}^{-1}$ ). Two harmonic peak (003) and (006) can be visible at  $3.9^\circ$  and  $7.9^\circ$   $2\theta$  positions, corresponding to d-values of 2.22 nm and 1.11 nm of OII dye in the layered structure (Figure 6). As in the previous case of MO, the third broad peak at  $11.5^\circ$   $2\theta$  position is difficult to be assigned. Therefore, the detection of the (006)  $\text{CO}_3$  and (006) Cl reflections allows the presence of carbonate phase to be confirmed in addition to OII species within the interlayer. The broad reflection was assigned to the mixture of two (009) OII and (003)  $\text{CO}_3$  peaks. The presence of carbonate phase is in line with the results of the chloride release from the LDH structure.

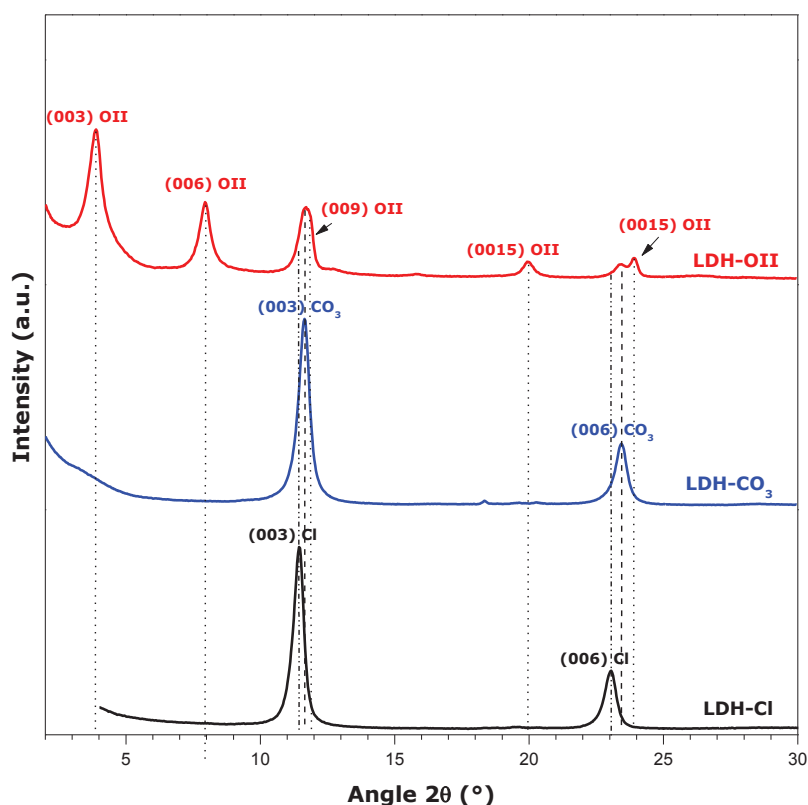


Figure 6. X-ray diffraction patterns in the  $2\theta$  range from  $2^\circ$  to  $30^\circ$  for the intercalation of OII in the Mg-Al-LDH-Cl structure corresponding to the selected point on the OII adsorption isotherm (as marked by crosses in Figure 3).

Figure 7 shows the XRD patterns of Mg-Al-LDH-Cl saturated with the OG units ( $Q_{\text{ads}} = 0.58 \text{ mmol g}^{-1}$ ). Very weak reflections of OG adsorbed in the interlayer at  $5.2^\circ$ ,  $15.8^\circ$  and  $21.1^\circ$   $2\theta$  positions can be assigned to the (003), (009) and (0012) harmonic peaks. However, broadening of the peak from  $10^\circ$  to  $11.5^\circ$  corresponds to the presence of three different phases in the adsorbent, namely the (006) OG, (003) CO<sub>3</sub> and (003) Cl. Moreover, the intensity of carbonate and chloride reflections in comparison with those of OG indicates that the two inorganic phases are predominant within the layer compared to the organic ion. The presence of the initial chloride phase is in good agreement with the results shown in Figure 4. The uncompensated layer charge during the release of chloride ions (around  $5.6 \mu\text{mol}$ ) is neutralized by the carbonate species dissolved in aqueous solution.

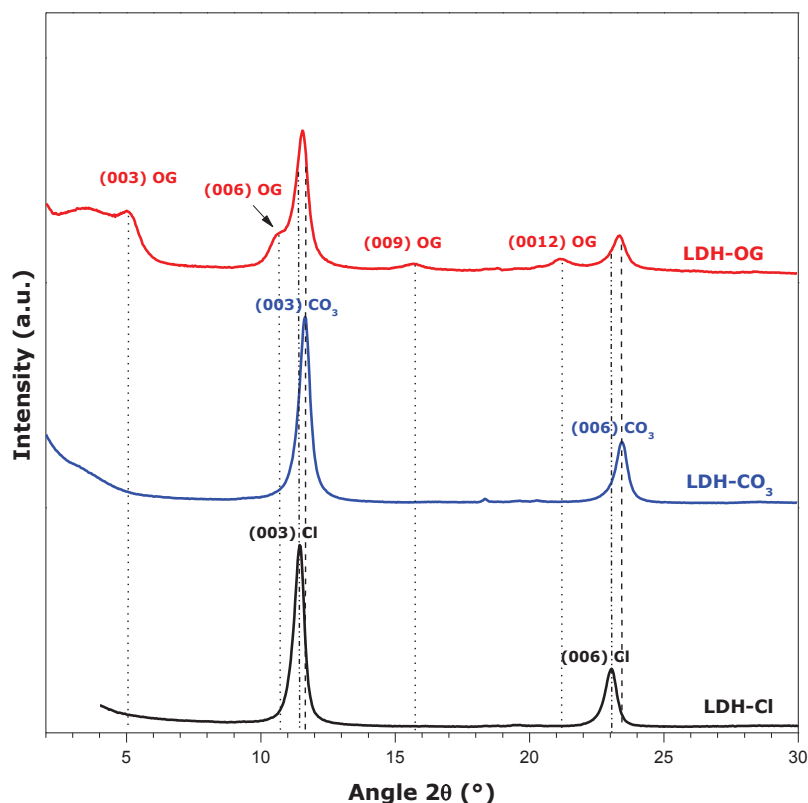


Figure 7. X-ray diffraction patterns in the  $2\theta$  range from  $2^\circ$  to  $30^\circ$  for the intercalation of OG in the Mg-Al-LDH-Cl structure corresponding to the selected point on the OG adsorption isotherm (as marked by crosses in Figure 3).

The main question which arises is why during anion exchange in Mg-Al-LDH-NO<sub>3</sub> [11], the OG species are adsorbed easily without a great competition with carbonates provided from the atmosphere, whereas OG anions have much difficulty to be adsorbed onto LDH when similar exchange is realized with chloride ions. To find the answer to this particular question, interactions involved in the dye adsorption should be compared. Therefore, the enthalpies of displacement during the process of exchange have been evaluated using the ITC experimental set.

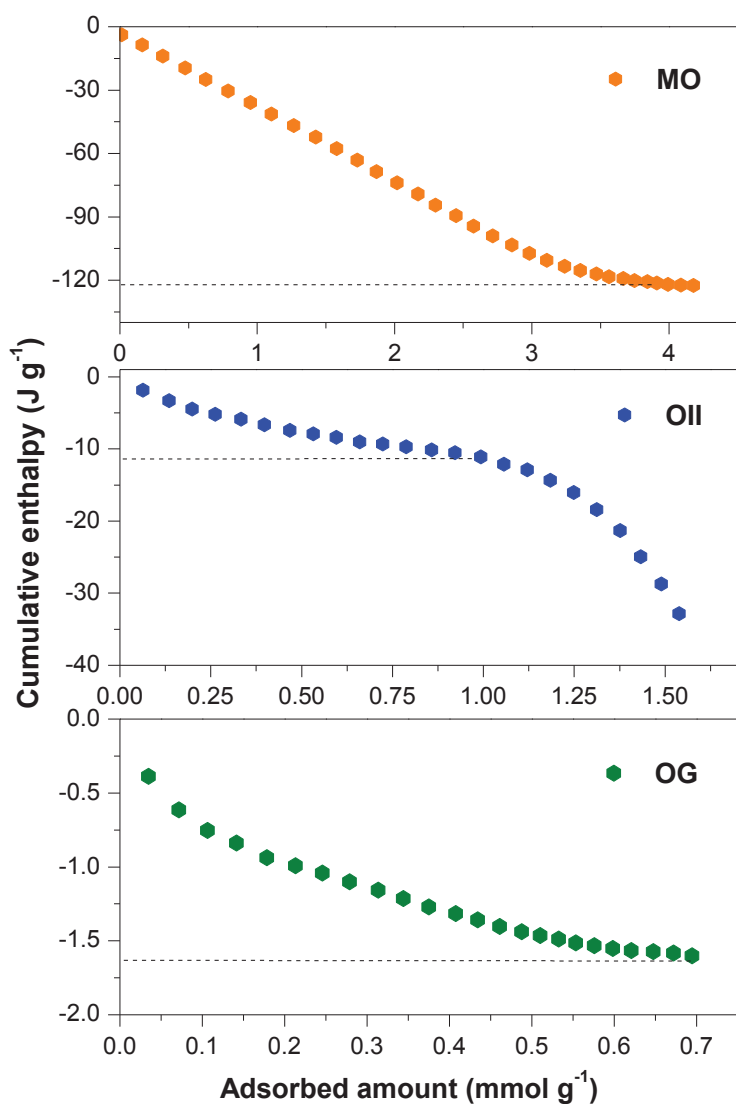


Figure 8. Variations of the cumulative enthalpy of displacement as a function of the amount of dye adsorbed.

In Figure 8 the variations of the cumulative enthalpy of displacement are plotted against the amount of dye adsorbed. The global character of the exchange process is exothermic. By analogy with the results obtained for Mg-Al-LDH-NO<sub>3</sub> [11] the thermal effect for MO and OG levels off at the end of the vertical part of the adsorption isotherm with values of the cumulative enthalpy of  $-122 J g^{-1}$  and  $-1.6 J g^{-1}$ , respectively. In the case of OII, the cumulative enthalpy curve can be divided into two parts: 1) the quasilinear dependence of  $\Delta_{dpl}H_{cum}$  on the amount adsorbed

over vertical part of the adsorption curve ( $Q_{ads} < 1 \text{ mmol g}^{-1}$ ), 2) the monotonous decrease from the beginning of the saturation plateau ( $Q_{ads} > 1 \text{ mmol g}^{-1}$ ). As it was explained in Chapter II, this phenomenon is due to the formation of OII complexes or aggregates with the Mg(II) ions, obtained by partial dissolution of the LDH.

To conclude, the exothermic effect of displacement accompanying the retention of OG is the lowest in comparison with other dyes (especially with those of MO). This value is even lower than those obtained for Mg-Al-LDH-NO<sub>3</sub> ( $-10 \text{ J g}^{-1}$ ) [11]. It was already mentioned earlier that cumulative enthalpy of displacement represents the global heat effect accompanying the adsorption processes. Hence, low value of  $\Delta_{dpl}H_{cum}$  for OG is in good agreement with lower amount of dye adsorbed, consequently the weak expansion of the layer, low interlayer anion displacement, etc. Thus, the affinity of the dye anions can be ordered as follows:  $MO^- > OII^- > Cl^- > OG^{2-} > NO_3^-$ .

In the next section of this chapter, we check whether adsorptive capacities of the three dyes onto Mg-Al-LDH-Cl are changed in the presence of equimolar proportions of the competing inorganic anions in solution, during adsorption.

#### ***4. Competitive adsorption of dye and inorganic anions from equimolar bi-solute and tri-solute solutions***

The analysis of results obtained in Chapter III on the competitive adsorption between inorganic anions (sulfates, chromates, carbonates and hydrogen phosphates) and dyes onto Mg-Al-LDH-NO<sub>3</sub> has demonstrated that carbonates and hydrogen phosphates have significant negative impact on the dye adsorption. In the present chapter the emphasis is mainly on the competitive adsorption of the dyes in the presence of inorganic ions. In addition, tri-component systems containing both inorganic anions and the dye in solution are tested. A comparison with the dye removal from mono-component solutions without competing species is also done.

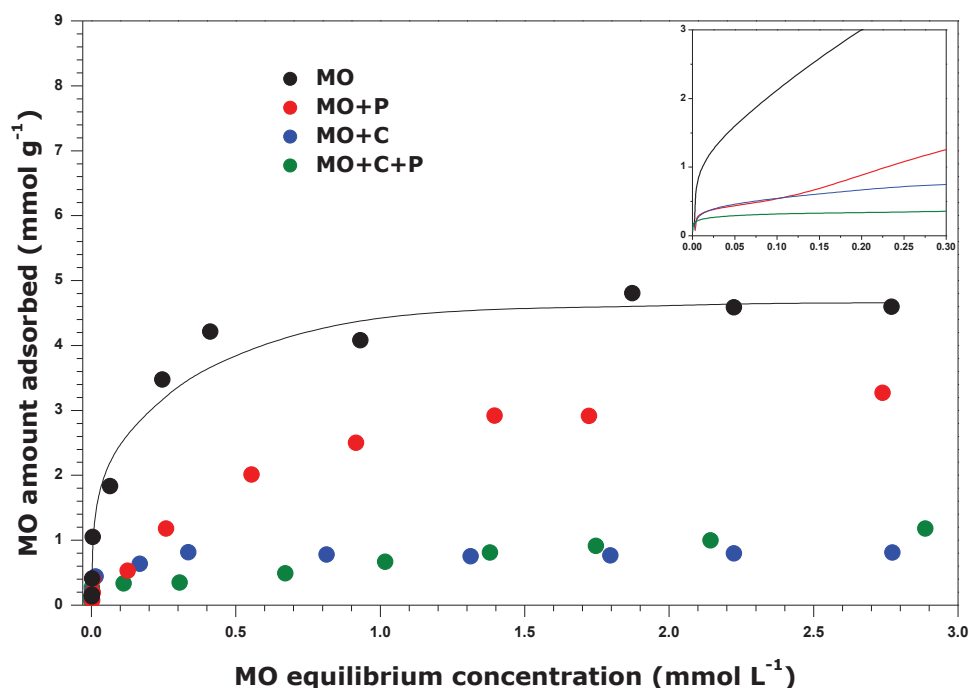


Figure 9. Isotherm of competitive adsorption between Methyl Orange (MO) and carbonate and hydrogen phosphate onto Mg-Al-LDH-Cl from equimolar bi-solute and tri-solute solutions, containing MO, hydrogen phosphates (P) or carbonates (C) anions.

Figure 9 shows the adsorption results of the MO in competition with inorganic ions (carbonates and hydrogen phosphates). The presence of both inorganic ions have the negative influence on the amount of dye adsorbed. The decrease in the MO adsorption is equal to 35% overall adsorption isotherm in the presence of  $\text{HPO}_4^{2-}$  species. In the presence of carbonates adsorption of MO decreases up by 83% from  $4.7 \text{ mmol g}^{-1}$  to  $0.8 \text{ mmol g}^{-1}$ . Thus, at equilibrium carbonate ions have higher influence on the dye adsorption than hydrogen phosphates have. However, at small MO equilibrium concentrations  $< 0.2 \text{ mmol L}^{-1}$ , the same MO adsorption behavior can be observed in the presence of both inorganic ions (see Figure 9). The initial portion of the dye adsorption isotherm in the presence of inorganic ions ( $0.3 \text{ mmol g}^{-1}$ ) can be related with the MO exchange onto LDH, indicating strong interactions between dye and solid in the range of small equilibrium concentrations (i.e. the vertical part of the isotherm). The subsequent increase in the MO retention can be related to the sorption on the external surface of the LDHs (see XRD analysis of the LDH loaded with mixture dye and inorganic ions in Chapter III).

In the presence of two inorganic competing species (tri-solute composition), MO exhibit different adsorption behavior, with rather small amounts adsorbed ( $Q_{\text{ads}} \approx 0.3 \text{ mmol g}^{-1}$ ) in the range of very dilute solutions  $< 0.5 \text{ mmol L}^{-1}$ . However, with the further increase in the dye equilibrium concentration, the steady increase in the MO amount adsorbed occurs. The global effect due to the presence of inorganic ions on the MO exchange capacity onto Mg-Al-LDH-Cl follows the next trend:  $P < C \approx C + P$ . Similar adsorption properties of MO in the bi-component mixture with carbonates and in the tri-component one (P+C) indicate that the carbonate is the main inhibitor of the adsorption of dye and phosphate ions.

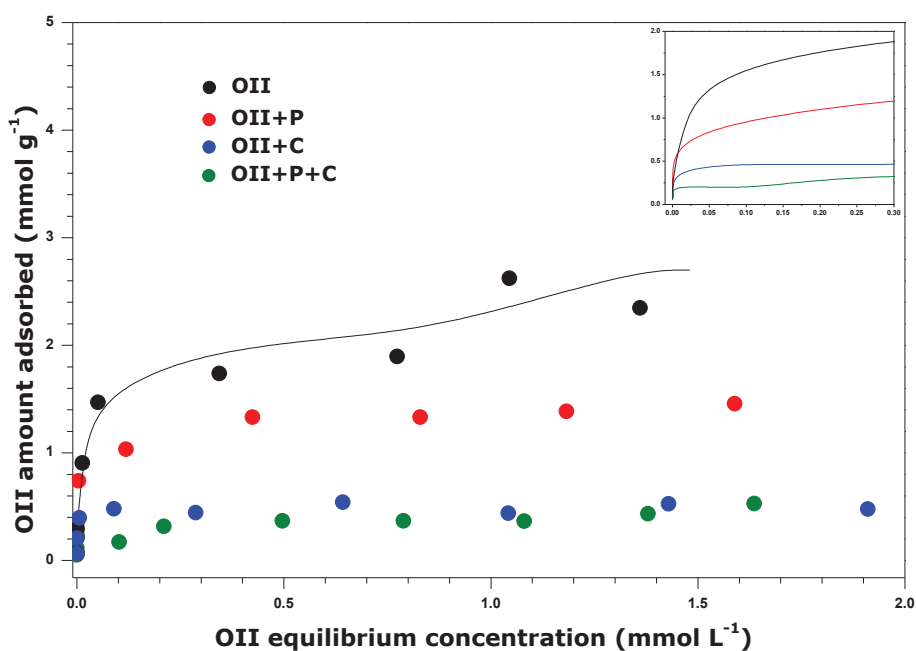


Figure 10. Isotherm of competitive adsorption between Orange II (OII) and carbonate and hydrogen phosphate onto Mg-Al-LDH-Cl from equimolar bi-solute and tri-solute solutions, containing OII, hydrogen phosphates (P) or carbonates (C) anions.

Competitive adsorption between OII and the inorganic anions is presented in Figure 10. By analogy with the results obtained for MO, two inorganic ions have negative influence on the dye adsorption. The presence of  $\text{HPO}_4^{2-}$  decreases the quantity of OII retained by the solid down to 50% ( $1.4 \text{ mmol g}^{-1}$ ) in comparison with the single-component system ( $2.7 \text{ mmol g}^{-1}$ ). In the

presence of carbonate, the OII adsorption is decreased by 81% to 0.5 mmol g<sup>-1</sup>. The latter value is in good agreement with those reported in the literature for OII adsorbed onto Mg<sub>2</sub>Al-CO<sub>3</sub> [12]. In the adsorption plateau region the dye adsorption from tri-solute solutions is equal to that obtained from bi-solute solutions with carbonate species. However, in the range of small equilibrium concentration, the adsorption of OII is more influenced by the mixture (P+C) than by the presence of carbonates or HPO<sub>4</sub><sup>2-</sup>. It is interesting to notice that during the adsorption onto Mg-Al-LDH-NO<sub>3</sub>, the presence of phosphate or carbonate units have the same influence on the OII adsorption from bi-solute solutions as when adsorbed onto Mg-Al-LDH-Cl. This can be related to the similar adsorption of hydrogen phosphate onto Mg-Al-LDH-NO<sub>3</sub> (i.e., 2.7 meq g<sup>-1</sup> as reported in Chapter III) and onto Mg-Al-LDH-Cl (i.e., 2.6 meq g<sup>-1</sup>, as can be seen in Figure AII-4 in Appendix II section V).

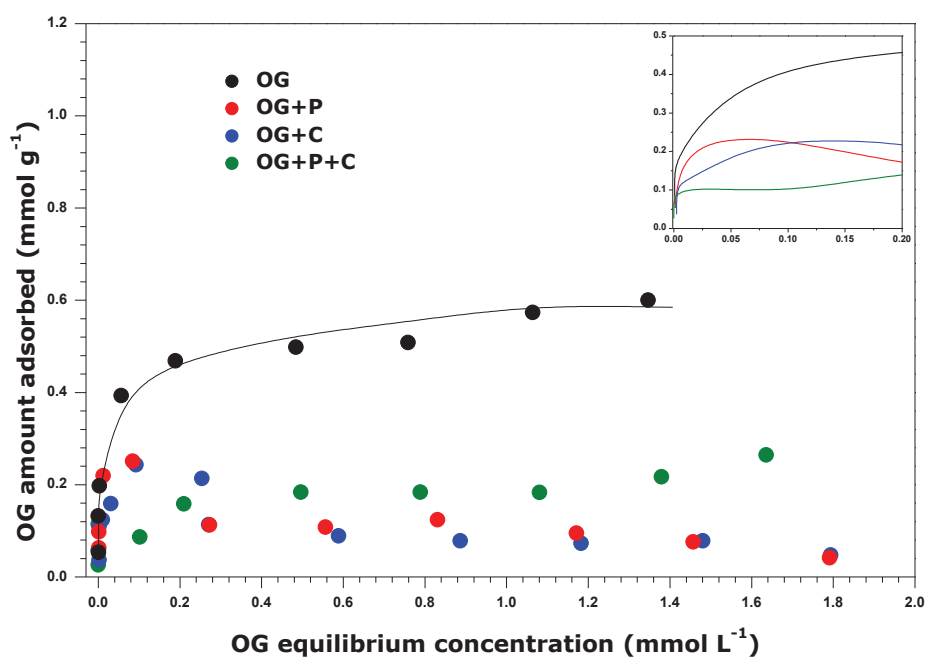


Figure 11. Isotherm of competitive adsorption between Orange G (OG) and carbonate and hydrogen phosphate onto Mg-Al-LDH-Cl from equimolar bi-solute and tri-solute solutions, containing OG, hydrogen phosphates (P) or carbonates (C) anions.

Figure 11 shows the results of competitive adsorption between OG and inorganic ions onto Mg-Al-LDH-Cl. Carbonates and phosphates have almost the same influence on the OG adsorption. Only the vertical parts of the adsorption curves in the presence of inorganic anions own somewhat different, with higher affinity of OG in the presence of hydrogen phosphate than that in the presence of carbonate ions. Then, the amount of dye adsorbed attains a value of  $0.25 \text{ mmol g}^{-1}$  in the presence of either (C or P) competing species at a low OG equilibrium concentrations ( $< 0.4 \text{ mmol L}^{-1}$ ). However, at higher concentrations of dye in the solution, the amount of dye adsorbed decreases monotonously. This depression of the OG uptake at higher concentration could be explained on the basis of pH measurements in aqueous suspensions, as reported at Figures AII-6 (a, b) in Appendix II in relation with the diagrams of speciation (Figures AII-5). The initial pH values measured at the beginning of the sorption process can give us information about the species initially present in the solution. The decrease in the dye adsorption is enhanced by increasing the concentration of dihydrogen phosphate in the solution and the same observation has been done for carbonate. For the first points on the adsorption plot where dye adsorbs progressively, bicarbonate is either the only or predominant phase in the solution. However, the depression of OG occurs when the percentage of carbonate is superior to the bicarbonate phase in solution ( $\text{pH} > 10.3$   $\text{pK}_{\text{a}2}=10.3$ ). At the maximum adsorption, the OG is decreased by 58% during the adsorption process in comparison with single-component adsorption. The uptake of OG in competition with carbonates and hydrogen phosphate corresponds to Type I according to the classification proposed in Chapter III.

A different shape of the adsorption isotherm is observed for OG adsorption from tri-solute solutions. At small equilibrium concentrations, the OG adsorption is decreased down to  $0.1 \text{ mmol g}^{-1}$ . Further increase in the dye concentration (above  $0.2 \text{ mmol L}^{-1}$ ) results in an increase in the dye adsorption up to  $0.2 \text{ mmol g}^{-1}$  and then it remains the same. To rationalize this observation, the competition between the two inorganic ions in the tri-solute solution for adsorption sites can be forwarded (Figure AII-6 (c)). Thus, for the first points, a competition can occur between OG, dihydrogen phosphate and bicarbonate. As the overall concentration of all adsorbed species in the solution is small, there are enough available sites for the adsorption of all competing species: in consequence, the dye units adsorb. In adsorption plateau of  $0.2 \text{ mmol g}^{-1}$  the presence of the mixed carbonate phase is postulated (at  $\text{pH}=9.3$ , 91%  $\text{HCO}_3^-$ , 9%  $\text{CO}_3^{2-}$ ). This mixture of

bicarbonate and carbonate anions can potentially compete with hydrogen phosphate for LDH surface sites, as reported by Shin et al. [13]. The explanation of the competitive results with pH measurement is just a hypothesis, as the charge of adsorbed species inside the layer should be better studied.

## **5. CONCLUSIONS**

In this Chapter, we described the adsorption experiments performed on the Mg-Al-LDH-Cl sample, with the aim to establish the difference between the adsorption properties of the two LDH solids, containing various interlayer anions: nitrates (Chapters II and III) and chlorides (this chapter). At first, the structural properties of adsorbent were characterized by TGA and XRD analysis. Single-solute adsorption experiment was then performed for three azo dyes (MO, OII and OG). The adsorption of MO and OG onto Mg-Al-LDH-Cl was smaller ( $4.7 \text{ mmol g}^{-1}$  MO,  $0.6 \text{ mmol g}^{-1}$  OG) than that onto Mg-Al-LDH-NO<sub>3</sub> ( $5.5 \text{ mmol g}^{-1}$  MO and  $1.7 \text{ mmol g}^{-1}$  OG). On the contrary, no influence of the interlayer anion was observed on the adsorption of OII. This difference was ascribed to the affinity of the pristine interlayer anion towards the layered double hydroxide (Cl > NO<sub>3</sub>). Moreover, the ITC measurements gave the same trend in the enthalpy of displacement during adsorption. The XRD patterns of the solid samples loaded with dye anions confirmed the presence of the chloride phase in the case of OG. In addition, the presence of the carbonate phase was noted for all dyes.

The multi-solute sorption study was then performed in the presence of bivalent inorganic anions. Hydrogen phosphates and carbonates were tested for their impact on the dye uptake when adsorbed from bi- and tri-solute solutions. For MO and OII, hydrogen phosphate ions had less influence (a decrease down to 35 and 50 %, respectively) on the retention uptake of such dyes, in comparison with that of carbonate ions (83% MO, 81% OII). During the dye adsorption from bi-solute solutions containing carbonates, MO and OII are influenced to the same extent as if they were adsorbed from tri-solute solutions (Dye+P+C). In the case of OG, the presence of both phosphate and carbonate ions had the same influence on the dye sorption capacity. During the adsorption from very diluted solution OG adsorbs to the great extent. With the increase in the

equilibrium dye concentration, the quantity adsorption of dye decreases. However, when the adsorption of OG is performed from tri-solute solutions in the presence of both carbonate and phosphate ions, the amount of dye adsorbed onto LDH sample remained the same after having reached the plateau value. The hypothesis about possible competition between carbonate and hydrogen phosphate ions present in the solution for the LDH adsorption sites was postulated.

In summary, Mg-Al-LDH-Cl is a good adsorbent material for MO and OII dyes, but its adsorption capacity towards OG is smaller, because of the lower surface affinity of the latter dye against chloride interlayer anions:  $\text{MO}^- > \text{OII}^- > \text{Cl}^- > \text{OG}^{2-} > \text{NO}_3^-$ . However, if the wastewater contains carbonate ions, there will be significant decrease in the retention performance of the LDH sample.

## 6. References

1. Rives, V., *Layered double hydroxides: present and future*. 2001, New York: Nova Publishers. 439.
2. Miyata, S., *Anion-exchange properties of hydrotalcite-like compounds*. *Clays Clay Miner*, 1983. **31**(4): p. 305-311.
3. Auerbach, S.M., K.A. Carrado, and P.K. Dutta, *Handbook of layered materials*. . 2004, New York: Marcel Dekker. pp. 650.
4. de Heredia, J.B., et al., *Nitrate removal from groundwater using Amberlite IRN-78: Modelling the system*. *Applied Surface Science*, 2006. **252**(17): p. 6031-6035.
5. Zhang, P., et al., *Removal of methyl orange from aqueous solutions through adsorption by calcium aluminate hydrates*. *Journal of Colloid and Interface Science*, 2014. **426**: p. 44-47.
6. Monash, P. and G. Pugazhenthii, *Utilization of calcined Ni-Al layered double hydroxide (LDH) as an Adsorbent for removal of methyl orange dye from aqueous solution*. *Environmental Progress & Sustainable Energy*, 2014. **33**(1): p. 154-159.
7. Sui, M., et al., *Adsorption of norfloxacin in aqueous solution by Mg-Al layered double hydroxides with variable metal composition and interlayer anions*. *Chemical Engineering Journal*, 2012. **210**: p. 451-460.
8. Violante, A., et al., *Sorption/desorption of arsenate on/from Mg-Al layered double hydroxides: Influence of phosphate*. *Journal of Colloid and Interface Science*, 2009. **333**(1): p. 63-70.
9. Suzuki, E., S. Idemura, and Y. Ono, *Properties of hexacyanocobaltate (III)-exchanged hydrotalcite-like minerals*. *Clays and Clay Minerals*, 1989. **37**(2): p. 173-178.
10. Châtelet, L., et al., *Competition between monovalent and divalent anions for calcined and uncalcined hydrotalcite: anion exchange and adsorption sites*. *Colloids and Surfaces A: Physicochemical and Engineering Aspects*, 1996. **111**(3): p. 167-175.
11. Darmograi, G., et al., *Study of Adsorption and Intercalation of Orange-Type Dyes into Mg-Al Layered Double Hydroxide*. *Journal of Physical Chemistry C*.
12. Géraud, E., et al., *Texture effect of layered double hydroxides on chemisorption of Orange II*. *Journal of Physics and Chemistry of Solids*, 2007. **68**(5): p. 818-823.
13. Shin, H.-S., et al., *Phosphorus removal by hydrotalcite-like compounds (HTLcs)*. *Water Science and Technology*, 1996. **34**(1-2): p. 161-168.



**Chapter V:**  
**Single-component and  
competitive adsorption of Dyes  
and Cr (VI) onto strongly basic  
Anion -Exchange Resin**



## **INTRODUCTION**

The mechanism of the three chosen Orange type dyes, Methyl Orange, Orange II and Orange G was discussed in details in Chapter II-IV using adsorbent-reference Layered Double Hydroxide. Hence, it was found that adsorption of these dyes on the anionic clay is a complex mechanism and it is greatly depends on several factors such as, concentration of anions in solution, work on the open air, properties of used adsorbing species, and interactions between solid and adsorbates. However, it will be interesting to find out if the same adsorbing system (Orange-type dyes) but this time either without the addition of any other competing organic anions or in the presence of competing inorganic anions such as chromium for instance will have similar effects during adsorption onto another anion exchanger.

Therefore, in this chapter the discussion will focus on the adsorption of Orange-type dyes but on another adsorbent-reference, organic anion exchanger, known as Amberlite® IRN-78. This adsorbent is a strongly basic anion-exchanger resin. That is why it is important to measure the initial as well as the equilibrium pHs in the working media, since the change in pH can give valuable information about the charge of adsorbing species initially present in the bulk.

Two contributions were investigated in this chapter. The first is the study of the mechanism of dye and Cr uptake from a single solute solution. <sup>13</sup>C CP/MAS NMR was used to confirm the mechanism of dye uptake on the resins. Regeneration test was performed for all investigated organic and inorganic species.

The second contribution was to study the retention of the dye and the oxyanion Cr (VI) from the multi-component system. The same methods as described in the previous chapters were used to investigate this competition. The selectivity of adsorbent for organic and inorganic species is an important parameter capable of influencing the adsorption of such system was also investigated in view of contributing to the understanding of different factors that can affect the adsorption of impurities in real wastewater systems.

Single-component and competitive  
adsorption of three anionic Orange-type  
dyes and Cr(VI) oxoanion from aqueous  
solutions  
onto strongly basic anion-exchange resin

*Ganna Darmograi, Bénédicte Prelot, Amine Geneste, Louis-Charles de Menorval, and  
Jerzy Zajac*

Institut Charles Gerhardt de Montpellier, UMR-5253 CNRS-UM-ENSCM,  
C.C. 1502 Place Eugène Bataillon, F-34095 Montpellier cedex 5, France

## 1. Introduction

The sorption-based technology for *in situ* treatment of polluted streams usually combines an easy handling, fast operational readiness, low operational costs, low-level discharge generation with significant reversibility of the removal process thus allowing the raw materials to be preserved. Given the sorption mechanism underlying a particular pollutant removal technology, the efficiency and selectivity of sorption material may be largely affected by certain substances, which are present in the aqueous stream and enter into competition with the main pollutant component. Within the framework of recovery of various ionic substances, ion-exchange resins are important examples of synthetic sorbents for wastewater treatment since they can be easily tailored to specific applications [1]. For example, the use of such ion exchangers has been considered for removal of heavy metals [2-5], common inorganic ions [6], precious metals and rare elements [7-9], as well as dyes, acids, insecticides, or phenols [10-20]. In view of understanding the selectivity of the resins employed, the sorption process was studied in multi-component systems containing a mixture of heavy metals [2, 5, 21, 22], rare metals [23] or inorganic anions [24, 25]. Only a few papers have reported the results of competitive adsorption between some organic and inorganic anions onto anion-exchange resins [19, 26, 27].

Deng *et al.* investigated the impact of sulfate and chromate anions on the retention of perfluorooctane sulfonate (PFOS) by polyacrylic IRA67 and IRA958 resins [19]. They demonstrated that the presence of  $\text{SO}_4^{2-}$  had little effect on the PFOS sorption, whereas Cr(VI) oxoanions caused a very significant decrease in the PFOS uptake. Wang and co-workers reported the effects of competition between nitrates and such organic acids as gallic (GA), tannic (TA) and humic (HA), making use of an anion-exchange resin containing amine groups [26]. The order of decreasing effectiveness of the acid in depressing the nitrate uptake was  $\text{HA} > \text{GA} > \text{TA}$  and this was correlated with the electronegativity of these acids. It was postulated that the electrostatic interactions between the exchangeable sites in the resin and charged organic acids were mainly responsible for the acid effect on the removal of nitrate anions. Karcher *et al.* considered the use of strongly basic S6328a and weakly basic MP62 resins to remove the Reactive Black 5 dye from aqueous solutions containing also  $\text{SO}_4^{2-}$ ,  $\text{CO}_3^{2-}$ , or  $\text{HPO}_4^{2-}$  [27]. The dye retention by both resins

appeared little influenced by inorganic anions. MP62 was efficient only up to pH 8 and showed good propensity for alkaline regeneration.

The objective of the present work was to test the efficiency and selectivity of strongly basic anion-exchange resin, Amberlite<sup>®</sup> IRN-78, in the removal of anionic Orange-type dyes and chromate anion from aqueous solutions. The study has been motivated by environmental issues since the textile industry can discharge various dyes and Cr(VI) oxoanions into aqueous streams, thereby causing severe impact to the environment [28]. The selected dyes included Methyl Orange, Orange II, and Orange G differing from one another by hydrophobic-hydrophilic character, molecular size, and electric charge. The competitive adsorption of three dye-chromate pairs from bi-solute equimolar solutions was compared with the corresponding single-component adsorption phenomena to monitor the mutual impact of the co-occurring compounds. Besides the equilibrium adsorption isotherms and selected desorption cycles, the nature of the dye species retained on the resin surface was studied with the aid of cross-polarization magic angle spinning <sup>13</sup>C NMR and the enthalpy change upon anion-exchange was quantified using isothermal titration calorimetry.

## **2. Experimental**

### **2.1. Materials**

Amberlite<sup>®</sup> IRN-78, Nuclear Grade resin, was purchased from Rohm and Haas (France) as yellow spherical beads in the 0.580–0.680 mm size range. This strongly basic gel-type anion exchange resin was supplied in the hydroxide form (at least 95% of the available exchange sites). It had a styrene divinylbenzene copolymer matrix with trimethylammonium functional groups. Its total exchange capacity, as specified by the manufacturer, was  $\geq 1.7$  meq L<sup>-1</sup>.

The three Orange-type dyes of high purity (dye content > 99%) were purchased from Sigma-Aldrich and used without further purification. They are further designated as follows: MO = Methyl Orange, OII = Orange II or Acid Orange 7, OG = Orange G or Acid Orange 10. The maximum absorbance in the ultraviolet (UV) spectra was observed at a wavelength of 466 nm, MO; 483 nm, OII; and 480 nm, OG. Potassium chromate (K<sub>2</sub>CrO<sub>4</sub>) was also a from Sigma-Aldrich product (purity > 99%). These solutes were employed as received. The 18.2 MΩ cm water used to

prepare aqueous solutions was obtained with the aid of a combined Purite Select Analyst (France Eau) and PURELAB<sup>®</sup> Classic (ELGA LabWater, France) water purification system.

## 2.2. Measurements of the adsorption isotherms in single-solute and bi-solute systems

The individual isotherms of adsorption onto Amberlite<sup>®</sup> IRN-78 from single- and bi-solute solutions were determined by equilibrating about 50 mg of the resin beads with 20 ml of aqueous solution at a given composition in 30 ml Nalgene<sup>®</sup> reactors. In the single-component adsorption experiments, the initial solute concentrations were varied within the following range: 0.02 – 2 mmol L<sup>-1</sup>, MO and OII; 0.03 – 3 mmol L<sup>-1</sup>, OG; 0.04 – 5 mmol L<sup>-1</sup>, CrO<sub>4</sub><sup>2-</sup>. To determine the individual adsorption isotherms of the two anionic species from bi-solute equimolar solutions, a mixed stock solution containing 2.5 mmol L<sup>-1</sup> of each solute was used to obtain appropriate diluted solutions to be poured into Nalgene<sup>®</sup> tubes. For comparison purposes, the dilution schemes were designed to generate the individual adsorption isotherms for the dye species covering ranges of the equilibrium dye concentration similar to those obtained in the single-solute systems. The pH of resin suspensions was checked before and after the attainment of adsorption equilibrium. Wawrzekiewicz and Hubicki reported the results of kinetic studies on the adsorption of sulphonated azo dyes onto strongly basic anion-exchange resins (macroporous polystyrene Amberlite<sup>®</sup> IRA-900 and IRA-910), thereby giving strong indications for the fast sorption kinetics [20]. Taking into account this conclusion, the Nalgene<sup>®</sup> reactors in the present work were slowly shaken overnight in a thermostated cage ( $\pm 0.1$  deg) at 298 K. The separation of solid phase from the supernatant liquid was achieved by centrifugation at 10 000 rpm for 10 min. The equilibrium concentration of a selected anion in the bulk phase was determined by UV-Vis spectroscopy (Jasco V-670 UV-Vis Spectrophotometer operating in the wavelength range from 350 to 550 nm). The corresponding amount adsorbed was calculated as follows:

$$\Delta_a n = \frac{V_o(C_i - C_{eq})}{m_s} \quad (1)$$

where  $C_i$  and  $C_{eq}$  represent, respectively, the initial and final (after attaining the equilibrium) concentrations of the adsorbed species,  $V_o$  is the initial volume of the aqueous solution, and  $m_s$  is the mass of the resin. All adsorption experiments were repeated at least twice

to test and verify the results. The worst repeatability was observed in the plateau adsorption region where it was within: 4%, MO; 2%, OII; 4%, OG; 6% CrO<sub>4</sub><sup>2-</sup>.

### 2.3. Reversibility and selectivity tests of solute retention by the resin

The resin was tested for one sorption-washing-elution cycle based on the same solution depletion method. Each solid sample, separated from the supernatant solution at the end of the first single-component adsorption step, was repeatedly washed with ultrapure water inside the Nalgene<sup>®</sup> tube. After each washing cycle, the resulting aqueous phase was collected and analyzed by UV-Vis spectroscopy to ensure that there were neither dye nor chromate units reversibly removable from the neighborhood of resin particles. Then the tube containing only the washed resin sample without the supernatant liquid was filled with 20 mL of a 0.02 or 1 mol L<sup>-1</sup> NaOH solution and slowly shaken at 298 K. In the meantime, 5 mL aliquots of the supernatant solution were collected at fixed time intervals of 2, 3, 4, and 20h and analyzed for the concentration of dye or chromate anion,  $C_{des}$ . The collected samples were subsequently returned to the Nalgene<sup>®</sup> tube in order to keep the same composition of the system. The quantity of dye desorbed from the resin was calculated from the following equation:

$$\Delta_{dn} = \frac{V \cdot C_{des}}{m_s} \quad (2)$$

where V is the volume of the NaOH solution in the tube.

The solute desorption was also presented as a percentage of the total amount adsorbed in the first adsorption cycle, i.e.,  $\frac{\Delta_{dn}}{\Delta_{an}} \times 100$  %.

The selectivity tests were carried out by starting with Amberlite<sup>®</sup> IRN-78 saturated with a selected component from a single-solute solution (the corresponding points located in the plateau region of the adsorption isotherms). The resin samples loaded with the maximum quantity of chromate anions were first washed with ultrapure water by following the procedure established for desorption tests. Then, they were equilibrated in the same Nalgene<sup>®</sup> tubes with 20 mL of dye solution having a concentration of 2 mmol L<sup>-1</sup>, MO and OII; 3 mmol L<sup>-1</sup>, OG. By analogy, the samples previously saturated with a given dye were put into contact with 20 mL of a 5 mmol L<sup>-1</sup>

K<sub>2</sub>CrO<sub>4</sub> solution. The tubes were slowly shaken overnight at 298 K and the corresponding amount adsorbed at equilibrium determined by using Eq. 1.

### *2.3. Calorimetry measurements of the enthalpy changes accompanying single-component and competitive adsorption of dye and chromate anions*

A TAM III differential microcalorimeter operating in a heat flow mode was used to measure the enthalpy of displacement accompanying both single-component and competitive adsorption of dye and chromate anions onto Amberlite<sup>®</sup> IRN-78 from aqueous solutions at 298 K. The experimental setup and operating procedures were detailed previously [2]. The 1 mL measuring ampoule containing about 2.5-4 mg of resin beads suspended in 0.8 mL of ultrapure water was placed in the microcalorimeter. The homogeneity of the solid suspension was maintained by means of an agitation system equipped with a Teflon paddle stirrer. The whole system including also a reference ampoule filled with the same amount of ultrapure water was equilibrated during 2h. Pulse injections of an appropriate stock solution were performed making use of a computer-controlled microsyringe injection device. In the single-component adsorption experiment, the concentration of stock solution was as follows: 7.5 mmol L<sup>-1</sup>, MO; 8 mmol L<sup>-1</sup>, OII; 10 mmol L<sup>-1</sup>, OG; 20 mmol L<sup>-1</sup>, CrO<sub>4</sub><sup>2-</sup>. When the competitive adsorption of dye and chromate anions was studied, the microsyringe was filled with an equimolar mixture of two components, each of which had the following concentration: 8 mmol L<sup>-1</sup>, MO + CrO<sub>4</sub><sup>2-</sup>; 7 mmol L<sup>-1</sup>, OII + CrO<sub>4</sub><sup>2-</sup> and OG + CrO<sub>4</sub><sup>2-</sup>. The operational parameters were kept the same for all calorimetry experiments, namely: 25 injections of 10 μL during 10 s, a stirring speed of 90 rpm, time of equilibration between two successive injections equal to 90 min. Further procedures for data processing were described previously [2]. The experimental enthalpy changes were subsequently corrected for dilution effects (see Supplementary Information for more details). The dilution experiments were carried out under the same experimental conditions but without a resin sample in the measuring ampoule. The enthalpy changes corresponding to the successive injection steps were finally summed up to obtain the cumulative enthalpy of displacement,  $\Delta_{dpl}H_{cum}$ , per unit mass of the solid material. The repeatability of the enthalpy measurement including the data

processing procedures was within: 10%, MO; 5%, OII, OG, and  $\text{CrO}_4^{2-}$  anions. Nevertheless, the trends in  $\Delta_{dpl}H_{cum}$  with the quantity of adsorption were the same in two calorimetric runs.

#### **2.4. $^{13}\text{C}$ CP/MAS NMR study of the resin samples loaded with dye anions**

The cross-polarization magic angle spinning (CP/MAS)  $^{13}\text{C}$  NMR was employed to get more insight into the nature of adsorbed dye species. Prior to NMR measurements, the resin sample loaded with dye anions were prepared by dispersing 75 mg of resin in 30 ml of a concentrated dye solution. The initial concentrations were chosen to produce samples saturated with the adsorbed dye species (i.e., in the adsorption plateau region). After the attainment of adsorption equilibrium, samples of the supernatant solution were collected to check the amount of dye adsorbed and its concentration in the equilibrium bulk phase. The dye-loaded solid sample was washed with ultrapure water, dried at 333 K for 2-3 h, and transferred to the NMR equipment. The NMR spectra were collected at 300 K using an ASX-300 Bruker spectrometer at 75.47 MHz with a contact time of 4 ms, 12 kHz spinning rate and 13 000 accumulations at 5 s intervals. Chemical shifts were referenced to the  $\text{CH}_2$  groups of solid adamantane at 38.5 ppm relative to the  $^1\text{H}$  resonance of TMS. For the purpose of comparison, the NMR spectra were also recorded on the Amberlite<sup>®</sup> IRN-78 degassed overnight at 303 K and untreated powdered dye samples.

### **3. Results and discussion**

In the present work, the results of adsorption measurements with azo dyes in basic aqueous solutions should be treated with caution since such dyes may exist in different anionic forms due to the azo-hydrazone tautomerism [29-31]. Methyl Orange possessing a sulfonic group has only one  $\text{pK}_a$  in the acidic region (i.e.,  $\text{pK}_a = 3.46$  [32]), so the MO units will be deprotonated in the present systems to form monovalent anions,  $\text{MO}^-$ . It was reported that the hydrazone form with a  $-\text{N}-\text{H}\cdots\text{O}=\text{}$  moiety was the most stable tautomer for Orange II and Orange G in the aqueous phase [29, 31, 33, 34]. Consequently, the  $\text{R}-\text{N}-\text{NH}-\text{R}$  group may be also deprotonated in the basic region (i.e.,  $\text{pK}_a = 10.6$ , OII [35]; 11.5, OG [36]). In strongly basic solutions, Orange II may exist as

divalent  $\text{OII}^{2-}$  anions, whereas the charge number of Orange G anions may be even equal to -3, i.e.,  $\text{OG}^{3-}$ . All these forms are depicted in Fig. S1 in Supporting Information.

### 3.1. Single-component adsorption of dye and chromate anions from single-solute solutions

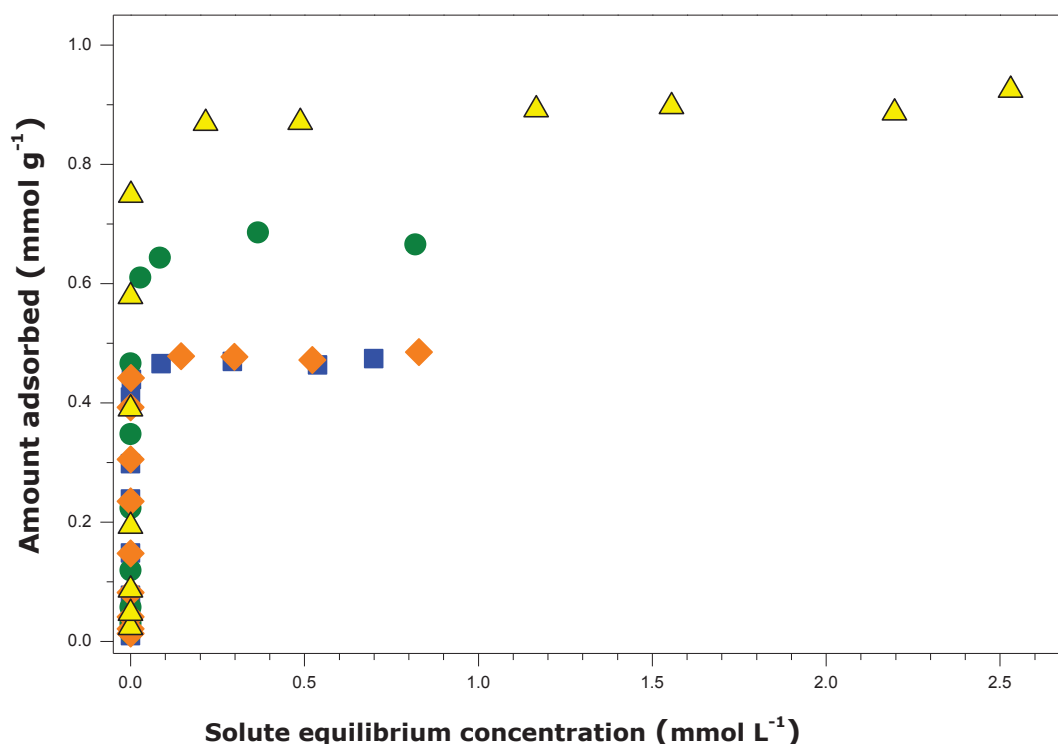


Figure 1. Single-component adsorption isotherms for Methyl Orange (orange diamonds), Orange II (blue squares), Orange G (green circles), and chromate anions (yellow triangles) retained on Amberlite® IRN-78 from single-solute aqueous solutions at 298 K.

Figure 1 presents the adsorption isotherms for the four solutes studied; the amount adsorbed is plotted against the solute concentration in the equilibrium bulk solution. The retention of dye species changes the color of the resin beads, as can be seen in Fig. S2 in Supporting Information. All solutes have high affinity towards the resin exchangeable sites especially for very low concentrations. Most of the solute species are adsorbed within this concentration range, thereby resulting in a quasi-vertical portion on the adsorption curve. Then, the amount adsorbed increases

a little and it levels off above  $0.25 \text{ mmol L}^{-1}$  at the very most. The maximum solute uptake in the adsorption plateau region decreases in the following order:  $\text{CrO}_4^{2-} > \text{OG} > \text{OII} \approx \text{MO}$ .

In order to rationalize the above observation, changes in the pH of resin suspensions monitored upon adsorption measurements should be taken into account. In the beginning, the dispersion of resin beads in ultrapure water did not modify the pH of the solvent. When some volume of the stock solution was put into the Nalgene<sup>®</sup> reactor to obtain the initial solution of a given composition, the pH of the resin suspension rose, after a few minutes of contact, to a new value between 9 and 10, depending on the solute nature and its concentration. In accordance with the fast kinetics of anion exchange onto strongly basic resins demonstrated previously for azo dyes [20] and chromate anions in alkaline solutions [37], an initial increase by a few pH units may be considered as a result of anion exchange with the pristine  $\text{OH}^-$  anions. For points localized in the plateau region of the adsorption isotherms, the equilibrium pH value after the attainment of adsorption equilibrium was as follows: about 11, MO, OII, and  $\text{CrO}_4^{2-}$ ; 11.5, OG.

The apparent capacity of strongly basic anion-exchange resins for various anions may be affected, on the one hand, by the charge number of the anion, size of the hydrated anion, and its degree of hydration, but on the other hand, by the extent of hydration of the resin, its porosity, or degree of crosslinking in the matrix of the resin phase [37, 38]. As a polystyrene gel-type resin, Amberlite<sup>®</sup> IRN-78 is relatively hydrophobic (a moisture holding capacity of 54-60%) and, as such, it should prefer less hydrated anions. It is known that  $\text{CrO}_4^{2-}$  is practically the only chromate species present in alkaline solutions at  $\text{pH} > 7$  [37]. Therefore, this is that Cr(VI) species that adsorbs onto Amberlite<sup>®</sup> IRN-78 in the present chromate system. The hydrated  $\text{CrO}_4^{2-}$  ion has a radius of 0.288 nm and it contains, on average, 2.8 water molecules in its hydration shell [39]. This is the smallest anion used in the present work. When expressed in equivalents per gram, the maximum amount of twofold negatively charged chromate ion (i.e.,  $1.8 \text{ meq g}^{-1}$ ) is close to the minimum value ( $1.7 \text{ meq g}^{-1}$ ) for anion exchange capacity (AEC) of Amberlite<sup>®</sup> IRN-78. The hydrated monovalent  $\text{OH}^-$  has a radius of 0.212 nm and its hydration number is 2.7 [39].  $\text{OH}^-$  and  $\text{CrO}_4^{2-}$  are characterized by similar hydration numbers, but they differ in size and, especially, in charge number. Chromate anion seems to be capable of displacing not only two hydroxides but also other divalent anions present in the resin, e.g., more hydrated  $\text{CO}_3^{2-}$  or  $\text{SO}_4^{2-}$  (according to the manufacturer's specification). The three dye anions are more hydrophobic than  $\text{CrO}_4^{2-}$ , as

evidenced by their endothermic dilution (see Fig. S3 in Supporting Information). At the same time, they have greater molecular sizes; the monovalent  $\text{MO}^-$  is the smallest among the three dye anions [40]. The maximum quantity of MO adsorption (i.e.,  $0.5 \text{ meq g}^{-1}$ ) is much lower than the minimum AEC of the resin, which may be ascribed to its great size. If the two other organic solutes were fully ionized (i.e.,  $\text{OII}^{2-}$  and  $\text{OG}^{3-}$ ), their maximum adsorption values, on a per-equivalent basis, would be  $0.9$  and  $1.9 \text{ meq g}^{-1}$ , respectively. This difference is not fully justified by the charge numbers of the two anions and it is at variance with the greater size of OG [40]. One explanation is that they adsorb as a mixture of anions of different valences. The results of  $^{13}\text{C}$  CP/MAS NMR study may shed more light on the nature of the adsorbing dye anions.

Figure 2 shows NMR spectra recorded on resin samples saturated with MO, OII, and OG in comparison with those obtained with degassed Amberlite<sup>®</sup> IRN-78 and powdered dye samples. The complete assignments of the  $^{13}\text{C}$  NMR spectra is out of the scope of the present analysis, particularly since the existence of significant overlap of numerous peaks specific to the dye with those specific to the resin. For example, the peak centered at  $\delta 39.9 \text{ ppm}$  in the NMR spectrum of MO (the carbon atoms of the terminal methylene groups [41]) overlaps with the corresponding peaks in the NMR spectrum of the resin (aliphatic carbons in the polystyrene-divinylbenzene backbone [42]), thereby changing its shape in the case of resin + MO system. Shoulders in some peaks characteristic of the resin point towards a partial overlap effect and suggest that the resin is the predominant component of the mixed system. In Fig. 2b, this case is exemplified by a small shoulder of the peak at  $\delta 126.6 \text{ ppm}$  (aromatic carbons in the resin backbone [42]) generated through interference with the OII signal centered at  $\delta 120.6 \text{ ppm}$  (carbon N<sup>°</sup>9 in the 2-oxonaphthalene moiety [33]). Outside the overlap domains, the peaks specific to a given dye are small in line with the low dye content in the mixed system (below 15 wt%). Within the above-mentioned interpretation limits, it can be concluded that no new dye-specific  $^{13}\text{C}$  signals appear in the NMR spectrum recorded on Amberlite<sup>®</sup> IRN-78 saturated with Methyl Orange. This means that the dye units preserve their molecular structure upon adsorption (see Fig. S1a in Supporting Information). On the contrary, the  $^{13}\text{C}$  signal centered at  $\delta 177.9$  in the NMR spectrum recorded on the OII-resin sample disappears and a new signal appears at  $\delta 157.2 \text{ ppm}$ . The former can be assigned to the carbon N<sup>°</sup>2 in the 2-oxonaphthalene moiety of Orange II [33] (marked with the red asterisk in Fig. S1b in Supporting Information).

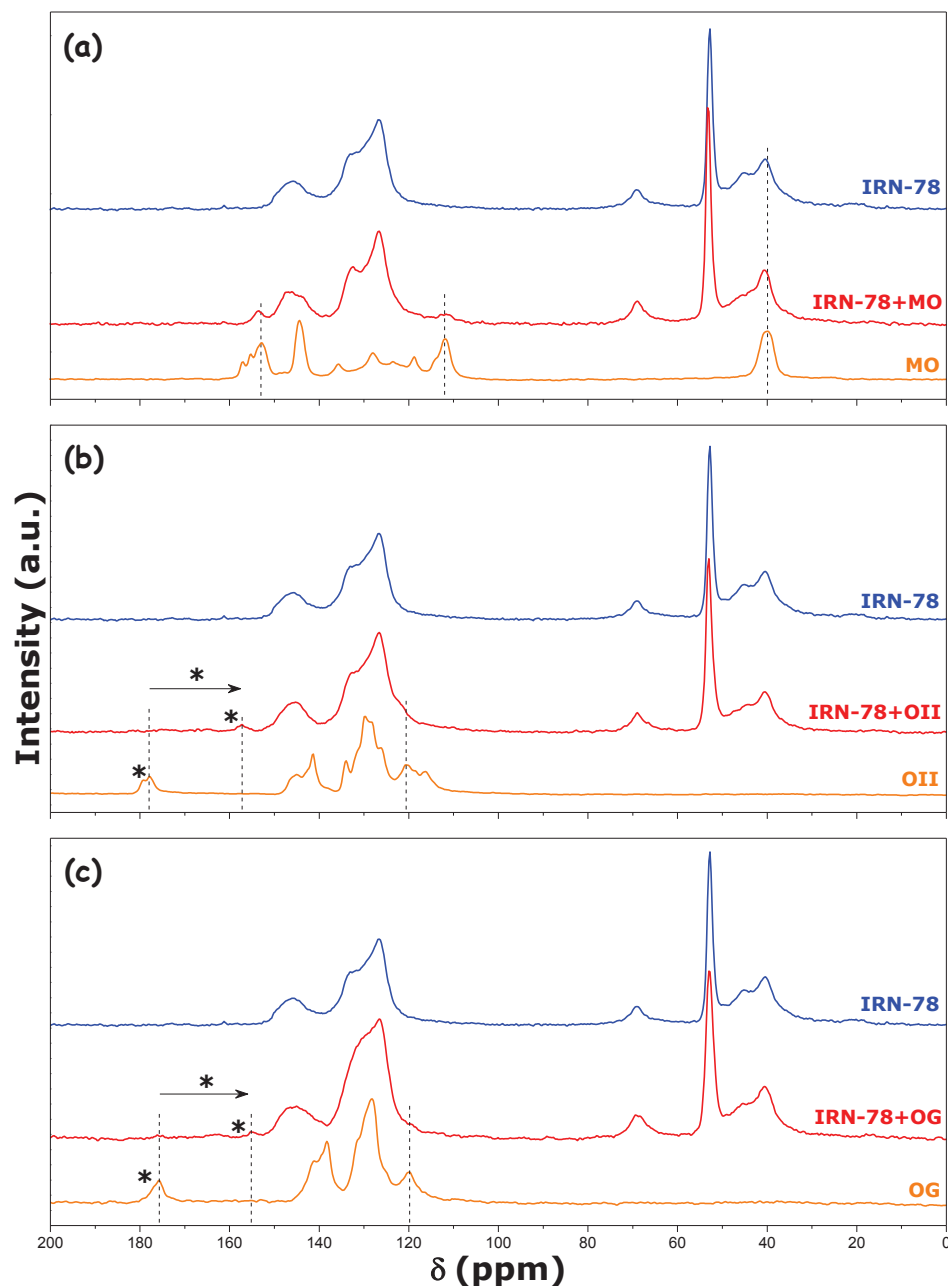


Figure 2.  $^{13}\text{C}$  CP/MAS NMR spectra for washed and dried Amberlite® IRN-78 previously saturated with Methyl Orange (a), Orange II (b), or Orange G (c) from concentrated single-solute aqueous solutions at 298 K. The NMR spectra recorded on pure Amberlite® IRN-78 degassed overnight at 303 K and those obtained from untreated powdered dye samples are reported for comparison purposes. In the case of OII and OG, a horizontal arrow has been added to emphasize a partial transformation of the R-N-NH-R group into a negatively charged center upon adsorption (the asterisks refer to the red and green marks in Fig. S1).

It is the most deshielded nucleus mainly because of the existence of intramolecular hydrogen bond between the oxygen and hydrogen linked to the azo-nitrogen. When the hydrogen bond is broken due to the deprotonation of R-NH-N-R group in alkaline medium, the  $^{13}\text{C}$  signal of this carbon (marked with the green asterisk in Fig. S1b) should be shifted upfield. By analogy with the shielding of the  $^{13}\text{C}$  nucleus in nitromethane adsorbed on different oxide surfaces [43], the surprising intensity of the present effect (about 20 ppm) may be explained by the strength of acid-base interactions underlying the adsorption of OII ions. Therefore, the appearance of the new resonance in the NMR spectrum of the resin + OII system provides a strong indication that the dye units are adsorbed onto Amberlite<sup>®</sup> IRN-78 as divalent anion,  $\text{OII}^{2-}$ . Similar conclusions can be drawn from the transformation of the  $\delta$  175.7 ppm signal into a new one centered at  $\delta$  155.2 ppm in the solid-state CP/MAS  $^{13}\text{C}$  NMR spectrum of the resin + Orange G system: Orange G is adsorbed onto Amberlite<sup>®</sup> IRN-78 as trivalent anion,  $\text{OG}^{3-}$ . However, a careful analysis of the NMR spectrum reveals that the signal at  $\delta$  175.7 ppm does not disappear completely. Some residual peak still remains at this location indicating the simultaneous adsorption of  $\text{OG}^{2-}$  anions. Finally, the trimethylammonium  $-\text{CH}_2-\text{N}^+(\text{CH}_3)_3$  functional groups on the polystyrene-divinylbenzene backbone of the resin likely interact with a mixture of  $\text{OG}^{3-}$  and  $\text{OG}^{2-}$  ions from aqueous solutions. This is because the equilibrium pH value of the resin suspension is too close to the second  $\text{pK}_a$  (11.5) of OG in alkaline solutions to produce only  $\text{OG}^{3-}$  species.

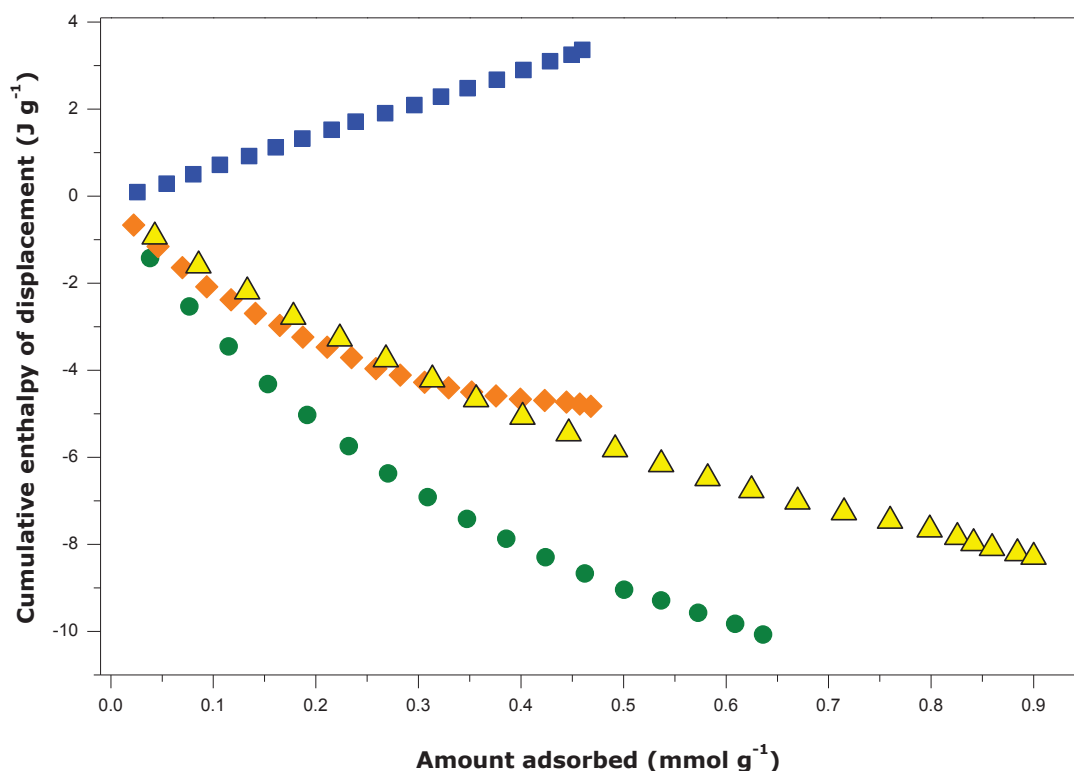


Figure 3. Cumulative enthalpy of displacement accompanying the adsorption of Methyl Orange (orange diamonds), Orange II (blue squares), Orange G (green circles), and chromate anions (yellow triangles) onto Amberlite<sup>®</sup> IRN-78 from single-solute aqueous solutions at 298 K.

The analysis of Figure 3 allows gaining insight into the energy balance upon single-component adsorption of three dye and chromate anions onto Amberlite<sup>®</sup> IRN-78 from single-solute solutions. It is important to emphasize here that the enthalpy of displacement,  $\Delta_{dpl}H_{cum}$ , includes all thermal effects recorded upon ion exchange between the pristine  $\text{OH}^-$  counter-ions and adsorbing anionic species: desorption and re-hydration of  $\text{OH}^-$ , adsorption and partial dehydration of  $\text{CrO}_4^{2-}$  and dye anions, changes in the hydration shell around the ionogenic groups in the resin structure, as well as thermodynamic consequences of constantly varying composition of the liquid phase as a function of the pH (e.g., shifts in  $\text{OII}/\text{OII}^{2-}$  and  $\text{OG}^{2-}/\text{OG}^{3-}$  equilibria). The last contribution is because the correction terms for dilution have been determined by diluting appropriate stock solutions in ultrapure water (see Fig. S3 in Supporting Information).

In the case of Orange II, the displacement process is endothermic and, as such, entropy-driven up to the adsorption plateau. On a qualitative level, this result obtained by direct calorimetry

is in accordance with the endothermic character of dye adsorption onto various anion-exchange resins, as inferred from the temperature dependence of the experimental adsorption isotherms [10-14]. Nevertheless, the adsorption of two other dyes, as well as that of  $\text{CrO}_4^{2-}$ , is systematically exothermic.

It is difficult to explain such a fundamental difference in the displacement energetics between the two types of systems, since the adsorption isotherm for OII exhibits no particular behavior compared to the other solutes. To rule out an explanation based on the wrong estimation of the enthalpy correction term for dilution, a new dilution experiment was carried out by increasing the pH of both the OII stock solution in the syringe and the solution inside the measuring ampoule of the calorimeter (see Fig. S4 in Supporting Information). At pH 12, the  $\text{OII}^{2-}$  anions should be the predominant species. Their dilution appears much less endothermic than that of  $\text{OII}^-$  ions. Nevertheless, the enthalpy of dilution contributes to a disproportionately small extent by comparison with the enthalpy of displacement and the correction term for dilution is negligible in all cases (cf. Fig. S4 in Supporting Information). Another hypothesis can be forwarded on the basis of the endothermicity of OII-water interactions. If one considers that the presence of water molecules is limited chiefly to the vicinity of ionogenic sites (i.e., trimethylammonium groups) in the resin structure, the dye anionic species adsorbed on such positively charged centers are pushed to interact with the surface-bound water. This probably gives rise to an endothermic contribution to  $\Delta_{dpl}H_{cum}$ , which could be the greatest for OII.

Since the enthalpy of displacement measured for the OII + Amberlite<sup>®</sup> IRN-78 system increases almost linearly with the amount adsorbed, the mechanism of dye retention by the resin likely follows only one pathway characterized by a constant molar enthalpy of  $7.3 \text{ kJ mol}^{-1}$ . In the case of MO, OG, and chromate, the retention mechanism undergoes some changes because the enthalpy of displacement is a convex (downward) function of the quantity of solute adsorption. The initial slope of the plot of  $\Delta_{dpl}H_{cum}$  vs. amount adsorbed corresponds to the following value of molar enthalpy:  $-16.0 \text{ kJ mol}^{-1}$ , MO;  $-29.7 \text{ kJ mol}^{-1}$ , OG;  $-16.4 \text{ kJ mol}^{-1}$ ,  $\text{CrO}_4^{2-}$ . On the other side, the ‘average’ mechanism may be described by the average value of molar enthalpy, which is as follows:  $-10.3 \text{ kJ mol}^{-1}$ , MO;  $-15.8 \text{ kJ mol}^{-1}$ , OG;  $-9.2 \text{ kJ mol}^{-1}$ ,  $\text{CrO}_4^{2-}$ . In both cases, the multivalent OG anions appear to have the highest binding affinity, *on a per-mole basis*, for the positively charged trimethylammonium centers in the resin structure.

Table 1. Results of desorption tests carried out with Amberlite® IRN-78 previously saturated with Orange-type dye or chromate anions from single-solute solutions at 298 K and put into contact with a 0.02 mol L<sup>-1</sup> or 1 mol L<sup>-1</sup> NaOH solution at different time intervals. The extent of desorption is presented as a percentage of the total amount adsorbed in the first adsorption cycle.

Solute	0.02 mol L <sup>-1</sup> NaOH				1 mol L <sup>-1</sup> NaOH			
	2	3	4	20	2	3	4	20
MO	0.6%	0.7%	0.7%	0.5%	0.8%	0.8%	0.8%	0.8%
OII	0.2%	0.1%	< 0.1%	0%	0.1%	0.1%	0.1%	0.1%
OG	0.7%	0.5%	0.4%	~ 0%	0.1%	0.1%	0.2%	0.2%
Cr(VI)	5.4%	5.6%	5.9%	6.1%	100%	100%	100%	100%

A subsequent desorption study was planned to verify the above findings through testing the thermodynamic reversibility of the anion exchange process. Changes in the UV-Vis absorbance of the supernatant solutions within the UV-Vis spectral range (examples corresponding to desorption by 0.02 mol L<sup>-1</sup> NaOH solution are given in Fig. S5 in Supporting Information) illustrate the extent of solute desorption. The resulting percentages of desorption at different time intervals have been collected in Table 1.

The efficiency of desorption by both NaOH solutions in removing dye species from the resin is very low because the percentage of dye removal is always below 1%. This points to the irreversible dye retention by Amberlite® IRN-78. Methyl Orange adsorbs irreversibly from single-solute solutions to a smaller extent than the two other dyes do, especially in strongly alkaline solutions. It is worth noting here that, contrary to MO, the UV-Vis absorption spectra of OII and OG in the supernatant solutions (after desorption) change their shape compared to the corresponding spectra in ultrapure water. They resemble those recorded with alkaline solutions of OG and OII, as can be seen in Fig. 4. Since the pH of these supernatant solutions ranges between 11 and 12, the comparison of UV-Vis spectra in Fig. 4 corroborates the conclusions drawn from the NMR studies of the resin samples saturated with the dyes. Depending on the actual pH value,

Orange II and Orange G occur in alkaline solutions in the form of multivalent anions or as a mixture containing anions of different valences. Following the results in Table 1, the irreversibility of dye retention somewhat increases at more alkaline pH values. In conclusion, the sorption irreversibility concerns rather dye anions with an ionized R-NH-N-R group. When they become the only species present in strongly alkaline solutions (e.g., 1 mol L<sup>-1</sup> NaOH), they compete efficiently against OH<sup>-</sup> for positively charged sites in the resin structure.

About 6% of chromate anions are desorbed during the first 2 h of equilibration with the 0.02 mol L<sup>-1</sup> NaOH solution. Further prolonged contact appears rather inefficient. When the desorption is performed by using 1 mol L<sup>-1</sup> NaOH solution, the removal of CrO<sub>4</sub><sup>2-</sup> from the resin is complete even after 15 min of equilibration. This indicates that hydroxide is a stronger competitor against chromate anion in highly concentrated OH<sup>-</sup> solutions.

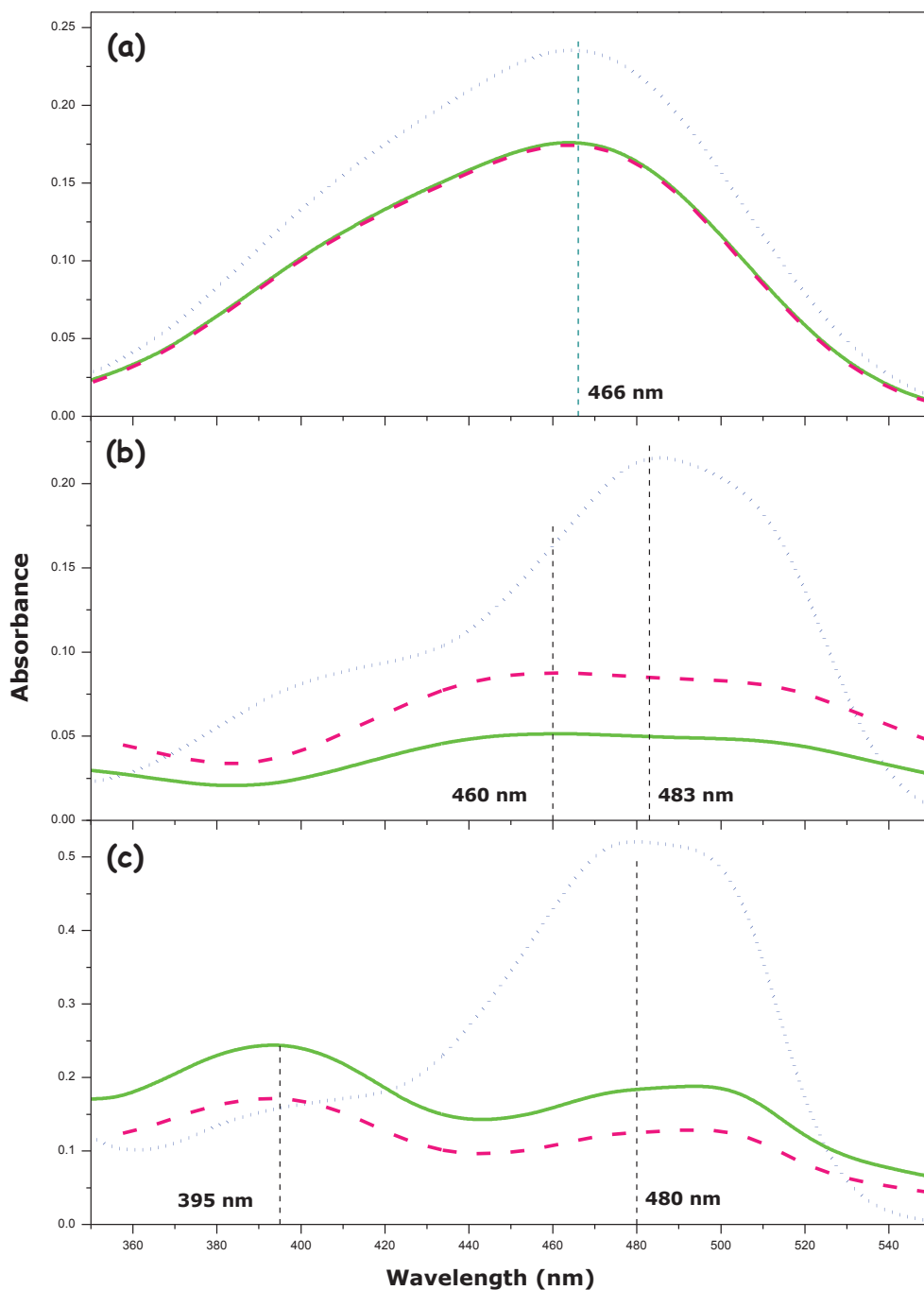


Figure 4. Room temperature UV-Vis absorption spectra of MO(a), OII (b), and OG (c) in various aqueous solutions: single-solute solution in ultrapure water (dotted blue lines), NaOH alkaline solution (dashed rose lines), supernatant solution collected after desorption study of Amberlite<sup>®</sup> IRN-78 previously saturated with dye species and put into contact with a 0.02 mol L<sup>-1</sup> NaOH solution during 2h (solid green lines).

### *3.2. Competitive adsorption of dye and chromate anions from bi-solute equimolar solutions*

When dye anions and  $\text{CrO}_4^{2-}$  co-exist in multi-component solutions, the difference between their affinities for positively charged centers in the resin structure will certainly contribute to the complexity of anion exchange at the Solid-Liquid interface. For the purpose of the present work, the selective retention of organic and inorganic anions was studied from bi-solute solutions containing a given dye and  $\text{CrO}_4^{2-}$ . The results of equilibrium adsorption and calorimetry measurements performed with such systems have been collected in Figures 5 and 6. In the case of MO and OII, the individual adsorption isotherms in the bi-solute systems do not differ greatly from the corresponding curves obtained with the single-component systems, which means that the presence of  $\text{CrO}_4^{2-}$  in the aqueous phase does not have much impact on the adsorption of the dye component. On the contrary, the retention of  $\text{CrO}_4^{2-}$  is decreased largely, especially for higher equilibrium concentrations. At low concentrations of the dye component in the equilibrium bulk solution, the two components strongly adsorb in equivalent amounts and this results in the vertical segments on both individual adsorption isotherms. Beyond this initial adsorption range, the quantity of dye adsorption reaches its equilibrium with the value of  $0.5 \text{ mmol g}^{-1}$ . The amount of chromate becomes to decrease and it subsequently decays either to zero (MO + chromate) or to a very small value (OII + chromate). Therefore, the composite isotherms, obtained by adding the individual component contributions, also attain a maximum value close to  $0.8 \text{ mmol g}^{-1}$  at the end of the initial vertical portions.

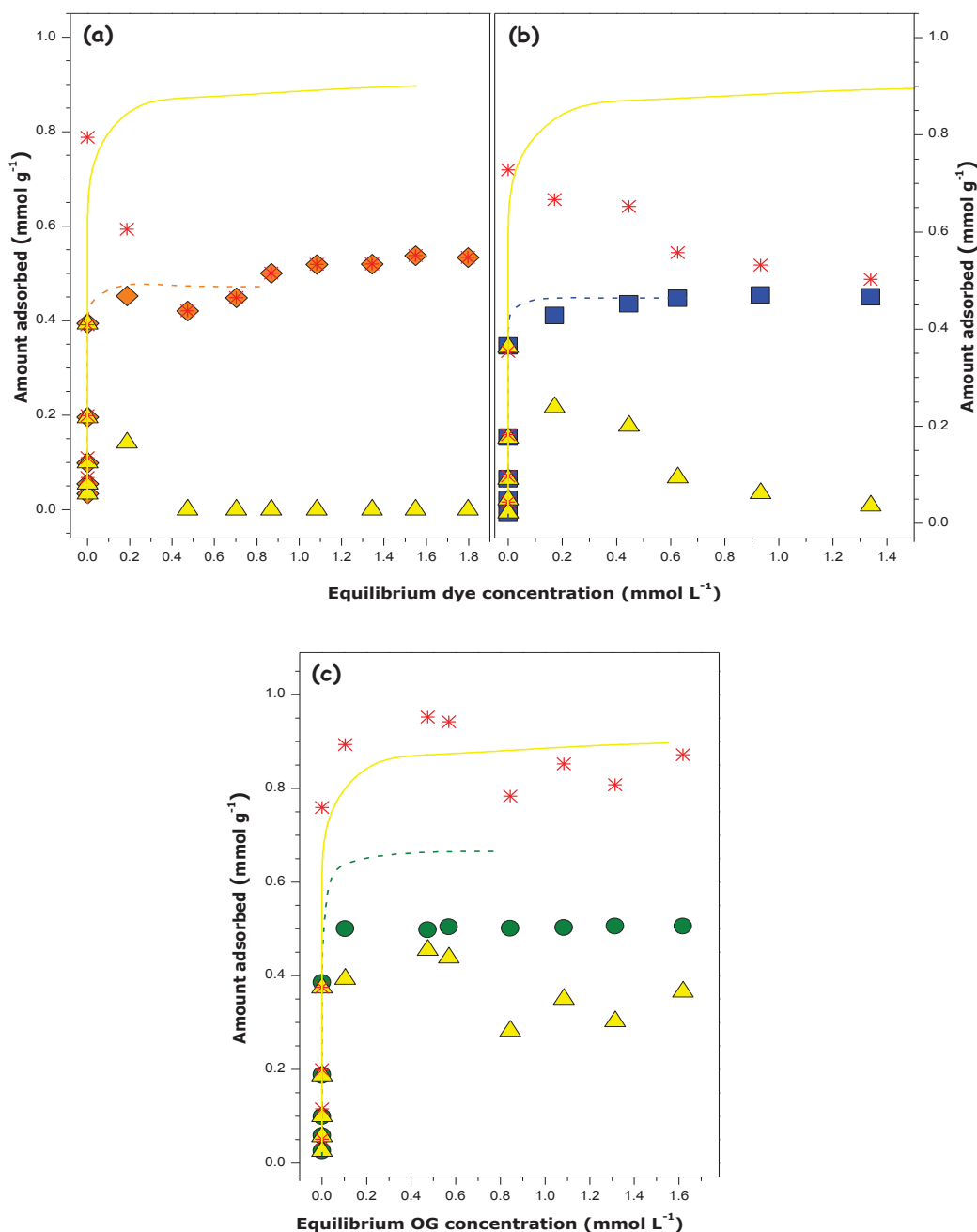


Figure 5. Results of equilibrium adsorption measurements of the competitive adsorption between MO (a), OII (b), or OG (c) and  $\text{CrO}_4^{2-}$  onto Amberlite<sup>®</sup> IRN-78 from bi-solute equimolar solutions at 298 K. The individual adsorption isotherms of the dye (orange (MO); blue (OII); green (OG) symbols) and chromate (yellow triangles), as well as the composite adsorption isotherms (crosses), are plotted against the equilibrium concentration of dye component. The dashed and solid lines represent the adsorption isotherms of the dye and inorganic ion, respectively, as determined in the separate single-solute systems (as a function of the equilibrium concentration of the corresponding solute).

In the OG + chromate system, the individual adsorption curves still possess initial vertical portions, where the adsorption of both solute occurs in equimolar proportion. Then, the isotherms undergo some changes in comparison with those determined for the other dyes. The quantity of OG adsorption increases to a plateau adsorption value of about  $0.5 \text{ mmol g}^{-1}$ , which is smaller than the ‘saturation’ value (i.e.,  $0.63 \text{ mmol g}^{-1}$ ) obtained in the single-solute system. The amount of  $\text{CrO}_4^{2-}$  retained by Amberlite® IRN-78 from bi-solute solutions firstly increases to  $0.45 \text{ mmol g}^{-1}$  and then it decreases to about  $0.34 \text{ mmol g}^{-1}$ , which represents 38% of its maximum adsorption in the single-solute system. Finally, the maximum composite adsorption oscillates around  $0.9 \text{ mmol g}^{-1}$  over the interval of moderate and high equilibrium concentrations.

In order to confirm the mechanism of anion exchange between hydroxides and the adsorbing species of both types, it is important to mention that the pH of the resin suspension for points in the adsorption plateau region increases from about 10 (after the first few minutes of solid-liquid contact) to an equilibrium value depending on the dye type: pH 11, MO; pH 11.2, OII; pH 11.4, OG. By analogy with the case of single-component adsorption, this indicates the possibility of  $\text{OII}^{2-}$  formation, though the existence of  $\text{OG}^{3-}$  anions is rather to be excluded. All this points to the conclusion that the competitive adsorption of dye and inorganic anions is again limited by the anion exchange capacity of Amberlite® IRN-78.

The energetic aspects of the anion exchange process in the bi-solute systems may be quantified by monitoring variations of the cumulative enthalpy of displacement. In Figure 6, the  $\Delta_{dpl}H_{cum}$  values are plotted as a function of the composite dye + chromate adsorption only throughout the vertical portion of the adsorption isotherm. The processing of the calorimetric data obtained with the bi-solute systems is quite straightforward in this particular adsorption range. Since the two solutes seem to be retained in equimolar amounts, their proportion in the equilibrium bulk solution within the calorimetric ampoule remains unchanged. Therefore, the results of dilution experiments carried out with the bi-solute equimolar solutions can be directly used to evaluate the dilution correction term. The thermal effects of dilution are presented in Fig. S6 in Supporting Information. The dilution of bi-solute equimolar solutions in ultrapure water is much less endothermic in comparison with that of single-solute dye solutions (see Fig. S3 in Supporting Information) because of the exothermic contribution provided by  $\text{CrO}_4^{2-}$ .

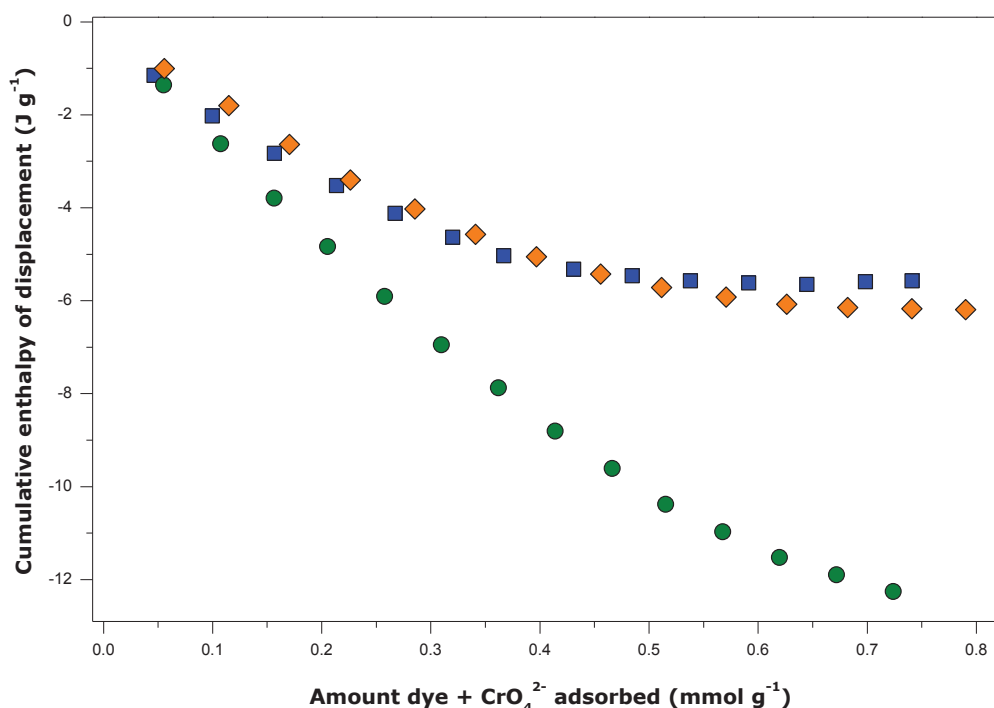


Figure 6. Cumulative enthalpy of displacement accompanying the competitive adsorption of MO (orange diamonds), OII (blue squares), OG (green circles) and, CrO<sub>4</sub><sup>2-</sup> anions, onto Amberlite<sup>®</sup> IRN-78 from equimolar bi-solute aqueous solutions at 298 K.

The displacement process in the bi-solute systems is exothermic, even in the case of Orange II. For MO and OII, the enthalpy curves look very similar to each other. They represent convex (downward) functions of the quantity of composite adsorption: in the second half of the adsorption range, the overall process becomes almost athermal. In the OG + chromate system, the  $\Delta_{dpl}H_{cum}$  values decrease monotonously up to the end. The initial slopes of the plots of  $\Delta_{dpl}H_{cum}$  vs. amount adsorbed are as follows:  $-15.4 \text{ kJ mol}^{-1}$ , MO;  $-17.6 \text{ kJ mol}^{-1}$ , OII;  $-23.1 \text{ kJ mol}^{-1}$ , OG. With the only exception of the OG + chromate system, these molar enthalpies correspond well to the arithmetic mean of the individual solute contributions as measured in appropriate single-solute systems. Firstly, this means that the two components are retained in a quite independent manner. Secondly, this is an extra argument for dominance of the OG<sup>2-</sup> species within this initial adsorption range, as the pH of the resin suspension is probably not sufficiently alkaline to generate OG<sup>3-</sup> anions. From the viewpoint of enthalpy, the displacement process accompanying the competitive interactions between Orange II and CrO<sub>4</sub><sup>2-</sup> is dominated by the exothermic contribution made by the inorganic anion.

The comparison of apparent affinities between dye and inorganic anions for positively charged centers in the resin structure may be also based on the selectivity tests in which the resin samples pre-saturated with one component have been equilibrated with a concentrated solution of the other. It is important to note that the selected solute concentrations are capable of saturating the resin sites with the oncoming solute in the appropriate single-solute system. Table 2 shows the results, which include the amount of the oncoming species retained by the resin, the quantity of the initially retained solute remaining in the resin after the attainment of a new sorption equilibrium (compared to the saturation value), and the sum of individual component contributions. When the resin is pre-saturated with a given dye (Table A), the oncoming  $\text{CrO}_4^{2-}$  may be still adsorbed without displacing many dye units. In consequence, the maximum quantity of adsorption being a sum of individual solute contributions can be even doubled like in the case of Methyl Orange. This means that the dye retention by Amberlite® IRN-78 does not saturate all available positive centers in the resin structure.

Table 2. Results of selectivity tests of solute retention by Amberlite® IRN-78: (A) the resin sample pre-saturated with a dye and subsequently equilibrated with a concentrated  $\text{CrO}_4^{2-}$  solution, (B) the resin sample pre-saturated with  $\text{CrO}_4^{2-}$  and subsequently equilibrated with a concentrated dye solution. The values are reported in  $\text{mmol g}^{-1}$

Table A

Dye used to pre-recover	MO	OII	OG
Reference value: initial individual adsorption i.e. saturation plateau reached during the pre-recovering process of dye (MO, OII or OG)	0.47	0.47	0.63
Cr amount adsorbed onto recovered with dye resin	0.59	0.38	0.15
Dye amount remaining in the dye-resin after dye adsorption	0.49	0.46	0.63
Sum of the two species contained in the resin after the second adsorption step (Cr secondary adsorbed together with not removed dye)	1.04	0.84	0.77

Table B

Dye to be adsorbed	MO	OII	OG
Reference value: initial individual adsorption i.e. saturation plateau reached during the pre-recovering process with Cr	0.82		
Dye amount adsorbed onto recovered with Cr resin	0.28	0.19	0.36
Cr amount remaining in the Cr-resin after dye adsorption	0.79	0.79	0.61
Sum of the two species contained in the resin after the second adsorption step (dye secondary adsorbed together not removed Cr)	1.07	0.98	0.96

Simultaneously, the conclusion of irreversible dye uptake, forwarded in the previous paragraph, finds again its confirmation. The capacity of individual chromate adsorption onto Amberlite® IRN-78 pre-saturated with a dye increases in the order: resin + MO > resin + OII > resin + OG.

When the resin sample is pre-saturated with  $\text{CrO}_4^{2-}$  and subsequently equilibrated with a concentrated solution of MO or OII, about 2% of the initial adsorbate (chromate anion) is desorbed from the interfacial region (Table B). In the case of oncoming OG species, the chromate desorption attains 25% of its initial adsorption value. The amount of dye retained by the resin is as follows: 0.2 mmol  $\text{g}^{-1}$ , OII; 0.3 mmol  $\text{g}^{-1}$ , MO; 0.4 mmol  $\text{g}^{-1}$ , OG. This is consistent with the high affinity of OG anions for the exchangeable resin sites. Surprisingly, the OII adsorption is smaller than that of MO. Nevertheless, it should be noted that the pH of the resin suspension is rather close to neutral because the alkaline supernatant solution in equilibrium with the chromate-resin sample is replaced by a new dye-solution in ultrapure water. Therefore, the divalent  $\text{OII}^{2-}$  ion cannot be formed in the aqueous phase. At equal charges, the more hydrophobic and smallest  $\text{MO}^-$  anion is preferentially adsorbed against  $\text{OII}^-$  by Amberlite® IRN-78 which likely explains the above results. Again, the sum of the individual solute contributions is greater than the initial  $\text{CrO}_4^{2-}$  adsorption.

#### **4. Conclusions**

Strongly basic anion-exchange resin Amberlite® IRN-78 has proven its usefulness in removing Orange-type anionic dyes from aqueous streams. The overall performance of the removal process depends on the composition of the aqueous phase and it is guided by the anion exchange capacity (AEC) of the resin. When the resin is in the hydroxide ion form, the adsorption follows the pathway of anion exchange between the pristine  $\text{OH}^-$  ions and the oncoming anionic species. This anion exchange makes the supernatant solution more alkaline, which, in some cases, may give rise to new dye species with an additionally ionized R-N-NH-R moiety, e.g.,  $\text{OII}^{2-}$  or even  $\text{OG}^{3-}$ . From the viewpoint of thermodynamics, the constantly changing composition of the aqueous phase and the diversity of dye anionic forms co-existing in the supernatant present a challenge for simultaneous adsorption and calorimetry studies.

In the single-solute systems, the retention capacity of the resin towards various anionic solutes, *on a per-mole basis*, decreased in the following order:  $\text{CrO}_4^{2-} > \text{OG} > \text{OII} \approx \text{MO}$ . The overall enthalpy effect of displacement was either exothermic ( $\text{CrO}_4^{2-}$ , OG, MO) or endothermic (OII). The retention of dyes was irreversible even in strongly alkaline media contrary to  $\text{CrO}_4^{2-}$ , which was completely desorbed from the resin by a  $1 \text{ mol L}^{-1}$  NaOH solution. The competition between dye and chromate anions from their equimolar solutions mainly caused a marked decrease in the uptake of  $\text{CrO}_4^{2-}$ , thereby pointing to preferential dye retention by Amberlite® IRN-78. Similar conclusion was drawn from the selectivity tests in which the resin samples pre-saturated with a dye or  $\text{CrO}_4^{2-}$  were equilibrated with a concentrated solution of the other solute. Orange G had the highest interaction affinity for positively charged trimethylammonium centers in the resin structure, irrespective of the composition of aqueous solution.

## *References*

- [1] S.D. Alexandratos, Ion-Exchange Resins: A Retrospective from Industrial and Engineering Chemistry Research, *Industrial & Engineering Chemistry Research*, 48 (2009) 388-398.
- [2] B. Prelot, I. Ayed, F. Marchandea, J. Zajac, On the real performance of cation exchange resins in wastewater treatment under conditions of cation competition: the case of heavy metal pollution, *Environmental Science and Pollution Research*, 21 (2014) 9334-9343.
- [3] D.L.d. Silva, G. Brunner, Desorption of heavy metals from ion exchange resin with water and carbon dioxide, *Brazilian Journal of Chemical Engineering*, 23 (2006) 213-218.
- [4] Q. Sun, P. Lu, L. Yang, The adsorption of lead and copper from aqueous solution on modified peat-resin particles, *Environmental Geochemistry and Health*, 26 (2004) 311-317.
- [5] N. El-Kholy, N. Badawy, A. El-Said, A.A. El Pasir, Competitive adsorption of Co (II) in a binary and tertiary system with metal ions Cr (III) and Ni (II) on Lewatite S-100 cation exchange resin, *Nature & Science*, 11 (2013) 41-48.
- [6] J.B. de Heredia, J. Domínguez, Y. Cano, I. Jiménez, Nitrate removal from groundwater using Amberlite IRN-78: Modelling the system, *Applied Surface Science*, 252 (2006) 6031-6035.
- [7] S.H. Lee, J.H. Yoo, J.H. Kim, Ion exchange characteristics of rhodium and ruthenium from a simulated radioactive liquid waste, *Korean Journal of Chemical Engineering*, 21 (2004) 1038-1043.

- [8] K.-R. Kim, M.-S. Lee, D.-H. Ahn, S.-P. Yim, H. Chung, Preparation of functional anion-exchange resin and its selective adsorption of palladium in nitric acid medium, *Journal of Industrial and Engineering Chemistry*, 8 (2002) 472-476.
- [9] S.H. Lee, K.R. Kim, J.-S. Shon, J.H. Yoo, H. Chung, Ion exchange characteristics of rhodium from a simulated radioactive liquid waste, *Journal of Industrial and Engineering Chemistry*, 5 (1999) 296-301.
- [10] S.M. Al-Rashed, A.A. Al-Gaid, Kinetic and thermodynamic studies on the adsorption behavior of Rhodamine B dye on Duolite C-20 resin, *Journal of Saudi Chemical Society*, 16 (2012) 209-215.
- [11] V. Dulman, C. Simion, A. Barsanescu, I. Bunia, V. Neagu, Adsorption of Anionic Textile Dye Acid Green 9 from Aqueous Solution onto Weak or Strong Base Anion Exchangers, *Journal of Applied Polymer Science*, 113 (2009) 615-627.
- [12] X. Lu, Y.S. Shao, N.Y. Gao, L. Ding, Equilibrium, Thermodynamic, and Kinetic Studies of the Adsorption of 2,4-Dichlorophenoxyacetic Acid from Aqueous Solution by MIEX Resin, *J. Chem. Eng. Data*, 60 (2015) 1259-1269.
- [13] M. Naushad, Z.A. Allothman, M.R. Khan, Removal of malathion from aqueous solution using De-Acidite FF-IP resin and determination by UPLC-MS/MS: Equilibrium, kinetics and thermodynamics studies, *Talanta*, 115 (2013) 15-23.
- [14] D. Suteu, D. Bilba, S. Coseri, Macroporous polymeric ion exchangers as adsorbents for the removal of cationic dye basic blue 9 from aqueous solutions, *Journal of Applied Polymer Science*, 131 (2014).
- [15] M.E. Thrash Jr, N.G. Pinto, Flow microcalorimetric measurements for bovine serum albumin on reversed-phase and anion-exchange supports under overloaded conditions, *Journal of Chromatography A*, 908 (2001) 293-299.
- [16] J.-b. Zhou, M. Green, A. Shaviv, Mineralization of organic N originating in treated effluent used for irrigation, *Nutrient Cycling in Agroecosystems*, 67 (2003) 205-213.
- [17] M. Chasanov, R. Kunin, F. McGarvey, Sorption of phenols by anion exchange resins, *Industrial & Engineering Chemistry*, 48 (1956) 305-309.
- [18] R. Anderson, R. Hansen, Phenol sorption on ion exchange resins, *Industrial & Engineering Chemistry*, 47 (1955) 71-75.
- [19] S. Deng, Q. Yu, J. Huang, G. Yu, Removal of perfluorooctane sulfonate from wastewater by anion exchange resins: Effects of resin properties and solution chemistry, *Water Research*, 44 (2010) 5188-5195.
- [20] M. Wawrzkiwicz, Z. Hubicki, Kinetics of adsorption of sulphonated azo dyes on strong basic anion exchangers, *Environmental Technology*, 30 (2009) 1059-1071.
- [21] B.H. Li, F.Q. Liu, J.F. Wang, C. Ling, L.J. Li, P. Hou, A.M. Li, Z.P. Bai, Efficient separation and high selectivity for nickel from cobalt-solution by a novel chelating resin: batch, column and competition investigation, *Chem. Eng. J.*, 195 (2012) 31-39.

- [22] L.J. Li, F.Q. Liu, X.S. Jing, P.P. Ling, A.M. Li, Displacement mechanism of binary competitive adsorption for aqueous divalent metal ions onto a novel IDA-chelating resin: Isotherm and kinetic modeling, *Water Research*, 45 (2011) 1177-1188.
- [23] J.L. Zhang, X.H. Liu, X.Y. Chen, J.T. Li, Z.W. Zhao, Separation of tungsten and molybdenum using macroporous resin: Competitive adsorption kinetics in binary system, *Hydrometallurgy*, 144 (2014) 77-85.
- [24] M. Alikhani, M.R. Moghbeli, Ion-exchange polyHIPE type membrane for removing nitrate ions: Preparation, characterization, kinetics and adsorption studies, *Chem. Eng. J.*, 239 (2014) 93-104.
- [25] K.K. Clark, A.A. Keller, Adsorption of perchlorate and other oxyanions onto magnetic permanently confined micelle arrays (Mag-PCMAs), *Water Research*, 46 (2012) 635-644.
- [26] B. Wang, H. Song, C. Wang, C. Shuang, Q. Li, A. Li, Evaluation of nitrate removal properties of magnetic anion-exchange resins in water, *Journal of Chemical Technology & Biotechnology*, DOI 10.1002/jctb.4723(2015) n/a-n/a.
- [27] S. Karcher, A. Kornmüller, M. Jekel, Anion exchange resins for removal of reactive dyes from textile wastewaters, *Water Research*, 36 (2002) 4717-4724.
- [28] J. Park, J. Shore, Water for the dyehouse: supply, consumption, recovery and disposal, *Journal of the Society of Dyers and Colourists*, 100 (1984) 383-399.
- [29] W.H. Ojala, L.K. Lu, K.E. Albers, W.B. Gleason, T. Richardson, R. Lovrien, E. Sudbeck, Intermolecular interactions of sulfonated azo dyes: crystal structures of the diammonium, dilithium, magnesium and calcium salts of 7-hydroxy-8-(phenylazo)-1, 3-naphthalenedisulfonic acid (Orange G), *Acta Crystallographica Section B: Structural Science*, 50 (1994) 684-694.
- [30] A.J. Barnes, M.A. Majid, M.A. Stuckey, P. Gregory, C.V. Stead, The resonance Raman spectra of Orange II and Para Red: molecular structure and vibrational assignment, *Spectrochimica Acta Part A: Molecular Spectroscopy*, 41 (1985) 629-635.
- [31] A.S. Özen, P. Doruker, V. Aviyente, Effect of cooperative hydrogen bonding in azo-hydrazone tautomerism of azo dyes, *The Journal of Physical Chemistry A*, 111 (2007) 13506-13514.
- [32] R.G. Sandberg, G.H. Henderson, R.D. White, E.M. Eyring, Kinetics of acid dissociation-ion recombination of aqueous methyl orange, *The Journal of Physical Chemistry*, 76 (1972) 4023-4025.
- [33] L.C. Abbott, S.N. Batchelor, J. Oakes, B.C. Gilbert, A.C. Whitwood, J.R. Lindsay Smith, J.N. Moore, Experimental and computational studies of structure and bonding in parent and reduced forms of the azo dye Orange II, *The Journal of Physical Chemistry A*, 109 (2005) 2894-2905.
- [34] K.-S. Cheon, Y.S. Park, P.M. Kazmaier, E. Buncel, Studies of azo-hydrazone tautomerism and H-bonding in azo-functionalized dendrimers and model compounds, *Dyes and Pigments*, 53 (2002) 3-14.
- [35] K. Bourikas, M. Styliidi, D.I. Kondarides, X.E. Verykios, Adsorption of acid orange 7 on the surface of titanium dioxide, *Langmuir*, 21 (2005) 9222-9230.

- [36] J. Madhavan, F. Grieser, M. Ashokkumar, Degradation of orange-G by advanced oxidation processes, *Ultrasonics Sonochemistry*, 17 (2010) 338-343.
- [37] A.K. Sengupta, D. Clifford, S. Subramonian, Chromate ion-exchange process at alkaline pH, *Water Research*, 20 (1986) 1177-1184.
- [38] J. Inczédy, *Analytical Applications of Ion Exchangers*, Pergamon Press, Oxford, 1966.
- [39] Y. Marcus, A simple empirical model describing the thermodynamics of hydration of ions of widely varying charges, sizes, and shapes, *Biophys. Chem.*, 51 (1994) 111-127.
- [40] G. Darmograi, B. Prelot, G. Layrac, D. Tichit, G. Martin-Gassin, F. Salles, J. Zajac, Study of Adsorption and Intercalation of Orange-Type Dyes into Mg–Al Layered Double Hydroxide, *The Journal of Physical Chemistry C*, 119 (2015) 23388-23397.
- [41] H. Laguna, S. Loera, I.A. Ibarra, E. Lima, M.A. Vera, V. Lara, Azoic dyes hosted on hydrotalcite-like compounds: Non-toxic hybrid pigments, *Microporous and Mesoporous Materials*, 98 (2007) 234-241.
- [42] A. Traboulsi, N. Dupuy, C. Rebufa, M. Sergent, V. Labeed, Investigation of gamma radiation effect on the anion exchange resin Amberlite IRA-400 in hydroxide form by Fourier transformed infrared and <sup>13</sup>C nuclear magnetic resonance spectroscopies, *Analytica Chimica Acta*, 717 (2012) 110-121.
- [43] E. Lima, L.C. de Ménorval, D. Tichit, M. Laspéras, P. Graffin, F. Fajula, Characterization of the Acid–Base Properties of Oxide Surfaces by <sup>13</sup>C CP/MAS NMR Using Adsorption of Nitromethane, *The Journal of Physical Chemistry B*, 107 (2003) 4070-4073.

## SUPPORTING INFORMATION

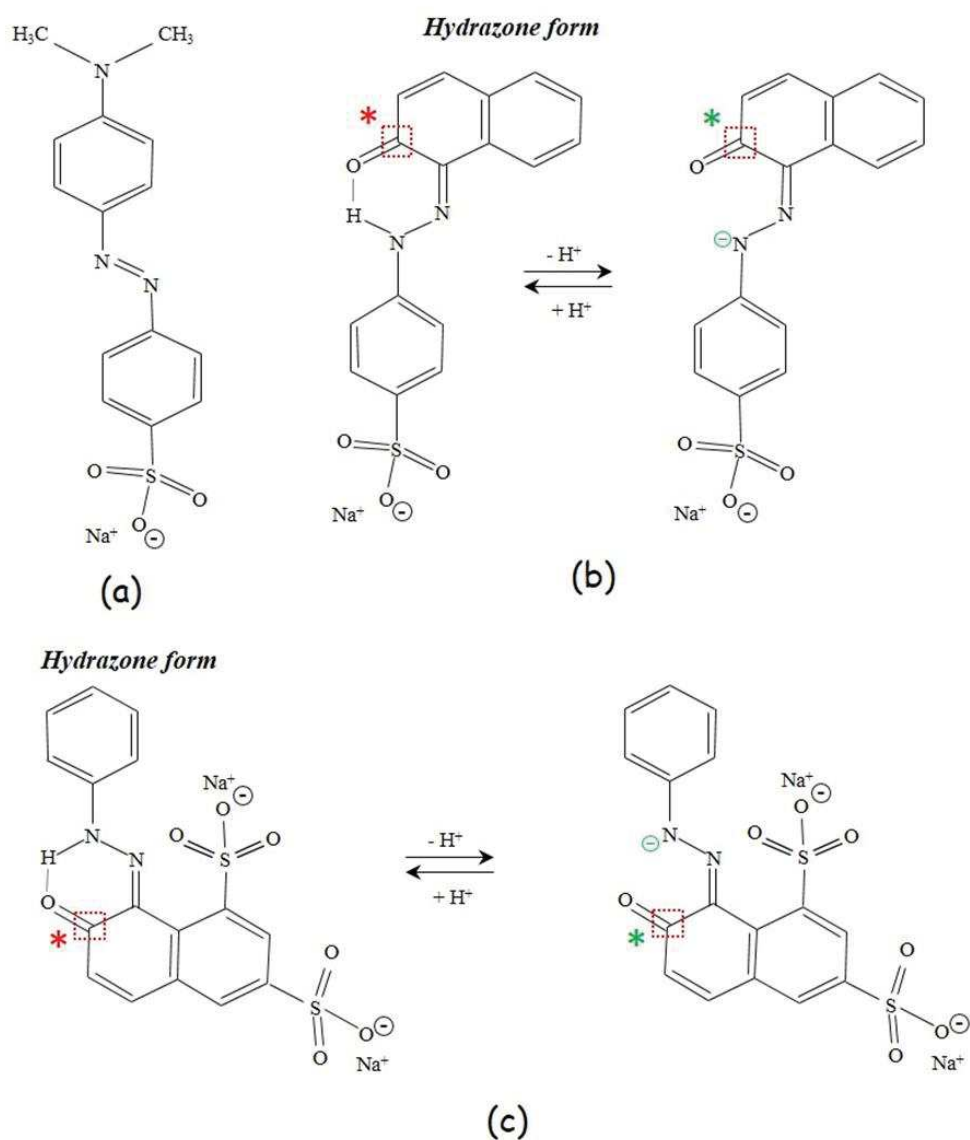


Figure S1. Orange-type dyestuff structures studied in the present work, represented in partially dehydrated (sulfonic group) hydrazone form: (a) Methyl Orange, (b) Orange II, (c) Orange G. The deprotonation pathway for R-N-NH-R group in the hydrazone structures of Orange II and Orange G leading to an additional negatively charged center in alkaline solutions is also shown schematically. The carbon atom within the 2-oxonaphthalene moiety bonded with oxygen has

been labelled with red (in the protonated forms) or green (in the deprotonated forms) asterisks to further assist the analysis of  $^{13}\text{C}$  CP/MAS NMR spectra in Fig. 2.

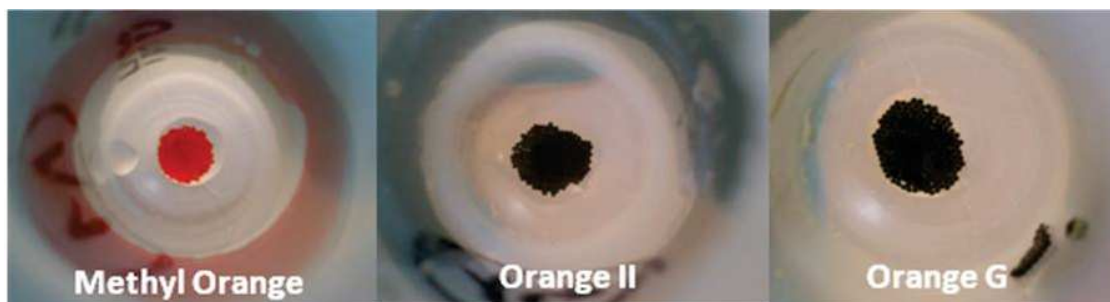


Figure S 2. Images of Amberlite<sup>®</sup> IRN-78 beads saturated with Methyl Orange, Orange II, and Orange G dyes from concentrated single-solute solutions. The resin beads have collected after wash at the bottom of Nalgene<sup>®</sup> tubes.

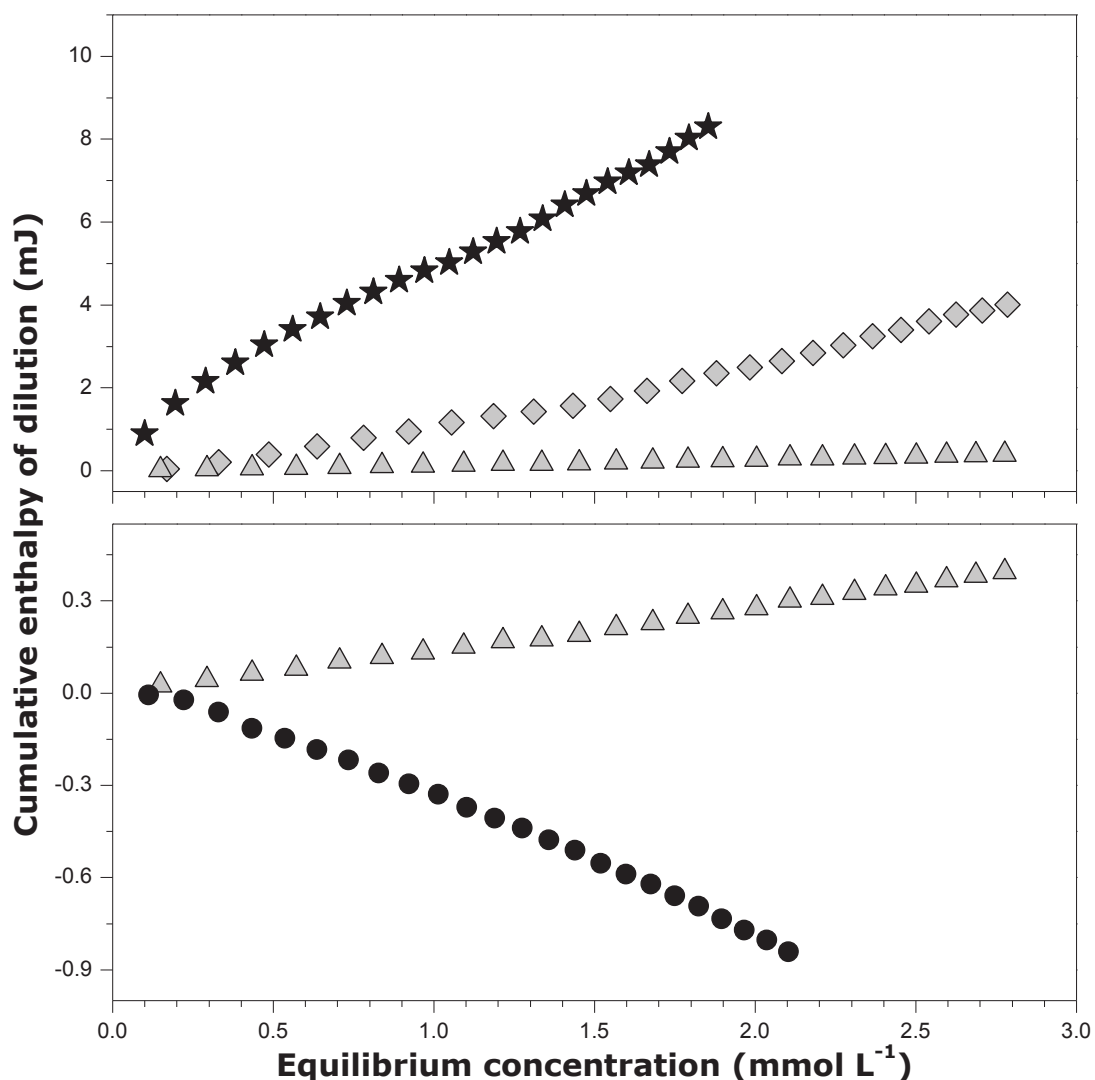


Figure S 3. Variations of the cumulative enthalpy of dilution at 298 K for single-solute solutions in ultrapure water containing: Methyl Orange (gray diamonds), Orange II (black stars), Orange G (gray triangles), or chromate anions (black circles) as a function of the equilibrium solute concentration (inside the calorimetric ampoule). The dilution experiments were carried out under the same experimental conditions as those employed in the adsorption runs but without putting a resin sample into the measuring ampoule. The scale of the vertical (enthalpy) axis is different in the upper and lower panel.

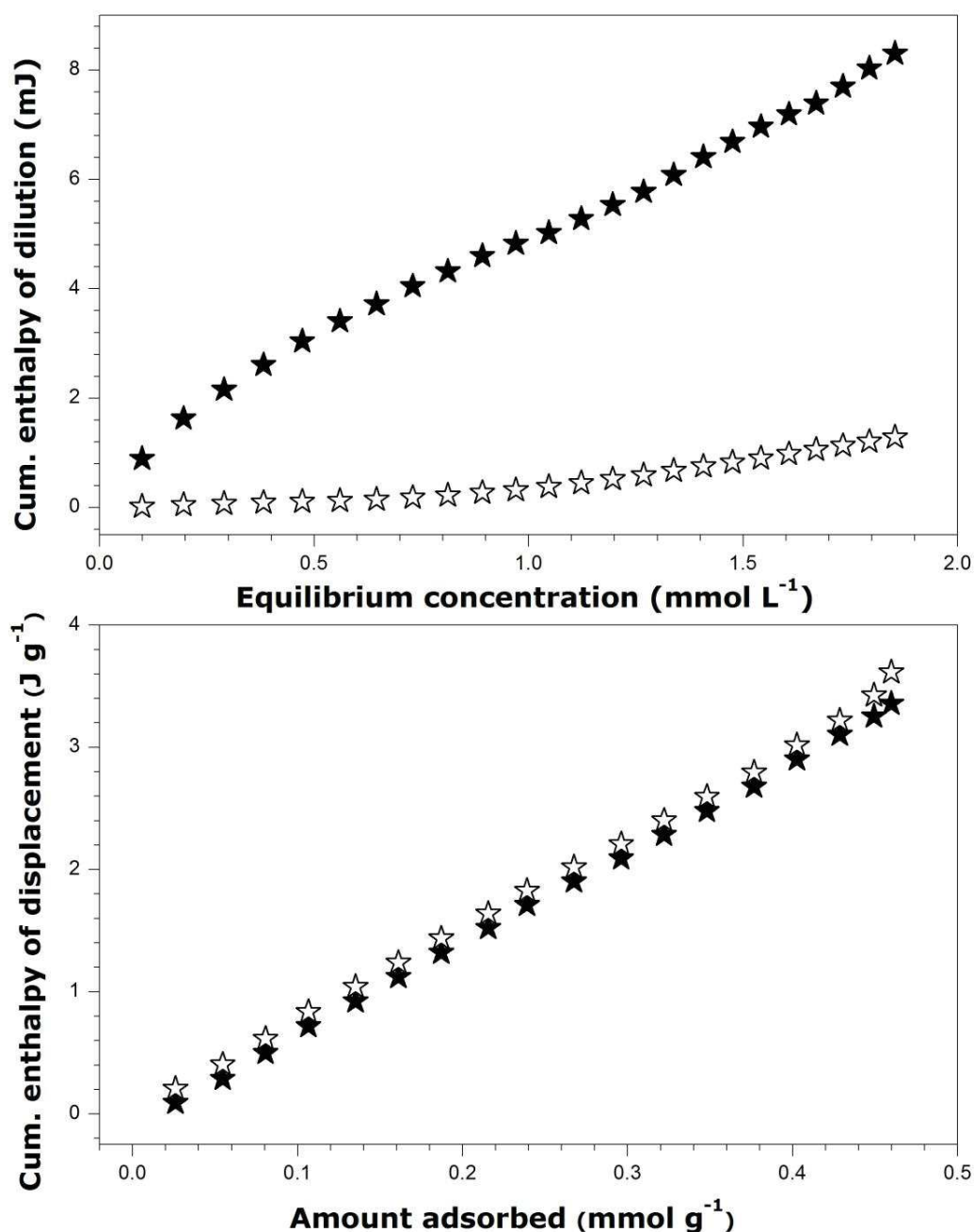


Figure S 4. Effect of pH on the cumulative enthalpy of dilution (upper panel) and cumulative enthalpy of displacement (lower panel) for Orange II dissolved in ultrapure water (solid stars) and an aqueous NaOH solution (pH 12) at 298 K. The dilution experiments were carried out under the same experimental conditions as those employed in the adsorption runs but without putting a resin sample into the measuring ampoule (injection volume: 10  $\mu\text{L}$ , injection speed: 10 s, agitation speed: 90 rpm, equilibration time between two successive injections: 30 min). In all cases, the dye concentration was 8 mmol L<sup>-1</sup>.

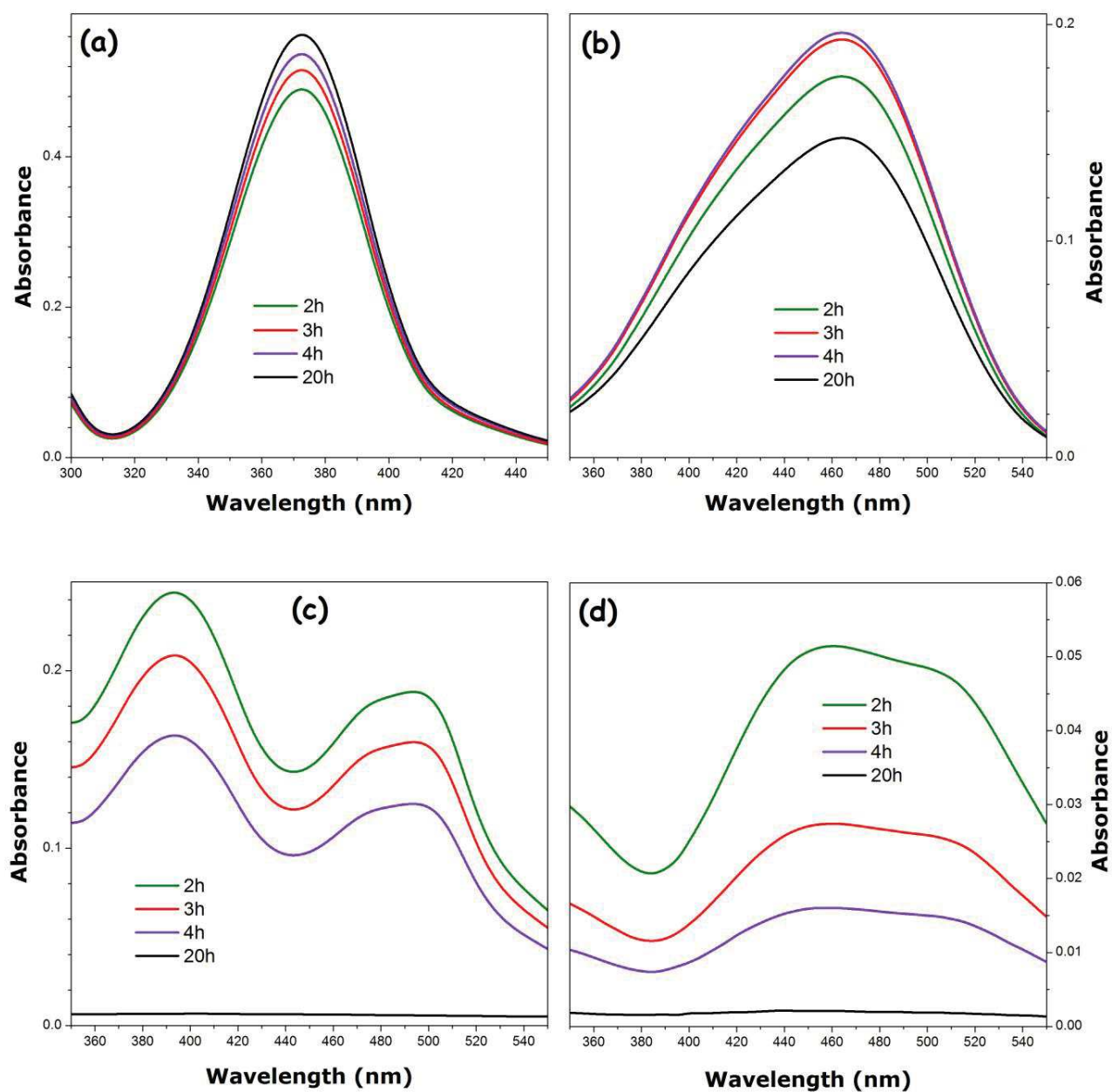


Figure S 5. Room temperature UV-Vis absorption spectra recorded in supernatant solutions collected after desorption study of Amberlite<sup>®</sup> IRN-78 previously saturated with  $\text{CrO}_4^{2-}$  (a), Methyl Orange (b), Orange II (c), or Orange G (d) and put into contact with a  $0.02 \text{ mol L}^{-1}$  NaOH solution at different time intervals (2, 3, 4, and 20 h).

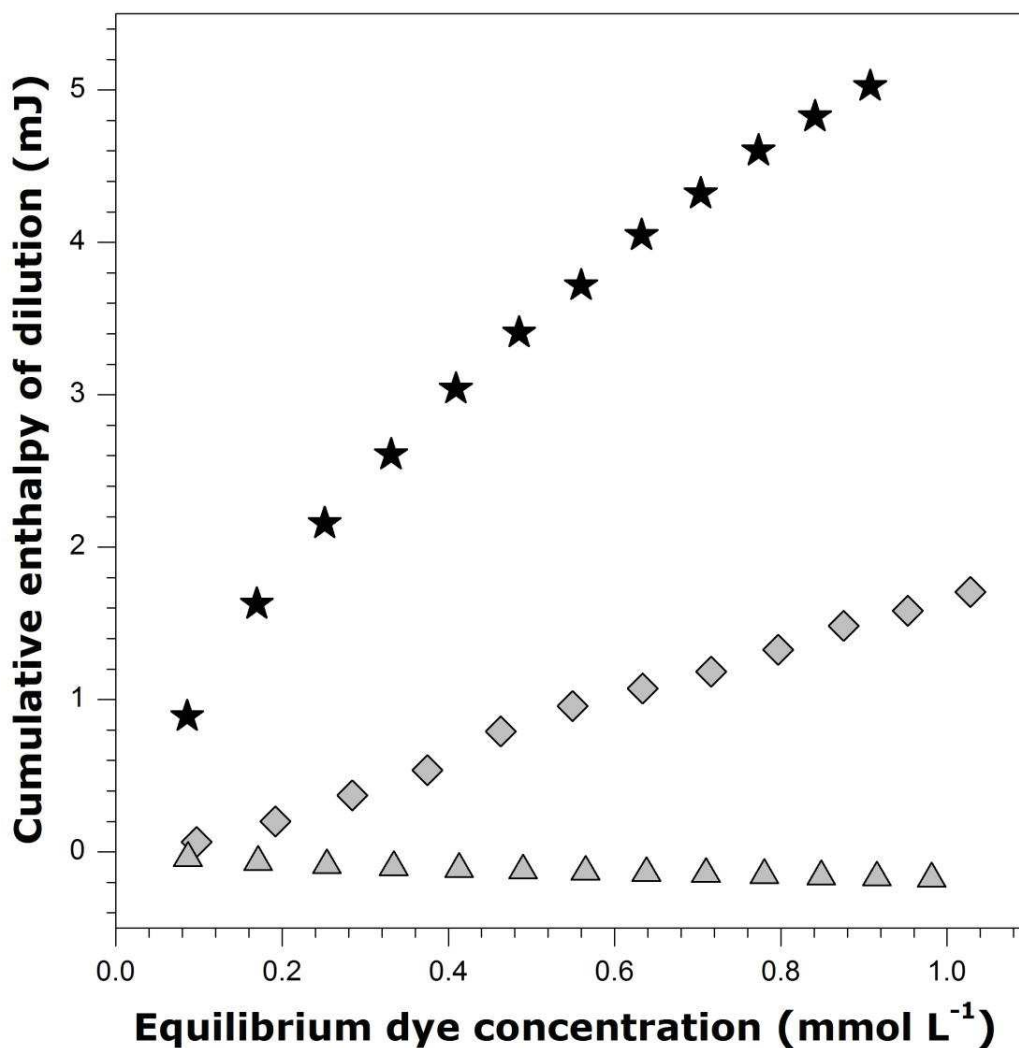


Figure S 6. Variations of the cumulative enthalpy of dilution at 298 K for two-solute equimolar solutions in ultrapure water containing: Methyl Orange + CrO<sub>4</sub><sup>2-</sup> (gray diamonds), Orange II + CrO<sub>4</sub><sup>2-</sup> (black stars), or Orange G + CrO<sub>4</sub><sup>2-</sup> (gray triangles), as a function of the equilibrium dye concentration (inside the calorimetric ampoule).

## **CONCLUSIONS**

In this chapter, we discussed the results obtained for the adsorption of Orange-type dyes and oxyanion Cr(VI) onto anion-exchange resin - Amberlite® IRN-78 from single-component as well as multi-component systems. This study has enabled not only the understanding but also has emphasized the importance of pH on the sorption processes. Adsorbed dyes can be easily deprotonated at higher pH with the formation of new species with higher charges.

Detail mechanisms of Methyl Orange, Orange II and Orange G removal on Amberlite® were discussed and we demonstrated that the <sup>13</sup>C CP/MAS NMR analysis has enabled the understanding of the nature of the charged species adsorbed in the resins matrix. The retention capacity of the resin towards various anionic solutes, decreased in the following order: CrO<sub>4</sub><sup>2-</sup> > OG > OII ≈ OM. Desorption studies using both 0.02 and 1M NaOH demonstrated the low desorption properties of these dyes from the solid.

The second study was based on the multi-component adsorption from bi-solute solutions of dye and inorganic competing species – chromates. It was quiet interesting to find out that the amount adsorbed of MO and OII is not influenced by the presence of chromate ions. However, the amount of OG adsorbed was decreased to some extent in presence of Cr(VI). Concerning the adsorption of the inorganic anion, its adsorption was negatively influenced by the presence of the dyes to a higher extent in presence of MO and OII and to a lower extent in presence of OG. The selectivity tests confirm the higher affinity of the organic dyes with the anion-exchange resins than those of inorganic ion. Therefore, the resin was firstly saturated with one of the adsorbing species and the later was put in contact with another competing specie. Hence, chromate ions were able to desorb from the resins by the presence of the dye. On the contrary, the dyes cannot be desorbed in the presence of chromate ions. These results confirm the higher affinity of the resins for the dyes and not for chromates.



# Conclusions and Perspectives



## ***CONCLUSIONS AND PERSPECTIVES***

The nature of the interactions between competing species within the bulk of the solution as well as at the solid-liquid interface during the adsorption process from the multi-component solutions are the two main factors governing the sorption selectivity of the sorbent material. The understanding of the nature of these interactions is primordial. Therefore, the aim of the present work was to investigate such interactions together with the sorption properties of various model materials. A few reference materials with good adsorption properties in regarding the removal of some selected pollutants were chosen for the study of the mechanism of sorption of organic dyes as well as the nature of interactions involved in the sorption process. Multi-component adsorption between organic and inorganic species onto the selected adsorbent was subsequently investigated in new of potential applications in the solid structure in the Environmental Remediation.

First year of this thesis was devoted to the work with the famous photocatalysis - titanium oxide nanoparticles. The aim was to approve the photocatalytic performance of this material towards degradation of organic dye Rhodamine 6G. The results of this dye adsorption from phosphates buffer solution showed that phosphates have the high affinity to  $\text{TiO}_2$  surface, therefore inhibit the dye adsorption. Even if we could not investigated more studies on this solid-reference, however, it shows the importance of adsorbent-adsorbate interactions imply during sorption process.

Second investigated model is the anionic clay also known as Layered Double Hydroxide (LDH) was chosen due to its interesting chemical and physical properties. The principal advantage of such type of material is that it can attract various negatively charged organic and inorganic contaminants, which makes it a perfect candidate for the study of the competitive adsorption. The first parts of the present study was made on an Mg-Al-LDH sample containing nitrate species as the pristine compensating anions (Chapters II-III). Nitrates ions as compensating anions were chosen due to its good exchange property. The X-ray diffraction technique was used to monitor the changes in the solid structure upon adsorption of pollutants shed more light on the mechanism of adsorption. Three Orange-type dyes, Methyl Orange, Orange II and Orange G, were chosen to

investigate the adsorption mechanism onto Mg-Al-LDH-NO<sub>3</sub>. For the three dyes, the kinetics of adsorption was fast, between 60 and 100 min, and the process followed a pseudo-second order model. It should be mentioned here that the three chosen dyes differ in terms of molecular sizes, electrical charges and hydrophobic/hydrophilic properties. Hence, it was interesting to observe the hydrophobicity of the molecules was the principal factor governing the dye adsorption onto LDH against electric charge of the anion. This conclusion was at variance with the importance of the charge effect in the adsorption of inorganic anions. Such a conclusion was drawn up from the comparison of the results obtained with Methyl Orange and Orange G. Here MO anions, being more hydrophobic, was adsorbed to a greater extent onto LDH. The adsorption mechanism for MO occurred via two processes, an anion exchange and an adsorption on the external surface of the LDH. Subsequently, MO adsorbed in quantities greater than the AEC of adsorbent. On the contrary, the less hydrophobic and bi-charged OG was adsorbed to a much lower extent onto the same adsorbent. In addition, the analysis of co-adsorption of Na<sup>+</sup> counter-ion showed that, in the region of small adsorption quantities OG used its two negative charges; in the range of higher adsorption values co-adsorption of sodium occurred in order to neutralize one of the negative charges bearing by dye anion. However, the third dye molecule (Orange II) had also its particularity in regard with the retention mechanism. Isothermal Titration Calorimetry was a very powerful tool in elucidating this complex mechanism and understanding the specific interactions between OII and Mg-Al-LDH, as well as the nature of the OII adsorption mechanism on this solid. It was found that OII was partially intercalated into the LDH interlayer space, followed by the complexation or aggregation of OII units by Mg and Al ions, present in the supernatant due to the partial dissolution of the LDH. In addition, X-ray diffraction patterns of the dye-loaded samples showed that co-adsorption of carbonates, provided from air, occurred simultaneously with the dye adsorption. In consequence, the complexity of adsorption mechanisms, which involved several species that could compete with one another for the active sites present in the LDH, was elucidated in Chapter II.

Chapter III reports the multi-component adsorption between the Orange-type dyes and some inorganic anions onto Mg-Al-LDH. The bi-solute component systems were investigated for the three dyes already mentioned earlier and various inorganic anions (sulfates, chromates, phosphates and carbonates) presented in different molar ratios. Moreover, the quantity of adsorption was calculated for the dyes and such inorganic ions as sulfates, chromates and phosphates. Therefore, it was possible to evaluate the influence of the presence of both competing

anions on each other. The variations of the total amount of adsorption were evaluated by the sum of the individual quantities of adsorption, thereby producing the so-called *composite isotherms*. This complex study allowed the classification systems studied with respect to the shape of their adsorption curves determined in the multi-component systems. Three main types were described. When the reduction in the adsorption extent concerned mainly only the one of solutes, Type 1 and Type 3 isotherms were obtained. When this reduction observed for the both solutes, a Type 2 isotherm was recorded. For inorganic anions, the order of decreasing effectiveness of the inorganic anion in reducing the retention capacity of Mg-Al-LDH-NO<sub>3</sub> towards a given dye, *on a per-equivalent basis*, was as follows: CO<sub>3</sub><sup>2-</sup> >> HPO<sub>4</sub><sup>2-</sup> > SO<sub>4</sub><sup>2-</sup> ≈ CrO<sub>4</sub><sup>2-</sup>, Methyl Orange; HPO<sub>4</sub><sup>2-</sup> ≈ CO<sub>3</sub><sup>2-</sup> > CrO<sub>4</sub><sup>2-</sup> > SO<sub>4</sub><sup>2-</sup>, Orange II; HPO<sub>4</sub><sup>2-</sup> ≈ SO<sub>4</sub><sup>2-</sup> > CO<sub>3</sub><sup>2-</sup> ≈ CrO<sub>4</sub><sup>2-</sup>, Orange G. The presence of phosphates and carbonates had a negative impact on the dye adsorption. These inorganic ions decreased the adsorption of MO and OII onto LDH. In the case of OG, only the presence of sulfates had also a negative impact. The presence of sulfates and chromates did not affected the MO adsorption. This could be assigned to the highly hydrophobic nature of the dye. Indeed, the latter was able to exceed the AEC value of LDH both in the single- and bi-solute systems. Concerning the two other dyes, i.e., OII and OG, it was surprising to learn that the phosphate ions had a more negative impact on the dye uptake against carbonates. The plausible explanation was that the effect was due to the change in pH and the charge of the competing inorganic species in the bulk solution.

Chapter IV was dedicated to the study of the single-solute and the multi-solute adsorption onto Mg-Al LDH containing chloride anions compensate for the positive interlayer charge. It was demonstrated that, for the three dyes studied, the mechanism of uptake was analogous to the Mg-Al-LDH-NO<sub>3</sub>. The same trend in dye adsorption was observed, concerning the quantity of adsorption decreasing in the order: MO > OII > OG. This was in good agreement with what has been observed in the literature concerning the affinity of the interlayer anion. It was found that the interlayer chloride anions were strongly bound to the layers, more than the nitrate anions were. Hence, the amounts of MO and OG were smaller than those obtained onto Mg-Al-LDH-NO<sub>3</sub>, at variance with the result obtained with OII, whose amount adsorbed had not changed. Moreover, the amount of OG adsorbed was too small. Thus was confirmed, by using HPLC and XRD techniques, that this dye was not capable for replacing the chloride anions within the LDH structure. Subsequently, this study allowed of decreasing a new order of adsorption capacity to be established as follows: MO > OII > Cl > OG > NO<sub>3</sub>.

The last Chapter V of the present manuscript was devoted to the single-component and the competitive adsorption of dyes and Cr(VI) anions onto last solid-reference used in this work, synthetic organic exchanger Amberlite® IRN-78. This adsorbent is interesting, because of the different factors: it is commercially available, often uses as synthetic organic model for anion exchange and because it can adsorb different organic and inorganic ions.

In this part, the importance of the pH of solid suspension was underlined, because of the strongly basic character of Amberlite® IRN-78. The pH was measured before the adsorption process and at equilibrium in order to obtain valuable information regarding the charge of the species adsorbing initially present in the solution at the solid-liquid interface as function of time. We demonstrated therein that the adsorption of dyes could depend on the nature of the adsorbent. Dye adsorption onto a strongly basic resin such as Amberlite® IRN-78 followed the pathway of an anion exchange between the pristine OH<sup>-</sup> ions and the oncoming anionic species. Consequently, the exchanged OH<sup>-</sup> ions increased the pH of the bulk solution and could therefore additionally deprotonate the dye species into anions with a higher valency. The retention capacity of the resin from the single-solute solution towards various anionic solutes, *on a per-mole basis*, decreased in the following order: CrO<sub>4</sub><sup>2-</sup> > OG > OII ≈ OM. The appropriate ITC experiments showed that the overall enthalpy effect of displacement was either exothermic (CrO<sub>4</sub><sup>2-</sup>, OG, OM) or endothermic (OII). The competition between dye and chromate anions from their equimolar bi-solute solutions mainly caused a marked decrease in the uptake of CrO<sub>4</sub><sup>2-</sup>, thereby pointing to the preferential dye retention by Amberlite® IRN-78. Moreover, higher affinity of the dye units towards the anion-exchange resin was confirmed by the reversibility and selectivity tests. The bi-solute MO + Cr(VI) and OII + Cr(VI) systems could be ascribed to the Type I isotherm, that containing OG + Cr(VI) to the Type II isotherm. According to the classification established and discussed previously in Chapter II.

Another intention of the present work was to propose the procedures for sorbent materials efficient in retaining pollutant compounds from the multi-component aqueous streams. Such studies will provide important information about the use of the selected sorbents in real wastewater systems. In this context, the following perspectives can be envisaged:

- It is necessary to determine the charge of the inorganic and even organic species inside the LDH interlayer. The combination of such techniques as IR, NMR, and Raman spectroscopy can potentially provide answers to the questions.

- There is a large variety of competing species in the wastewater system, which can compete with each another for the interlayer space and thus may be tested in regards with the competitive adsorption. These compounds include such toxic oxyanions as arsenate, vanadate, bromate, etc.
- The study of the co-adsorption of sodium accompanying MO and OG has opened a new perspective leading to establish the total balance of exchanging species other positively charges compounds uptake, e.g., heavy metals potentially presented in the mills.
- Some complementary information about the kinetics of adsorption for each of the competing species in the multi-component systems can be useful to explain the mechanism of competitive adsorption.
- The recently reported information about the temperature of wastewater streams coming from the textile industry (i.e., around 40° C) the necessity indicates the importance of carrying out the adsorption studies at different temperatures. The competitive adsorption of pollutants onto LDH may follow a somewhat different mechanism at higher temperature.
- Another important perspective will be to investigate new adsorbents, new dye-containing systems, other inorganic species, which will contribute to better understand the competitive interaction involved in interfacial phenomena.



# List of Figures and Tables



# LIST OF FIGURES

## Chapter I

Figure 1. Lennard - Jones type diagrams (non-activated adsorption): potential energy versus distance. _____	15
Figure 2. Model of double layer structure of the solid-liquid interface with examples of specific and non-specific ion adsorption [5], together with their hydration shell. _____	17
Figure 3. Schematic representation of $\text{Na}^+$ - $\text{Ca}^{2+}$ exchange [6]. _____	18
Figure 4. Classification of solution adsorption isotherms according to Giles et al. [12]. _____	21
Figure 5. Example of chromophores related with non-conjugated (left) and conjugated (right) systems [13]. _____	22
Figure 6. Examples of molecules that represent different chemical classes: anthraquinone (a), indigoid (b), phthalocyanine (c), xanthene (d) and nitroso (e) dyes. _____	24
Figure 7. Tautomeric forms of Orange II molecules depending from pH [19]. _____	26
Figure 8. Schematic representation of brucite layer (A) and that of LDHs (B) [26]. _____	27
Figure 9. Different kinds of anions, which could be intercalated in the LDHs. _____	28
Figure 10. Schema of the possible applications of LDHs [33]. _____	29
Figure 11. Cation (left) and anion (right) exchange resins, with schematic representation of negatively charged matrix and positively charged functional groups [44]. _____	31
Figure 12. Structure of the anionic resin, which contains styrene divinylbenzene copolymer matrix with trimethylammonium functional groups. _____	32
Figure 13. Schema of different competing species presented in solutes. _____	35

## Chapter II

Figure 1. Structural formulas of MO (a), OII (b), OG (c), and their 2D molecular sizes, as estimated with the aid of ChemDraw 3D 5.0 software package. _____	59
Figure 2. Pseudo-second order kinetics model of MO (a), OII (b) and OG (c) adsorption onto Mg-Al-LDH- $\text{NO}_3$ for different initial concentrations. _____	63

<i>Figure 3. Left panels: adsorption isotherms for MO (a), OII (b), and OG (c) anions and sodium cations from aqueous solutions onto Mg-Al-LDH-NO<sub>3</sub> at 25 °C; Right panels: variations of the cumulative enthalpy of displacement as a function of the amount of dye adsorbed.</i>	66
<i>Figure 4. X-ray diffraction patterns in the 2θ range from 2° to 30° for the intercalation of MO in the Mg-Al-LDH-NO<sub>3</sub> structure corresponding to 5 points in the MO adsorption isotherm (as marked by crosses in Figure 3).</i>	69
<i>Figure 5. X-ray diffraction patterns in the 2θ range from 2° to 30° for the intercalation of OII in the Mg-Al-LDH-NO<sub>3</sub> structure corresponding to 4 points in the OII adsorption isotherm (as marked by crosses in Figure 3).</i>	70
<i>Figure 6. X-ray diffraction patterns in the 2θ range from 2° to 30° for the intercalation of OG in the Mg-Al-LDH-NO<sub>3</sub> structure corresponding to 5 points in the OG adsorption isotherm (as marked by crosses in Figure 3).</i>	72
<i>Figure S7. SEM image (upper panel) and X-ray powder diffraction pattern (lower panel) of Mg-Al-LDH-NO<sub>3</sub></i>	78
<i>Figure 8. Sorption isotherm of OII on Mg-Al-LDH-NO<sub>3</sub> from aqueous solution (upper panel) and calculated cumulative enthalpies of displacement as a function of the OII amount adsorbed (lower panel).</i>	91
<i>Figure S 1. SEM image (upper panel) and X-ray powder diffraction pattern (lower panel) of Mg-Al-LDH-NO<sub>3</sub></i>	78
<i>Figure S 2. Amount of MO (a), OII (b) and OG (c) adsorbed onto Mg-Al-LDH-NO<sub>3</sub> as a function of the contact time for different initial concentrations.</i>	81
<i>Figure S 3. First order sorption kinetics of MO (a), OII (b) and OG (c) adsorption onto Mg-Al-NO<sub>3</sub> LDH for different initial concentrations.</i>	83
<i>Figure S 4. Intra-particle mass transfer diffusion model for MO (a), OII (b) and OG (c) adsorption onto Mg-Al-NO<sub>3</sub> LDH for different initial dye concentrations.</i>	84
<i>Figure 9. TEM images of fibers formed during adsorption onto LDHs (A, B) and by direct contact between OII Mg(NO<sub>3</sub>)<sub>2</sub> solution (C, D). In the presence of LDH (A, B), only a small part of the LDH solid particles was taken from in the base of the tube, with the aim to avoid too high number of particles and keep better image quality.</i>	92

Figure 10. Thermograms for OII adsorption onto Mg-Al-LDH-NO<sub>3</sub> (a), OII dilution in water (under the same conditions as for sorption onto Mg-Al-LDH-NO<sub>3</sub>) (b), OII interaction with Mg(NO<sub>3</sub>)<sub>2</sub> (c) and with Al(NO<sub>3</sub>)<sub>3</sub> (d) solutions. \_\_\_\_\_ 93

Figure 11. XRD patterns of Mg-Al-LDH-OII (1), fibers OII-LDH (2) and of fibers / particles formed during OII dilution in Mg(NO<sub>3</sub>)<sub>2</sub> (3). \_\_\_\_\_ 95

Figure S 5. The following tubes contain the solid particles removed from supernatant after sorption process for HPLC analysis. The tube (a) contains 0.35 mmol g<sup>-1</sup> released Mg and 2.78 mmol g<sup>-1</sup> adsorbed OII; (b) contains 0.36 mmol g<sup>-1</sup> of Mg and 2.38 mmol g<sup>-1</sup> OII. \_\_\_\_\_ 100

### Chapter III

Figure 1. Three different competition schemes exemplified by the individual adsorption isotherms for dye anions (big orange symbols) and inorganic anions (big violet symbols), as well as the composite adsorption isotherm (red stars) plotted as a function of the concentration of the dye component in the equilibrium bulk solution: (a) MO + SO<sub>4</sub><sup>2-</sup> system (Type I), (b) OG + CrO<sub>4</sub><sup>2-</sup> system (Type II), (c) OII + HPO<sub>4</sub><sup>2-</sup> system (Type III). The solid (with small orange symbols) and dashed lines (with small violet symbols) represent the adsorption isotherms of the dye and inorganic ion, respectively, as determined in the separate single-solute systems (as a function of the equilibrium concentration of the corresponding solute). The vertical dotted line is used to indicate the theoretical anion exchange capacity (AEC) of LDH. \_\_\_\_\_ 118

Figure 2. X-ray diffraction patterns in a 2θ range from 2° to 30° for Mg-Al-LDH-NO<sub>3</sub> loaded with various anionic species from single- and bi-solute equimolar solutions. For the three mixtures of MO and sulfate anions, the amounts adsorbed are as follows: (1) 0.65 meq g<sup>-1</sup>, MO; 1.29 meq g<sup>-1</sup>, SO<sub>4</sub><sup>2-</sup>; (2) 2.69 meq g<sup>-1</sup>, MO; 0.96 meq g<sup>-1</sup>, SO<sub>4</sub><sup>2-</sup>; (3) 3.93 meq g<sup>-1</sup>, MO; 0.68 meq g<sup>-1</sup>, SO<sub>4</sub><sup>2-</sup>. \_\_\_\_\_ 119

Figure 3. X-ray diffraction patterns in a 2θ range from 2° to 30° for Mg-Al-LDH-NO<sub>3</sub> loaded with various anionic species from single- and bi-solute equimolar solutions. For the two mixtures of OG and chromate anions, the amounts adsorbed are as follows: (1) 1.01 meq g<sup>-1</sup>, OG; 0.99 meq g<sup>-1</sup>, CrO<sub>4</sub><sup>2-</sup>; (2) 1.57 meq g<sup>-1</sup>, OG; 1.42 meq g<sup>-1</sup>, CrO<sub>4</sub><sup>2-</sup>. \_\_\_\_\_ 121

Figure 4. X-ray diffraction patterns in a 2θ range from 2° to 30° for Mg-Al-LDH-NO<sub>3</sub> loaded with various anionic species from single- and bi-solute equimolar solutions. For the two

<i>mixtures of OII and hydrogen phosphate anions, the amounts adsorbed are as follows: (1) 0.27 meq g<sup>-1</sup>, OII; 0.83 meq g<sup>-1</sup>, HPO<sub>4</sub><sup>2-</sup>; (2) 0.20 meq g<sup>-1</sup>, OII; 2.56 meq g<sup>-1</sup>, HPO<sub>4</sub><sup>2-</sup>.</i>	122
<i>Figure 5. Effect of the addition of inorganic anions on the retention capacity of Mg-Al-LDH-NO<sub>3</sub> towards Methyl Orange (panel a), Orange II (panel b), and Orange G (panel c) from bi-solute solutions at different molar ratios between dye and inorganic anion.</i>	125
<i>Figure 6. Effect of the addition of dye anions on the retention capacity of Mg-Al-LDH-NO<sub>3</sub> towards divalent hydrogen phosphate (panel a), sulfate (panel b), and chromate (panel c) anions from bi-solute solutions at different molar ratios between inorganic anion and dye.</i>	126
<i>Figure 7. X-ray diffraction patterns in a 2θ range from 2° to 30° for Mg-Al-LDH-NO<sub>3</sub> loaded with various anionic species from single- and bi-solute equimolar solutions. For the three mixtures of MO and carbonate anions, the amounts of dye adsorbed are as follows: (1) 0.48 meq g<sup>-1</sup>, (2) 0.97 meq g<sup>-1</sup>, (3) 1.2 meq g<sup>-1</sup>.</i>	128
<i>Figure 8. X-ray diffraction patterns in a 2θ range from 2° to 30° for Mg-Al-LDH-NO<sub>3</sub> loaded with various anionic species from single- and bi-solute equimolar solutions. For the two mixtures of OG and carbonate anions, the amounts of dye adsorbed are as follows: (1) 1.12 meq g<sup>-1</sup>, (2) 1.17 meq g<sup>-1</sup>.</i>	129
<i>Figure 9. Effect of the addition of carbonate anions to the aqueous phase on the retention capacity of Mg-Al-LDH-NO<sub>3</sub> towards Methyl Orange (MO), Orange II (OII), and Orange G (OG) from bi-solute solutions at different molar ratios between dye and carbonate species. AEC refers to the anion exchange capacity of the LDH sample.</i>	130
<i>Figure S 1. Isotherms of dye adsorption from single-solute solutions onto Mg-Al-LDH-NO<sub>3</sub> at 298 K. The solid lines represent the smoothed isotherms constructed on the basis of the results of repeated adsorption experiments. The vertical dotted line is used to indicate the theoretical anion exchange capacity (AEC) of LDH. Adapted from G. Darmograi et al., Study of Adsorption and Intercalation of Orange-Type Dyes into Mg-Al Layered Double Hydroxide, Journal of Physical Chemistry, DOI: 10.1021/acs.jpcc.5b05510</i>	136
<i>Figure S 2. Adsorption isotherms for inorganic anions from single-solute solutions onto Mg-Al-LDH-NO<sub>3</sub> at 298 K. The solid lines represent the smoothed isotherms constructed on the basis of the results of repeated adsorption experiments. The vertical dotted line is used to indicate the theoretical anion exchange capacity (AEC) of LDH.</i>	137

Figure S 3. Variations of the cumulative enthalpy of displacement accompanying adsorption of dye and inorganic anions from single-solute solutions onto Mg-Al-LDH-NO<sub>3</sub> at 298 K as a function of the amount of a given species retained by the solid sample, as plotted in an adsorption range corresponding to the initial quasi-vertical portion on the adsorption isotherm, i.e., up to  $\Delta n^*$ ;  $\Delta dplHcum^*$  represents the enthalpy value at the end of this interval: (a) Methyl Orange, (b) SO<sub>4</sub><sup>2-</sup>, (c) Orange II, (d) CrO<sub>4</sub><sup>2-</sup>, (e) Orange G, (f) HPO<sub>4</sub><sup>2-</sup>. \_\_\_\_\_ 138

Figure S 4. Individual (panels a and b) and composite (panel c) adsorption isotherms for Methyl Orange and hydrogen phosphate anions adsorbed at 298 K onto Mg-Al-LDH-NO<sub>3</sub> from bi-solute solutions at different molar ratios between dye and inorganic anion under conditions of exposure to the ambient atmosphere employed in the present study. The dotted lines are used to indicate the anion exchange capacity (AEC) of the LDH sample. \_\_\_\_\_ 139

Figure S 5. Individual (panels a and b) and composite (panel c) adsorption isotherms for Methyl Orange and sulfate anions adsorbed at 298 K onto Mg-Al-LDH-NO<sub>3</sub> from bi-solute solutions at different molar ratios between dye and inorganic anion under conditions of exposure to the ambient atmosphere employed in the present study. The dotted lines are used to indicate the anion exchange capacity (AEC) of the LDH sample. \_\_\_\_\_ 140

Figure S 6. Individual (panels a and b) and composite (panel c) adsorption isotherms for Methyl Orange and chromate anions adsorbed at 298 K onto Mg-Al-LDH-NO<sub>3</sub> from bi-solute solutions at different molar ratios between dye and inorganic anion under conditions of exposure to the ambient atmosphere employed in the present study. The dotted lines are used to indicate the anion exchange capacity (AEC) of the LDH sample. \_\_\_\_\_ 141

Figure S 7. Individual (panels a and b) and composite (panel c) adsorption isotherms for Orange II and hydrogen phosphate anions adsorbed at 298 K onto Mg-Al-LDH-NO<sub>3</sub> from bi-solute solutions at different molar ratios between dye and inorganic anion under conditions of exposure to the ambient atmosphere employed in the present study. The dotted lines are used to indicate the anion exchange capacity (AEC) of the LDH sample. \_\_\_\_\_ 142

Figure S 8. Individual (panels a and b) and composite (panel c) adsorption isotherms for Orange II and sulfate anions adsorbed at 298 K onto Mg-Al-LDH-NO<sub>3</sub> from bi-solute solutions at different molar ratios between dye and inorganic anion under conditions of exposure to the

*ambient atmosphere employed in the present study. The dotted lines are used to indicate the anion exchange capacity (AEC) of the LDH sample.* \_\_\_\_\_ 143

*Figure S 9. Individual (panels a and b) and composite (panel c) adsorption isotherms for Orange II and chromate anions adsorbed at 298 K onto Mg-Al-LDH-NO<sub>3</sub> from bi-solute solutions at different molar ratios between dye and inorganic anion under conditions of exposure to the ambient atmosphere employed in the present study. The dotted lines are used to indicate the anion exchange capacity (AEC) of the LDH sample.* \_\_\_\_\_ 144

*Figure S 10. Individual (panels a and b) and composite (panel c) adsorption isotherms for Orange G and hydrogen phosphate anions adsorbed at 298 K onto Mg-Al-LDH-NO<sub>3</sub> from bi-solute solutions at different molar ratios between dye and inorganic anion under conditions of exposure to the ambient atmosphere employed in the present study. The dotted lines are used to indicate the anion exchange capacity (AEC) of the LDH sample.* \_\_\_\_\_ 145

*Figure S 11. Individual (panels a and b) and composite (panel c) adsorption isotherms for Orange G and sulfate anions adsorbed at 298 K onto Mg-Al-LDH-NO<sub>3</sub> from bi-solute solutions at different molar ratios between dye and inorganic anion under conditions of exposure to the ambient atmosphere employed in the present study. The dotted lines are used to indicate the anion exchange capacity (AEC) of the LDH sample.* \_\_\_\_\_ 146

*Figure S 12. Individual (panels a and b) and composite (panel c) adsorption isotherms for Orange G and chromate anions adsorbed at 298 K onto Mg-Al-LDH-NO<sub>3</sub> from bi-solute solutions at different molar ratios between dye and inorganic anion under conditions of exposure to the ambient atmosphere employed in the present study. The dotted lines are used to indicate the anion exchange capacity (AEC) of the LDH sample.* \_\_\_\_\_ 147

*Figure S 13. X-ray diffraction patterns in a  $2\theta$  range from  $2^\circ$  to  $18^\circ$  for Mg-Al-LDH-NO<sub>3</sub> loaded with various anionic species from single- and bi-solute equimolar solutions. For the three mixtures of MO and chromate anions, the amounts adsorbed are as follows: (1) 0.99 meq g<sup>-1</sup>, MO; 1.86 meq g<sup>-1</sup>, CrO<sub>4</sub><sup>2-</sup>; (2) 2.95 meq g<sup>-1</sup>, MO; 1.53 meq g<sup>-1</sup>, CrO<sub>4</sub><sup>2-</sup>; (3) 5.72 meq g<sup>-1</sup>, MO; 0 meq g<sup>-1</sup>, CrO<sub>4</sub><sup>2-</sup>.* \_\_\_\_\_ 148

*Figure S 14. X-ray diffraction patterns in a  $2\theta$  range from  $2^\circ$  to  $18^\circ$  for Mg-Al-LDH-NO<sub>3</sub> loaded with various anionic species from single- and bi-solute equimolar solutions. For the three mixtures of OII and sulfate anions, the amounts adsorbed are as follows: (1) 0.25 meq g<sup>-1</sup>, OII;*

0.52 meq g<sup>-1</sup>, SO<sub>4</sub><sup>2-</sup>; (2) 0.70 meq g<sup>-1</sup>, OII; 1.41 meq g<sup>-1</sup>, SO<sub>4</sub><sup>2-</sup>; (3) 0.94 meq g<sup>-1</sup>, OII; 1.61 meq g<sup>-1</sup>, SO<sub>4</sub><sup>2-</sup>. \_\_\_\_\_ 149

Figure S 15. X-ray diffraction patterns in a 2θ range from 2° to 30° for Mg-Al-LDH-NO<sub>3</sub> loaded with various anionic species from single- and bi-solute equimolar solutions. For the two mixtures of OII and chromate anions, the amounts adsorbed are as follows: (1) 0.58 meq g<sup>-1</sup>, OII; 1.14 meq g<sup>-1</sup>, CrO<sub>4</sub><sup>2-</sup>; (2) 1.15 meq g<sup>-1</sup>, OII; 1.34 meq g<sup>-1</sup>, CrO<sub>4</sub><sup>2-</sup>. \_\_\_\_\_ 150

Figure S 16. X-ray diffraction patterns in a 2θ range from 2° to 30° for Mg-Al-LDH-NO<sub>3</sub> loaded with various anionic species from single- and bi-solute equimolar solutions. For the three mixtures of OG and sulfate anions, the amounts adsorbed are as follows: (1) 0.93 meq g<sup>-1</sup>, OG; 0.95 meq g<sup>-1</sup>, SO<sub>4</sub><sup>2-</sup>; (2) 1.05 meq g<sup>-1</sup>, OG; 1.18 meq g<sup>-1</sup>, SO<sub>4</sub><sup>2-</sup>; (3) 0.92 meq g<sup>-1</sup>, OG; 1.46 meq g<sup>-1</sup>, SO<sub>4</sub><sup>2-</sup>. \_\_\_\_\_ 151

Figure S 17. X-ray diffraction patterns in a 2θ range from 2° to 30° for Mg-Al-LDH-NO<sub>3</sub> loaded with various anionic species from single- and bi-solute equimolar solutions. For the three mixtures of MO and hydrogen phosphate anions, the amounts adsorbed are as follows: (1) 0.40 meq g<sup>-1</sup>, MO; 0.81 meq g<sup>-1</sup>, HPO<sub>4</sub><sup>2-</sup>; (2) 1.33 meq g<sup>-1</sup>, MO; 2.54 meq g<sup>-1</sup>, HPO<sub>4</sub><sup>2-</sup>; (3) 2.6 meq g<sup>-1</sup>, MO; 2.11 meq g<sup>-1</sup>, HPO<sub>4</sub><sup>2-</sup>. \_\_\_\_\_ 152

Figure S 18. X-ray diffraction patterns in a 2θ range from 2° to 30° for Mg-Al-LDH-NO<sub>3</sub> loaded with various anionic species from single- and bi-solute equimolar solutions. For the two mixtures of OG and hydrogen phosphate anions, the amounts adsorbed are as follows: (1) 0.70 meq g<sup>-1</sup>, OG; 2.01 meq g<sup>-1</sup>, HPO<sub>4</sub><sup>2-</sup>; (2) 0.28 meq g<sup>-1</sup>, OG; 2.95 meq g<sup>-1</sup>, HPO<sub>4</sub><sup>2-</sup>. \_\_\_\_\_ 153

Figure S 19. Effect of the addition of carbonate anions to the aqueous phase on the adsorption of Methyl Orange (panel a), Orange II (panel b), and Orange G (panel c) at 298 K onto Mg-Al-LDH-NO<sub>3</sub> from bi-solute solutions at different molar ratios between dye and carbonate species. The dotted lines are used to indicate the anion exchange capacity (AEC) of the LDH sample. 154

Figure S 20. X-ray diffraction patterns in a 2θ range from 2° to 18° for Mg-Al-LDH-NO<sub>3</sub> loaded with various anionic species from single- and bi-solute equimolar solutions. For the two mixtures of OII and carbonate anions, the amounts of dye adsorbed are as follows: (1) 0.23 meq g<sup>-1</sup>, (2) 0.49 meq g<sup>-1</sup>. \_\_\_\_\_ 155

## Chapter IV

Figure 1. TG - DTA plots of uncalcined Mg-Al-LDH-Cl	161
Figure 2. XRD pattern of Mg-Al-LDH-Cl adsorbent.	161
Figure 3. Isotherms of dye adsorption from single-component solutions onto Mg-Al-LDH-Cl at 298 K. The solid lines represent the smoothed isotherms constructed on the basis of the results of repeated adsorption experiments. Red points represent the dye loaded LDH samples taken for XRD.	162
Figure 4. Dye adsorbed onto LDH as a function of chloride leached during exchange. Straight lines represent an expected equivalent exchange.	164
Figure 5. X-ray diffraction patterns in the $2\theta$ range from $2^\circ$ to $30^\circ$ for the intercalation of MO in the Mg-Al-LDH-Cl structure corresponding to 2 selected points at $Q_{ads} = 1.9$ and $4.0 \text{ mmol g}^{-1}$ on the MO adsorption isotherm (as marked by crosses in Figure 3).	165
Figure 6. X-ray diffraction patterns in the $2\theta$ range from $2^\circ$ to $30^\circ$ for the intercalation of OII in the Mg-Al-LDH-Cl structure corresponding to the selected point on the OII adsorption isotherm (as marked by crosses in Figure 3).	167
Figure 7. X-ray diffraction patterns in the $2\theta$ range from $2^\circ$ to $30^\circ$ for the intercalation of OG in the Mg-Al-LDH-Cl structure corresponding to the selected point on the OG adsorption isotherm (as marked by crosses in Figure 3).	168
Figure 8. Variations of the cumulative enthalpy of displacement as a function of the amount of dye adsorbed.	169
Figure 9. Isotherm of competitive adsorption between Methyl Orange (MO) and carbonate and hydrogen phosphate onto Mg-Al-LDH-Cl from equimolar bi-solute and tri-solute solutions, containing MO, hydrogen phosphates (P) or carbonates (C) anions.	171
Figure 10. Isotherm of competitive adsorption between Orange II (OII) and carbonate and hydrogen phosphate onto Mg-Al-LDH-Cl from equimolar bi-solute and tri-solute solutions, containing OII, hydrogen phosphates (P) or carbonates (C) anions.	172
Figure 11. Isotherm of competitive adsorption between Orange G (OG) and carbonate and hydrogen phosphate onto Mg-Al-LDH-Cl from equimolar bi-solute and tri-solute solutions, containing OG, hydrogen phosphates (P) or carbonates (C) anions.	173

## Chapter V

Figure 1. Single-component adsorption isotherms for Methyl Orange (orange diamonds), Orange II (blue squares), Orange G (green circles), and chromate anions (yellow triangles) retained on Amberlite® IRN-78 from single-solute aqueous solutions at 298 K. \_\_\_\_\_ 189

Figure 2. <sup>13</sup>C CP/MAS NMR spectra for washed and dried Amberlite® IRN-78 previously saturated with Methyl Orange (a), Orange II (b), or Orange G (c) from concentrated single-solute aqueous solutions at 298 K. The NMR spectra recorded on pure Amberlite® IRN-78 degassed overnight at 303 K and those obtained from untreated powdered dye samples are reported for comparison purposes. In the case of OII and OG, a horizontal arrow has been added to emphasize a partial transformation of the R-N-NH-R group into a negatively charged center upon adsorption (the asterisks refer to the red and green marks in Fig. S1). \_\_\_\_\_ 193

Figure 3. Cumulative enthalpy of displacement accompanying the adsorption of Methyl Orange (orange diamonds), Orange II (blue squares), Orange G (green circles), and chromate anions (yellow triangles) onto Amberlite® IRN-78 from single-solute aqueous solutions at 298 K. \_\_\_\_ 194

Figure 4. Room temperature UV-Vis absorption spectra of MO(a), OII (b), and OG (c) in various aqueous solutions: single-solute solution in ultrapure water (dotted blue lines), NaOH alkaline solution (dashed rose lines), supernatant solution collected after desorption study of Amberlite® IRN-78 previously saturated with dye species and put into contact with a 0.02 mol L<sup>-1</sup> NaOH solution during 2h (solid green lines). \_\_\_\_\_ 198

Figure 5. Results of equilibrium adsorption measurements of the competitive adsorption between MO (a), OII (b), or OG (c) and CrO<sub>4</sub><sup>2-</sup> onto Amberlite® IRN-78 from bi-solute equimolar solutions at 298 K. The individual adsorption isotherms of the dye (orange (MO); blue (OII); green (OG) symbols) and chromate (yellow triangles), as well as the composite adsorption isotherms (crosses), are plotted against the equilibrium concentration of dye component. The dashed and solid lines represent the adsorption isotherms of the dye and inorganic ion, respectively, as determined in the separate single-solute systems (as a function of the equilibrium concentration of the corresponding solute). \_\_\_\_\_ 200

Figure 6. Cumulative enthalpy of displacement accompanying the competitive adsorption of MO (orange diamonds), OII (blue squares), OG (green circles) and, CrO<sub>4</sub><sup>2-</sup> anions, onto Amberlite® IRN-78 from equimolar bi-solute aqueous solutions at 298 K. \_\_\_\_\_ 202

Figure S1. Orange-type dyestuff structures studied in the present work, represented in partially dehydrated (sulfonic group) hydrazone form: (a) Methyl Orange, (b) Orange II, (c) Orange G. The deprotonation pathway for R-N-NH-R group in the hydrazone structures of Orange II and Orange G leading to an additional negatively charged center in alkaline solutions is also shown schematically. The carbon atom within the 2-oxonaphthalene moiety bonded with oxygen has been labelled with red (in the protonated forms) or green (in the deprotonated forms) asterisks to further assist the analysis of  $^{13}\text{C}$  CP/MAS NMR spectra in Fig. 2. \_\_\_\_\_ 210

Figure S 2. Images of Amberlite<sup>®</sup> IRN-78 beads saturated with Methyl Orange, Orange II, and Orange G dyes from concentrated single-solute solutions. The resin beads have collected after wash at the bottom of Nalgene<sup>®</sup> tubes. \_\_\_\_\_ 210

Figure S 3. Variations of the cumulative enthalpy of dilution at 298 K for single-solute solutions in ultrapure water containing: Methyl Orange (gray diamonds), Orange II (black stars), Orange G (gray triangles), or chromate anions (black circles) as a function of the equilibrium solute concentration (inside the calorimetric ampoule). The dilution experiments were carried out under the same experimental conditions as those employed in the adsorption runs but without putting a resin sample into the measuring ampoule. The scale of the vertical (enthalpy) axis is different in the upper and lower panel. \_\_\_\_\_ 211

Figure S 4. Effect of pH on the cumulative enthalpy of dilution (upper panel) and cumulative enthalpy of displacement (lower panel) for Orange II dissolved in ultrapure water (solid stars) and an aqueous NaOH solution (pH 12) at 298 K. The dilution experiments were carried out under the same experimental conditions as those employed in the adsorption runs but without putting a resin sample into the measuring ampoule (injection volume: 10  $\mu\text{L}$ , injection speed: 10 s, agitation speed: 90 rpm, equilibration time between two successive injections: 30 min). In all cases, the dye concentration was 8 mmol  $\text{L}^{-1}$ . \_\_\_\_\_ 212

Figure S 5. Room temperature UV-Vis absorption spectra recorded in supernatant solutions collected after desorption study of Amberlite<sup>®</sup> IRN-78 previously saturated with  $\text{CrO}_4^{2-}$  (a), Methyl Orange (b), Orange II (c), or Orange G (d) and put into contact with a 0.02 mol  $\text{L}^{-1}$  NaOH solution at different time intervals (2, 3, 4, and 20 h). \_\_\_\_\_ 213

Figure S 6. Variations of the cumulative enthalpy of dilution at 298 K for two-solute equimolar solutions in ultrapure water containing: Methyl Orange +  $\text{CrO}_4^{2-}$  (gray diamonds), Orange II +

$\text{CrO}_4^{2-}$  (black stars), or Orange G +  $\text{CrO}_4^{2-}$  (gray triangles), as a function of the equilibrium dye concentration (inside the calorimetric ampoule). \_\_\_\_\_ 214

# LIST OF TABLES

## Introduction

<i>Table 1. Classification of pollutants in textile effluents [2]</i>	4
---	---

## Chapter I

<i>Table 1. Examples of chromophoric groups presented in organic dyes.</i>	22
<i>Table 2. Physico-chemical characterization and heavy metals concentrations in textile mills effluents [57].</i>	34

## Chapter II

<i>Table 1. Chemical composition and proposed formula of Mg-Al-LDH-NO<sub>3</sub> as inferred from the elemental analysis (the element contents are given in wt %).</i>	58
<i>Table S 1. Kinetic parameters of Orange dyes adsorption onto Mg-Al LDHs for different initial dye concentrations.</i>	82

## Chapter III

<i>Table 1. Maximum retention capacity, <math>\Delta n_{max}</math>, and average affinity, <math>\Delta d_{plHcum}</math>, of Mg-Al-LDH-NO<sub>3</sub> toward various dye and inorganic anions when adsorbed from single-solute solutions under conditions of exposure to the ambient atmosphere employed in the present study; the <math>\Delta d_{plHcum}^*</math> represents the value of the cumulative enthalpy of displacement at the end of the initial vertical portion on the adsorption isotherm (i.e., at <math>Q_{ads}^*</math>)</i>	115
<i>Table 2. Affiliation of the bi-solute systems studied in the present work to one of the four types of the competition scheme, as defined in Fig. 2 (the molar ratio of dye to inorganic anion is specified in the brackets)</i>	124
<i>Table S 1. Operating parameters used in the adsorption experiments carried out with the aid of isothermal titration calorimeter TAM III</i>	137

## Chapter V

<i>Table 1. Results of desorption tests carried out with Amberlite® IRN-78 previously saturated with Orange-type dye or chromate anions from single-solute solutions at 298 K and put into</i>	
--	--

*contact with a 0.02 mol L<sup>-1</sup> or 1 mol L<sup>-1</sup> NaOH solution at different time intervals. The extent of desorption is presented as a percentage of the total amount adsorbed in the first adsorption cycle.* \_\_\_\_\_ 196

*Table 2. Results of selectivity tests of solute retention by Amberlite® IRN-78: (A) the resin sample pre-saturated with a dye and subsequently equilibrated with a concentrated CrO<sub>4</sub><sup>2-</sup> solution, (B) the resin sample pre-saturated with CrO<sub>4</sub><sup>2-</sup> and subsequently equilibrated with a concentrated dye solution.* \_\_\_\_\_ 203



# Appendices

# APPENDIX I

This Appendix presents the work investigated onto TiO<sub>2</sub> nanoparticles, which was chosen as potential adsorbent for the study of the simple as well as the multi-component adsorption in the beginning of this thesis. Titanium oxide is a material of paramount technological importance that have shown great potential as ideal and powerful photocatalysts for water decontamination. In numerous studies of photocatalytic degradation of organic pollutants, the main emphasis is usually placed on the modification and fine-tuning of the catalyst surface properties to improve their photocatalytic efficiency under UV or Visible radiation. Much less attention is paid to the pollutant adsorption stage, which is a pre-requisite for the ultimate photocatalytic reactions. Such characteristics of the adsorbed pollutant species as the strength and reversibility of their adsorption on the catalyst surface or their orientation and concentration within the interfacial region may certainly affect the performance of the photocatalytic process. Moreover, the use of this photocatalysis in the polluted water streams implies the knowledge of an adsorbent's behaviour in the real wastewaters conditions. There is thus an urgent need for systematic studies of the underlying adsorption mechanisms and the test of this material for performance in the multi-component solutions.

Adsorption of dye reference – Rhodamine 6G was investigated onto different nanomorphologies: nanotubes, nanofibers and nanopowders of TiO<sub>2</sub> with aim to study the influence of structure on the adsorbing properties. Even if this adsorbent could not be used for the investigation of the multi-component adsorption (Rhodamine 6G dye adsorbs to a very small extent) however it was possible to evidence a competition between the organic dyes and inorganic ions (phosphate buffer, added for pH stabilization). Hence, phosphate buffer was considered as important competing species, because of their good affinity onto TiO<sub>2</sub>. This study demonstrate the importance of the competitive adsorption study with aim to better understand adsorbing properties of used adsorbent especially in the real wastewater systems.

## **Adsorption process of Rhodamine 6G on TiO<sub>2</sub> particles and the influence of competitive species from buffer solutions**

Ganna DARMOGRAI<sup>1</sup>, Monika KUS<sup>2</sup>, Vera MEYNEN<sup>2</sup>, Sara CAVALIERE<sup>1</sup>, Gaëlle MARTIN-GASSIN<sup>1</sup>, Jerzy ZAJAC<sup>1</sup>, Benedicte PRELOT\*<sup>1</sup>

<sup>1</sup>Institut Charles Gerhardt, UMR-5253 CNRS-UM-ENSCM, C.C. 1502,

Place Eugène Bataillon, F-34095 Montpellier cedex 5, FRANCE

Phone: +33 4 67 14 33 05; E-mail : benedicte.prelot@um2.fr

<sup>2</sup>Laboratory of Adsorption and Catalysis, Department of Chemistry, University of Antwerpen, Campus Drie Eiken, Universiteitsplein 1, B-2610 Wilrijk, BELGIUM

Keywords: titanium oxides, titanate, Rhodamine 6G, adsorption, competition, phosphate buffer.

### ABSTRACT:

Because of their numerous applications, mainly in the field of photocatalysis, the surface behaviour of titanium dioxides is an important issue to be addressed in order to better understand the mechanisms and optimize their performance in specific applications. Various materials were chosen from commercial suppliers, or synthesized specially for this study, to obtain series of solids with various properties (structure, texture, morphology, surface reactivity...): nanopowder P25 Degussa and commercial anatase; nanofibers, synthesized by using electrospinning technique; trititanate nanotubes and mixed-phase anatase/trititanate, which were prepared using a hydrothermal approach. The adsorption of Rhodamine 6G onto these materials was studied from aqueous solution in different conditions, at natural pH and from phosphate buffer 0.1M at two different pHs: 6 and 8. The adsorption capacities were obviously dependent of the type of particles and the nature and pH of the solutions. In all conditions, the anatase and the ES nanofibers had the lowest and the highest adsorption capacity respectively. In phosphate buffers at pH 8, the

adsorption capacity was higher than at pH 6, due to the negative surface charge. This influence was rather small in the case of anatase, which exhibits huge phosphate adsorption. This demonstrates the competition between anionic species, and its consequence on the affinity for Rhodamine 6G in the presence of phosphates. At pH6 in water and in phosphate buffer, the adsorption capacity was also reduced, due to a combined effect of surface charge increase, in addition with the adsorption of competing ions.

### ***INTRODUCTION***

In recent years, titanium dioxide has attracted much attention for the treatment of dye-containing wastewater. Because of their powerful oxidation strength, high chemical and photostability in water, nontoxicity, low cost, and insolubility in water under most environmental conditions, they have shown great potential as ideal and powerful photocatalysts [1, 2]. The optimization of catalysts performance is based on the understanding of the main driving forces and mechanisms for their oxidative removal [3], and especially the selectivity of adsorbent that can be affected by many factors such as properties of the reactant (size, polarity, structure, etc.), surface charging, solvent, surface atomic structure. Numerous studies have been carried out to better explain TiO<sub>2</sub> surface chemistry and especially at the solid-liquid interface [4]. Because most organic pollutants have weak adsorption on the TiO<sub>2</sub> particles, surface treatment or textural modification could enhance the adsorption capacity and potentially their photocatalytic properties when they are used in degradation process [5-8]. In various shapes/morphologies, such as nanoparticles, tubes, wires, fibres etc..., nanomaterials show a better performance in environmental remediation than other conventional techniques because of their high surface-to-volume ratio [9] especially when using innovative synthesis for original one-dimensional (1D) electrospun nanostructured materials [10, 11] or tubes such as titanate nanotubes [12].

The best approach to express adsorption performance of materials does not reach a consensus, since for some photocatalytic studies, the sorption properties can be expressed %, mol/g, and then correlated with particle size [13] or directly to specific surface area [5]. It is obvious that accurate information are obtained when working in mol m<sup>-2</sup>, and taking into account the detailed analysis of the isotherm, its shape, including the idea of considering the possible

## Appendices

---

multilayer adsorption or the strength of the adsorption [14]. In addition, the morphology and the crystallinity of particles play crucial roles on surface reactivity. Indeed, various acidic character and location of polar sites on the TiO<sub>2</sub> surface [15] or differences in proton affinity distributions (PADs) and the strength (pK position) of various local domains of proton adsorption [16] have been observed on anatase with various shapes and exposed surfaces. The complexity of the liquid-solid interface implies to consider more variables in comparison to the gas-solid system, with parameters such as the surface site, preparation procedures, and concentration of the particles, the pH of the solution and its effect on the surface structure, the concentration of the reactants, ... [1]. These include also the control of the surface charge by adjusting the pH, anchoring specific molecules to the surface for the selective adsorption of reactants [6, 17] and even some times the idea of the competitive solute solvent adsorption [18].

Competitive adsorption onto TiO<sub>2</sub> surfaces is studied in different manners. Yang and Davis [19] reported Cu(II) and EDTA adsorption from single and bi-component systems onto P25 TiO<sub>2</sub> sample. They have shown that the behaviour in single component system was strongly modified when ionic and cationic species were mixed, with the occurrence of ligand bridged ternary complexes. In the case of glutamate and lysine molecules in the presence of Ca<sup>2+</sup>, Lee et al. [20] have evidenced cooperative, or competitive, effects, depending on the modification of surface charge after adsorption of Ca<sup>2+</sup>, inducing attraction or repulsion of the organic species to be the adsorbed. Weng et al [21] have shown that in the presence of humic (HA) or fulvic (FA) acids together with phosphate, the sorption on goethite FeOOH exhibits much stronger competition effects of FA in comparison with HA, in relation with the difference in the spatial distribution more or less close to the oxide surface. In some cases, when the sorption is performed in buffers [22], the sorption of humic acids (HA) in phosphate buffer may be reduced, not only due to the effect of pH or ionic strength, but phosphate might compete with HA on the surface of adsorbent, or may interact with the HA in the solution and affecting HA adsorption.

To evidence the influence of competitive effect in particular in presence of phosphate, adsorption of Rhodamine 6G, a cationic orange-fluorescent dye often used in degradation tests was extensively studied in different conditions (in water or in buffer, at various pHs), in order to establish the influence of physicochemical conditions. Different types of Titanium based nanomaterials, nanopowder (P25, Anatase Commercial), nanofibres and nanotubes in two forms calcined and not calcined, denoted TNT-C and TNT-NC, respectively, were chosen as adsorbent

for the organic dye Rhodamine 6G. Nanotubes and nanofibers samples were prepared using a hydrothermal chemical route and electrospinning method, respectively. As reference, commercial P25 and Anatase commercial Nanopowder were used. In the end, the sorption properties were correlated with the competitive character of the mechanism on the surface active sites.

## 1. EXPERIMENTAL SECTION

### 1.1 Materials and syntheses of adsorbents / photocatalysts

The dye Rhodamine 6G was purchased from E. Merck India. The formula is shown on the Figure 1 and was labelled Rh6G. Commercial TiO<sub>2</sub> nanopowder P25 was obtained from Degussa AG and Titanium (IV) oxide, Anatase from Aldrich. They were used as received. The phosphate buffers and all solutions of Rh6G were prepared in ultrapure water (resistivity of 18.2 MΩ) produced by using an Elga LabWater Model PL 5241 system. Nanofibers and nanotubes were prepared using the conditions described in the following.

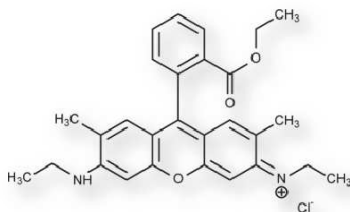


Figure 1 Molecular structure of Rhodamine 6G

#### *Electro-spun ES nanofibers*

For the synthesis of TiO<sub>2</sub> ES nanofibers, a procedure similar to that in [23] was followed. A carrier polymer solution made of 230 mg of polyvinyl pyrrolidone (PVP, M<sub>w</sub> ~1,300,000, Aldrich) in 3.3 mL of absolute ethanol (puriss., Sigma-Aldrich) was added to a precursor solution made of 0.52 mL of titanium(IV) isopropoxide (97 %, Aldrich, stored in a glove box) and 1 mL of acetic acid (Sigma-Aldrich). The solutions were degassed by ultrasonication for 15 min, mixed together, stirred for 1 hour and loaded into the syringe. Electrospinning of the final solution was

## *Appendices*

---

carried out in air at room temperature with a standard syringe and a grounded collector plate configuration with the following conditions: distance between the needle tip and the collector plate of 10 cm, applied voltage of 15 kV and flow rate of 0.5 mL h<sup>-1</sup>. The as-prepared fibres were calcined in air at 500 °C at a heating rate of 5 °C min<sup>-1</sup> for 6 hours in order to decompose and remove PVP and obtain pure inorganic fibres.

### *Nanotubes*

For preparation of tubes 4.5 g of TiO<sub>2</sub> (Sigma Aldrich) was dispersed into 80 ml of 10 M NaOH (Acros Organics) and stirred for 1 hour. Further, the mixture was transferred to an autoclave and kept in an oven at 150 °C for 48 hours. The obtained solid was recovered by centrifugation and further washed with distilled water, which resulted in sodium trititanate nanotubes. Afterwards, the sample was ion-exchanged by stirring the obtained material for 30 min in 480 ml of 0.1 M solution of HCl at room temperature. The sample was recovered by centrifugation and further washed three times with water and two times with ethanol. Finally, the washed sample was dried at 100 °C for 3 days. The as-obtained samples are denoted as TNT NC. Some of the material was calcined in order to change the content of anatase in the sample (re-crystallization while maintaining morphology) according to the following procedure 1 °C min<sup>-1</sup> to 350 °C for a duration of 6 hours in ambient atmosphere followed by stepwise cooling. The obtained calcined material is denoted as TNT C.

### *1.2 Characterization of the solid materials*

The specific surface areas  $S_{\text{BET}}$  (m<sup>2</sup> g<sup>-1</sup>) were deduced from nitrogen adsorption at -196 °C using a Micromeritics ASAP2020 and calculated with the Brunauer-Emmet-Teller BET method. The samples were previously outgassed at 200 °C for 16 h under a residual pressure of 10<sup>-2</sup> Pa. The crystal phase of the titanium nanoparticles was determined by X-ray diffraction (XRD) on a PANalytical X'pert powder diffractometer equipped with CuK<sub>α</sub> radiation ( $\lambda = 1.542 \text{ \AA}$ ) and by FT-Raman spectroscopy [24, 25]. The morphology of all samples was analysed by using a Hitachi S-4800 scanning electron microscope (SEM).

### 1.3 Isotherms of Rhodamine 6G adsorption

Adsorption of Rh6G was carried out using a batch process, in pure water or in buffer. Phosphate buffer solutions ( $0.1 \text{ mol L}^{-1}$ ) were used throughout the experiment to maintain a pH value of 6.0 or 8.0. They were prepared by mixing various amounts of two stock solutions,  $0.2 \text{ mol L}^{-1}$  monobasic and  $0.2 \text{ mol L}^{-1}$  dibasic sodium phosphate. For pH 6, the volumes are 87.7 ml and 12.3 ml of  $\text{NaH}_2\text{PO}_4 \cdot \text{H}_2\text{O}$  and  $\text{Na}_2\text{HPO}_4$  respectively, with ultrapure water to 200 ml. For pH 8, the volumes are 5.3 ml and 94.7 ml with ultrapure water to 200 ml. The same buffer solution was used to prepare Rh6G stock solution with concentration  $10 \mu\text{mol L}^{-1}$ . It was then diluted to prepare the solutions at various initial concentrations ( $0.25 - 10 \mu\text{mol L}^{-1}$ ) for the various experimental points on the adsorption isotherm. In each tube, a solid sample of titanium oxide (5 mg) was dispersed in 10 ml Rh6G solution of already known initial concentration. Then, the tubes were stirred overnight at  $25^\circ\text{C}$  by using a rotary shaker at 10 rpm to obtain adsorption equilibrium. The pH of the suspension was then carefully checked. The separation of the solid phase from the liquid was achieved by centrifugation at 10 000 rpm for 12 min. The supernatant was then analysed by using V-670 UV-Vis Spectrophotometer (interval of wavelength 400-600 nm) to determine the equilibrium concentration. The adsorption capacity ( $Q_{\text{ads}}$ ,  $\mu\text{mol m}^{-2}$ ) is the calculated as follows and displayed as function of equilibrium concentration.

$$Q_{\text{ads}} = \frac{V_0(C_i - C_{\text{eq}})}{m_s S_{\text{BET}}}$$

$C_i$  and  $C_{\text{eq}}$  are the initial and final (equilibrium) concentration of Rh6G respectively expressed in  $\mu\text{mol L}^{-1}$ ,  $V_0$  (L) is the initial volume of the sample solution, and  $m_s$  and  $S_{\text{BET}}$  are the weight (in g) and the specific surface area (in  $\text{m}^2 \text{g}^{-1}$ ) of the adsorbent, respectively.

### 1.4 Zeta potential measurements

The dependence of  $\zeta$  potential on pH was studied in aqueous suspension with a concentration of  $1 \text{ mg L}^{-1}$  for all investigated samples, by using the Malvern instrument Zetasizer 3000HSa. The pH values of the aqueous mixtures were adjusted, adding  $1 \text{ mol L}^{-1}$  HCl and  $1 \text{ mol L}^{-1}$  NaOH, respectively. Zeta potentials for different solids were measured in phosphate buffer solutions at pH 8.

## 2. RESULTS AND DISCUSSION

The Figure 2 shows the Scanning Electron Microscopy (SEM) images of the various TiO<sub>2</sub> samples. The P25 material is known to exhibit spherical primary particles with 21 nm, with significant aggregation of the elementary particles. The Anatase is also composed of agglomerated nanoparticles (10-20 nm). The ES nanofibers are very long filaments, with 100- 200 nm diameter and several  $\mu\text{m}$  in length. TNT (NC or C) display needles or flakes with 10 nm thickness and 1  $\mu\text{m}$  length.

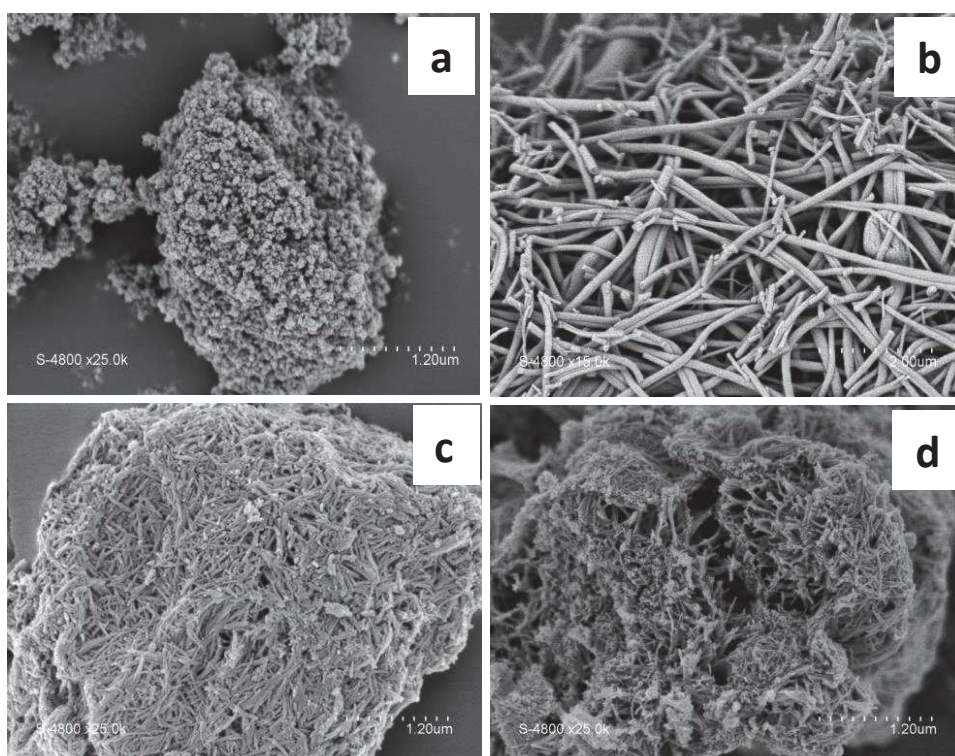


Figure 2. SEM images of Anatase (a), nanofibers (b) and nanotubes calcined (c) and not calcined (d).

Table 1 summarizes the characteristic of all commercial and synthesized materials used in this study. Concerning the textural parameters, two classes of materials could be distinguished,

## Appendices

each of them with similar specific surface area. The first set of materials, with nanotubes TNT, exhibits high  $S_{\text{BET}}$ , 342 and 340  $\text{m}^2 \text{g}^{-1}$  for not calcined and calcined samples respectively. Their specific surface areas are approximately seven times higher than the three other samples, which possess  $S_{\text{BET}}$  between 46 and 57  $\text{m}^2 \text{g}^{-1}$ . On the other hand, XRD analysis (data not shown) confirmed that the commercial Anatase sample is pure anatase phase. Besides, P25 and ES nanofibers contain the mixture of rutile and anatase phases, with mainly anatase in both cases [26]. For nanotubes, the not calcined sample contain only TNT phase, whereas a small percentage of anatase appears after calcination.

Table 1. Specific surface area and crystal phase of the various titanium oxide samples.

Sample name	Crystal phase <sup>a</sup>	$S_{\text{BET}}$ ( $\text{m}^2 \text{g}^{-1}$ )
Anatase Commercial	100% anatase	57
P25	81% anatase 19% rutile	49
ES nanofibers	68% anatase 32% rutile	46
TNT-NC	TNT	342
TNT-C	TNT + Anatase	340

<sup>a</sup> Crystal phase determined with XRD or FT-Raman Spectroscopy [25]

In order to evaluate the influence of surface charge and pH, the dye adsorption was performed at natural pH (pH 5.2-5.7) and in phosphate buffer at two different pHs, pH 6 and pH 8. The adsorption isotherms of Rh6G on the spherical nanoparticles P25 are presented on Figure 3. The values of maximum amount of dye adsorbed on all titanium oxide samples from  $\text{H}_2\text{O}$  at natural pH and from phosphate buffer solution at pH 8 and pH 6 are reported in Table 2.

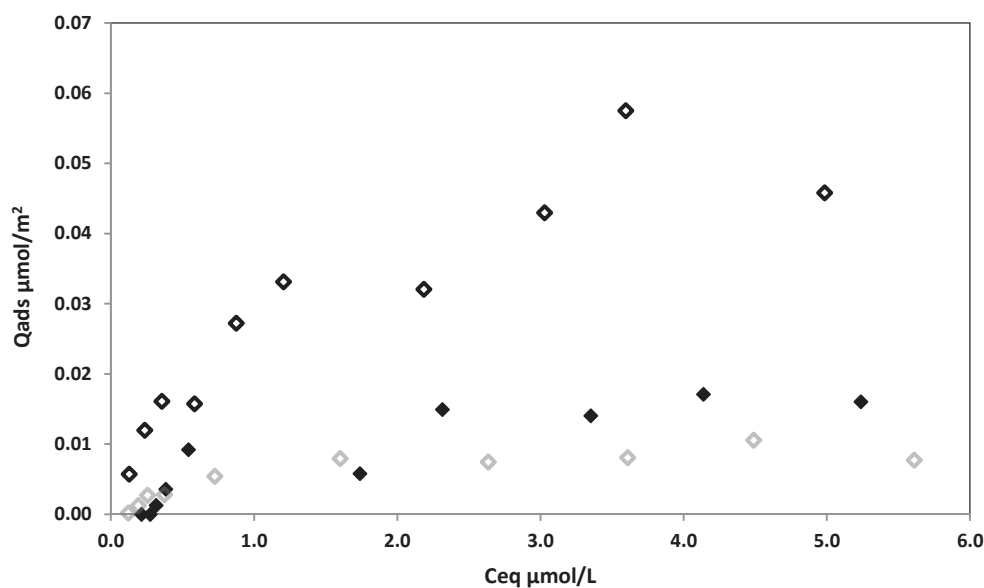


Figure 3. Adsorption isotherms for Rhodamine 6G onto P25 nanoparticles at 25°C from H<sub>2</sub>O at natural pH (◇), from phosphate buffer at pH 6 (◇) and at pH 8 (◆)

Table 2. Maximum amounts of dye adsorbed onto titanium oxide samples from H<sub>2</sub>O at natural (nat.) pH and from phosphate buffer solutions at pH 8 and pH 6. (nd = not determined)

	Qads max. (10 <sup>-2</sup> μmol m <sup>-2</sup> )		
	Buffer pH=6	Buffer pH=8	H <sub>2</sub> O nat. pH
<b>P25</b>	0.8	1.6	5.9
<b>TNT-NC</b>	nd	0.9	4.8
<b>TNT-C</b>	nd	1.1	2.7
<b>ES fibers</b>	4.7	8-10	10-14
<b>Anatase</b>	0.5	0.5	2.5

In buffered solutions, it can be noticed that for P25 adsorption capacity increases from 0.8 x 10<sup>-2</sup> μmol m<sup>-2</sup> to 1.5 x 10<sup>-2</sup> μmol m<sup>-2</sup> with increasing pH from 6 to 8, respectively. These amounts are very low, especially when compared with those obtained on modified solid. For example Tada et al. [6] reported in his work that experimental conditions or surface treatment could increase 2.6-fold the saturated adsorption amount. It is well known that the adsorption onto oxides with variable surface charge is strongly pH dependent. Since the point of zero charge (PZC) of P25 is

## Appendices

evaluated at  $\text{pH} \approx 6$  [27], adsorption of cationic molecule Rh6G is favoured under basic conditions compared to acidic conditions in similar ionic strength or without competing species and specific interactions [28]. When pH increases from 6 to 8, Rh6G is more easily attracted by the P25 surface, and the adsorption is more favourable as observed on Figure 3. This results point to importance of electrostatic interaction between Rh6G and the surface of the adsorbent.

For commercial Anatase nanoparticles (Figure 4), the difference between the maximum adsorbed at  $\text{pH}=6$  and  $\text{pH}=8$  is not significant ( $0.48 \times 10^{-2}$  and  $0.51 \times 10^{-2} \mu\text{mol m}^{-2}$ , respectively within the experimental error range). It can be explained by the limited affinity of the Anatase sample for the dye adsorption from the buffer solutions. The maximum of adsorption capacity was already achieved at  $\text{pH} = 6$ . In contrast to the P25 for which adsorption is pH dependent, the increase of pH has no influence on the amount adsorbed onto Anatase.

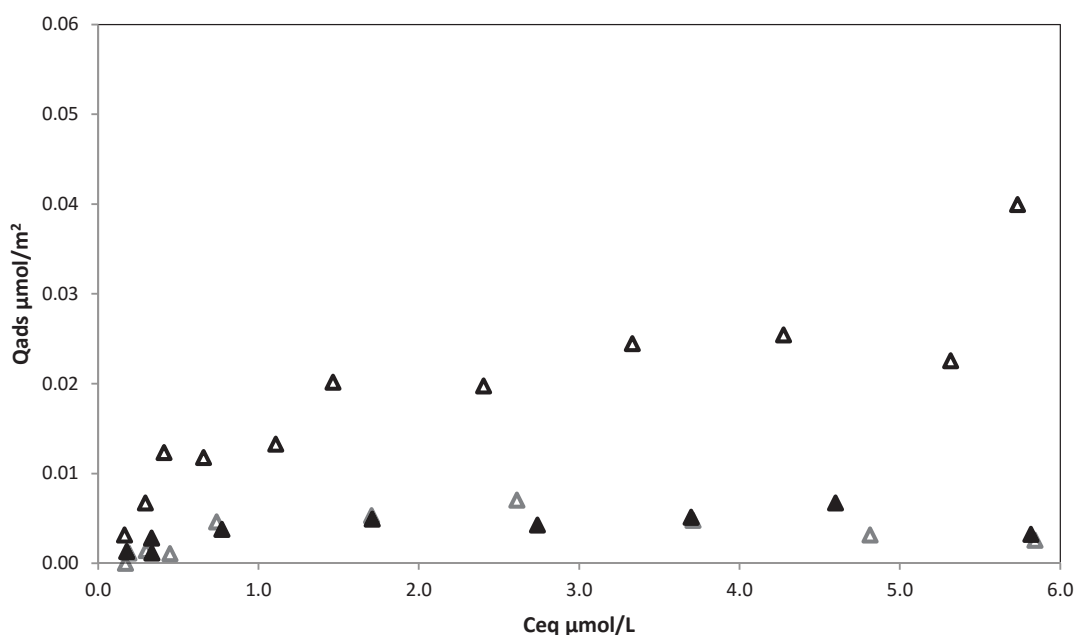


Figure 4. Adsorption isotherms for Rhodamine 6G onto Anatase Commercial nanoparticles at 25°C from water at natural pH ( $\Delta$ ), from phosphate buffer at pH 6 ( $\Delta$ ) and at pH 8 ( $\blacktriangle$ ).

In both cases for P25 and Anatase, the adsorption capacity in pure water, at natural pH (5.2-5.7 for P25, 4.7-5.3 for Anatase), is 4 or 5 times higher than in buffer solution. This cannot be explained by the simple influence of pH, since adsorption should be lower at acid pH when the surface decreases. Similar conclusions were also drawn for nanotubes. The obtained results are shown on

## Appendices

Figure 5 and in Table 2 Adsorbed quantities for not calcined and calcined samples are lower in the buffer solution ( $0.9 \times 10^{-2} \mu\text{mol m}^{-2}$  and  $1 \times 10^{-2} \mu\text{mol m}^{-2}$ , respectively), than those in water ( $4.8 \times 10^{-2} \mu\text{mol m}^{-2}$  and  $2.7 \times 10^{-2} \mu\text{mol m}^{-2}$ ). The same influence of buffer could be observed for ES nanofibers (see Figure 1 in ESI and Table 2). Maximum adsorbed amount from buffer at pH=6 is  $4.7 \times 10^{-2} \mu\text{mol m}^{-2}$  while it increases in the range 8 to  $10 \times 10^{-2} \mu\text{mol m}^{-2}$  at pH=8, whereas it reaches 12 or 14 in water  $10^{-2} \mu\text{mol m}^{-2}$ .

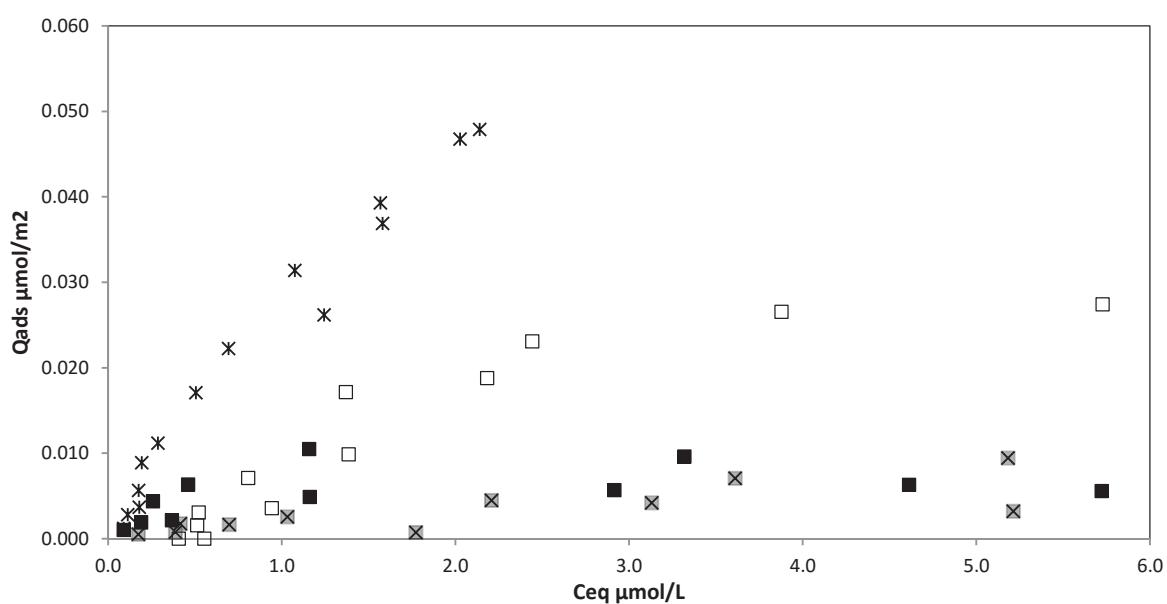


Figure 5. Adsorption isotherms for Rhodamine 6G onto nanotubes H TNT-C at 25°C from water at natural pH (□) and from phosphate buffer at pH 8 (■) and onto nanotubes H TNT-NC at 25°C from water at natural pH (\*) and from phosphate buffer at pH 8 (\* with grey).

For all samples, there is an increase of the amount adsorbed in the pure water (see Table 2), in comparison with experiments in the buffer solution. In order to clarify these differences in adsorption, zeta-potential measurement were carried out. Figure 6 shows the results obtained for all titanium oxide particles at pH 8 in water (pH adjusted with NaOH) and pH 8 in buffer solution.

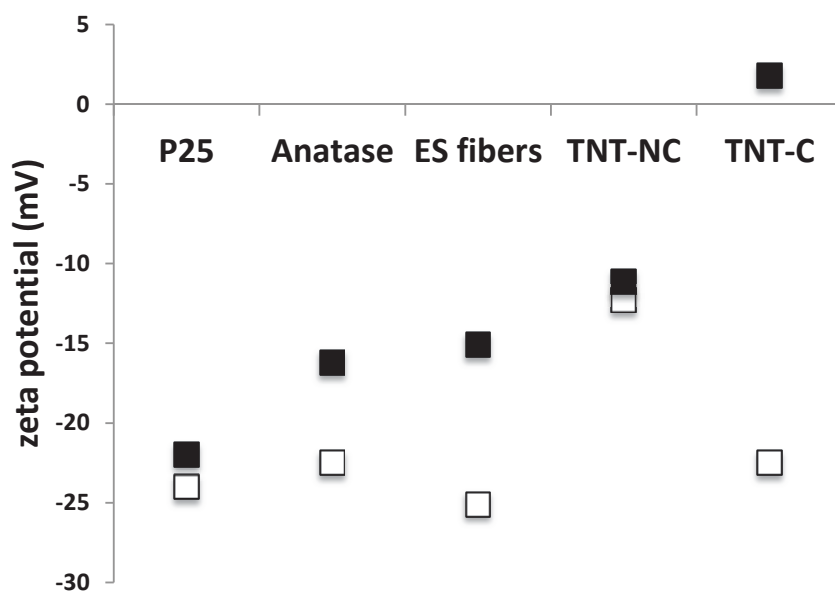


Figure 6. Zeta-potential measurements in water with pH=8 (full symbols), and in phosphate buffer at pH=8 (empty symbols).

Except for calcined nanotubes in water, the values of zeta potential are negative for all samples. This result was expected since IEP of rutile and anatase are evaluated at pH 5.8-6, whereas it is evaluated at 3 or 4 for TNT depending on their synthesis conditions [12]. As it can be observed, zeta potential values measured in buffer are higher than the values obtained in water (except for not calcined nanotubes). It shows clearly the influence of the buffer on the surface properties of adsorbents. Theoretically, because of the higher zeta potential of the surfaces in buffer solution, Rh6G should be more attracted and adsorbed in buffer surroundings. Nevertheless, Rh6G is more adsorbed in water, with lower values of zeta potential.

In order to explain the difference between Rh6G adsorption on Anatase and P25 from the buffer solutions at different pHs, adsorption of phosphates on these two solids was performed. Results of the adsorption isotherms of  $\text{HPO}_4^{2-}$  are shown on Figure 7. It can be observed that Anatase exhibits completely different behaviour compared to P25. Phosphate adsorption onto P25 is insignificant ( $1.5 \cdot 10^{-2} \mu\text{mol m}^{-2}$ ), whereas Anatase displays high adsorption capacity ( $Q_{\text{max}} = 0.9 \mu\text{mol m}^{-2} = 90 \cdot 10^{-2} \mu\text{mol m}^{-2}$ ), and higher affinity to phosphate species. From these data, it is obvious that for Anatase particle, phosphates are highly adsorbed. This firstly explains the decrease of adsorption capacity in buffer solution compared to measurements in pure water. Moreover, this

is the evidence of the presence of the competitive adsorption between the Rh6G molecules and the phosphates on the titanium oxide surfaces. Similar competition behaviour was already reported for humic or fulvic acids onto titanium dioxide nanoparticles from phosphate buffer solutions [22] or goethite in the presence of phosphate [21].

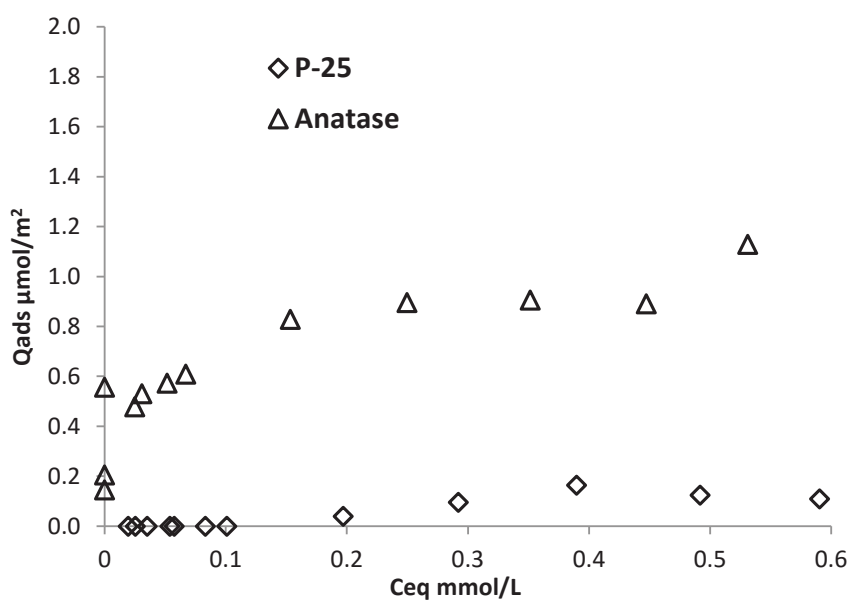


Figure 7. Adsorption isotherms for  $\text{HPO}_4^{2-}$  onto P25 and Commercial Anatase nanoparticles at  $25^\circ\text{C}$  from water at natural pH.

When adsorption of the dye is performed in buffer solution, the competitive adsorption between phosphate and dye take place. Surface sites are strongly hindered by phosphate species, which are adsorbed on it. They are thus not available for dye adsorption. Finally, the influence of pH is negligible, since, even if the surface charge is higher at pH 8, all the new ionized sites are occupied by phosphate. Anatase is more affected by adsorption of phosphates, and that is why there is no difference in adsorption capacity at pH 6 or 8 for this sample. In the case of P25, the sites are less sensitive to phosphate sorption. However, in the buffer solution, there is still slight effect of pH, with  $0.8$  and  $1.6 \cdot 10^{-2} \mu\text{mol m}^{-2}$  for pH 6 and pH 8 respectively. The strength of the interaction between  $\text{TiO}_2$  and phosphate species was also evidenced by Connor et McQuillan. From phosphate absorbance collected with internal reflection spectroscopy they obtained isotherm typical of a strongly binding adsorbate, with adsorption increasing to saturation coverage at

## *Appendices*

---

relatively low concentrations. They observed that phosphate binds strongly to TiO<sub>2</sub> surface through surface complexes and influences the interfacial and surface chemistry of TiO<sub>2</sub> [29].

Furthermore, for the TNT, maximum adsorbed amounts were influenced by calcination treatment, with higher adsorption for NC samples  $4.8 \times 10^{-2} \mu\text{mol m}^{-2}$  compared to calcined solids ( $2.7 \times 10^{-2} \mu\text{mol m}^{-2}$ ). This can be attributed to the slightly positive value of zeta potential (Figure 6), leading to repulsion, and lower adsorption on calcined samples. Even though the change in properties of TNT materials in case of calcination was mainly appointed to a partial change in crystal phase (formation of anatase), it is clear from the results that strongly altered surface properties have been generated compared to the not calcined materials but also in comparison to Anatase, which has a clearly negative zeta potential.

To conclude, for all tested nanomorphologies adsorption is higher in the water media with natural pH. Moreover, the tendency of Rh6G adsorption onto various solids is observed as follows: nanofibers ES >> nanopowder P25 > nanotubes TNT > nanopowder Anatase. This result can be related with structural properties of each solid. From Table 1, it can be noted that the nanotubes TNT have the highest specific surface areas, nevertheless, the amount adsorbed is not the highest on these type of adsorbents. It is also interesting to observe that the percentage of rutile phase is increased in the materials with the higher adsorption properties (i.e. ES and P25). While percentage of anatase phase is decreased in these two samples.

## **CONCLUSION**

Titanium oxide nanoparticles with different morphologies have been employed for the removal of organic Rhodamine 6G dye. Nanotubes and ES nanofibers were synthesized by hydrothermal and electrospinning methods. Commercial nanopowder P25, as best photocatalytic material, was used as reference solid together with commercial Anatase. At first, structural characterization of these adsorbents was performed before adsorption study investigation.

Adsorption isotherms were carried out with batch-mode experiments from the water at the natural pH and from phosphate buffer at pH 6 and pH 8. The results have shown that increasing the buffer pH from 6 to 8 give rise to the increase of adsorption capacity for P25 and ES nanofibers, due to the negative surface charge. That is in a good agreement with the results of zeta potential

## *Appendices*

---

measurements. Nevertheless, this influence of pH is rather small, especially in the case of Anatase. Indeed, Anatase exhibits great adsorption capacity for phosphate. Hence, this explains the low affinity for Rh6G in the presence of phosphate buffer, because of the competition between anionic species. At pH 6 in water and in phosphate buffer, the adsorption capacity is also reduced, due to a combined effect of surface charge increase, in addition with the adsorption of competing ions. This could explain the modification of the catalytic performances. Adsorption from water at natural pH compared to adsorption in buffer has shown the presence of competitive adsorption between Rh6G and phosphates species on the surface of the TiO<sub>2</sub>. The best adsorption capacity was achieved by ES nanofibers.

### *Acknowledgments*

The research leading to these results has received funding from the European Research Council under the European Union's Seventh Framework Programme (FP/2007-2013) / ERC Grant Agreement n. 306682.

### *References*

- [1] A.L. Linsebigler, G.Q. Lu, J.T. Yates, Photocatalysis on TiO<sub>2</sub> surfaces - Principles, Mechanisms, and selected results, *Chemical Reviews*, 95 (1995) 735-758.
- [2] P. Pattanaik, M.K. Sahoo, TiO<sub>2</sub> photocatalysis: progress from fundamentals to modification technology, *Desalination and Water Treatment*, 52 (2013) 6567-6590.
- [3] J. Schneider, M. Matsuoka, M. Takeuchi, J. Zhang, Y. Horiuchi, M. Anpo, D.W. Bahnemann, Understanding TiO<sub>2</sub> Photocatalysis: Mechanisms and Materials, *Chemical Reviews*, 114 (2014) 9919-9986.
- [4] K. Bourikas, C. Kordulis, A. Lycourghiotis, Titanium Dioxide (Anatase and Rutile): Surface Chemistry, Liquid–Solid Interface Chemistry, and Scientific Synthesis of Supported Catalysts, *Chemical Reviews*, 114 (2014) 9754-9823.
- [5] J. Sun, X. Yan, K. Lv, S. Sun, K. Deng, D. Du, Photocatalytic degradation pathway for azo dye in TiO<sub>2</sub>/UV/O<sub>3</sub> system: Hydroxyl radical versus hole, *Journal of Molecular Catalysis A: Chemical*, 367 (2013) 31-37.

## Appendices

---

- [6] H. Tada, M. Akazawa, Y. Kubo, S. Ito, Enhancing effect of SiO<sub>x</sub> monolayer coverage of TiO<sub>2</sub> on the photoinduced oxidation of rhodamine 6G in aqueous media, *J. Phys. Chem. B*, 102 (1998) 6360-6366.
- [7] L.L. Bao, M.J. Meng, K.Y. Sun, W.B. Li, D.X. Zhao, H.M. Li, M.Q. He, Selective Adsorption and Degradation of Rhodamine B with Modified Titanium Dioxide Photocatalyst, *J. Appl. Polym. Sci.*, 131 (2014) 12.
- [8] K. Lv, J. Yu, K. Deng, J. Sun, Y. Zhao, D. Du, M. Li, Synergistic effects of hollow structure and surface fluorination on the photocatalytic activity of titania, *J Hazard Mater*, 173 (2010) 539-543.
- [9] M.M. Khin, A.S. Nair, V.J. Babu, R. Murugan, S. Ramakrishna, A review on nanomaterials for environmental remediation, *Energy Environ. Sci.*, 5 (2012) 8075-8109.
- [10] X.D. Wang, Z.D. Li, J. Shi, Y.H. Yu, One-Dimensional Titanium Dioxide Nanomaterials: Nanowires, Nanorods, and Nanobelts, *Chemical Reviews*, 114 (2014) 9346-9384.
- [11] S. Cavaliere, S. Subianto, I. Savych, D.J. Jones, J. Rozière, Electrospinning: designed architectures for energy conversion and storage devices, *Energy Environ. Sci.*, 4 (2011) 4761-4785.
- [12] V. Bem, M.C. Neves, M.R. Nunes, A.J. Silvestre, O.C. Monteiro, Influence of the sodium/proton replacement on the structural, morphological and photocatalytic properties of titanate nanotubes, *Journal of Photochemistry and Photobiology A: Chemistry*, 232 (2012) 50-56.
- [13] Y.M. Xu, C.H. Langford, UV- or visible-light-induced degradation of X3B on TiO<sub>2</sub> nanoparticles: The influence of adsorption, *Langmuir*, 17 (2001) 897-902.
- [14] D.K. Singh, P.K. Iyer, P.K. Giri, Role of molecular interactions and structural defects in the efficient fluorescence quenching by carbon nanotubes, *Carbon*, 50 (2012) 4495-4505.
- [15] M. Ali Ahmad, B. Prelot, A. Razafitianamaharavo, J.M. Douillard, J. Zajac, F. Dufour, O. Durupthy, C. Chanéac, F. Villiéras, Influence of Morphology and Crystallinity on Surface Reactivity of Nanosized Anatase TiO<sub>2</sub> Studied by Adsorption Techniques. 1. The Use of Gaseous Molecular Probes. , *The Journal of Physical Chemistry C*, 116 (2012) 24596–24606.
- [16] M. Ali Ahmad, B. Prelot, F. Dufour, O. Durupthy, A. Razafitianamaharavo, J.M. Douillard, C. Chanéac, F. Villiéras, J. Zajac, Influence of Morphology and Crystallinity on Surface Reactivity of Nanosized Anatase TiO<sub>2</sub> Studied by Adsorption Techniques. 2. Solid–Liquid Interface, *The Journal of Physical Chemistry C*, 117 (2013) 4459-4469.
- [17] G. Liu, H.G. Yang, J. Pan, Y.Q. Yang, G.Q. Lu, H.-M. Cheng, Titanium Dioxide Crystals with Tailored Facets, *Chemical Reviews*, 114 (2014) 9559-9612.
- [18] J. Cunningham, G. Al-Sayyed, Factors influencing efficiencies of TiO<sub>2</sub>-sensitized photodegradation. Part 1.-Substituted benzoic acids: discrepancies with dark-adsorption parameters, *Journal of the Chemical Society, Faraday Transactions*, 86 (1990) 3935-3941.
- [19] J.-K. Yang, A.P. Davis, Competitive Adsorption of Cu(II)–EDTA and Cd(II)–EDTA onto TiO<sub>2</sub>, *Journal of Colloid and Interface Science*, 216 (1999) 77-85.
- [20] N. Lee, D.A. Sverjensky, R.M. Hazen, Cooperative and Competitive Adsorption of Amino Acids with Ca<sup>2+</sup> on Rutile (α-TiO<sub>2</sub>), *Environmental Science & Technology*, 48 (2014) 9358-9365.

## Appendices

---

- [21] L. Weng, W.H. Van Riemsdijk, T. Hiemstra, Humic nanoparticles at the oxide–water interface: Interactions with phosphate ion adsorption, *Environmental Science & Technology*, 42 (2008) 8747-8752.
- [22] M. Erhayem, M. Sohn, Effect of humic acid source on humic acid adsorption onto titanium dioxide nanoparticles, *Science of The Total Environment*, 470–471 (2014) 92-98.
- [23] M. Fehse, S. Cavaliere, P.E. Lippens, I. Savych, A. Iadecola, L. Monconduit, D.J. Jones, J. Rozière, F. Fischer, C. Tessier, L. Stievano, Nb-Doped TiO<sub>2</sub> Nanofibers for Lithium Ion Batteries, *The Journal of Physical Chemistry C*, 117 (2013) 13827-13835.
- [24] S. Ribbens, V. Meynen, G.V. Tendeloo, X. Ke, M. Mertens, B.U.W. Maes, P. Cool, E.F. Vansant, Development of photocatalytic efficient Ti-based nanotubes and nanoribbons by conventional and microwave assisted synthesis strategies, *Microporous and Mesoporous Materials*, 114 (2008) 401-409.
- [25] S. Ribbens, I. Caretti, E. Beyers, S. Zamani, E. Vinck, S. Van Doorslaer, P. Cool, Unraveling the Photocatalytic Activity of Multiwalled Hydrogen Trititanate and Mixed-Phase Anatase/Trititanate Nanotubes: A Combined Catalytic and EPR Study, *The Journal of Physical Chemistry C*, 115 (2011) 2302-2313.
- [26] I. Savych, J. Bernard d'Arbigny, S. Subianto, S. Cavaliere, D.J. Jones, J. Rozière, On the effect of non-carbon nanostructured supports on the stability of Pt nanoparticles during voltage cycling: A study of TiO<sub>2</sub> nanofibres, *Journal of Power Sources*, 257 (2014) 147-155.
- [27] K. Mogyorosi, N. Balazs, D.F. Sranko, E. Tombacz, I. Dekany, A. Oszko, P. Sipos, A. Dombi, The effect of particle shape on the activity of nanocrystalline TiO<sub>2</sub> photocatalysts in phenol decomposition. Part 3: The importance of surface quality, *Appl. Catal. B-Environ.*, 96 (2010) 577-585.
- [28] S. Hamad, J.R. Sanchez-Valencia, A. Barranco, J.A. Mejias, A.R. Gonzalez-Elipe, Molecular dynamics simulation of the effect of pH on the adsorption of rhodamine laser dyes on TiO<sub>2</sub> hydroxylated surfaces, *Mol. Simul.*, 35 (2009) 1140-1151.
- [29] P. Connor, A.J. McQuillan, Phosphate adsorption onto TiO<sub>2</sub> from aqueous solutions: an in situ internal reflection infrared spectroscopic study, *Langmuir*, 15 (1999) 2916-2921.

SUPPORTING INFORMATION

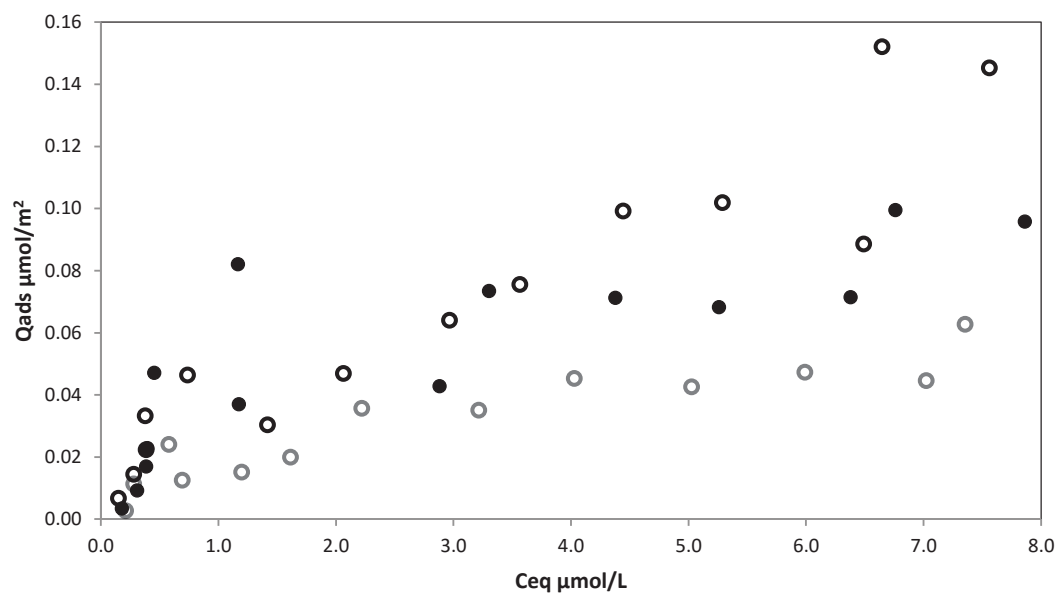


Figure 8. Adsorption isotherms for Rhodamine 6G onto Nanofibres SC at 298 K from water at natural pH (○), from phosphate buffer at pH 6 (◐) and at pH 8 (●)

# APPENDIX II:

## Complement for Chapter IV

### I. Experimental description

#### 1. Materials

Mg-Al-Cl LDH was prepared by co-precipitation method as described in Chapter II using  $\text{Mg}(\text{Cl})_2 \cdot 6\text{H}_2\text{O}$  and  $\text{Al}(\text{Cl})_3 \cdot 6\text{H}_2\text{O}$  provided by Sigma - Aldrich. All chemicals used for adsorption experiments were the same as those described in Chapters II and III.

#### 2. Characterization

X-ray diffraction patterns of the pristine sample were recorded on X'Pert diffractometer over the  $2\theta$  range from  $3^\circ$  to  $70^\circ$  using Cu  $K\alpha$  radiation ( $\lambda = 1.5418 \text{ \AA}$ ) and a nickel filter. The time of acquisition was fixed at 440 seconds with a  $2\theta$  step of  $0.0334^\circ$ . In the case of LDH samples containing different amounts of retained dye species, the XRD patterns were collected at a scan rate of  $0.003 \text{ deg min}^{-1}$  in the  $2\theta$  range from  $2^\circ$  to  $30^\circ$  at 30 mA, 45 kV, using an incident beam mask of 10 mm and a zero background sample holder.

The amount of interlayer water was determined from the analysis of TG-curve recorded on a NETZSCH STA409PC LUXX<sup>®</sup> apparatus. Experiment was performed under nitrogen atmosphere at a heating rate of  $2 \text{ }^\circ\text{C min}^{-1}$  in the temperature range from 298 to 1073K with a  $50\text{cm}^3 \text{ min}^{-1} \text{ N}_2$  flow.

### 3. Adsorption experiments

Adsorption study from single-solute or multi-solute solutions was made using the procedure described in Chapters II and III. Adsorption from bi- and tri- solute solutions was investigated when mixing up the various solutes in equimolar proportions. Thus, the concentration of inorganic anion was the same as that of the dye component: 5 mM MO; 4 mM OII; 3 mM OG.

The supernatant was also analyzed with the aid of ionic chromatography analyzer (Shimadzu HPLC) equipped with a CDD-6A conductivity detector operating at 313 K (Shim-pack IC-A1 column, 2 mmol L<sup>-1</sup> potassium hydrogen phthalate at pH 4.2 as the mobile phase) so as to study the amount of chloride anions released from the LDH sample during dye adsorption. The detection analysis was repeated twice with aim to evaluate the repeatability which was as follows: 21%, MO; 18%, OII; 20% OG.

### 4. Titration microcalorimetry and XRD study

The calorimetric and XRD procedures were detailed in Chapters II and III.

## II. Determination of the number of H<sub>2</sub>O molecules in the LDH

The theoretical formula of LDH without water molecules is Mg<sub>0.67</sub>Al<sub>0.33</sub> (OH)<sub>2</sub> Cl<sub>0.33</sub> and this corresponds to a molar mass to 70.88 g·mol<sup>-1</sup>. This chemical formula represents 85.5 % of the total mass of the LDH sample. The water contents is equal to 14.5%. The number of H<sub>2</sub>O molecules, n, can be calculated as follows:

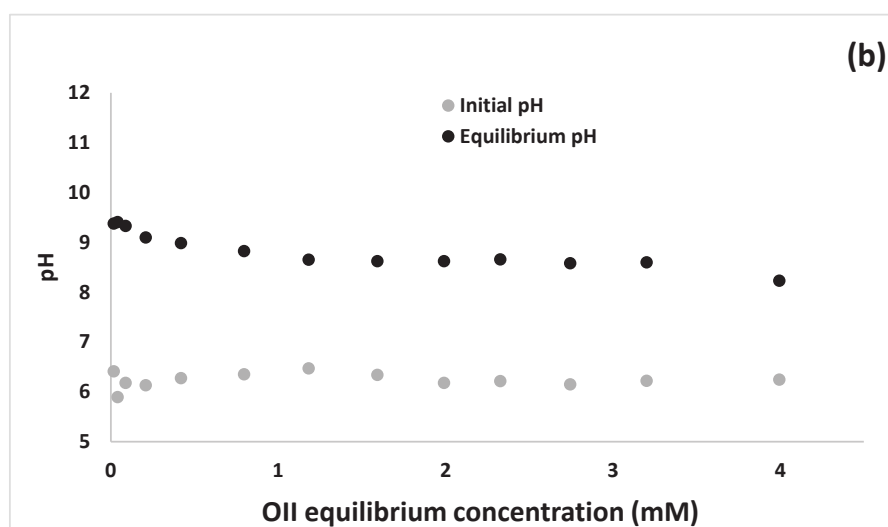
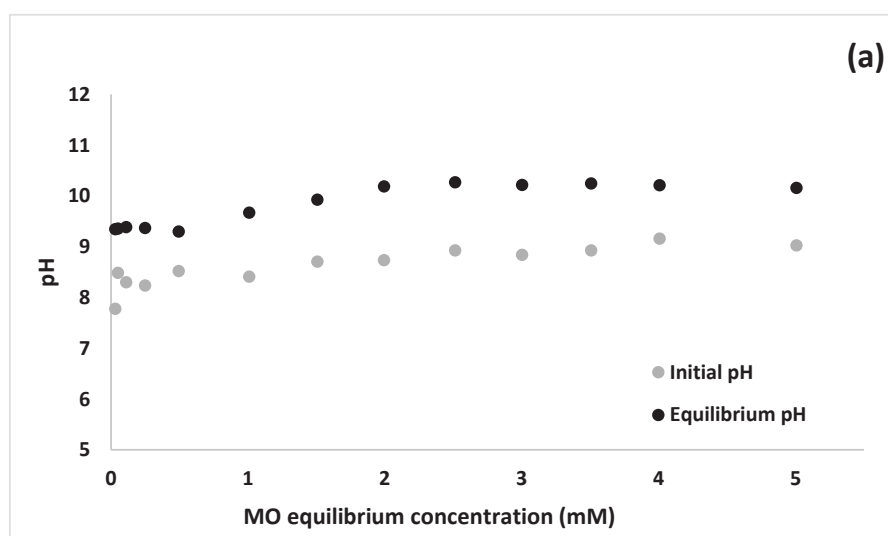
$$n = \frac{x_{H_2O}/M(H_2O)}{x(HDL)/M(HDL)} = \frac{0.145/18}{0.855/70.88} = 0.67$$

Therefore, the final formula of the present LDH sample as: Mg<sub>0.67</sub>Al<sub>0.33</sub> (OH)<sub>2</sub> Cl<sub>0.33</sub> • 0.67 H<sub>2</sub>O.

## Appendices

The anion exchange capacity (AEC) is inferred from the amount of  $M^{III}$  per gram of the sample.  $AEC = Al^{III} / M (Mg_{0.67}Al_{0.33} (OH)_2 Cl_{0.33} \cdot 0.67 H_2O) = 0.33 / 82.94$  or around  $4 \text{ mmol} \cdot \text{g}^{-1}$ .

### III. pH measurement during adsorption experiment



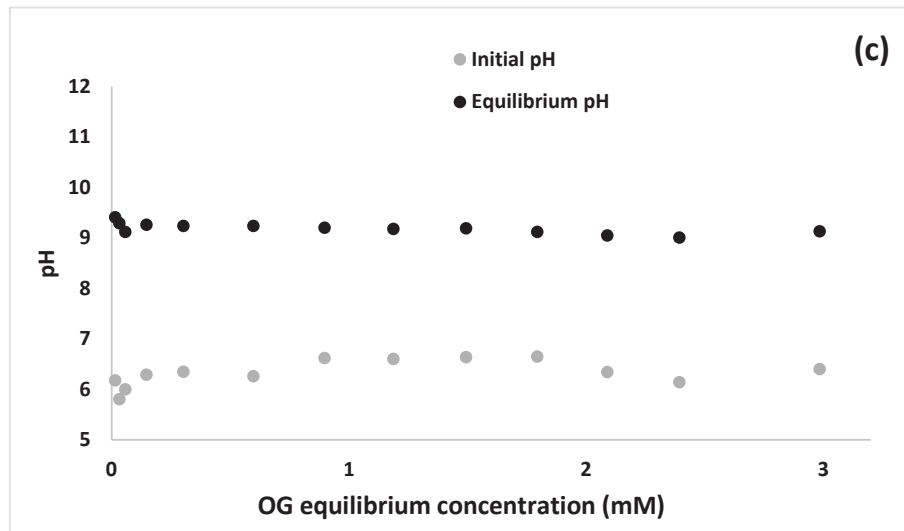
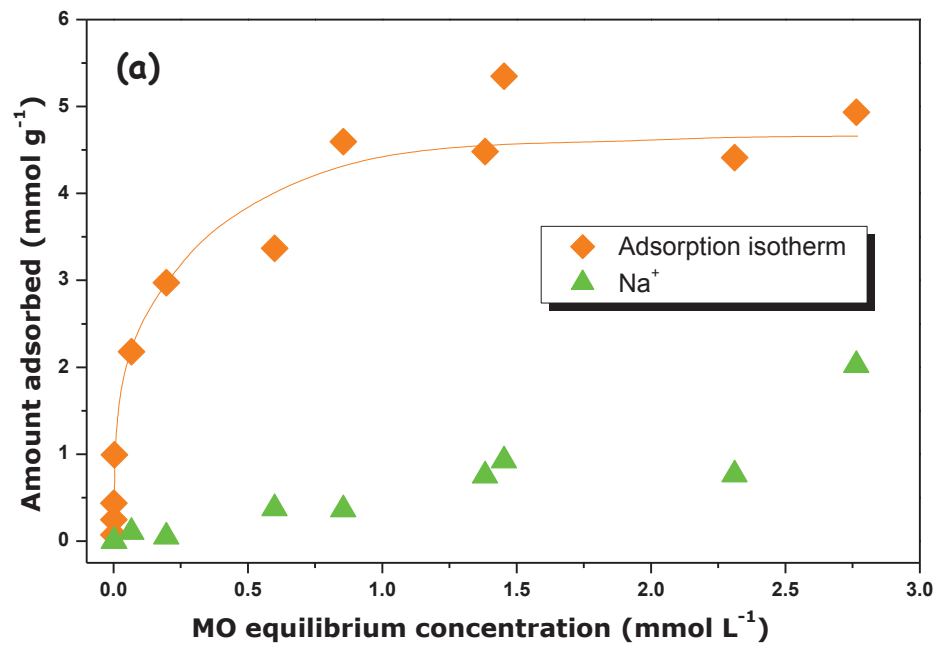


Figure AII- 1. Evolution of the initial and final pH during adsorption of Methyl Orange (a), Orange II (b) and Orange G (c) as a function of the dye concentration.

**IV. Measurements of the sodium counter-ions co-adsorption accompanying dye retention onto LDH**



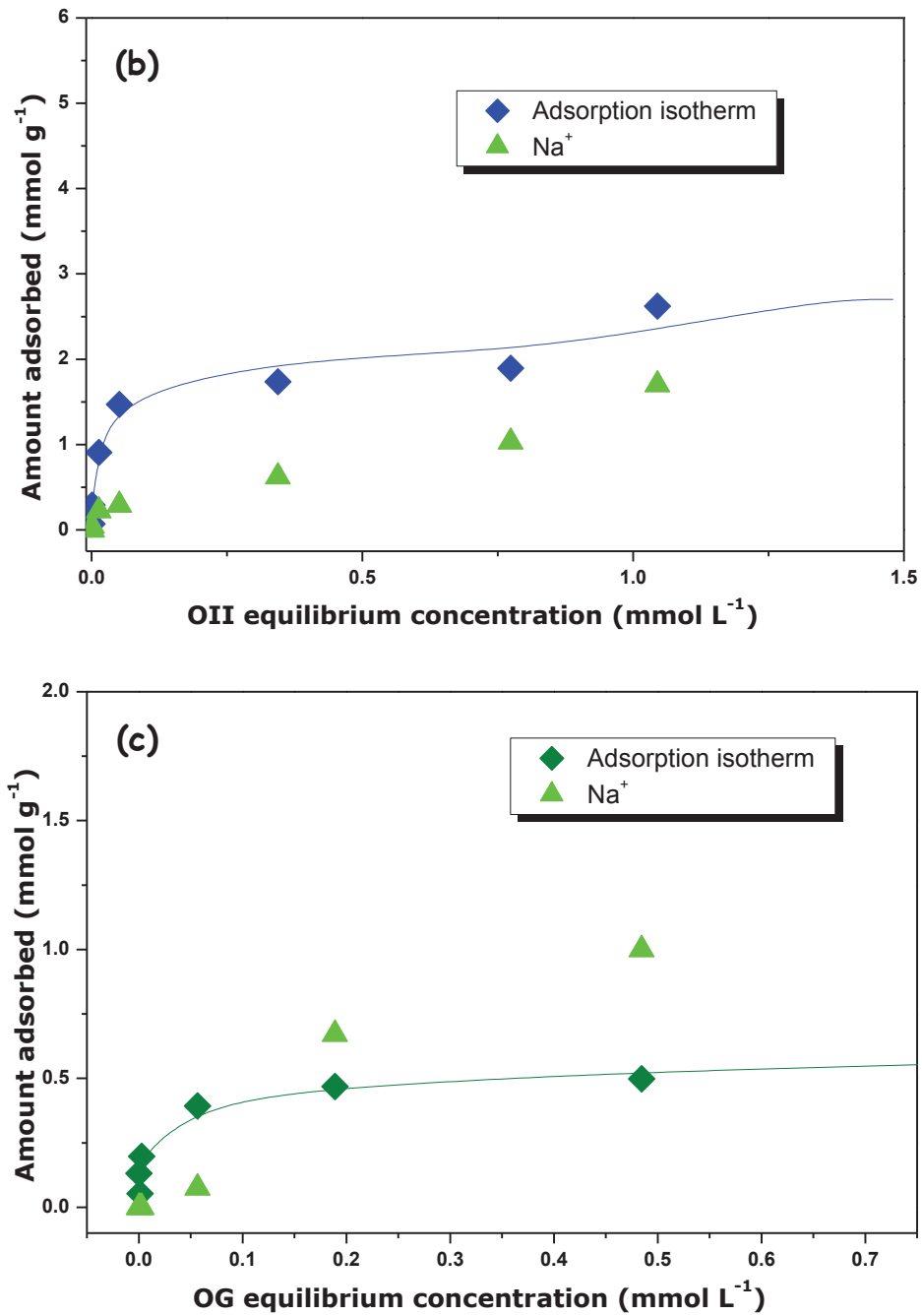


Figure AII- 2. Adsorption isotherms for MO (a), OII (b) and OG (c) with simultaneous co-adsorption of sodium (green triangles).

## Appendices

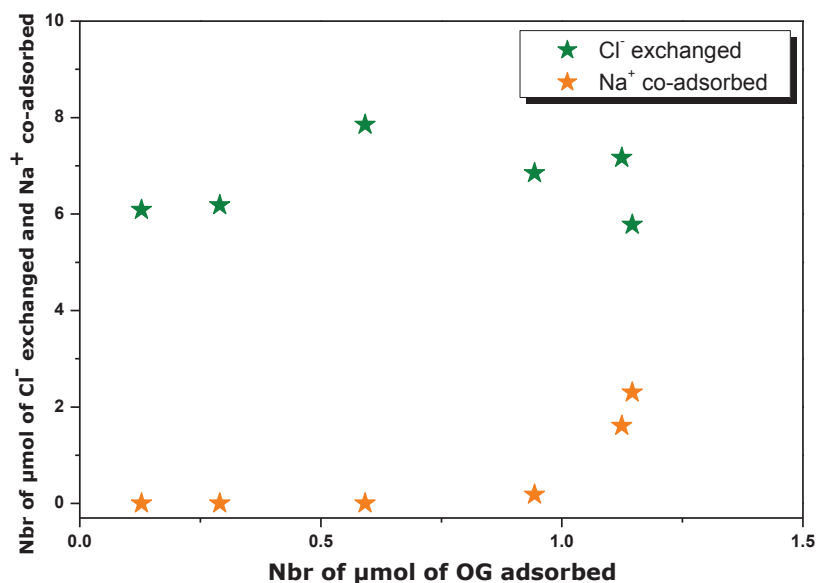


Figure AII- 3. Amount of chloride released from LDH and the sodium uptake as a function of the amount of OG adsorbed.

Table AII- 1. Calculations of uncompensated charge on the basis of OG adsorbed, Na co-adsorbed and Cl released from the structure during adsorption.

OG amount adsorbed ( $\mu\text{mol}$ )	OG amount adsorbed ( $\mu\text{eq}$ )	Cl amount released ( $\mu\text{mol}$ or $\mu\text{eq}$ )	Na amount co-adsorbed ( $\mu\text{mol}$ )	Molar OG: Na ratios	Uncompensated charges
0.1	<b>0.3</b>	6.1	$C_{\text{Na}^+} < \text{LOQ}$	-	<b>5.8*</b>
0.3	<b>0.6</b>	6.2	$C_{\text{Na}^+} < \text{LOQ}$	-	<b>5.6*</b>
0.6	<b>1.2</b>	7.9	$C_{\text{Na}^+} < \text{LOQ}$	-	<b>6.7*</b>
0.9	<b>1.9</b>	6.9	0.2	10.4	<b>5.0*</b>
<b>1.1</b>	2.2	7.2	1.6	1.4	<b>6.0*</b>
<b>1.1</b>	2.3	5.8	2.3	1	<b>4.6*</b>

\*The values of uncompensated charge, highlighted in blue were calculated by taking into account the bi-charged OG molecule, while those highlighted in orange presents the values calculated with values of mono-charged OG moieties (because of counter-ion sodium co-adsorption). Limit of quantification (LOQ): Sodium  $0.1 \text{ mmol L}^{-1}$ ; Chloride  $0.01 \text{ mmol L}^{-1}$ ; OG  $10^{-5} \text{ mmol L}^{-1}$ .

As it can be inferred from the analysis of Figure AII-2 and Table AII-1, it not possible to know the behavior of sodium in the first three points of adsorption isotherm about the possible simultaneous co-adsorption of sodium with OG uptake (values are lower than LOQ). Therefore we consider that no co-adsorption of sodium occurs simultaneously with dye in these points. However, from the fourth point it is possible to observe the sodium uptake with  $\text{Na}^+$  to OG ratio

equal to 1. The number of uncompensated charges was calculated by comparing the amount of OG adsorbed onto LDH and chloride ions released from the structure. For the first four points, it is considered that OG have two free charges and can neutralized 2 cationic charges. For the last two points, OG probably have only one free charge because another one is compensated by the co-adsorption of sodium. The mean value of uncompensated charges is equal to 5.6. Therefore it can be concluded that some another anionic species enter together with the adsorbing OG units.

### V. Competitive adsorption between the dye and the inorganic species

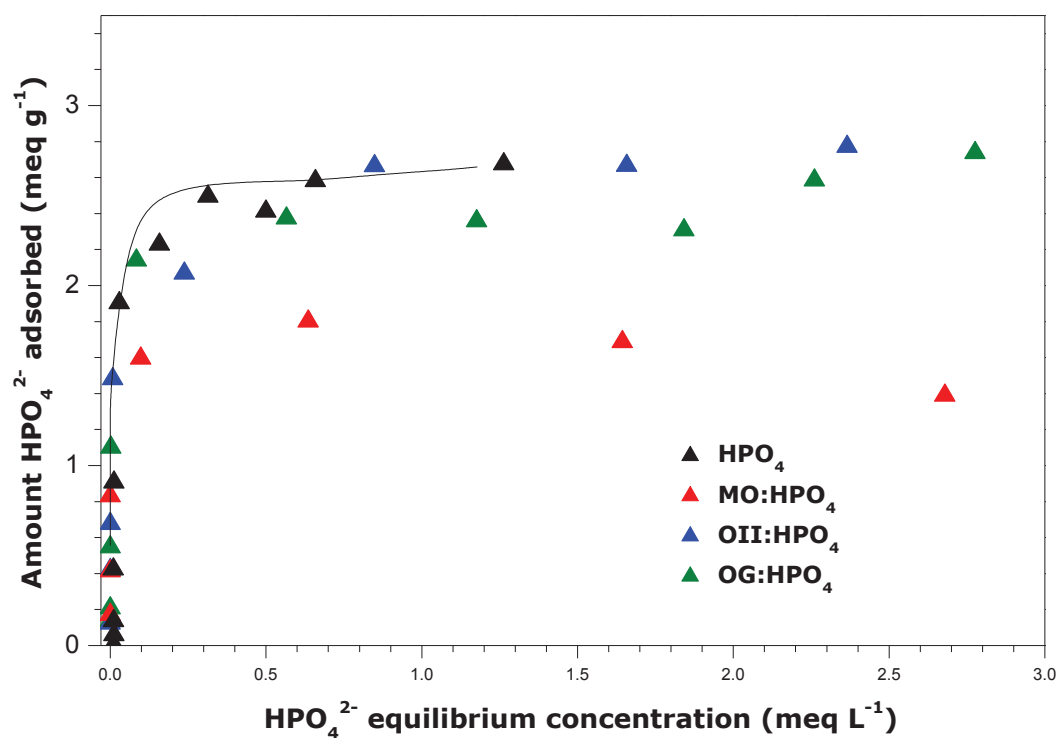


Figure AII- 4. Individual adsorption isotherm for hydrogen phosphate anions adsorbed at 298 K onto Mg<sub>2</sub>Al-LDH-Cl from bi-solute solution with dye.

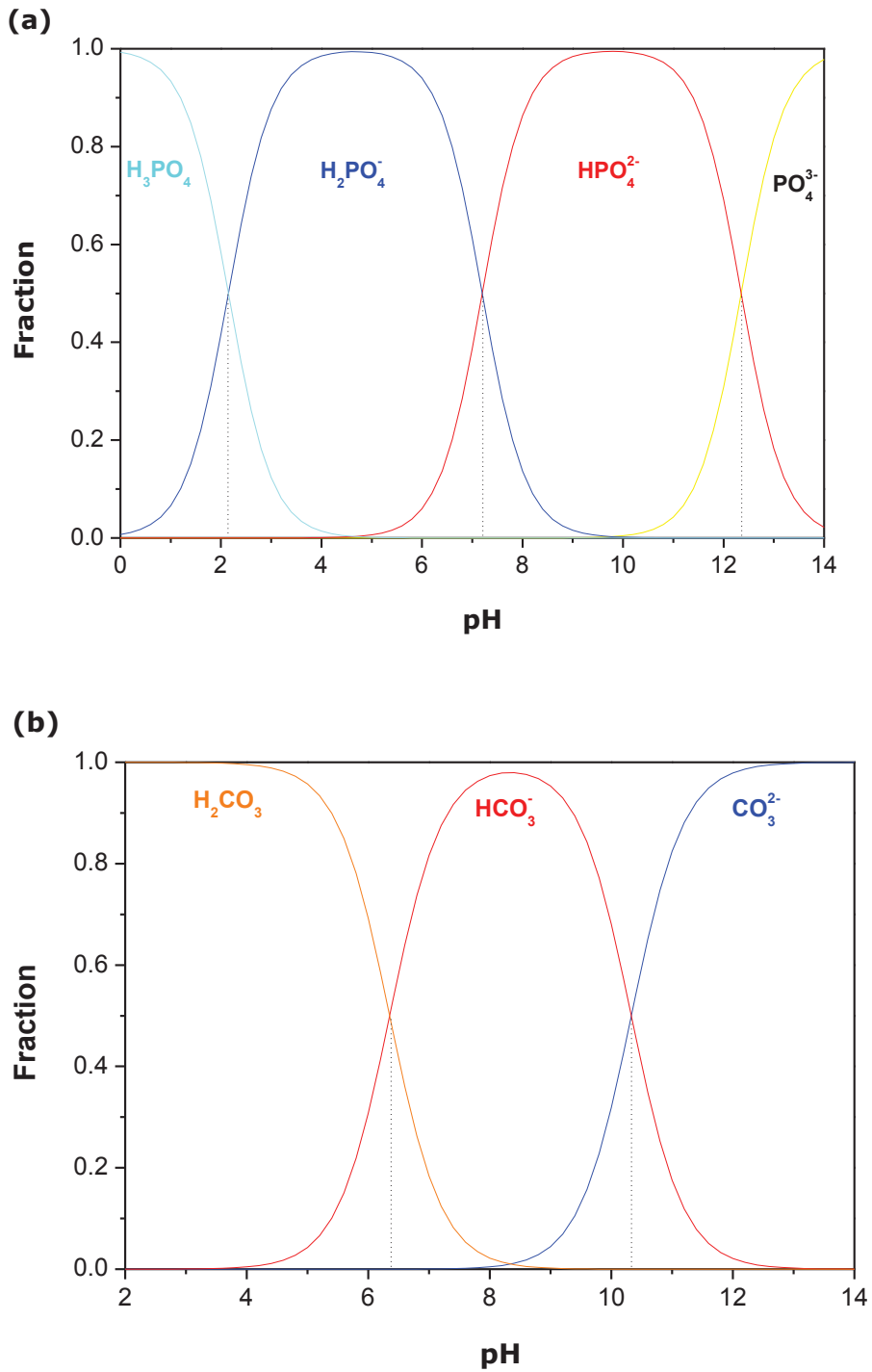
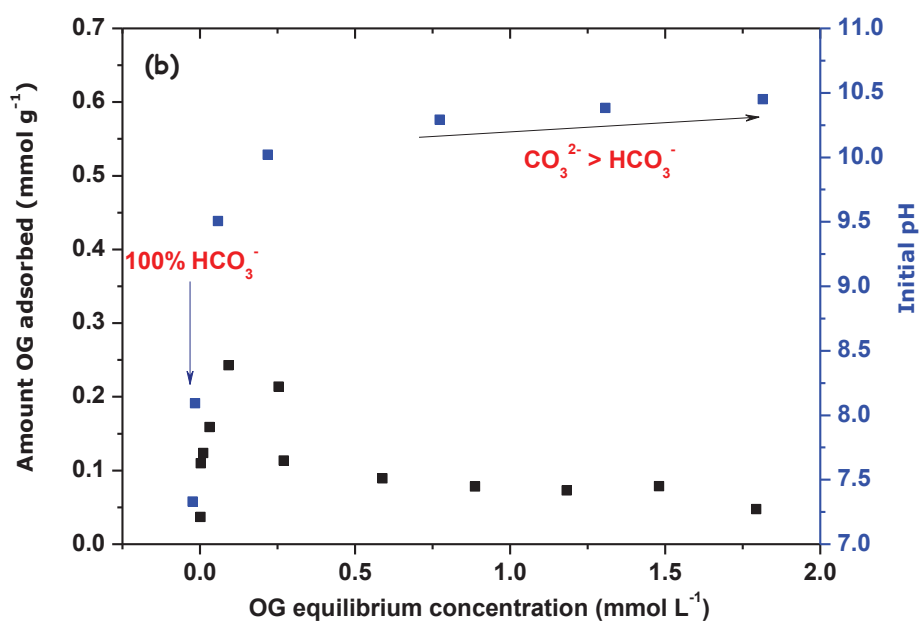
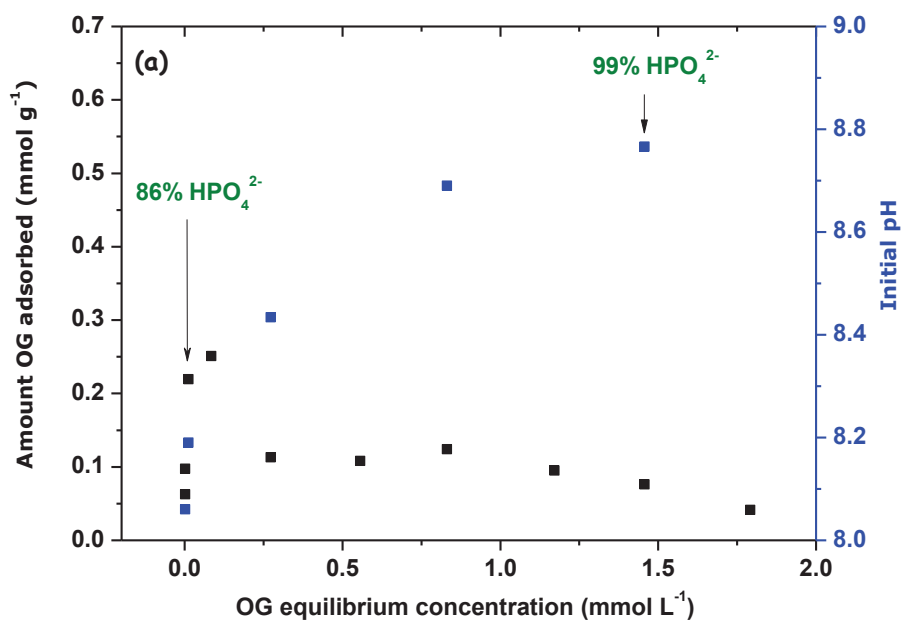


Figure AII- 5. Diagrams of the speciation for the phosphates (a) and carbonates (b) ions.

Appendices



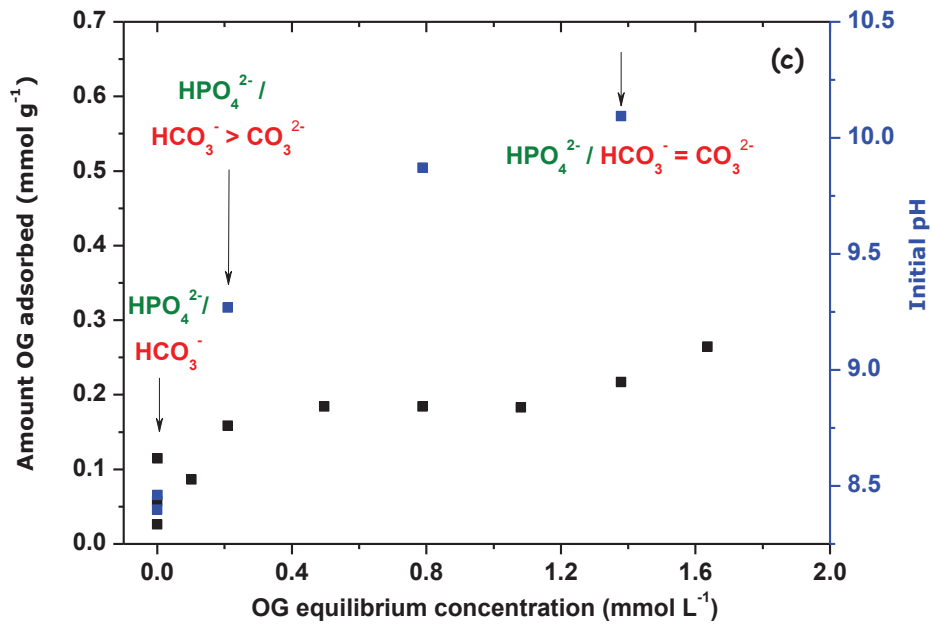


Figure AII- 6. Isotherms of competitive adsorption between OG dye with values of initial pH, measured at the first contact of the solid with solutes for some points on adsorption isotherm: bi-component systems OG+P (a) and OG+C (b); tri-component system OG+P+C (c).